(2)

# NAVAL POSTGRADUATE SCHOOL
# MONTEREY, CALIFORNIA






# DISSERTATION

LARGE-SCALE CIRCULATION REGIMES
AND TROPICAL CYCLONE CHARACTERISTICS
OVER THE WESTERN PACIFIC OCEAN

by

Patrick A. Harr

June, 1993

Dissertation Supervisor: Russell L. Elsberry

Approved for public release: distribution is unlimited

# REPORT DOCUMENTATION PAGE

Form Approved
OMB No 0704-0188



| 1. AGENCY USE ONLY (Leave blank) | 2. REPORT DATE | 3. REPORT TYPE AND DATES COVERED |
|---|---|---|
| | June, 1993 | PhD Dissertation |

**4. TITLE AND SUBTITLE**

Large-Scale Circulation Regimes and Tropical Cyclone Characteristics Over the Western Pacific Ocean

**5. FUNDING NUMBERS**

N0001493 WR 24009
PE 0601153N
PR RR033-03-01

**6. AUTHOR(S)**

Patrick A. Harr

**7. PERFORMING ORGANIZATION NAME(S) AND ADDRESS(ES)**

Naval Postgraduate School
Monterey, CA 93943-5000

**8. PERFORMING ORGANIZATION REPORT NUMBER**

**9. SPONSORING / MONITORING AGENCY NAME(S) AND ADDRESS(ES)**

Office of Naval Research (Code 1122MM)
Arlington, VA 22217-5000

**10. SPONSORING / MONITORING AGENCY REPORT NUMBER**

**11. SUPPLEMENTARY NOTES**

The views expressed in this thesis are those of the author and do not reflect the official policy or position of the Department of Defense or the U.S. Government

**12a. DISTRIBUTION / AVAILABILITY STATEMENT**

Approved for public release, distribution is unlimited

**12b. DISTRIBUTION CODE**

**13. ABSTRACT** *(Maximum 200 words)*

The basic structure of the variability of the large-scale circulations over the tropical western North Pacific is investigated with respect to its influence on tropical cyclone characteristics. A vector empirical orthogonal function analysis and a fuzzy cluster algorithm are used to define six recurrent 700 mb circulation patterns that represent large-scale variabilities associated with the monsoon trough and subtropical ridge. Three circulation patterns are associated with an active monsoon trough, and two patterns represent an inactive monsoon trough. One pattern depicts small deviations from the long-term climatology. The 700 mb circulation patterns are shown to be physically consistent with outgoing longwave radiation anomalies and the 200 mb streamfunction and velocity potential anomalies. A seventh set of circulation patterns is defined to contain transition periods between the active, inactive and small anomaly patterns. Transitions between recurrent circulation patterns may be within the active or the inactive patterns, or be transitions across the active/inactive boundary that are associated with major circulation changes. These significant transitions occur over a very limited set of paths, which are shown to be associated with interactions among tropical and midlatitude circulation systems. The recurrent circulation patterns and their transitions are shown to explain much of the observed intraseasonal variability in the occurrence and track types (recurving versus straight-moving) of tropical cyclones over the western North Pacific.

**14. SUBJECT TERMS**

tropical cyclones, circulation regimes, low-frequency variability, tropical cyclone motion, monsoons, cluster analysis

**15. NUMBER OF PAGES**

300

**16. PRICE CODE**

| 17. SECURITY CLASSIFICATION OF REPORT | 18. SECURITY CLASSIFICATION OF THIS PAGE | 19. SECURITY CLASSIFICATION OF ABSTRACT | 20. LIMITATION OF ABSTRACT |
|---|---|---|---|
| UNCLASSIFIED | UNCLASSIFIED | UNCLASSIFIED | UNLIMITED |

Approved for public release; distribution is unlimited

Large-Scale Circulation Regimes and Tropical Cyclone Characteristics
Over the Western Pacific Ocean

by

Patrick A. Harr
B.S., Miami University, 1976
M.S., Colorado State University, 1978

Submitted in partial fulfillment of the
requirements for the degree of

DOCTOR OF PHILOSOPHY IN METEOROLOGY

from the

NAVAL POSTGRADUATE SCHOOL
June 1993

Author: 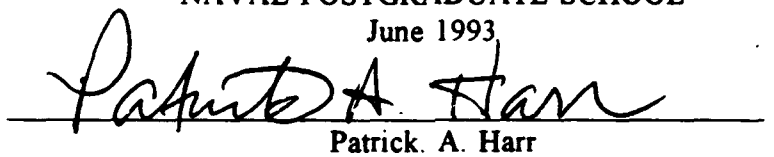
Patrick. A. Harr

Approved by: 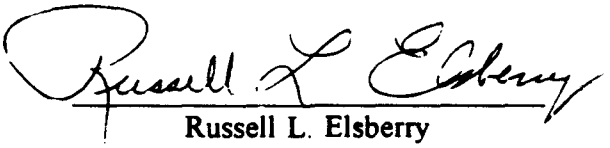
Russell L. Elsberry
Professor of Meteorology
Dissertation Supervisor

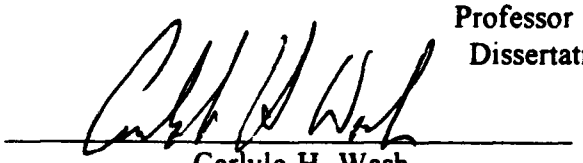
Carlyle H. Wash
Professor of Meteorology

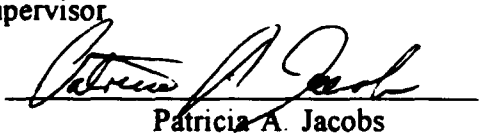
Patricia A. Jacobs
Professor of Operations Research

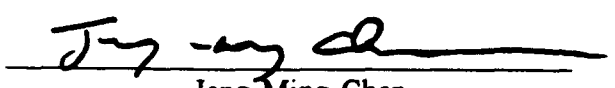
Jeng-Ming Chen
Research Assistant Professor of Meteorology

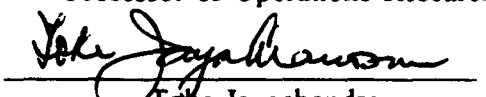
Toke Jayachandran
Dean, Computer and Information Services

Approved by: 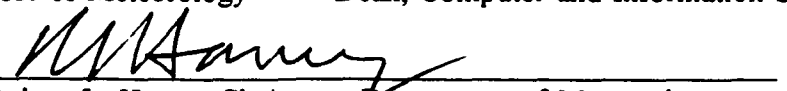
Robert L. Haney, Chairman, Department of Meteorology

Approved by: 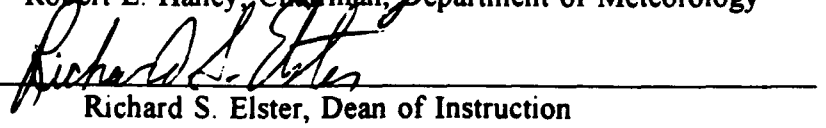
Richard S. Elster, Dean of Instruction

## ABSTRACT

The basic structure of the variability of the large-scale circulations over the tropical western North Pacific is investigated with respect to its influence on tropical cyclone characteristics. A vector empirical orthogonal function analysis and a fuzzy cluster algorithm are used to define six recurrent 700 mb circulation patterns that represent large-scale variabilities associated with the monsoon trough and subtropical ridge. Three circulation patterns are associated with an active monsoon trough, and two patterns represent an inactive monsoon trough. One pattern depicts small deviations from the long-term climatology. The 700 mb circulation patterns are shown to be physically consistent with outgoing longwave radiation anomalies and the 200 mb streamfunction and velocity potential anomalies. A seventh set of circulation patterns is defined to contain transition periods between the active, inactive and small anomaly patterns. Transitions between recurrent circulation patterns may be within the active or the inactive patterns, or be transitions across the active/inactive boundary that are associated with major circulation changes. These significant transitions occur over a very limited set of paths, which are shown to be associated with interactions among tropical and midlatitude circulation systems. The recurrent circulation patterns and their transitions are shown to explain much of the observed intraseasonal variability in the occurrence and track types (recurving versus straight-moving) of tropical cyclones over the western North Pacific.

## TABLE OF CONTENTS

## LIST OF TABLES

## LIST OF FIGURES

## ACKNOWLEDGMENTS

I would like to express my sincerest thanks to my advisor, Professor Russell L. Elsberry for providing the opportunity for me to work with him. His guidance, support and enthusiasm created a learning environment that taught meteorology, research and organization skills that I hope to apply throughout my professional life. I would also like to thank the members of the doctoral committee, Profs. C. H. Wash, P. A. Jacobs, T. Jayachandran and J.-M. Chen for constructive comments regarding this research. I also acknowledge stimulating discussions regarding statistical analysis techniques with Prof. J.-M. Chen. I am also thankful for the constant encouragement of Mr. William Clune of the Fleet Numerical Oceanography Center.

Special thanks are due my wife Sally, son Adam, daughter Emily and my parents.. They excused my absences with patience and understanding, but most of all they were constant reminders of the priorities in my life.

This research has been supported by the Office of Naval Research Marine Meteorology Program and the Naval Postgraduate School Direct Research Funds.

# I. INTRODUCTION

Tropical cyclone motion characteristics are significantly affected by the large-scale climatological circulations over each basin containing tropical cyclones (Elsberry 1987). Additionally, interannual variability in tropical cyclone characteristics due to deviations from the climatologically normal large-scale circulations have been documented. The eastward shift in the location of tropical cyclones over the western Pacific during El Nino years is one example of such an interannual variability (Chan 1985b).

Gray (1985) showed that the global frequency of tropical cyclone occurrences also varies on an intraseasonal time scale. Alternating active and inactive periods occur at intervals that range between 20 to 40 days. Sandgathe (1987; Figs.3-6) illustrated that considerable intraseasonal variability in the western Pacific tropical cyclone track types occurred during 1984. Examination of a climatology of western Pacific tropical cyclone tracks reveals many instances of intraseasonal variability in track types. For example (Fig. 1a), only recurving tropical cyclones occurred during May 1980, then four straight-moving tropical cyclones occurred between 24 June and 24 July, and only recurving tracks occurred from 27 July to 15 August. However, a period of variable track types occurred between 24 August and 14 September (Fig. 1b).

Tropical cyclone motion is primarily associated with a large-scale "steering" flow, which is usually associated with a deep-layer mean that encompasses the lower and middle troposphere. A secondary component of tropical cyclone motion that results in deviations of the motion of the tropical cyclone from the steering flow is caused by the interaction of the

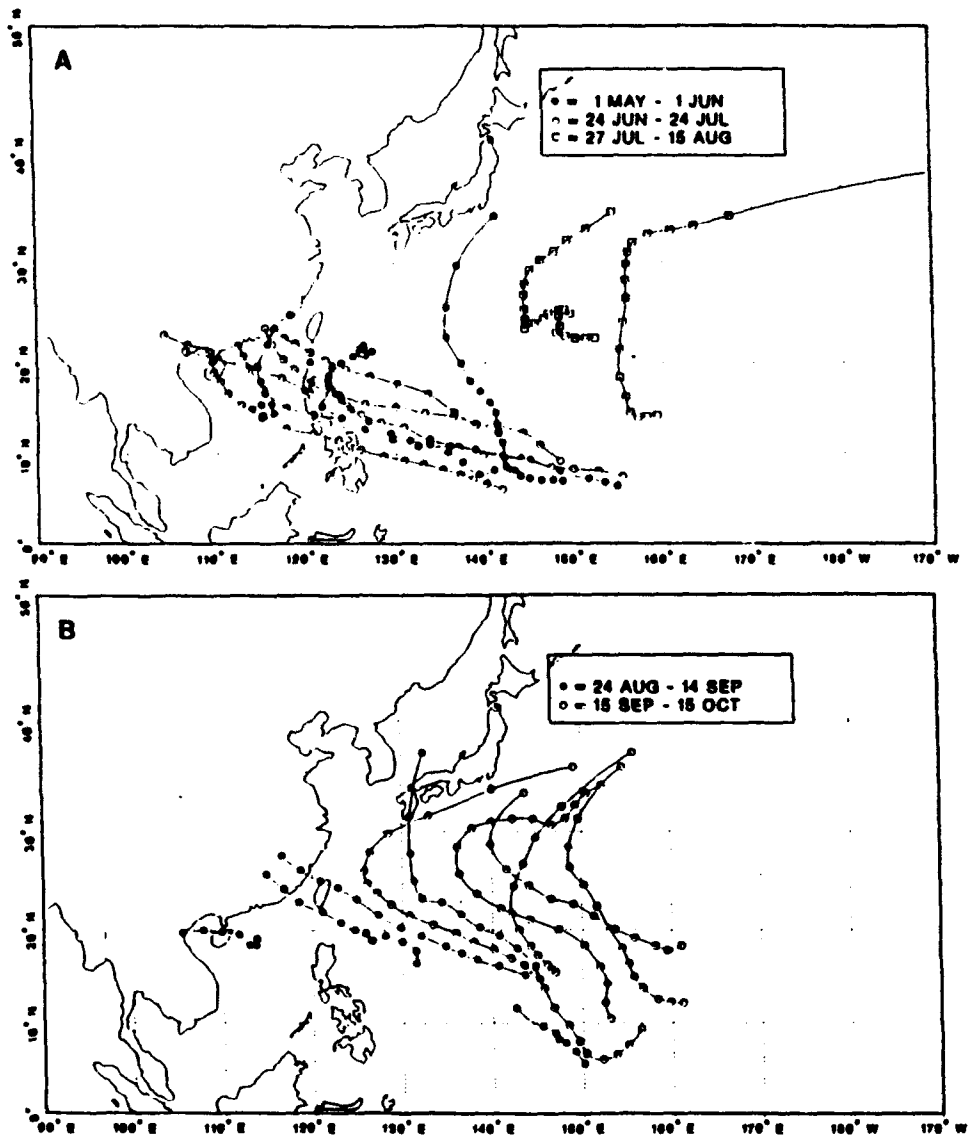


**Fig. 1** Best-track positions of 1980 tropical cyclones during (a) 1 May-15 August and (b) 24 August-15 October.

tropical cyclone circulation with the Earth's vorticity and the environmental vorticity (Elsberry 1987).

Many factors contribute to the variability of the large-scale circulation over the tropical western Pacific. These factors involve a broad range of space and time scales. Small space and short time scales are dominated by individual cloud clusters and tropical cyclones. Synoptic-scale features include larger tropical cyclones, super cloud clusters, easterly waves, cold surges, the monsoon trough, the subtropical ridge, and the tropical upper-tropospheric trough (TUTT). Large-scale features include global-scale propagating divergent circulations (Madden and Julian 1972; Knutson and Weickmann 1987), Rossby wave-like responses to tropical heating (Hoskins and Karoly 1981), and monsoon circulations. The climatological background over the tropical western Pacific within which these features exist is typically characterized by equatorial westerlies, a monsoon trough, trade wind easterlies and the subtropical ridge. The upper-tropospheric large-scale circulation includes the TUTT, subtropical anticyclone and equatorial easterlies associated with the Southwest Asian monsoon. Lau et al. (1989) and Sui and Lau (1992) propose a unified view of the interactions among the various scales defined above, and their relationships to the overall large-scale circulation of the western Pacific.

In the unified view of tropical circulation variability put forth by Lau et al. (1989), many of the attributes associated with the physical components of the large-scale tropical circulations are associated with global-scale oscillations (Knutson and Weickmann 1987). This implies that some circulation characteristics such as different phases of the 30-60 day oscillation may be recurrent patterns. Investigations of recurrent large-scale circulation

circulation patterns have concentrated on midlatitude flow regimes that are primarily related to blocking and zonal flow characteristics. These studies have concentrated on both the observational (Dole and Gordon 1983) and theoretical (Charney and DeVore 1979) aspects of recurrent large-scale circulation patterns.

The observed recurrence of periods that have similar tropical cyclone characteristics suggests that these may be related to the recurring large-scale circulation patterns. This statement assumes that direct relationships exist between recurrence of similar tropical cyclone patterns and the large-scale circulation. However, a more general approach would be to identify recurrent large-scale circulations independent of tropical cyclone characteristics, and then examine whether these circulations have any relationship to the observed variability in tropical cyclone characteristics.

Based upon investigations of large-scale midlatitude circulations, it is assumed that the recurrent circulation patterns may be represented in terms of the basic structures of the large-scale circulation variability (Mo and Ghil 1987). Therefore, these basic structures must be identified prior to the recognition of recurrent characteristics of the large-scale circulation over the tropical western Pacific. Typically, an empirical orthogonal function (EOF) analysis (Lorenz 1957) is used to define the intrinsic variability associated with large-scale atmospheric circulations (Barnston and Livezy 1987; Richman 1986). Because of the statistical nature of the EOF analysis, which was originally applied as a data reduction technique, no guarantee exists that the resultant functions describe physically realistic patterns. The constraints placed upon the EOF analysis only require an optimal representation of the structure of the variance within the data set. Whether these structures actually represent

attributes of the tropical atmosphere must be individually determined for each application. If the relationships between the recurrent circulation patterns, which are based upon the basic structure of the variability within the data field, and tropical cyclones are to be identified, then the physical characteristics of each basic mode of variability must be established.

Based upon the above discussions, the basic hypotheses of this research can be stated as:

- The variability of the large-scale tropical western Pacific circulation can be characterized by a small set of recurrent patterns.
- Recurrent circulation patterns are separated by transition periods when circulation characteristics may not be well defined.
- A limited set of preferred transition paths are observed between the recurrent patterns, and the corresponding field representations are physically consistent.
- Variations within the framework defined by recurrent circulation patterns and preferred transition periods significantly contribute to the observed variabilities in tropical cyclone characteristics such as activity/inactivity, genesis locations, and track types.

The approach in this research is to apply an EOF analysis to the 700 mb anomalous wind fields over the tropical Indian Ocean and western Pacific to identify the primary structures of circulation variability over these regions. The physical realism of the vector EOF analysis is established by comparing the variability associated with EOF structures with observed variability contained in the data set, as represented by the tropical cyclone-based circulation patterns defined by Harr and Elsberry (1991). The significance of these comparisons is established by performing similar analyses on several sets of meteorological variables. An EOF analyses of the zonal wind component and an EOF analysis of anomalous outgoing longwave radiation (OLR) are also compared to the observed variability of the large-scale

circulation to confirm the physical realism and consistency of the large-scale circulation representations.

Recurrent anomalous circulation patterns are then defined by a cluster analysis that is based upon the leading modes of the large-scale circulation variability. A large diffuse portion of the cluster analysis phase space is also defined that contains anomaly maps that are not similar to the main recurrent patterns. This diffuse cluster essentially identifies the transient portion of large-scale circulation variability, and can be used to define the preferred transition paths between the recurrent clusters.

The physical relationships between tropical cyclone characteristics and the recurrent circulation patterns is then established using the cluster patterns, which represent an instantaneous depiction of the circulation variability. The relationships with tropical cyclone characteristics during periods of large-scale transitions between the cluster patterns are also established. These are important relationships that have implications concerning the ability to predict expected tropical cyclone attributes, or changes in attributes, based upon the characterization of the atmospheric variability in the cluster analysis framework.

This dissertation begins with a summary of a preliminary study by Harr and Elsberry (1991) in Chapter II, Sections A and B, which defined large-scale circulation patterns based upon the occurrence of tropical cyclones or inactive periods. Definitions of the basic structure of large-scale circulation variability using a scalar EOF analysis of the zonal winds and a vector EOF of the total wind are described in Chapter III. This chapter establishes the physical basis of the EOF structures that will be carried throughout the cluster analysis. Chapter IV defines the cluster method and the cluster patterns that are based upon the basic

structures of anomalous 700 mb large-scale circulation variability. The physical significance of the cluster patterns is defined by examining their structure using several meteorological variables to more fully describe the large-scale, three-dimensional structure of the cluster patterns. The relationships between the cluster patterns and tropical cyclone characteristics is also established in Chapter IV. The internal consistency and relationships between the clusters are defined in Chapter V. These relationships are defined with respect to preferred transition paths, which lead to major circulation changes over the western Pacific. The evolution of the large-scale circulation during the preferred transition paths is established along with the effect of the transitions on tropical cyclone characteristics. Conclusions are provided in Chapter VI.

# II. PRELIMINARY ANALYSIS

The descriptions in Chapter I indicate significant variations in both western North Pacific (WPAC) tropical cyclone characteristics and tropical circulation features over interannual and intraseasonal time scales. On interannual time scales, Chan (1985b) describes a relationship between the large-scale circulation and an eastward shift in WPAC tropical cyclone formation positions during an El Nino/Southern Oscillation event. As a preliminary step, Harr and Elsberry (1991) identified interrelationships between intraseasonal variabilities of the large-scale circulation and tropical cyclone characteristics. Their analysis investigated whether certain large-scale circulation features are directly related to specific tropical cyclone track types and periods of inactivity. In the Harr and Elsberry (1991) analysis, the large-scale circulation is described by the departure of the 700 mb zonal wind from climatology. The primary procedures and results of Harr and Elsberry (1991) will be summarized in Sections A and B as their analysis was the basis for the remainder of this research.

The large-scale circulation may influence tropical cyclone track characteristics indirectly through controls on genesis location (McBride and Zehr 1981; Love 1982). Examination of climatological WPAC tropical cyclone tracks (Miller et al. 1988) indicated that straight-moving storms tend to form in particular genesis regions, whereas recurving tropical cyclones are more likely to occur within other regions. However, the distribution between straight-moving and recurving tropical cyclones appears to be almost even in other regions. The relationship between track type and genesis location is evident in Fig. 1. Straight-moving tropical cyclones that occurred between 24 June and 24 July formed in a

region that was distinct from the recurving cyclones during 27 July and 15 Aug, but in the same region as recurving cyclones that occurred between 1 May and 1 June. Harr and Elsberry (1991) first demonstrated an association between genesis location and subsequent track type and then established a direct relationship between the large-scale circulation control on track type (Section A below). Operationally-analyzed wind fields were then used to demonstrate whether distinct circulation patterns exist for each tropical cyclone track type. These large-scale circulations were identified by compositing time periods containing tropical cyclones that have similar track types. The relative utility of these relationships was then established by comparing predictions of tropical cyclone track type given genesis location with track-type predictions made by using a description of the large-scale circulation (Section B below).

## A. CLIMATOLOGICAL PROBABILITIES OF TRACK TYPE

The relationship between genesis location and subsequent track type is identified by defining the spatial distributions of the probability of each track type based on genesis location. From the climatology compiled by Miller et al. (1988), the numbers of WPAC tropical cyclones occurring during 10 half-month periods centered on either the first or sixteenth of the months June - October are counted for each track type. The spatial probability distributions of track type in relation to the genesis location is computed for each half-month period by dividing the frequencies pertaining to each track type by the frequency of the total set of cyclones. Only the distributions pertaining to straight-moving or recurving tropical cyclone are computed. It is assumed that tropical cyclones following odd-moving

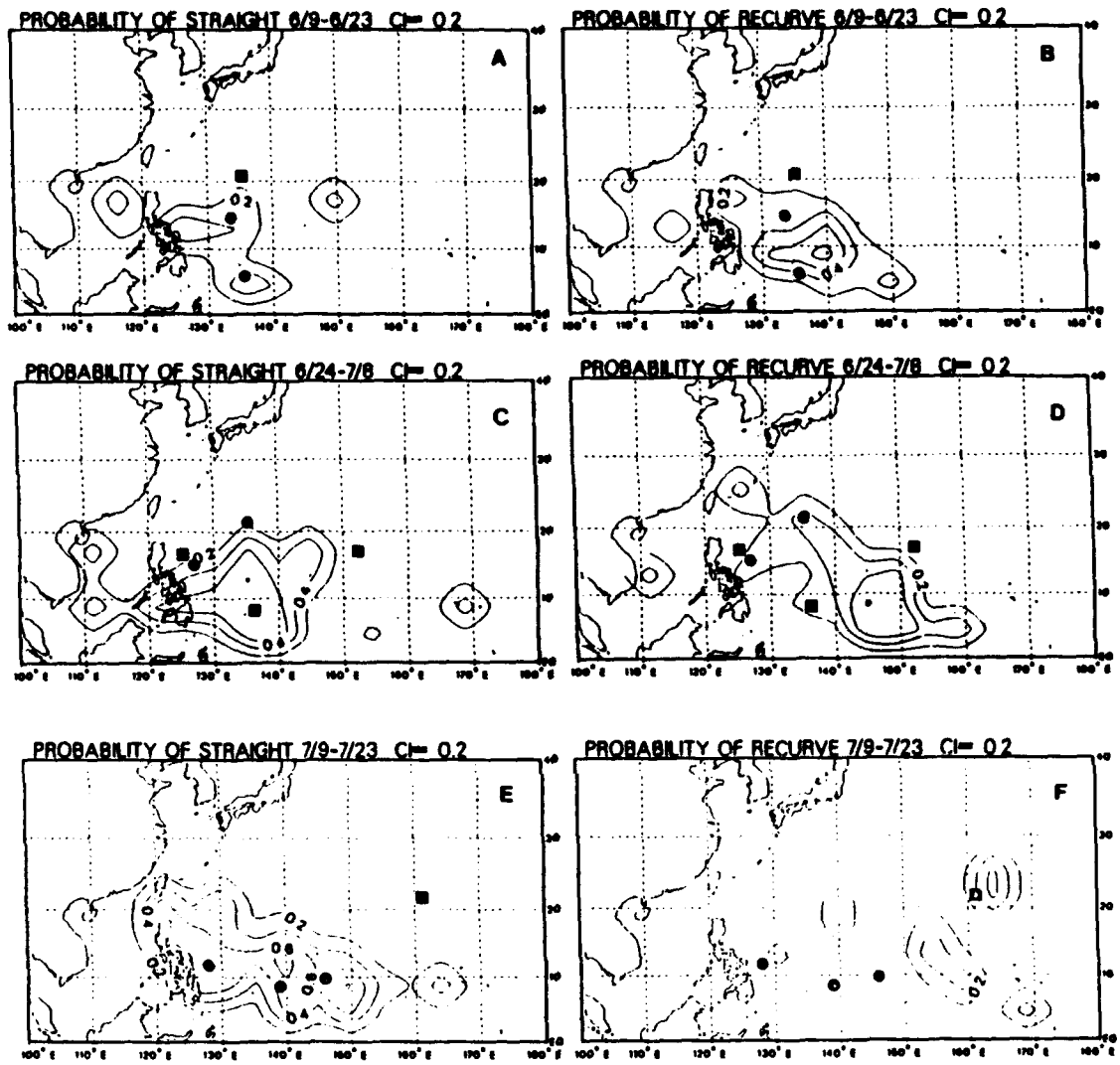


**Fig. 2(a)-(f)** Probability (contour interval of 0.2) of a tropical cyclone following either a straight (left column) or recurving (right column) track given the genesis location and the time of year. The probability values are defined in 5° lat.-long. boxes. Smoothed contours are produced by adding four times a center point to the four surrounding points and dividing the sum by eight. Each chart represents a two-week period centered on either the first or fifteenth of each month. The squares represent the genesis locations of 1983-85 recurving storms used in a prediction scheme defined in the text. The circles represent the genesis positions of straight-moving storms.

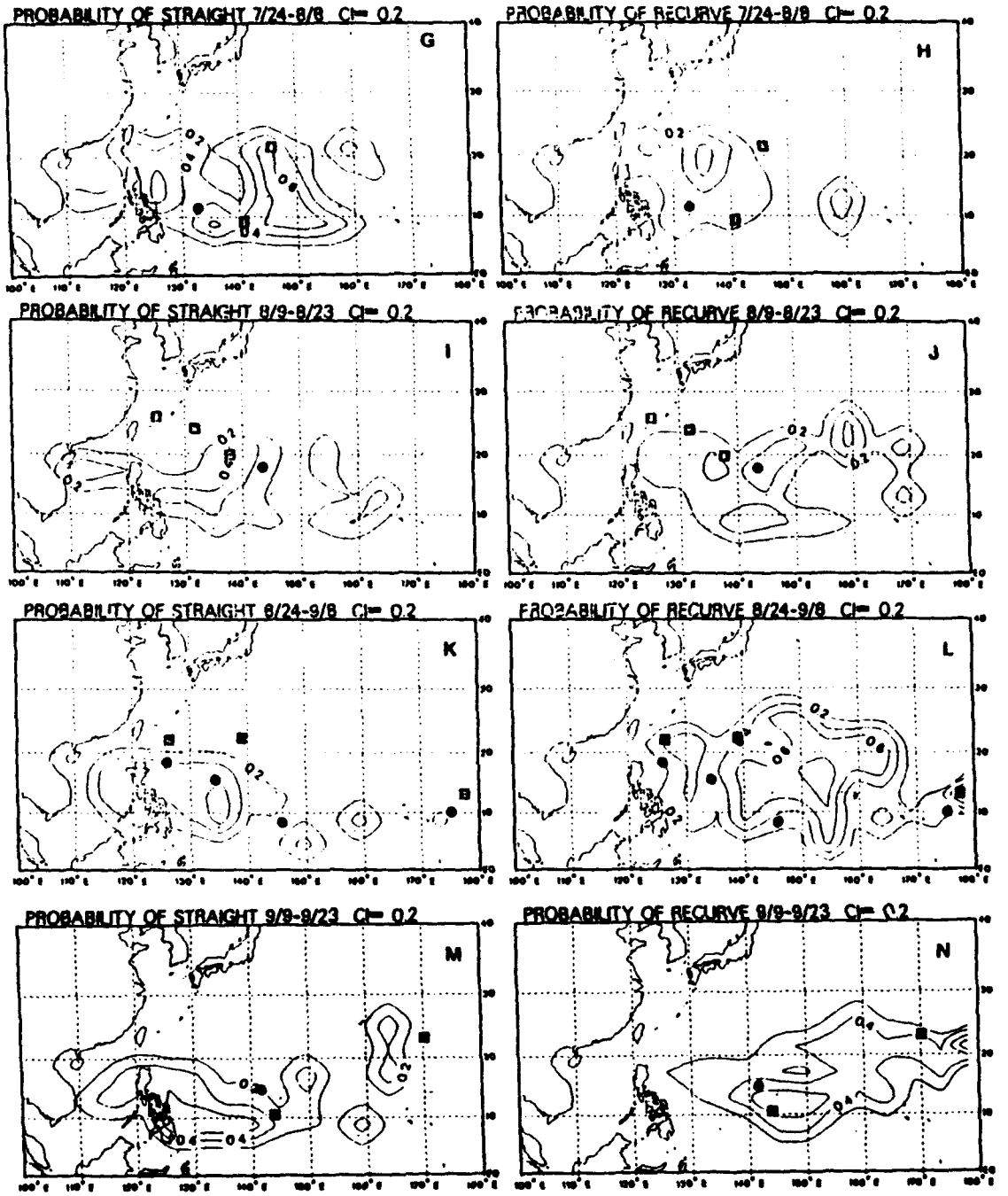


**Fig. 2(g)-(n)** As in Fig. 2(a)-(f), except for the indicated time periods

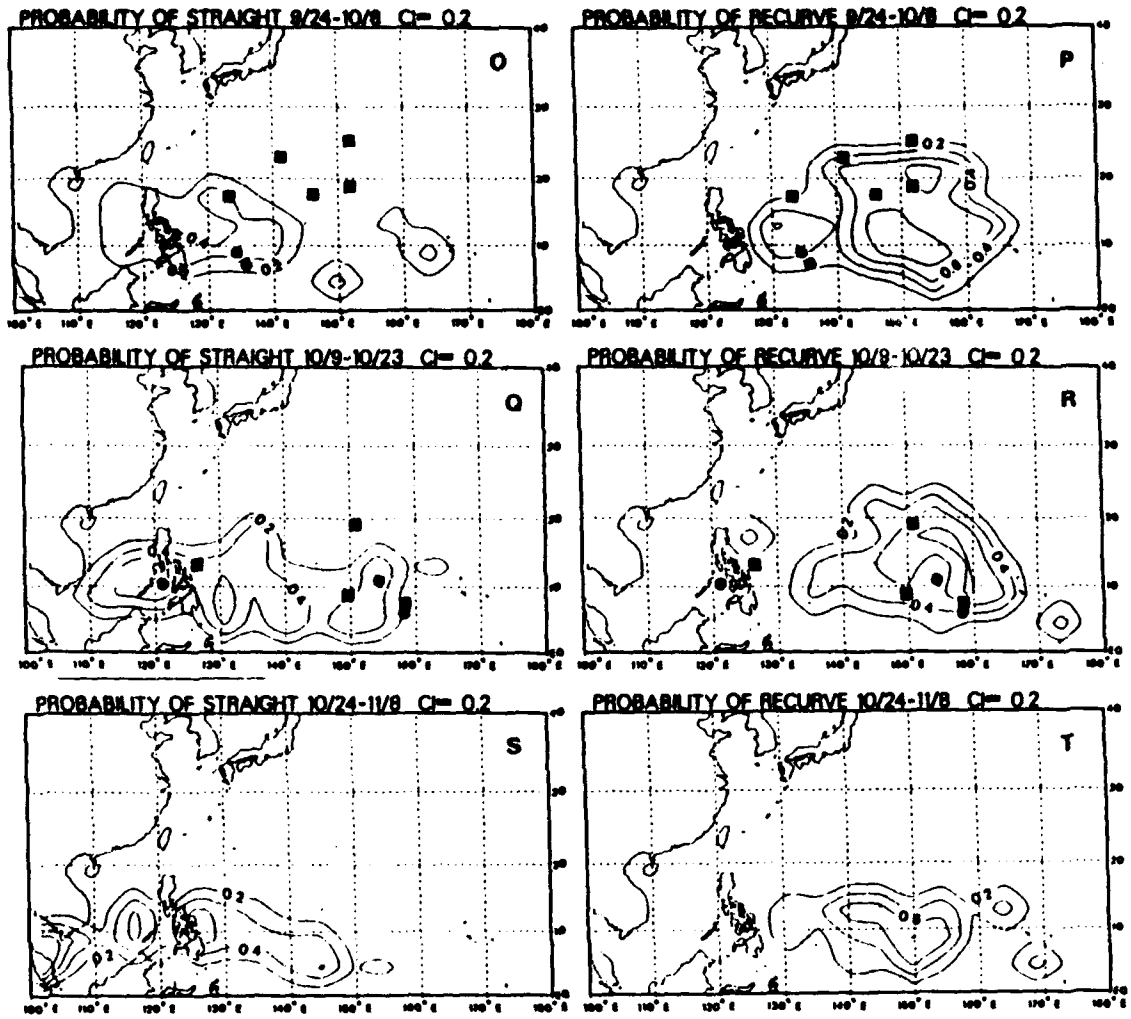


**Fig. 2(o)-(t)** As in Fig. 2(a)-(d), except for the indicated time periods.

tracks are essentially straight-moving or recurving cyclones that are influenced by factors considered to be external to those being examined here (e.g., other tropical cyclones, midlatitude systems).

During June, when tropical cyclone genesis usually occurs over the South China Sea and Philippine Sea, nearly equal probability is found that subsequent track types will be either straight-moving or recurving (Figs. 2a-b). During July, the climatological probability of a straight-moving track given that genesis occurs over the South China Sea or Philippine Sea remains high (Figs. 2c,e,g). The distribution of probabilities associated with recurving tracks are more variable. During early July, the probability of a recurving track is high when genesis occurs east of 140°E (Fig. 2d). During late July, the genesis regions for recurving tropical cyclones are much smaller than for straight-moving tropical cyclones (Fig. 2f). During early August, a large overlap exists between the primary regions of high probability of a straight track and a recurving track (Fig. 2h). Therefore, it would be difficult to determine whether a tropical cyclone will follow a straight-moving or recurving track based only on genesis location during this period. During the peak of the tropical cyclone season, the regions of maximum probability of each track type become more separate (Figs. 2 i-p). Regions of maximum probability of straight tracks remain south of 20°N over the South China Sea and the Philippine Sea. Regions of high probability of recurving tracks shift eastward to 155°E and northward to 25°N. Throughout the remainder of the season, the regions of maximum probable straight-moving and recurving track types remain fairly distinct and the areas of tropical cyclone genesis become smaller (Figs. 2o-t). The likelihood of a straight track is greatest south of 20°N and east of 145°E. The likelihood of a recurving track is

greatest east of 145°E and extends to 25°N during October before it shifts south in early November. The reproducability of these results has been examined by splitting the 43-year climatology into equal halves and then repeating the analysis on each half. The distributions are essentially identical to those obtained with the full 43-year climatology.

This track-type climatology indicates that genesis location does contribute to observed track characteristics. When genesis occurs north of 20°N, or east of 150°E and north of 10°N, the probability of a recurving track is larger than the probability of a straight track. South of these regions, the probabilities of each track are nearly even. Because of this result, recurving tropical cyclones that form in regions that clearly favor recurving tracks are classified recurving-north (RN). Recurving tropical cyclones that form in regions where it is equally likely to follow straight or recurving tracks are classified recurving-south (RS).

## B. LARGE-SCALE CIRCULATIONS ASSOCIATED WITH TRACK TYPES AND GENESIS LOCATIONS

Specific atmospheric circulation parameters have been linked to tropical cyclone genesis (Gray 1979; McBride and Zehr 1981). The objective of this section is to demonstrate that specific large-scale circulation patterns are associated with each track type and/or genesis region. The genesis region is accounted for by considering the separate groups of recurving storms defined from the conditional probabilities of track type given the genesis location.

The global band analyses (GBA) of wind data produced between 1979-1982 by the U.S. Navy Fleet Numerical Oceanography Center (FNOC) at 700 mb are used to identify large-scale circulations associated with each track type. The GBA fields are produced with a grid spacing of 2.5° on a Mercator projection true at 22.5°N. The latitudinal range of the

analysis is roughly 60°N-40°S, and the meridional extent is global. The analysis procedure utilizes surface, ship, aircraft, pilot balloon, radiosonde and satellite cloud-drift wind data. A successive corrections technique is used with 6-h persistence as the first-guess field. Details of the entire analysis procedure are provided in Grayson (1971). Anomalies of the 700 mb u- and v-component winds are derived by subtracting a daily climatology computed using 1979-1982.

The basic hypothesis of the study relates the variability of the tropical WPAC large-scale circulations and the "steering" concept of tropical cyclone motion. The large-scale circulation during May-October may be characterized by equatorial southwesterlies, the monsoon trough and the subtropical ridge. Although these features are present at lower levels, and tropical cyclone steering is best correlated with midtropospheric flow (Elsberry 1987), the 700-mb level is used since it represents a logical compromise between these factors.

Because of the weak gradients in geopotential height throughout the tropics, wind data are preferable for identifying the circulation features that affect tropical cyclone motion. Many studies of tropical cyclones and other tropical circulations have used winds directly from rawinsonde observations (George and Gray 1976; Gray 1979; Madden 1986; Madden and Gutzler 1989). Chan (1985a) investigated the relationships between tropical cyclone motion and steering flow derived from the GBA fields and concluded that the results were consistent with those obtained using rawinsonde data.

Large-scale circulation features associated with tropical cyclone track types are defined by compositing the 700 mb anomalous wind fields during periods when WPAC tropical

cyclones followed either straight or recurving tracks. Only tropical cyclones that attained a minimum of tropical storm intensity are considered. Tropical cyclones that formed and remained over the South China Sea are also omitted. Because such storms typically form deep within the monsoon trough with weak steering flow, they follow erratic tracks that are difficult to classify as either straight-movers or recurvers. The track classifications are defined using the climatological data in Miller et al. (1988). Recurving tracks are stratified into RS or RN classes as defined above.

Individual 700 mb wind anomaly fields may contain residual anomalous circulations from the surface bogus used in the GBA to define the position of mature tropical cyclones (at least tropical storm intensity). Consequently, the composite patterns could be contaminated by the superposition of many tropical cyclone circulations in the same region. The effect of the surface bogus is eliminated by constructing composites using only the first 24 h of the entire storm period. None of the tropical cyclones used in the analysis reached tropical storm intensity within the first 24 h defined in the best-track data. Although this procedure reduces the number of samples in each composite, it reduces the possible contamination of the anomalous wind anomalies due to a series of tropical cyclone circulations passing through the same region.

Time periods that contain multiple tropical cyclones following the same track type are only included once in the analysis. However, time periods that contain multiple tropical cyclones following different track types are excluded from the analysis. Because of the large WPAC area experiencing tropical cyclones, different track type regimes may exist simultaneously. However, the goal of this preliminary analysis is to identify large-scale

circulations associated with distinct track types. Finally, time periods containing tropical cyclones that are concurrent with tropical depression(s) and/or South China Sea storm(s) are not included in the analysis.

The composite patterns must have both physical and statistical significance if they are to provide more information about track type than is available from the climatological expectation based only on genesis position. Physical significance is established by identifying specific attributes of the composites with large-scale circulation features that are known to favor straight-moving versus recurving tracks. The method defined by Livezey and Chen (1983) is used to establish statistical significance of composites used in this analysis. This method is discussed in Appendix A. This method is based upon determining two levels of statistical significance. Local significance is defined for each point independent of all other space points by a Student's t test of the equality of two means. The problem of spatial independence between the space points is addressed using a Monte Carlo simulation procedure to determine the global significance associated with the distribution of the locally significant points. Appendix A contains specific results pertaining to the application of this technique to the large-scale circulation anomalies that are based on each track type. Therefore, subsequent remarks concerning significant features on composite charts in this study are based on the test defined in Appendix A.

### 1. Straight-moving Tropical Cyclones

The average large-scale anomalous circulation features associated with straight-moving (SM) tropical cyclones are shown in Fig. 3. An anticyclonic anomaly exits along

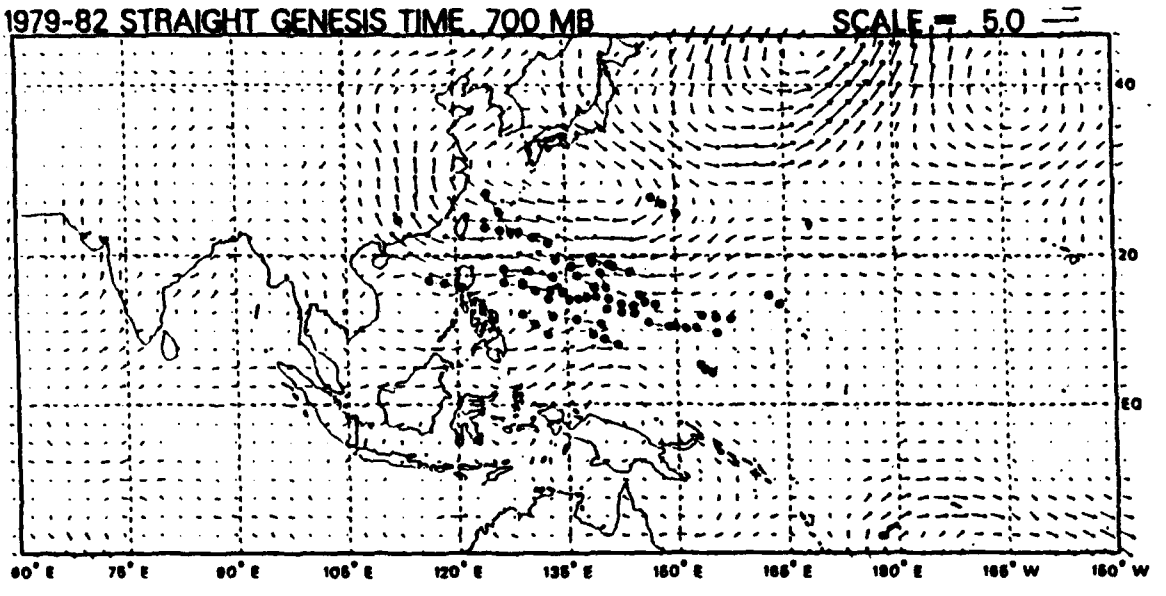


**Fig. 3** Anomalous 700 mb winds (m $s^{-1}$) composited from the initial 24 h of straight-moving tropical cyclones. The positions of the tropical cyclones are represented by the dots. Fifty-four individual maps are included in this composite.

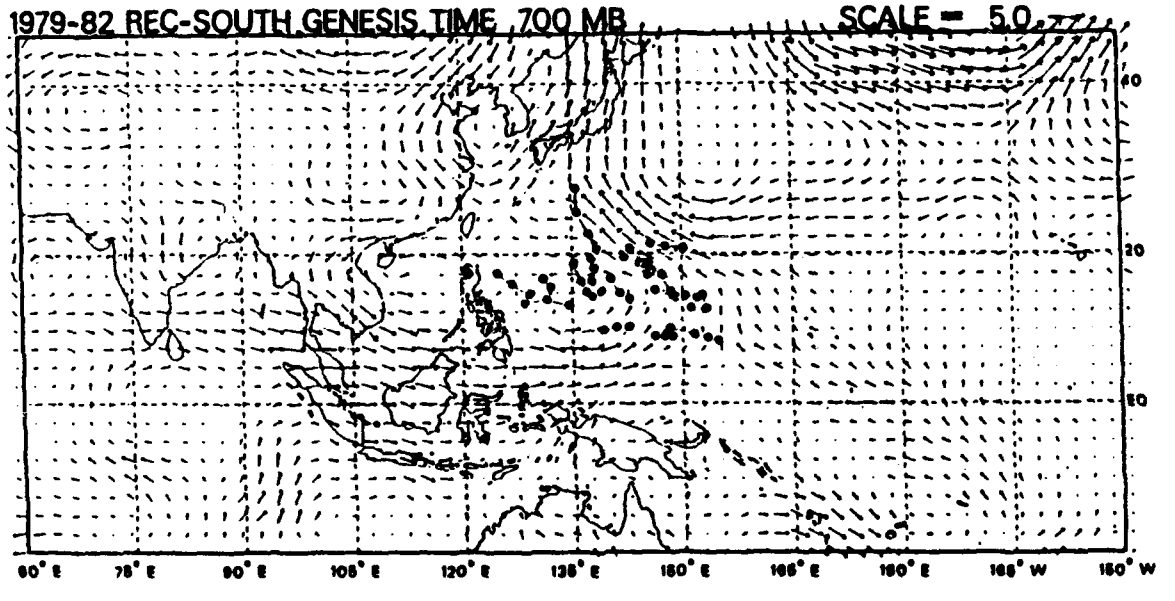


**Fig. 4** As in Fig. 3, except for recurving-south tropical cyclones. Fifty-two individual maps are included in this composite.

30°N and between 105° and 150°E, and cyclonic anomalies are found over the South China Sea and Philippine Sea.

A large region of anomalous cyclonic shear between 75° and 145°E exists between the equatorial southwesterlies and anomalous easterlies on the southern portion of the anomalous anticyclone centered along 30°N. This is associated with an enhanced monsoon trough extending into the tropical western North Pacific, which is an environment favorable for tropical cyclone genesis (Love 1982). Summarizing, these large-scale circulation anomalies define a physically consistent environment that favors tropical cyclone genesis within an active monsoon trough followed by a straight track associated with an enhanced subtropical ridge over the East China Sea.

### 2. Recurving-south Tropical Cyclones

Recurving-south (RS) tropical cyclones form south of 20°N and west of 150°E, which is a region that has no climatological preference between straight-moving and recurving tropical cyclones given the genesis location only (Fig. 2). Large equatorial westerly anomalies exist between 90° and 150°E. Anomalous cyclonic circulations exist over the Philippine Sea, South China Sea, and Bay of Bengal. A north-south oriented anomalous anticyclonic circulation is centered at 30°N between 135° and 180°E. Weak anomalies exist over the East China Sea and a cyclonic anomaly is found over the Yellow Sea.

Major differences exist between the SM and RS anomaly patterns over both the equatorial and subtropical regions. Over the equatorial regions, the anomalous westerlies between the equator and 5°N are stronger and cover a larger meridional area in the RS composite. Cyclonic circulation centers south of 20°N in the RS pattern extend farther east

(150°E) and west (75°E) than in the SM composite. Also, the centers of the cyclonic anomalies over the South China Sea and Philippine Sea are farther north in the RS composite than in the SM composite. These features indicate that the monsoon trough is more active and shifted northward during the initial 24 h of tropical cyclones following RS compared to those following SM tracks.

Over subtropical latitudes, the anomalous strong subtropical ridge present in the SM composite is replaced by a cyclonic anomaly over the Yellow Sea, which suggests that the western portion of the subtropical ridge is anomalously weak. The large anticyclonic anomalies east of Japan in the RS pattern indicate that the eastern portion of the subtropical ridge is anomalously strong.

In summary, the RS circulation pattern is characterized by an active monsoon trough with favorable genesis conditions, and a subtropical ridge that is weaker than normal between 120° and 135°E. The strengthening of the monsoon trough circulation is indicated by the strong equatorial westerly anomalies and evidence of anomalous cross-equatorial flow between 90° and 100°E. These factors may contribute to the northward shift of the anomalous monsoon trough compared to the SM pattern. A major contributor to the weakening of the western portion of the subtropical ridge may be the cyclonic anomalies over the Yellow Sea, which seem to represent a midlatitude feature. All these factors provide a physically consistent basis for the distinction between the SM and RS composites.

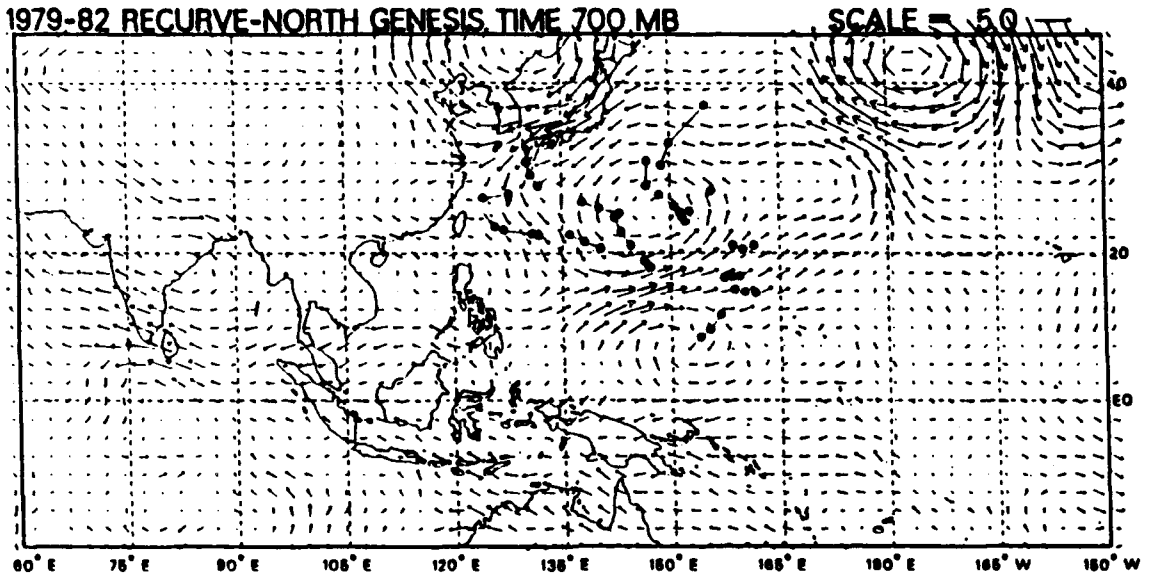


**Fig. 5** As in Fig. 3, except for recurving-north tropical cyclones. Fifty-five individual maps are included in this composite.

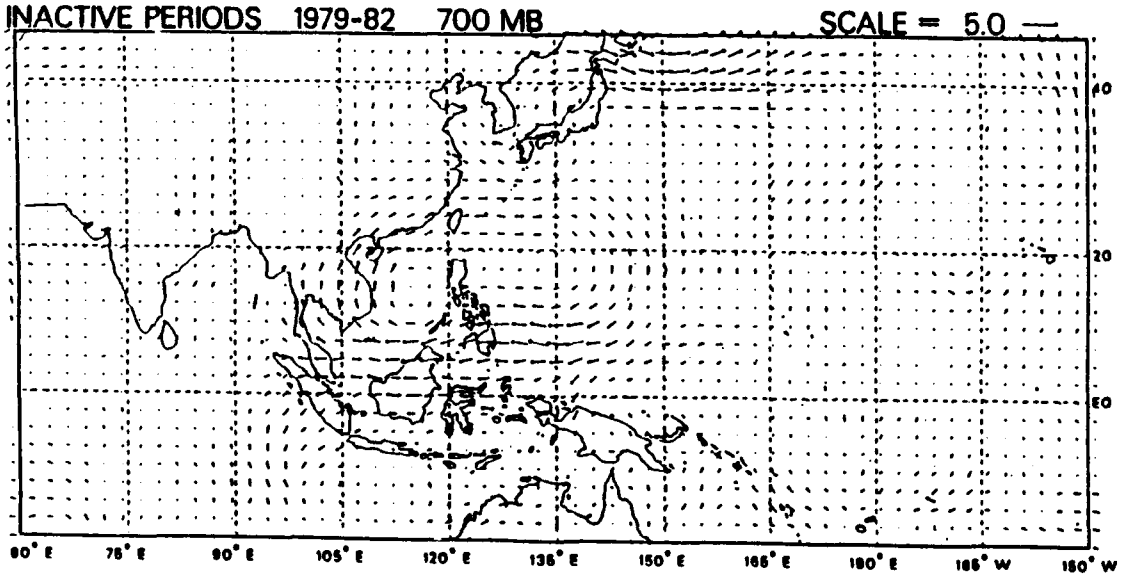


**Fig. 6** As in Fig. 3, except for inactive tropical cyclones. Two hundred sixty-three individual maps are included in this composite.

### 3. Recurve-north Tropical Cyclones

Recurve-north tropical storms are defined to be recurving storms that form north of 20°N. The anomalous large-scale circulation pattern for these types of tracks (Fig. 5) are very different from the patterns associated with straight or recurve-south tracks (Figs. 3,4). An anomalous ridge is oriented west-northwest to east-southeast between the equator-25°N from 70° to 100°E, and between the equator and 20°N from 100° to 160°E. Maximum anomalous equatorial easterlies exist between 70° and 120°E, which are associated with the most intense portion of the anomalous ridge that lies immediately to the north. Cyclonic anomalies are found along 25°N between 90°E and 165°W. These anomalous circulation patterns suggest that the monsoon trough is very weak or displaced to the north, and the subtropical ridge is also very weak.

### 4. Inactive Periods

Inactive periods are defined as consecutive 10 day periods between June-October during which no tropical cyclones exist over the western Pacific. The entire region of the South China Sea and Philippine Sea is covered by anticyclonic anomalies (Fig. 6). This is an amplification of the anticyclonic anomalies in the recurving-north composite (Fig. 5). However, the largest anomalous easterlies are shifted 20° east during the inactive periods. The sensitivity of the composite results to the length of the inactive period is investigated by compositing inactive periods that lasted between 5-10 and 3-5 days. During inactive periods that last between 3-5 days, the anomalous circulations are not organized into large-scale patterns (not shown). This suggests that short periods of inactivity are not forced by any coherent large-scale circulation variability. During inactive periods that last between 5-10

days, the anticyclonic anomalies are more intense and cover a larger area than longer periods of inactivity (not shown). Cyclonic anomalies are found north of 30°N between 110° and 140°E, which suggest the possible influence of midlatitude troughs that may shift the subtropical ridge southward.

### 5. Discussion of Composites

The composite results are summarized by averaging the anomalous 700 mb zonal (u) component of the wind between 100° and 140°E in 5° lat. bands from the equator to 30°N. This region includes the majority of the regions that contain significant variability among the composites.

Anomalous equatorial westerlies that extend to 10°-15°N in the straight-moving composite are stronger and extend to 15°-20°N in the recurving-south composite (Figs.7a,b). The increase is caused by anomalous cross-equatorial flow that is coupled to the anomalous trough extending from the Bay of Bengal through the Philippine Sea in the recurving-south composite (Fig. 4). Anomalous equatorial easterlies extend to 10°N in the recurve-north composite (Fig. 7c). During inactive periods, these easterly anomalies become stronger and extend to 15°N (Fig. 7d). This increase is associated with an eastward propagation of the maximum easterly anomalies from 70° to 120°E in the recurving-north composite (Fig. 5) to 100°-140°E in the inactive composite (Fig. 6). The eastward shift is coupled to a corresponding shift in the maximum anomalous anticyclonic circulations.

The above composites indicate that physically distinct and statistically significant anomalous large-scale circulation patterns exist during the initial 24 h of WPAC tropical cyclones following similar tracks, or during extended (at least 5 days) inactive

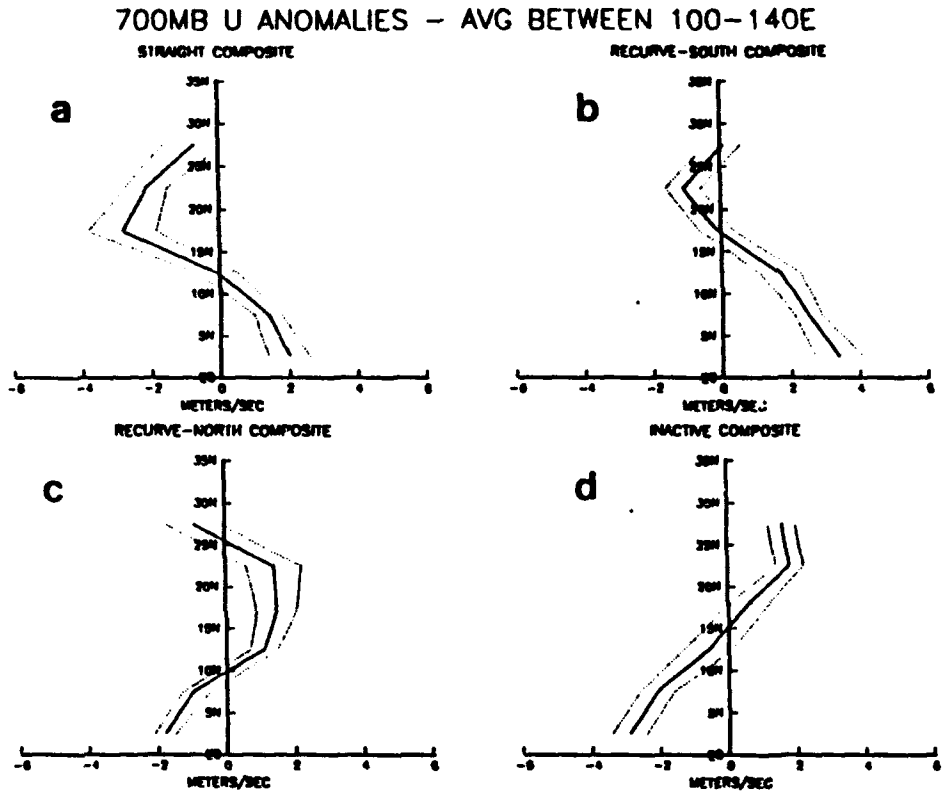


**Fig. 7** Latitudinal profiles of 700 mb u-component anomalies for the (a) straight-moving composite, (b) recurving-south composite, (c) recurving-north composite, and (d) composite of inactive periods. The dotted lines represent plus/minus one standard deviation from the mean profile.

periods. These composites were based on tropical cyclone tracks and inactive periods during 1979-82. The strength of the relationships defined by the composite analysis is examined by using the composite circulation patterns to predict the track type of tropical cyclones occurring during 1983-85, which is an independent data set. Track-type predictions are based upon latitudinal profiles of the 700 mb u components defined in Fig. 7. A distance measure between the actual profile and a composite profile is computed by summing the absolute differences between profiles over all latitude bands. The track-type prediction is simply the composite profile with the smallest absolute distance measure to the actual profile at the genesis time of a developing tropical cyclone. If the inactive composite profile is the best match, then a prediction of recurving-north is made, assuming that an external mechanism (i.e. TUTT ) could have forced genesis during an otherwise inactive period.

Fourteen of the 18 straight-moving storms and 20 of the 25 recurving storms are correctly predicted (Table 1). A prediction of straight-moving is made 19 times and 14 are correct, and a prediction of recurve is made 24 times and 20 are correct. A hypothesis test using the chi-square criteria (Freund 1971) is applied to Table 1 to determine if there is a relationship between the predicted and observed track types. The test statistic computed from Table 1 is 14.2, which exceeds the chi-square value at the 0.01 significance value with one degree of freedom. Therefore, the null hypothesis that no relationship exists between the observed and predicted track types could not be accepted. A chi-square test of the relationship between observed tracks and predicted track from the climatological data in Fig. 2 results in an acceptance of the hypothesis that there is no relationship between the climatologically predicted and observed tracks.

**TABLE 1** PREDICTIONS OF 1983-1985 TROPICAL CYCLONES. Predictions are based on 700 mb zonal wind anomalies at the time of genesis. The numbers of observations in each cell that would be expected if there was no relationship between predicted and observed track types are given in parentheses.

| | | OBSERVED | |
|---|---|---|---|
| | | Straight | Recurve |
| PREDICTED | Straight | 14(7.9) | 5(11.0) |
| | Recurve | 4(10.0) | 20(13.9) |

## C. DISCUSSION

The discussion in Section B clearly indicates that the four large-scale circulation anomaly patterns are identified with specific track types or inactive periods. Each of the anomalous circulations is characterized by an index constructed from the anomalous zonal wind averaged between 100°-140°E and the equator and 30°N in 5° lat. bands (Fig. 7). Although this index is based on anomalous circulation patterns defined during the initial 24 h of tropical cyclones having each track type, or for inactive periods, it may be computed from any 700 mb anomalous circulation pattern to describe the variability of the large-scale circulation over the tropical WPAC. The index was computed each 12 h for the 700 mb anomaly pattern during 1979-1987 whether or not a tropical cyclone existed. Therefore, each anomaly map is classified into one of four patterns, SM, RS, RN, or inactive.

### 1. Persistence of Anomaly Patterns

The variation of this index (Fig. 8) suggests the existence of a rather pronounced low-frequency component in the variability of large-scale circulation anomalies that are related to tropical cyclone track types and inactive periods. The average duration of

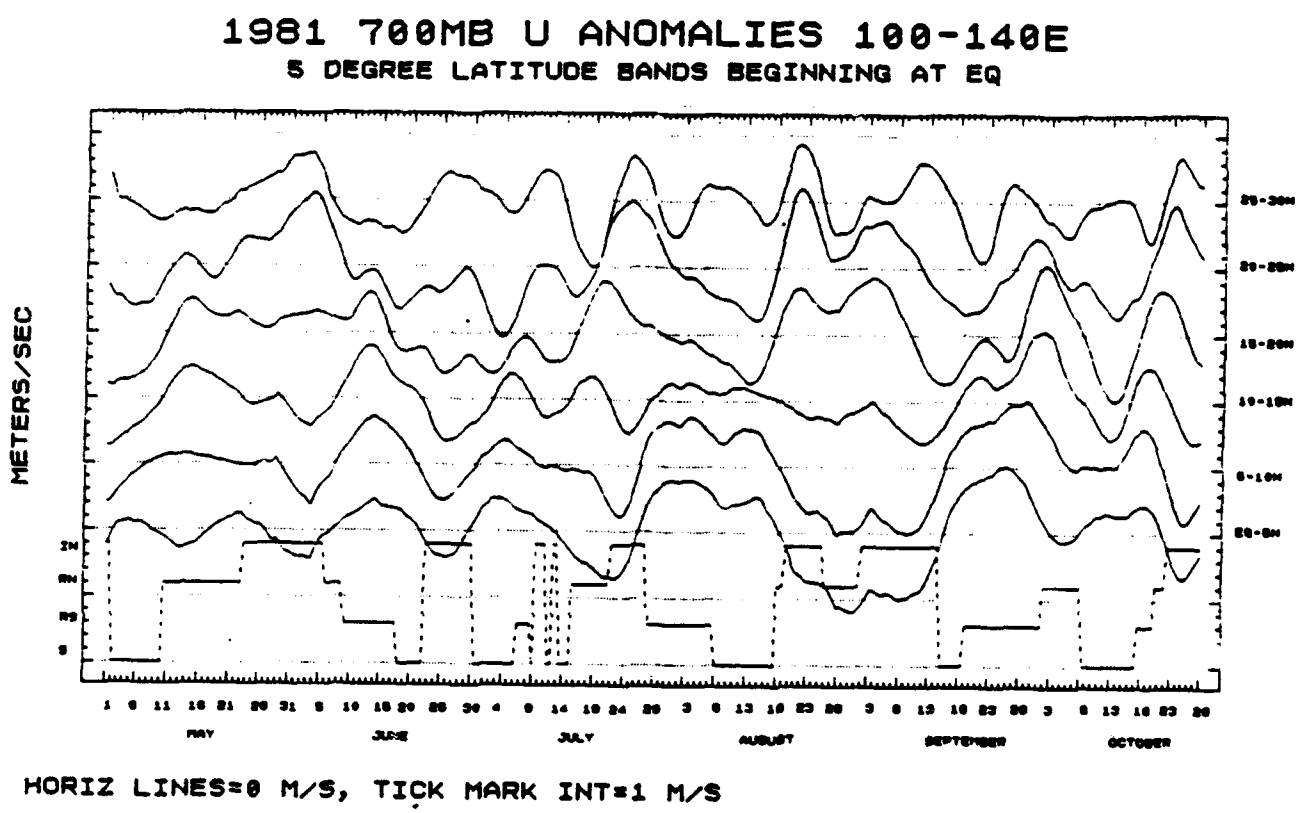


**Fig. 8** Time series of 700 mb u-component anomalies averaged from 100°-140°E in 5° lat. bands during 1981. The bottom dotted line represents the classification of the circulation pattern based upon the latitudinal profile of the zonal wind anomalies.

the anomaly patterns is provided in Table 2. The persistence of the anomaly pattern related to inactive periods is slightly longer than those associated with each track type, which are nearly equal. This is probably due to the definition of the inactive periods, which had to persist for at least 5 days.

TABLE 2 AVERAGE PERSISTENCE TIME FOR EACH TRACK-TYPE PATTERN

| PATTERN TYPE | AVERAGE DURATION(DAYS) | STD. DEVIATION(DAYS) |
|---|---|---|
| Straight | 6.1 | 3.2 |
| Recurve-south | 5.7 | 4.5 |
| Recurve-north | 5.0 | 3.0 |
| Inactive | 9.3 | 3.8 |

In Chapter I, the relationship between persistent events and the potential for extended-range prediction was discussed. Since specific tropical cyclone track characteristics (i.e., track types, inactivity) are associated with certain large-scale flow patterns, it is important to examine the persistence characteristics of the patterns to best use that information to provide extended-range forecasts of tropical cyclone characteristics. This has been the approach taken with respect to persistent anomalies and long-range prediction of midlatitude flows (Dole and Gordon 1983; Legras and Ghil 1985). In those studies, the duration of anomalous flow patterns (i.e., blocking, zonal flow) were investigated to determine if they were different from a first-order autoregressive process, which has often been used to model typical atmospheric variability (Leith 1973; Moritz and Sutera 1981). These two midlatitude anomalous flow patterns had different persistence properties from each other and from a typical autoregressive model.

The large-scale anomaly patterns defined for the tropical cyclone track types and inactive periods may also be categorized into two basic types of anomalous flow based upon the sense of the zonal wind anomalies over the near-equatorial latitudes. Straight-mover and recurve-south anomaly patterns are classified as "westerly" because they contain westerly zonal wind anomalies between the equator and 10°N. The recurve-north and inactive composites are classified as "easterly" since they contain easterly anomalies over the same region.

The durations of these westerly and easterly patterns are presented in Fig. 9 on a log-linear plot. For a first-order linear autoregressive process, the local slope is proportional to the probability that the run will continue (Legras and Ghil 1985). Shallow slopes indicate a higher probability of continuation than steep slopes. Several of the persistence properties of the anomalous tropical circulations related to tropical cyclone characteristics are similar to the properties of midlatitude flow anomalies. Persistent westerly or easterly sequences are not equal in length since the number of events decreases as the duration increases. However, the reduction in event lengths does not exactly follow a straight line as would occur if the variability followed a first-order autoregressive process (Dole and Gordon 1983). No preferred durations of persistent events are indicated since no pronounced plateaus are found in either the easterly or westerly curve.

The statistics pertaining to the persistence of easterly events are different from the persistence of westerly events. Prior to 17 days, westerly patterns tend to persist longer. After 17 days, easterly events persist longer. Each curve has some changes in slope. The slope of the westerly curve is nearly constant to 17 days and then becomes more steep.

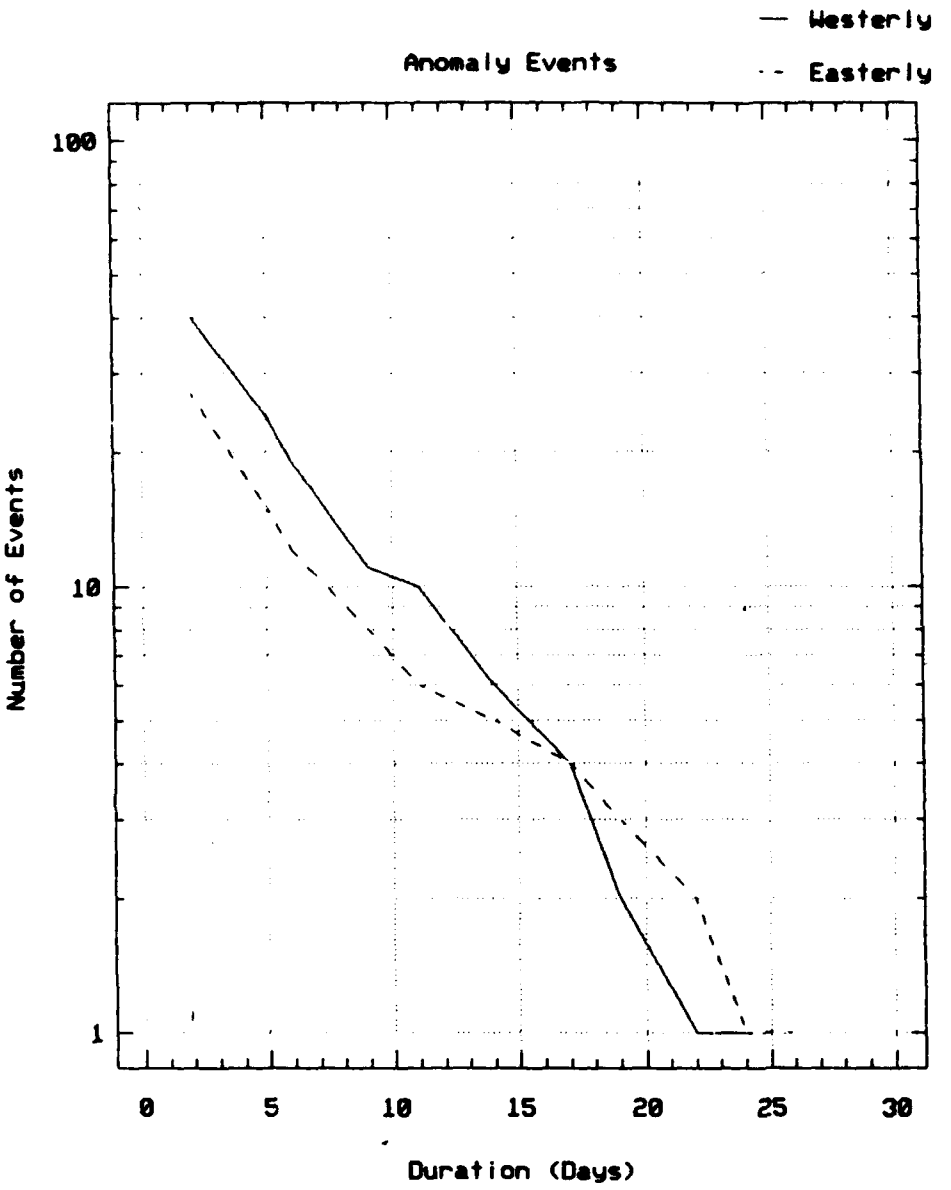


**Fig. 9** The duration of westerly and easterly large-scale 700 mb anomaly patterns.

Therefore, the near-constant slope prior to 17 days for the westerly events indicates a near constant probability of continuation. Beyond 17 days, the probability decreases that a westerly anomaly pattern will persist. The slope of the easterly curve is nearly constant up to 10 days, it then becomes more shallow, and finally the slope becomes more steep at 22 days. Comparison of the slopes of the two curves between 10 and 22 days indicates that an easterly anomaly pattern has a greater probability of continuing than a westerly pattern does within this time range.

### 2. Transitions Between Anomaly Patterns

The above analysis examines the persistence properties of large-scale circulation anomalies associated with tropical cyclone tracks and inactive periods as defined by the anomalous zonal wind index. These properties may be utilized to partition the time variability of the zonal wind index into periods when one particular anomaly pattern is persistent, or transient periods when no anomaly pattern is dominant in terms of persistence. If a particular anomaly pattern persists for a length of time that is at least equal to its average duration plus one standard deviation (Table 2), then it is considered a persistent period. Anomaly patterns that span periods of time less than the average are classified as transient periods. Furthermore, transient periods are classified as either westerly (transient-west, TR-W) or easterly (transient-east, TR-E) based on the direction of the anomalous zonal winds between the equator and 10°N. These two anomaly classifications are added to the four classes based on tropical cyclone characteristics and inactive periods.

It is also possible to use the strength of a particular anomaly pattern, defined as the relative magnitude of the index value compared to the values for all other patterns, to define periods when the circulation anomalies are not well defined. These small magnitude anomaly periods may or may not be persistent and perhaps should not be classified into one of the six anomaly patterns. Because of the relatively short data period, all periods are classified regardless of the strength of the anomaly pattern.

If $T_{i,j}$ equals the number of transitions between class i and j, and $n_i$ equals the total number of periods in class i, then the empirical probability of a transition between class i and j is $p_{i,j}= T_{i,j}/n_i$. The significance of transitions between classes may be assessed assuming an equal probability model of transitions from one regime to the other five regimes. That is, the transition probability between class i and class j is assumed to be $p_{i,j}=p=1/(N-1)$, where N equals the total number of classes. The expected number of transitions between class i and j is then $e_i=n_i p_{i,j}$, and the standard deviation is $s_i = p(1-p)^{1/2}$.

A transition path from class i to class j is then defined to be significant if $T_{i,j} > e_i + 1.5(s_i)$. The resulting significant transition paths are shown in Fig. 10. The four large-scale circulation anomaly patterns associated with tropical cyclone track types and inactive periods are shown outside the transient west and east classes. No significant transitions are found directly between the four persistent anomaly classes. All transitions from these classes proceed either to the west or east transient classifications where transitions between the east and west transient classes occur. The only direct transition leading from a transient class to the one of the four persistent classes occurs between the transient-east and inactive classes. An appealing physical characteristic of the transition diagram is that persistent periods of

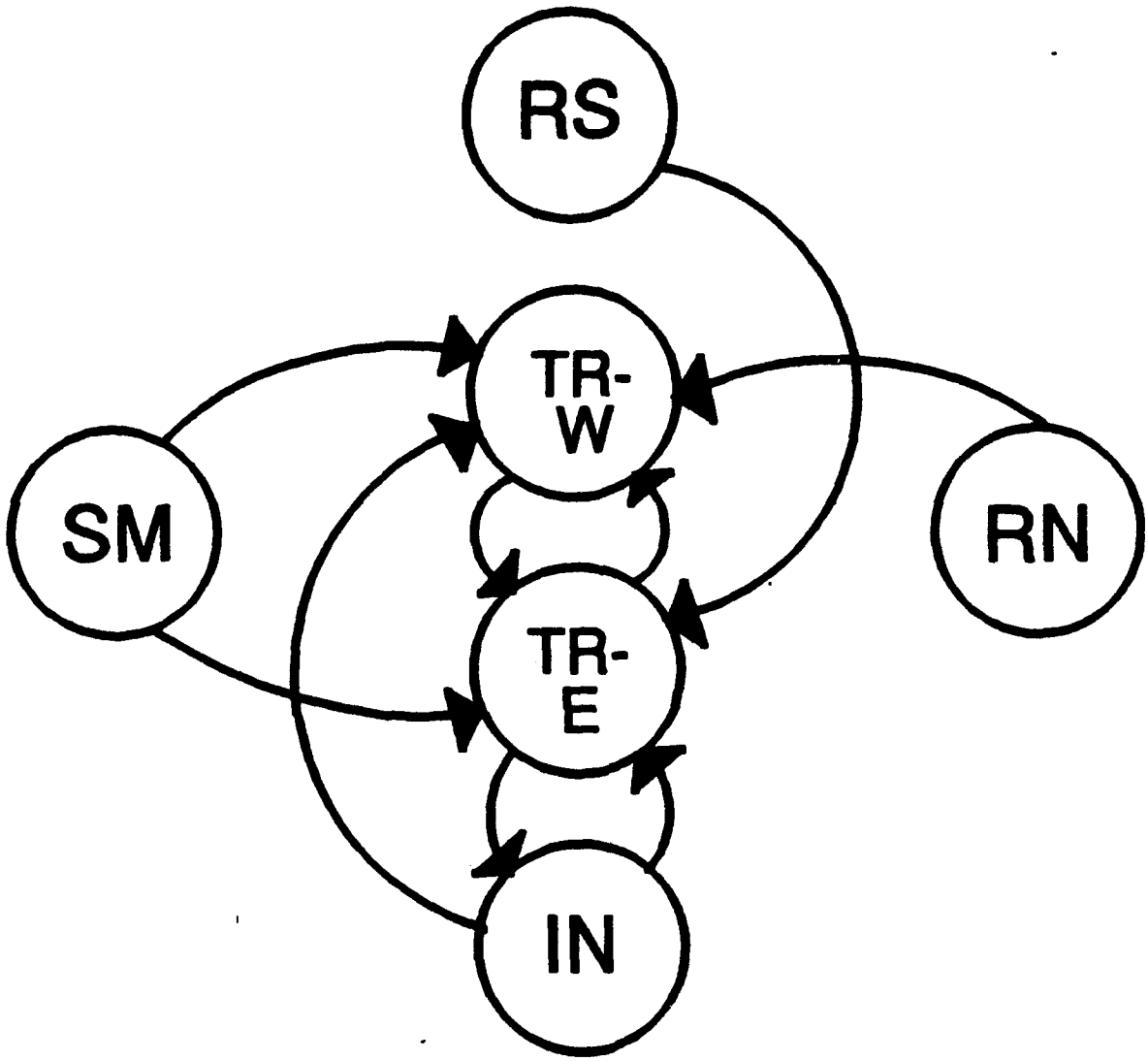


**Fig. 10** Significant transition paths between persistent and transient large-scale 700 mb anomalous circulation patterns.

anomalous large-scale circulations are followed by periods of transient patterns that may eventually lead to other persistent periods.

From an extended-range forecasting point of view, the utility of this type of a diagram initially seems limited. However, closer examination does reveal some symmetries to the significant transition paths. For instance, significant transitions from the recurve-south (inactive) class lead to the transient-east(transient-west) class, which signifies a major circulation change from a westerly (easterly) to an easterly (westerly) class. Similarly, significant transitions exist between the straight-moving (recurve-north) and transient-east (transient-west) classes. Furthermore, the recurve-south and recurve-north patterns only have significant transitions to a single transient class, whereas straight-movers and inactive patterns can transition to either westerly or easterly transient patterns. The recurve-south and inactive classifications are dominated by the largest zonal wind anomalies along the equatorial latitudes between 100°-140°E (Figs. 4,6), while the straight-moving and recurve-north classifications are dominated by anomalous subtropical circulations (Figs. 3,5). Therefore, these sets of transitions portrayed on opposite sides of the transition diagram may describe different physical controls on the anomalous large-scale circulation variability.

The significance criterion was reduced to $T_{i,j} = e_i + 0.75(s_i)$ to identify the preferred transition paths in greater detail (Fig. 11). Now significant transitions occur from the straight-moving class to the recurve-south class, and from the recurve-north class to the inactive class. Even with the addition of several transition paths, the symmetric quality of the transition diagram is preserved. Exits from the transient classes are more clear with the addition of transition paths that lead from the transient-east (transient-west) class to the

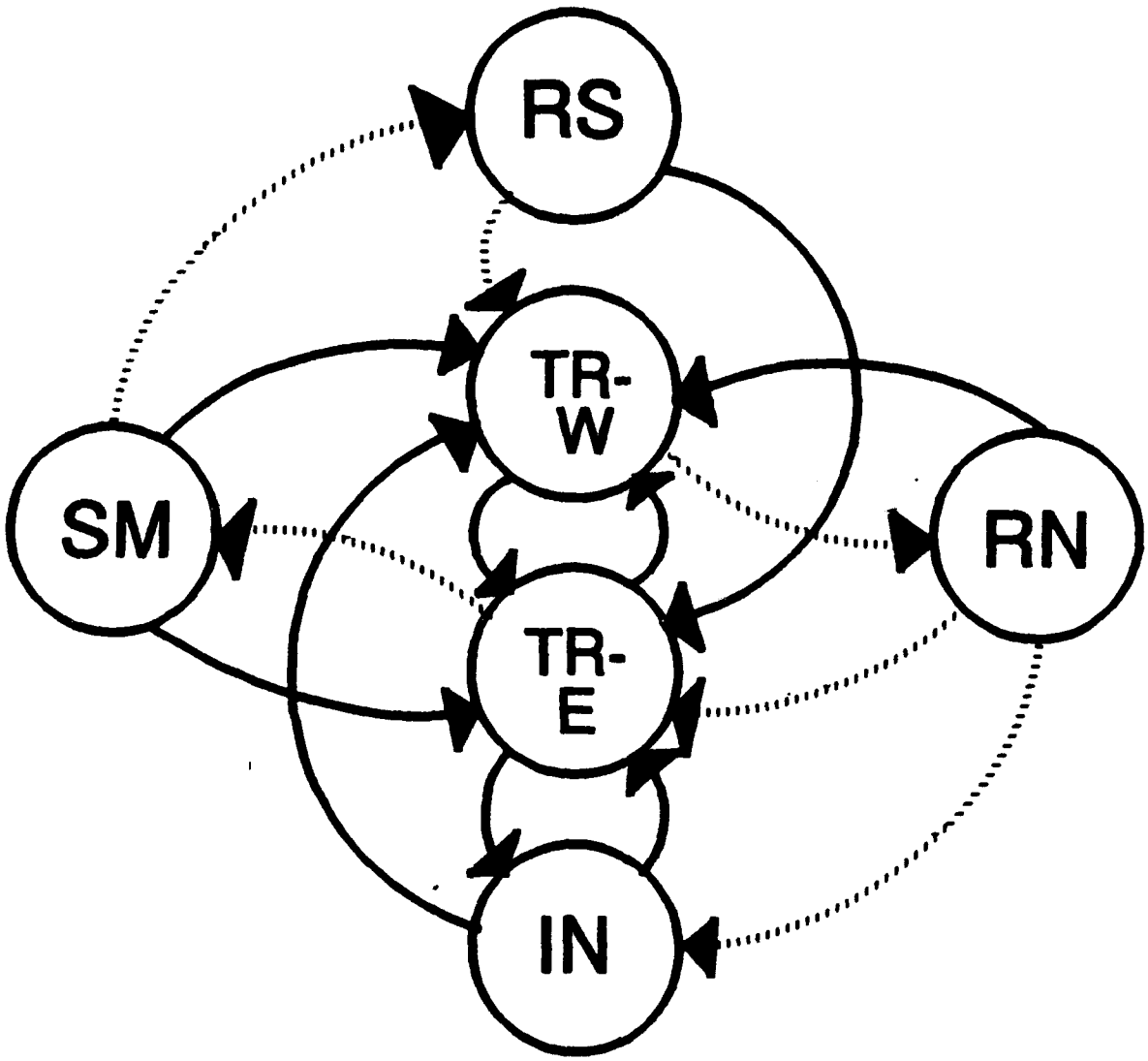


**Fig. 11.** As in Fig. 10, except that the criterion of significance has been relaxed, which yields additional significant transition paths (dotted).

straight-moving(recurve-north) class. However, no direct significant transitions are found from the transient classes to the recurve-south class.

## D. SUMMARY

Ideally, identifying the association between tropical circulation components such as those described in Chapter I with the establishment, maintenance and transition of the large-scale circulation anomalies influencing tropical cyclone will improve our understanding of the large-scale controls on tropical cyclone motion. Although the basic prediction scheme of Harr and Elsberry (1991) that uses the zonal wind index to forecast track type is quite successful, the description of the state of the large-scale circulation by the zonal wind index does not provide much detail concerning the evolution of the large-scale circulation patterns (Figs. 10,11). This may be because the index that is used to describe the classification of anomalous tropical circulations was based on tropical cyclone track types, but computed for all times whether or not a tropical cyclone exists. Furthermore, because the index is based on the anomalous circulations over a relatively small region of the tropical WPAC, it may be overly sensitive to the presence of tropical cyclones within the region used to compute the index. In these cases, the index would not provide an accurate description of the large-scale anomalous circulation.

The discussion in Chapter I suggested that the best hope for long-range prediction of tropical cyclone characteristics or activity is that the large-scale flow patterns associated with th. :haracteristics can be placed into a few identifiable classes and that they are somewhat persistent. The results of this preliminary study indicate that these criteria are

satisfied. However, the potential success of any extended-range predictions is also dependent upon identification of the physical relationships connected to the flow classifications and the transitions between them. Therefore, the goal is to identify more general classifications of the anomalous large-scale tropical circulations that are not directly based on tropical cyclone characteristics, and compare them to the classifications defined in this preliminary study. Generalized classifications would identify the association between large-scale variability observed in tropical cyclone characteristics with the basic modes of the tropical circulation variability.

# III. VARIABILITY OF THE LARGE-SCALE CIRCULATION ANOMALIES OVER THE TROPICAL WESTERN NORTH PACIFIC

In Chapter II, an index based on the latitudinal variation of the anomalous zonal wind between 100°-140°E was used to classify twice-daily anomaly maps into one of a set of large-scale circulation patterns. Because these patterns were based upon tropical cyclone track characteristics and inactive periods, the index may not provide an accurate representation of the variability of the large-scale anomalous circulations. A more realistic measure may be obtained by first examining the basic structure of the variability of the large-scale anomalous circulations. If the structure of the basic modes of variability could be classified within several large-scale patterns, then a more general description of the large-scale circulation variability could be obtained. This description would have the intrinsic variability of the tropical WPAC circulation as its basis rather than tropical cyclone characteristics. However, one objective is to compare the large-scale circulation features related to tropical cyclone characteristics with the basic structures of the tropical WPAC large-scale circulation variability, and thereby identify the controlling factors of the large-scale circulation on tropical cyclone characteristics.

In this study, an empirical orthogonal function (EOF) analysis is used to define the coherent variability within the anomalous large-scale tropical WPAC circulation between 1979-1987. EOF analysis, which is an eigentechnique that is usually applied to a covariance matrix, has become an increasingly popular data analysis tool in meteorology since its introduction by Lorenz (1957) (e.g., see Richman 1986 and references therein). The

covariance matrix is computed from a data matrix that contains several realizations (i.e., time) of different observations (i.e., gridded data fields). A more detailed description of the EOF technique is provided in Appendix B.

A spatial-mode EOF analysis (Richman 1986) provides two main descriptions of the structure of variability within a large data set. Spatial patterns, defined as the eigenvectors of the covariance matrix and labeled EOFs, identify the distribution of "centers of action" where variability is concentrated. The patterns are constrained to be orthogonal to each other, and are arranged in decreasing order according to the amount of the total variance within the data set they explain. EOF analysis varies from the more universal technique of principal component analysis (Hotelling 1933) by the manner in which the resulting eigenvectors are scaled. Typically, the first few spatial patterns describe the larger-scale variability with successive patterns becoming more complicated as the amount of explained variance associated with them decreases. The eigenvalues associated with each eigenvector of the covariance matrix are used to define the total variance explained by each EOF. The relative partition of the variance in any one realization contained within the original data matrix is defined by coefficients associated with each spatial pattern. Time series of each coefficient describe the variability of the variance contribution of each spatial pattern over time.

Ideally, it would be desirable that each spatial pattern represent a physical characteristic that could be assigned a physical interpretation to explain that particular mode of variability. The time series of the coefficients assigned to each pattern could then be used to describe the variability of the physical trait. Physical interpretation of the spatial EOF

patterns requires careful consideration of several factors such as sampling errors (North et al. 1982) and rotations of the EOF axes (Richman 1986, 1987; Jolliffee 1987).

Initially, EOF analysis is applied to the anomalous zonal winds that were used to define the tropical cyclone-based anomalous circulation patterns. Direct comparison between variabilities associated with tropical cyclone characteristics and the basic modes of variability in the large-scale anomalous circulation can then be made. A second EOF analysis is applied to outgoing longwave radiation (OLR) data over the tropical Indian Ocean and WPAC regions, which is taken as a measure of the deep convection and precipitation in the tropics (Gruber and Krueger 1984). The goal of this analysis is to compare coherent variations between the large-scale convection patterns and the tropical cyclone-based anomalous circulation patterns. Finally, a vector EOF analysis is applied to the total anomalous wind field to provide a more complete description of the anomalous large-scale tropical circulation variability.

## A. EOF ANALYSIS OF THE ANOMALOUS ZONAL WINDS

Initially, an EOF analysis is applied to the anomalous zonal wind components at 700 mb from 1979-1987 computed from the FNOC GBA analysis described in Chapter II. The data coverage extends from 20°S-40°N and 60°-180°E. The EOF axes are rotated using the varimax criteria as described by Richman (1987). The EOFs are computed using only the zonal wind components to be consistent with the index used to describe the circulation variability in Chapter II. The variabilities described by the EOFs of zonal wind may then be directly compared with the circulation anomalies based on the tropical cyclone characteristics.

The first six spatial patterns (EOFs) are shown in Fig. 12. Interpretation of the EOFs is more dependent on the spatial patterns within each EOF since the sign associated with the pattern is arbitrary. For a particular time, whether the pattern contributes in a positive or negative sense to the total field variance is determined by the sign of the coefficient associated with the pattern at that time. The percentages of variance explained by each EOF and their standard deviations are given in Table 3. The standard deviations are estimated from the eigenvalues using the method from North et al. (1982) as

$$\frac{\delta\lambda}{\lambda} = [2/N]^{1/2},$$

where $\delta\lambda$ is the standard deviation for eigenvalue $\lambda$, and N is the number of independent samples. Although the total number of data samples is 9(years) times 306(twice-daily analyses during June-October), the value of N is conservatively assigned to be 120. This value assumes a decorrelation time of approximately 15 days which is twice as long as the decorrelation time estimated for midlatitude atmospheric variability (Leith 1973).

**TABLE 3** PERCENT OF THE TOTAL VARIANCE EXPLAINED BY EACH EOF. The standard deviation is computed from the estimated error associated with each eigenvalue.

| EOF NUMBER | PERCENT VARIANCE | STD. DEVIATION |
|---|---|---|
| 1 | 10.2 | 1.1 |
| 2 | 7.5 | 1.0 |
| 3 | 6.2 | 0.5 |
| 4 | 5.4 | 0.4 |
| 5 | 4.2 | 0.4 |
| 6 | 2.9 | 0.3 |

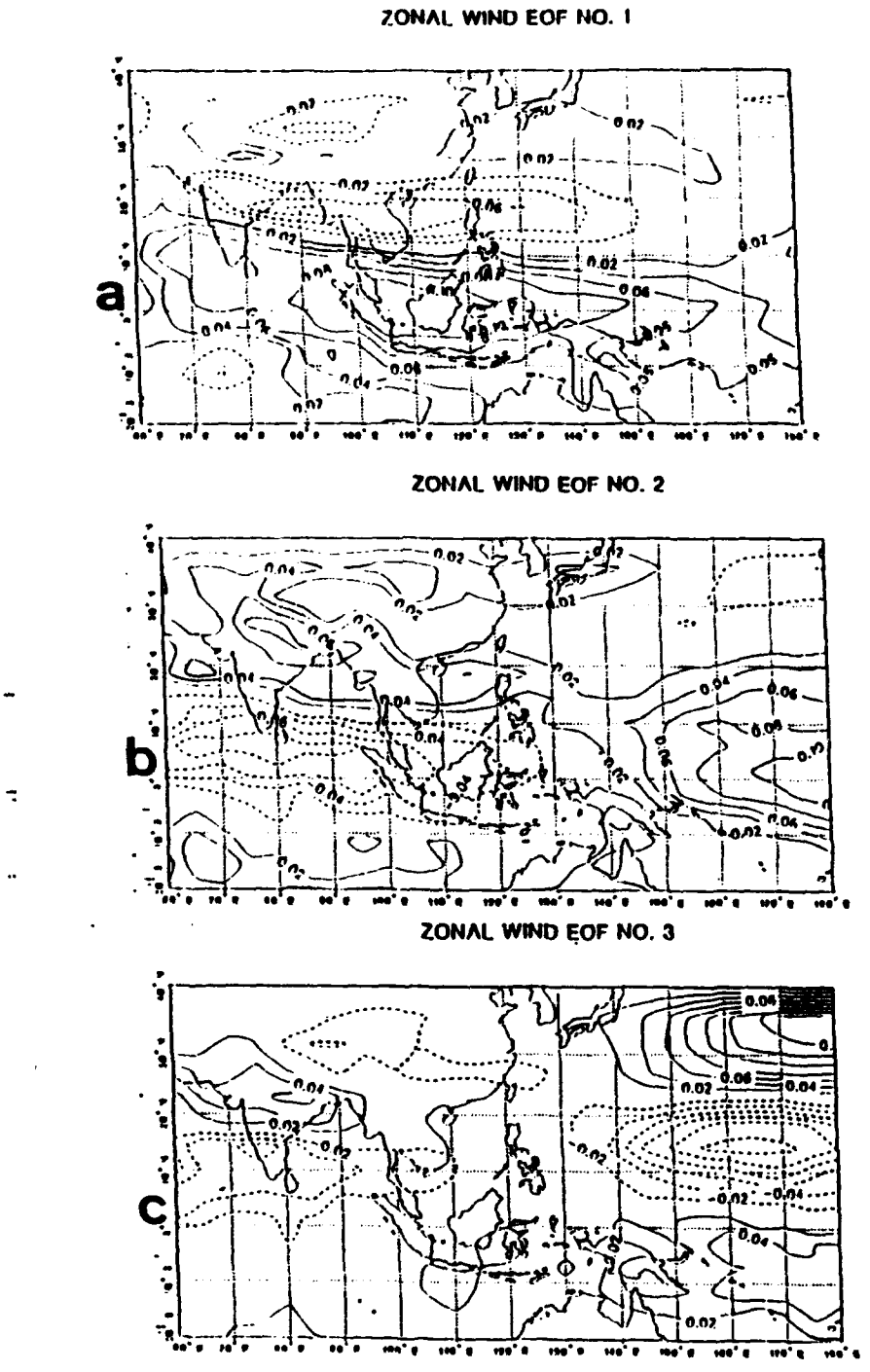


**Fig. 12(a)-(c)** Spatial structures of the first three EOFs based upon the 700 mb zonal wind anomalies. Units are nondimensional.

ZONAL WIND EOF NO. 4

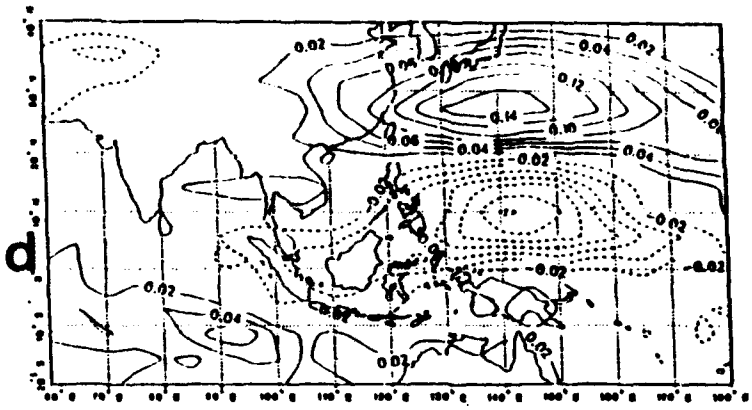


ZONAL WIND EOF NO. 5

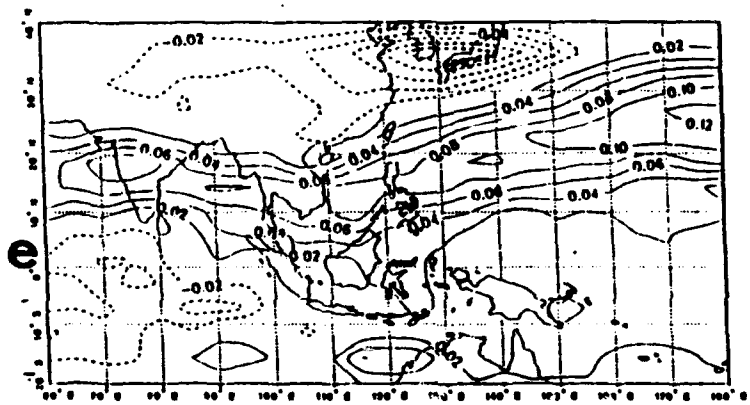


ZONAL WIND EOF NO. 6

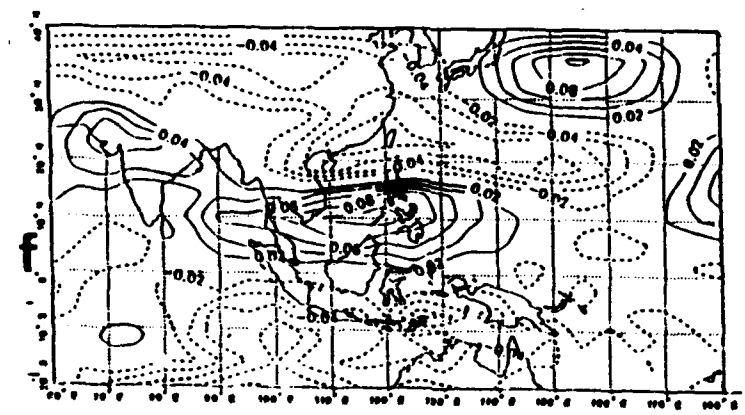


**Fig. 12(d)-(f)** As in Fig. 12(a)-(c), except for the fourth through sixth EOFs.

The first six EOFs explain 36.4% of the total variance. The standard deviations indicate that the eigenvalues are sufficiently separated so the expansion does not suffer from sampling errors (North et al. 1982). The slow rate of convergence of the EOF expansion is due to the size of the analysis domain, which includes a large midlatitude area in which the zonal wind is much more variable than over the tropical WPAC.

With a positive sign, EOF number 1 in Fig. 12a represents an anomalous large-scale zonal wind pattern that contains westerlies (positive zonal wind) over equatorial latitudes between 70°E and 160°E. The maximum westerly anomalies are centered on the equator between 100°E and 130°E. Over the same longitudinal area, easterly anomalies (negative zonal wind) are concentrated to the north between 10°N and 25°N. A band of weak westerly anomalies is centered on 30°N between 120°E and 160°E. In a positive (negative) sense, this pattern represents anomalous cyclonic (anticyclonic) shear over the monsoon trough region and a slightly enhanced (weakened) subtropical ridge over the East China Sea.

The second EOF pattern (Fig. 12b) also describes anomalous zonal winds between the equator and 10°N, but they are concentrated over the Indian Ocean and in an opposite sense to the pattern in EOF 1. Furthermore, the subtropical pattern is not well-defined in EOF 2. The second EOF does describe the variability over the equatorial latitudes in the central Pacific. In a positive sense, the second EOF pattern describes anomalous 700 mb easterlies to the west of 130°E and anomalous westerlies to the east of 140°E. Therefore, there would be anomalous 700 mb divergence over the equatorial WPAC. Opposite conditions would be described by the negative sense of EOF 2, and would be associated with anomalous 700 mb convergence over the region.

The third EOF pattern (Fig. 12c) is dominated by anomalous zonal winds over the subtropical latitudes between 140°E and 180°E. In a positive (negative) manner, this pattern describes an anomalous anticyclonic (cyclonic) circulation over this region. Therefore, the third EOF is associated with variability of the eastern portion of the subtropical ridge. A weak zonal anomaly pattern over India is also described by EOF 3. In a positive (negative) sense, anomalous anticyclonic (cyclonic) circulations would exist over India.

The fourth EOF pattern (Fig. 12d) describes the variability of the western Pacific portion of the subtropical ridge. A positive (negative) sign of EOF 4 is identified with an enhanced (weakened) ridge. A connection between zonal wind anomalies over Indonesia and anomalies over the Philippine Sea is indicated by the variability along the southern portion of the subtropical ridge.

The fifth EOF (Fig. 12e) also describes a connection between zonal wind anomalies over Indonesia and the Indian Ocean with anomalies over the subtropical regions of the WPAC. However, this band of anomalous zonal winds is located farther north with a pronounced southwest to northeast orientation that reaches to the dateline.

A positive sign of the sixth EOF pattern (Fig. 12f) indicates westerly anomalies that extend from the Indian subcontinent to the South China Sea and Philippine Sea along 10°N. Easterly anomalies are oriented east-west between 20°-30°N over the East China Sea. Westerly anomalies occur along 35°N just to the east of Japan. This type of anomaly pattern represents an enhanced monsoon trough (anomalous cyclonic shear) that is also shifted northward and oriented west to east over the tropical WPAC. The couplet of positive and negative anomaly

centers over the subtropical latitudes between 140°-170°E indicates an anomalous anticyclonic circulation that is farther north than the typical position of the subtropical ridge. The negative sense of the EOF 6 pattern describes a weak monsoon trough (anomalous anticyclonic circulation) and a weakened subtropical ridge (cyclonic circulation).

The remainder of the EOF patterns are not discussed since the amount of total variance explained becomes rather small. The EOF analysis partitions the variability of the 700 mb anomalous large-scale circulation into distinct patterns that represent variations in the monsoon trough (EOFs 1 and 2), subtropical ridge (EOFs 3 and 4), and combinations of equatorial and subtropical anomalies (EOFs 4 and 5). This partition of the total variability is similar to the anomalous circulation patterns that were defined in Chapter II based on tropical cyclone track characteristics. The primary difference between the two sets of patterns is that the EOFs seem to represent large-scale features that link variability over the Indian Ocean with variability over the western and central Pacific. Although the primary anomaly centers in the patterns based on tropical cyclone characteristics are larger in scale than would be expected if they only represented tropical cyclone variability, they do not indicate as much association between the Indian Ocean, WPAC, or CPAC as in Fig. 12.

The relationships between the large-scale anomaly patterns that are based on tropical cyclone characteristics and the EOF patterns are investigated further by examining the time variability of the EOF patterns in relation to the transitions between the various tropical cyclone-based anomaly patterns that are defined by Fig. 10. The variability of the EOF patterns is defined by the coefficients (principal components or PC) associated with each spatial pattern. As in Chapter II, the transitions defined in Fig. 10 can be generalized

according to the sense of the zonal wind anomalies over the equatorial WPAC region. The SM, RS and TR-W patterns are classified as westerly, and the IN, RN and TR-E are easterly. Transitions from the four persistent patterns (SM, RS, RN, IN) will be classified as defined by Table 4. By definition, it is not possible for one pattern to transition to itself without first transitioning to another persistent or transient pattern.

Although Fig. 10 indicates only the significant transition paths, all possible transitions in Table 4 are utilized in this analysis. All transitions are determined by the classifications based on the anomalous zonal wind index.

**TABLE 4** DESTINATIONS OF TRANSITIONS FROM THE FOUR PERSISTENT TROPICAL CYCLONE-BASED ANOMALY PATTERNS. Anomaly patterns are classified according to the sign of the equatorial anomalies over the tropical WPAC.

| ANOMALY PATTERN | TRANSITION TO WEST | TRANSITION TO EAST |
|---|---|---|
| Straight-moving (SM) | Recurve-south<br>Transient-west | Recurve-north<br>Inactive<br>Transient-east |
| Recurve-south<br>(RS) | Straight-moving<br>Transient-west | Recurve-north<br>Inactive<br>Transient-east |
| Recurve-north<br>(RN) | Straight-moving<br>Recurve-south<br>Transient-west | Inactive<br>Transient-east |
| Inactive<br>(IN) | Straight-moving<br>Recurve-south<br>Transient-west | Recurve-north<br>Transient-east |

The time of transition from one pattern to another is defined to be when the value of the anomalous zonal wind indicates a classification change. Therefore, transitions are

considered to be instantaneous. The variability of each of the first six EOF patterns is identified for the 15 days prior to the transition time and the 5 days after the transition time. Fifteen days are chosen because the mean persistence time plus one standard deviation (Table 2) is less than 15 days for all track-type patterns. Furthermore, this allows identification of the variability of the EOF patterns during periods when the tropical cyclone-based pattern is persistent prior to the transition to another pattern. The variability of the EOF coefficients is discussed in relation to the physical descriptions applied above to each spatial pattern.

Based upon the EOF patterns described above, the variability of the monsoon trough is defined by the first and second principal components (PCs). Approximately five days prior to the transition of a SM pattern to another westerly pattern, the monsoon trough becomes more enhanced (positive PC 1, negative PC 2) (Figs. 13a,b). Variability of the eastern portion of the subtropical ridge is described by PC 3 (Fig. 12c), but this pattern has a very small amplitude and large standard deviations throughout the persistent and transition periods (Fig. 13c). During the persistent SM period prior to -5 days, the eastern portion of the subtropical ridge is enhanced. The variation in PC 4 (Fig. 13d) indicates that this portion of the ridge weakens as the transition approaches and then strengthens within the following westerly pattern. The amplitudes of PC 5 and PC 6 are centered near zero (Figs. 13e,f) with large standard deviations.

The amplitudes associated with the EOF patterns are larger during a SM to east transition (Fig. 14). The variabilities of PCs 1 and 2 indicate that cyclonic anomalies associated with the monsoon trough reach a maximum near -6 days, and then begin to change to anticyclonic at the transition time. The strength of the eastern portion of the subtropical

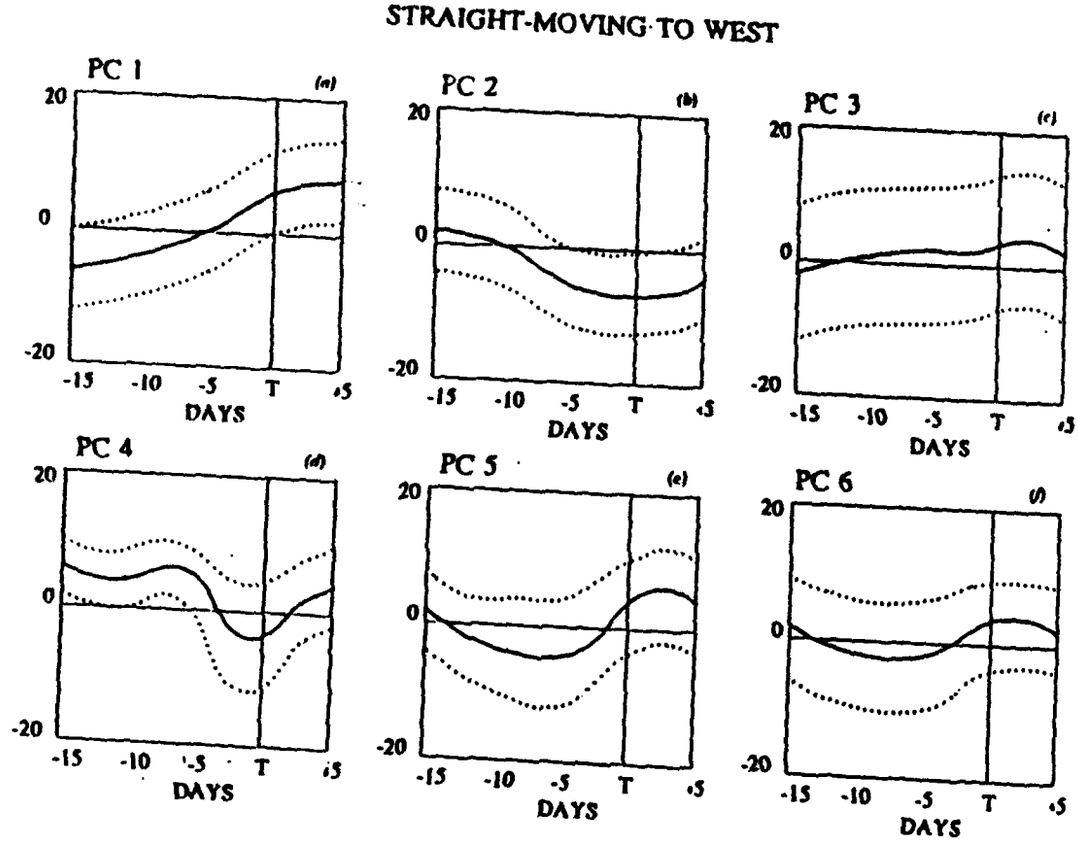


**Fig. 13** Variability of each of the leading six zonal wind EOF principal components related to the transition from the straight-moving tropical cyclone-based anomaly pattern to any westerly pattern. The abscissa defines the time (days) relative to the time of the transition, which is marked by the T. Principal component units are m $s^{-1}$. Dotted lines represent plus/minus one standard deviation.

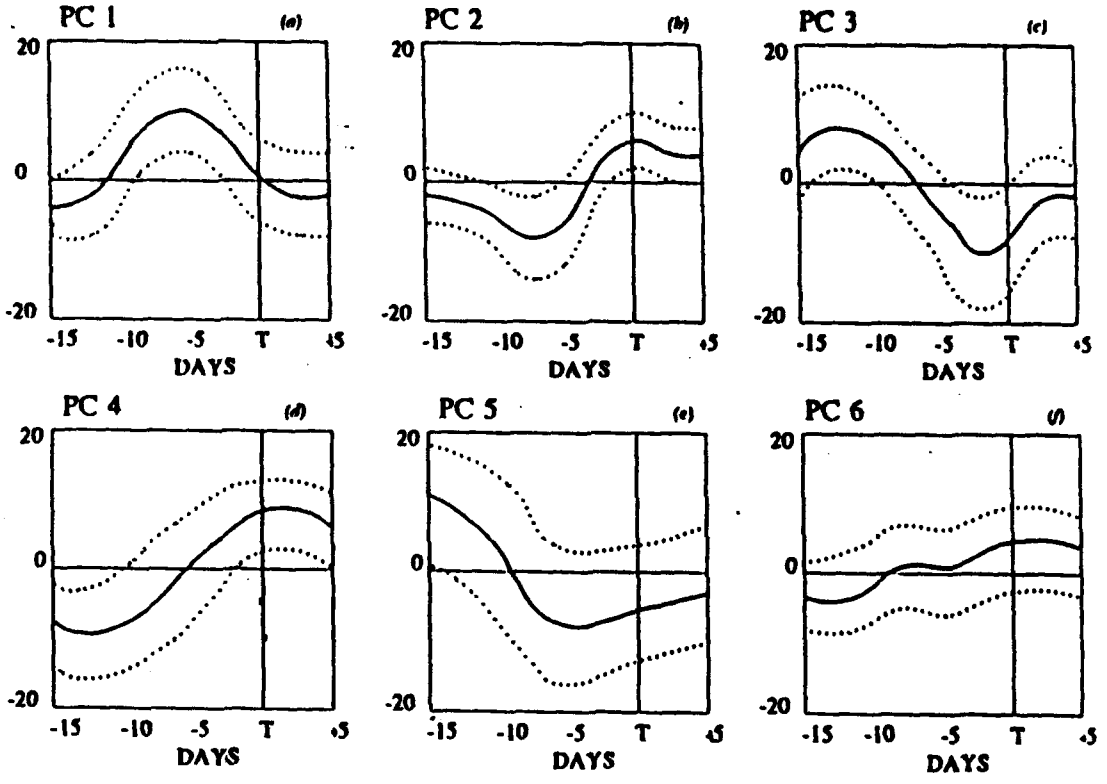


**Fig. 14** As in Fig. 13, except for transitions from a straight-moving tropical cyclone-based pattern to any east pattern.

ridge (described by PC 3) is amplified during the persistent SM period, and then weakens as the transition approaches. As the transition approaches, the western portion of the ridge strengthens (PC 4 positive). A negative EOF 4 pattern during -15 to -10 days is also associated with westerly anomalies over Indonesia (Fig. 12d), which would be consistent with the change in the monsoon trough indicated by PCs 1 and 2.

The RS to west transition is dominated by the large amplitude of the PC 1 coefficient (Fig. 15), which indicates an enhanced monsoon trough. The eastern portion of the subtropical ridge (PC 3) is stronger than normal until -11 days. The intensity of the western portion of the ridge fluctuates as the transition time approaches. After the transition, cyclonic anomalies dominate the eastern portion of ridge (PC 3 negative). The amplitudes of the remaining PCs are small except for PC 4 between -5 and -12 days. The large negative amplitudes indicate that the western portion of the ridge is weak which would be consistent with the occurrence of recurving tropical cyclones during the persistent portion of the RS pattern.

Similar to the SM to east transition, the largest cyclonic anomalies associated with the monsoon trough during the RS to east transition (PC 1, Fig. 16) occur between -15 and -10 days. A smooth change to anticyclonic anomalies occurs at the transition to an easterly pattern. Between -5 and -10 days, PC 4 and 6 indicate that weakening of the western portion of the subtropical ridge (PC 4 negative) is associated with a northward shift in the cyclonic anomalies identified with the enhanced monsoon trough (PC 6 positive). The PCs 4 and 6 coefficients reach their maximum values one day after the peak in the enhancement of the monsoon trough indicated by PC 1. The coefficients of PC 4 and 6 then tend to zero while

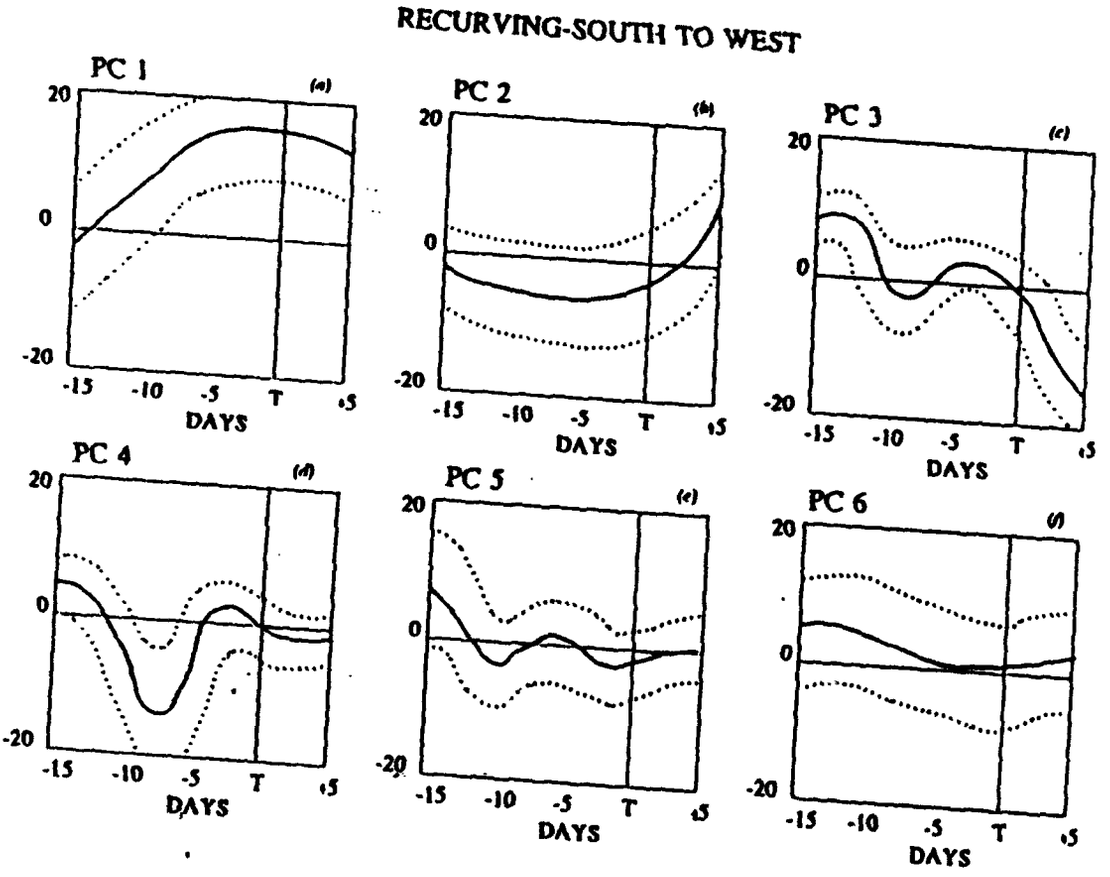


**Fig. 15** As in Fig. 13, except for transitions from a recurving-south tropical cyclone-based pattern to any other west pattern.

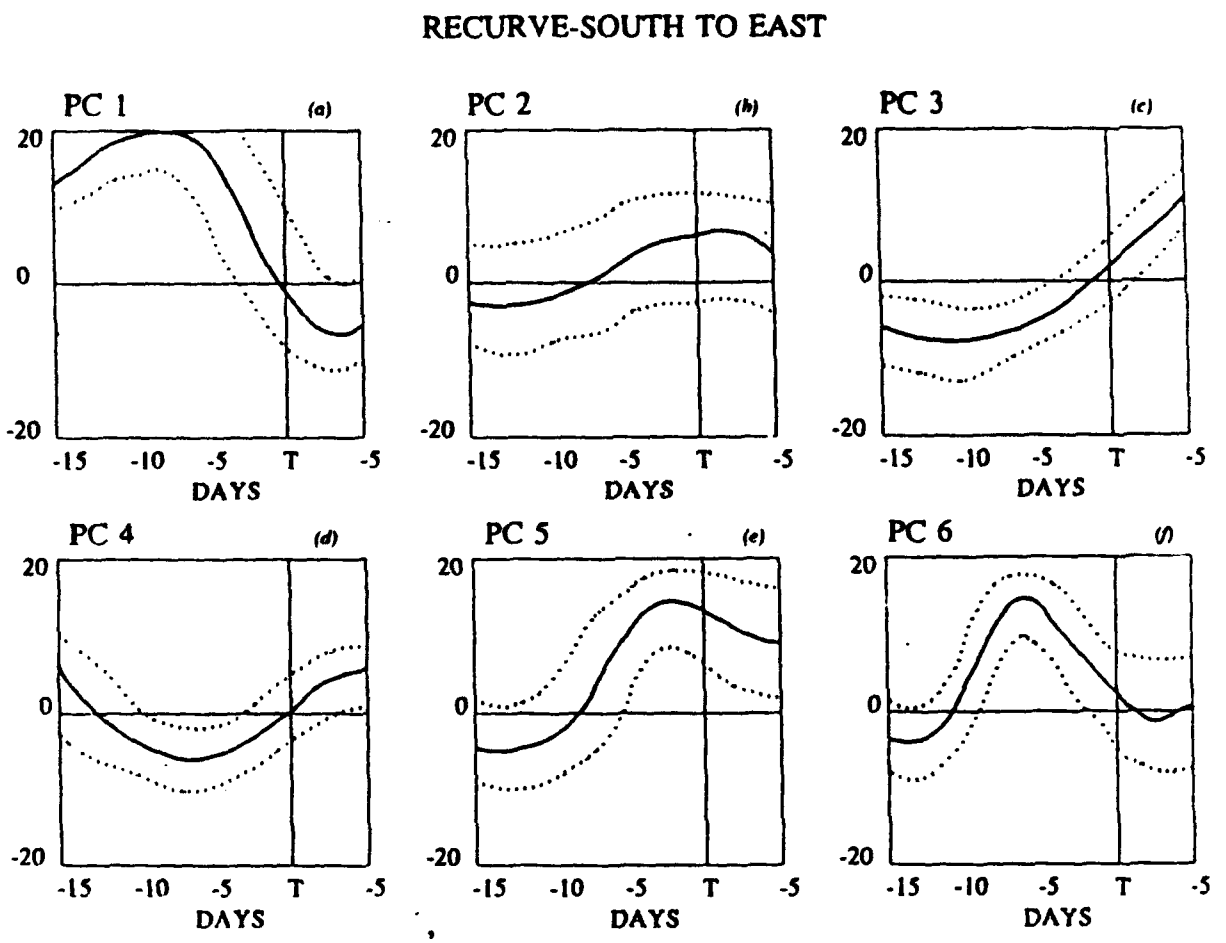


**Fig. 16** As in Fig. 13, except for transitions from a recurving-south tropical cyclone-based pattern to any east pattern.

the relative contribution to the total field variance by EOF 5 reaches a maximum. The combination of the variability in EOF patterns 1, 4, 5, and 6 suggest that the RS-east transition is characterized by a gradual northward shift in the westerly anomalies associated with the extremely strong monsoon trough.

The symmetry in relation to the transition diagrams (Figs. 10, 11) discussed in Chapter II also applies to the variability of the EOF coefficients. The PC variations during persistent easterly regimes are similar to those during westerly regimes described above, except with opposite signs. During a RN-east transition, a change from cyclonic to anticyclonic anomalies over the monsoon trough region occurs at -5 days (Fig. 17) during the persistent portion of the easterly RN pattern. All other PC coefficients are small except for negative values of PC 4 between -5 and -15 days, which indicate that the western portion of the subtropical ridge is weak.

All PC amplitudes are rather small during a RN-west transition (Fig. 18). An indication of a change from anticyclonic to cyclonic anomalies over the monsoon trough region ( PC 1) at the transition time is found.

During the persistent inactive pattern prior to a transition to another easterly pattern (Fig. 19), anticyclonic anomalies dominate the monsoon trough region (PC 1 negative, PC 2 positive). However, a change to opposite conditions occurs after the transition. This may be because the inactive pattern only transitions to a transient-east pattern, which may not be well defined. The values of PCs 3 and 4 indicate that both the eastern and western portions of the subtropical ridge are amplified during the persistent inactive pattern.

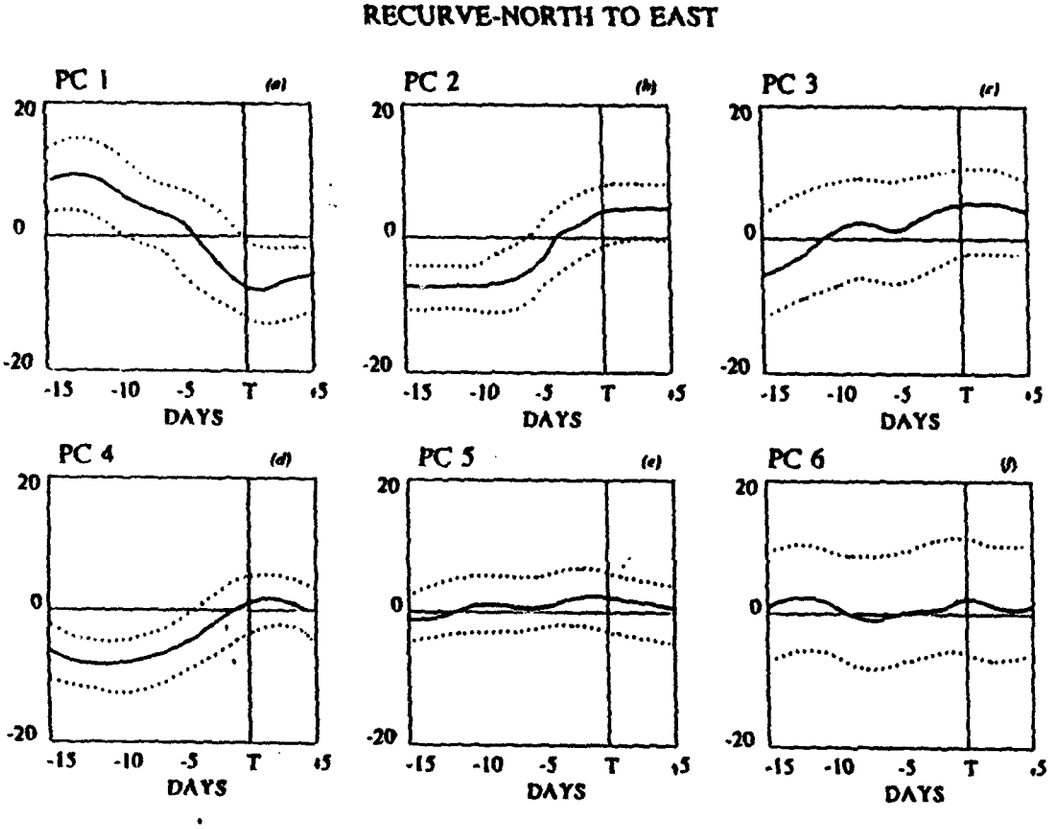


**Fig. 17** As in Fig. 13, except for transitions from a recurving-north tropical cyclone-based pattern to another east pattern.

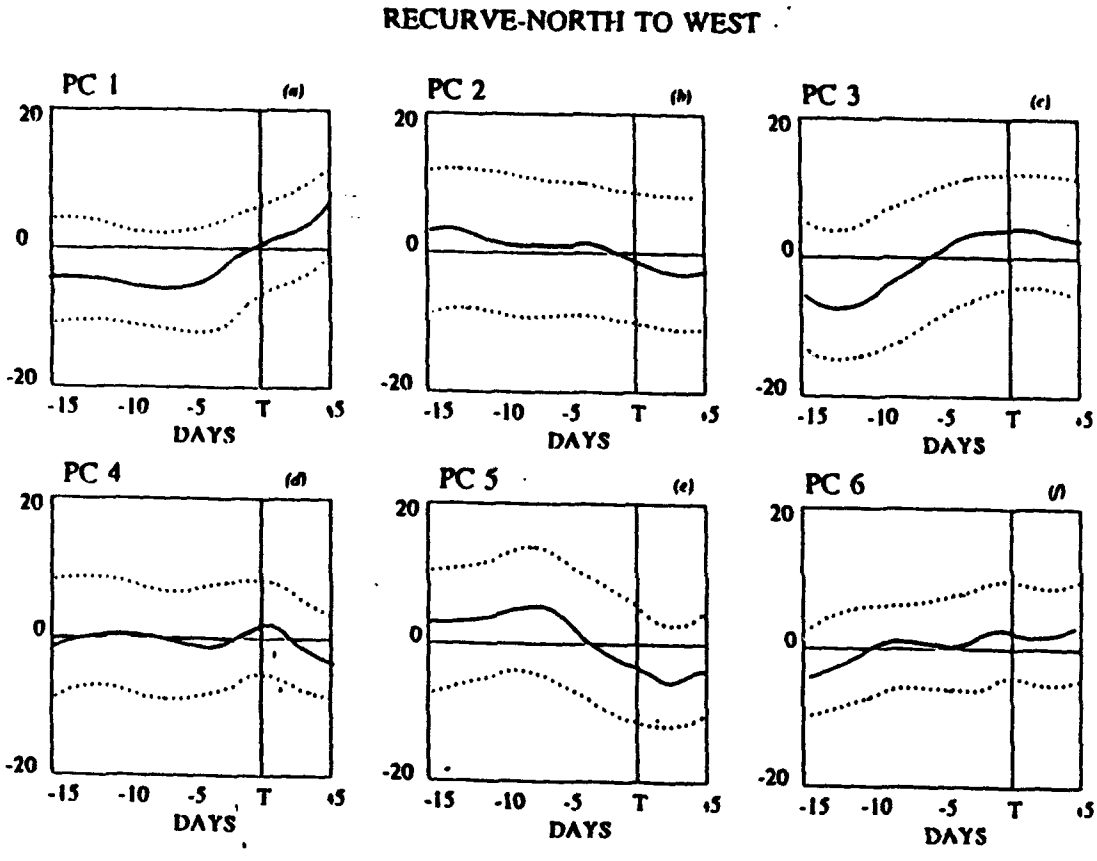


**Fig. 18** As in Fig. 13, except for transitions from a recurving-north tropical cyclone-based pattern to any west pattern.

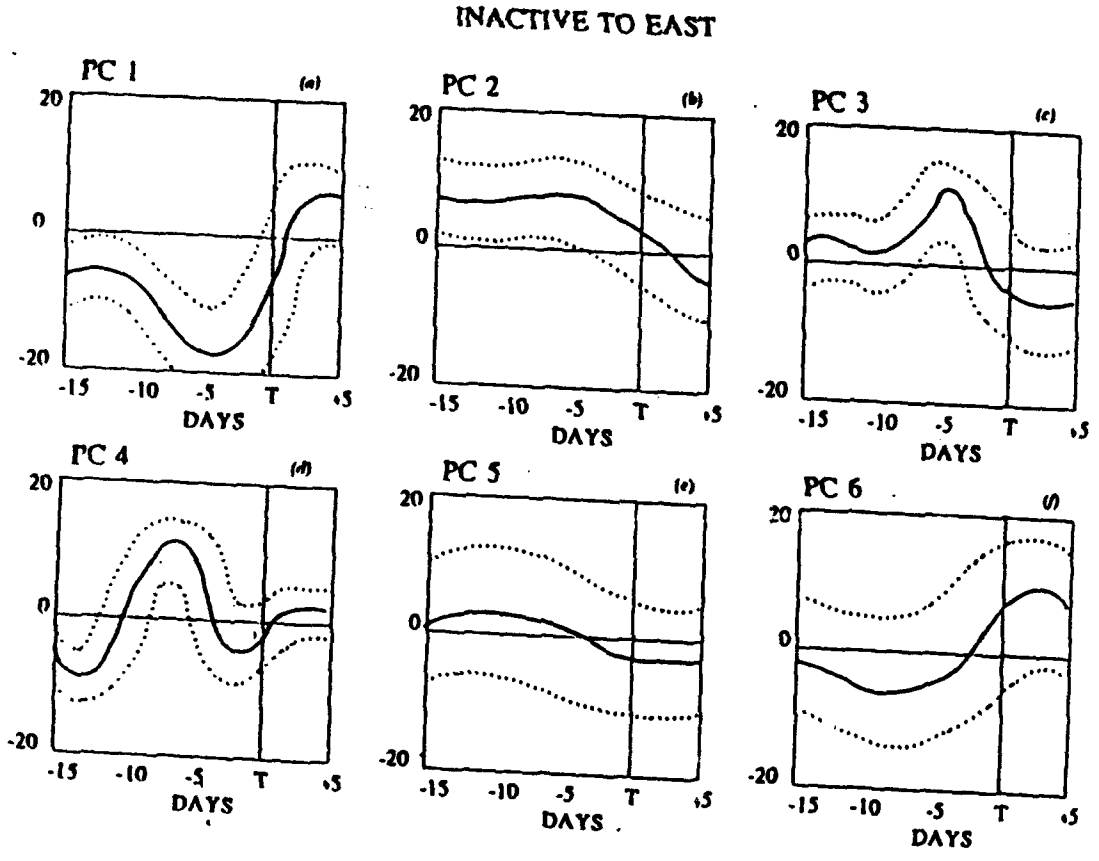


**Fig. 19** As in Fig. 13, except for transitions from an inactive tropical-cyclone based pattern to another east pattern.

The transition from a persistent inactive pattern to a west pattern is dominated by a change from anticyclonic anomalies to cyclonic anomalies over the monsoon trough region (Fig. 20). The anticyclonic anomalies reach a maximum at -9 days, and the transition to cyclonic anomalies occurs at day -3. During the transition, the eastern portion of the subtropical ridge is strengthened (PC 3 positive).

It may be concluded that the variability of anomalous large-scale circulations associated with tropical cyclone characteristics is related to the intrinsic variability of the large-scale tropical circulation defined by the EOF patterns. That is, the association of each EOF pattern with physical characteristics of the large-scale anomalous tropical WPAC circulation compares favorably with the anomalous circulation patterns based on tropical cyclone characteristics. Furthermore, the coherent variabilities associated with the EOF patterns during persistent and transition periods of the tropical cyclone-based patterns also indicate a strong association between the two sets. Because the EOF patterns describe variabilities that are larger scale than those based on tropical cyclone characteristics, the tropical cyclone-based patterns may be driven by the variations described by the EOFs.

The variabilities in EOF coefficients associated with transitions of the tropical cyclone-based patterns indicate the usefulness of the EOF patterns and coefficients for defining more general classifications of tropical circulation variability. Because these patterns and their variability are based only on the anomalous zonal wind component, they still may not provide a comprehensive description of tropical circulation variability. Although the zonal wind is a good indicator of large-scale circulation variability (Gutzler 1991), other synoptic-scale tropical circulations are identified by variations in the meridional wind (Lau and Lau 1990,

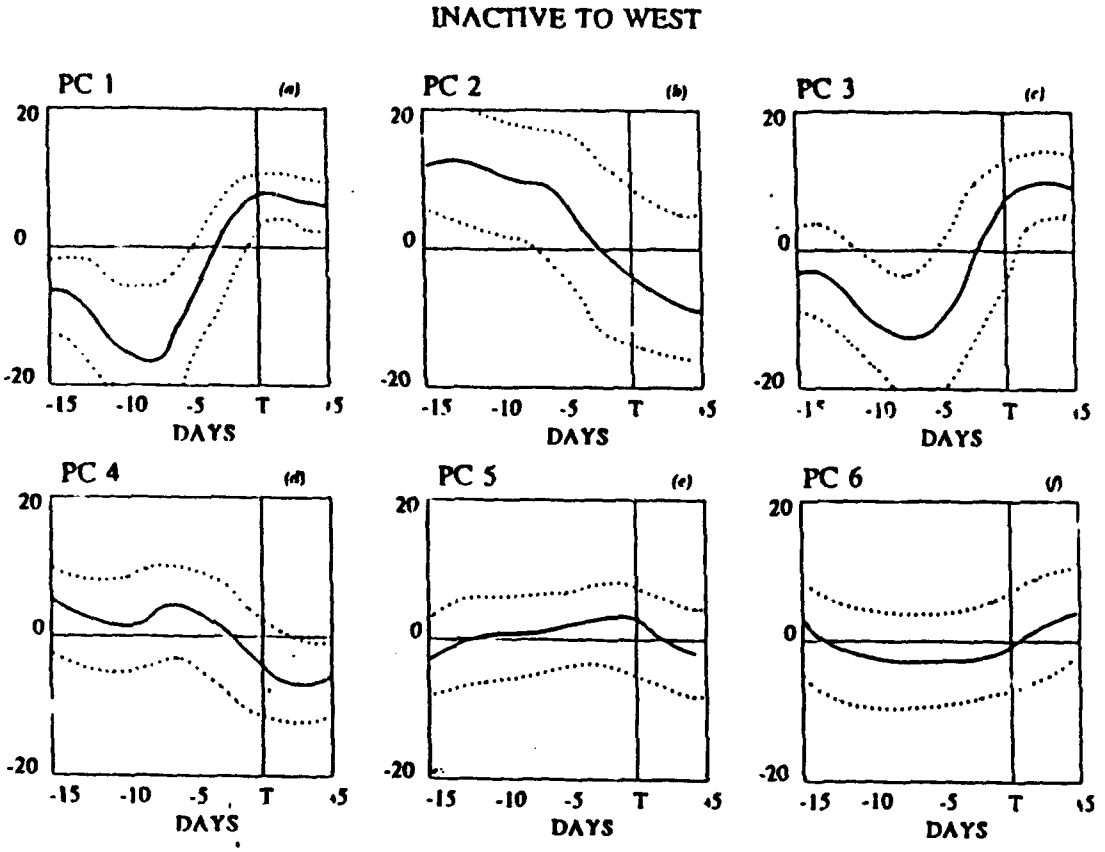


**Fig. 20** As in Fig. 13, except for transitions from an inactive tropical cyclone-based pattern to any west pattern.

1992; Liebmann and Hendon 1990). A more general description of the anomalous tropical circulations may be necessary to better classify the basic circulation variabilities. This aspect will be explored below by considering a vector EOF analysis that includes both wind components.

## B. EOF ANALYSIS OF ANOMALOUS OUTGOING LONGWAVE RADIATION

Although the above EOF patterns of the anomalous zonal wind components represent larger scale features, comparison with patterns based on tropical cyclone characteristics reveal a physically consistent relationship between the two sets. It would also be of interest to identify the relationship between the tropical cyclone-based large-scale anomalous circulation features and the variability of large-scale convection anomalies over the tropical Indian and western North Pacific Oceans.

The intensity of tropical convection is estimated by outgoing longwave radiation (OLR) data obtained from polar orbiting satellites (Gruber and Krueger 1984). Note that the original OLR data are placed on a 2.5° by 2.5° lat./long. grid so that it only describes large -scale convection features. These data are interpolated to the global-band grid between 60°E-180°E and 20°S-40°N, which is the same spatial domain used in the EOF analysis of the anomalous zonal wind data. The 12-h OLR data are averaged to provide one field per day centered on 00 UTC. Anomaly values are computed in the same manner as the wind data by subtracting a daily average computed for the June-October periods of 1979-1988. Negative OLR anomalies are associated with enhanced convection while positive anomalies are associated with reduced convection.

An EOF analysis is applied to the OLR anomalies, and the first five EOFs explain 25.2% of the total variance (Table 5). The relatively equal eigenvalues of EOFs 2 and 3 may be attributed to coupled physical characteristics, or to sampling errors. The proportionally larger decrease in the amount of variance explained between the third and fourth EOFs may indicate a limit in the physical interpretation in the EOF patterns.

**TABLE 5** PERCENT OF THE TOTAL VARIANCE AND STANDARD DEVIATION OF ANOMALOUS OLR EXPLAINED BY EACH EOF.

| EOF NUMBER | PERCENT VARIANCE | STD. DEVIATION |
|---|---|---|
| 1 | 7.0 | 1.2 |
| 2 | 5.6 | 0.8 |
| 3 | 5.1 | 0.4 |
| 4 | 3.9 | 0.4 |
| 5 | 3.6 | 0.3 |

Similar spatial EOF patterns of summertime OLR anomalies have been computed by several investigators (e.g., Lau and Chan 1985; Magana and Yanai 1991). In most analyses, the OLR data were filtered to highlight fluctuations in the intraseasonal frequencies (20 to 60 days). Although no filtering is applied to the OLR data in this analysis, the first spatial EOF pattern (Fig. 21a) is very similar to those obtained in other investigations. This implies that the basic variability of the large-scale OLR is dominated by intraseasonal variations. The first EOF describes a dipole pattern between the equatorial Indian Ocean and the WPAC. The orientation of the shaded anomaly pattern suggests that this EOF describes the variability of the convective activity associated with a monsoon trough that extends farther east than

normal, and is oriented from west to east rather than a more typical northwest to southeast orientation. A positive (negative) sign associated with this OLR pattern would be expected for an inactive (active) monsoon trough over the western equatorial Pacific.

A dipole-type pattern is also described by the second OLR EOF (Fig. 21b). In this case, the pattern depicts more of a seesaw between the eastern equatorial Indian Ocean and the equatorial central Pacific (Weickmann and Khalsa 1990).

The third EOF pattern (Fig. 21c) describes the OLR variability expected with a more climatologically oriented monsoon trough. In a positive sense, this pattern describes cloudiness associated with a trough that is oriented from the Indian subcontinent to Indonesia and the equatorial western Pacific, with reduced convective activity over the South China Sea and Philippine Sea. Conversely, a negative sign of this EOF pattern depicts enhanced convection over the Philippine Sea (15°N, 135°E).

The spatial patterns of the anomalous OLR variability contain smaller scale features as the amount of explained variance decreases. Although the amount of variance explained by the fourth and fifth EOFs becomes rather small, they both seem to describe variability in convection that is oriented from the southwest to the northeast. The fourth EOF (Fig. 21d) describes a continuous center of variability that is oriented from the equatorial Indian Ocean at 70°E to the Philippine Sea. The fifth EOF (Fig. 21e) defines centers of variability over the equatorial eastern Indian Ocean (5°S, 90°E) and subtropical Pacific along 15° between 140°-160°E.

The variability of the first four OLR EOF coefficients associated with persistent and transition periods of the tropical cyclone-based anomalous circulation patterns is examined in

OLR EOF NO. 1

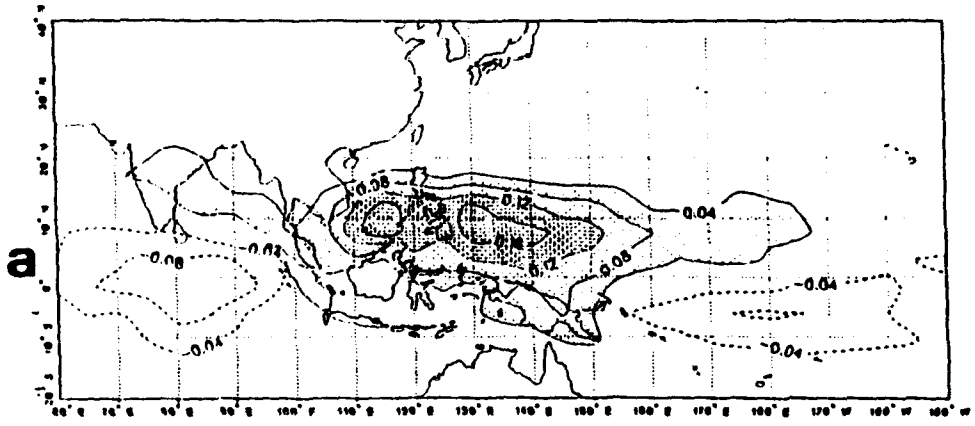


OLR EOF NO. 2

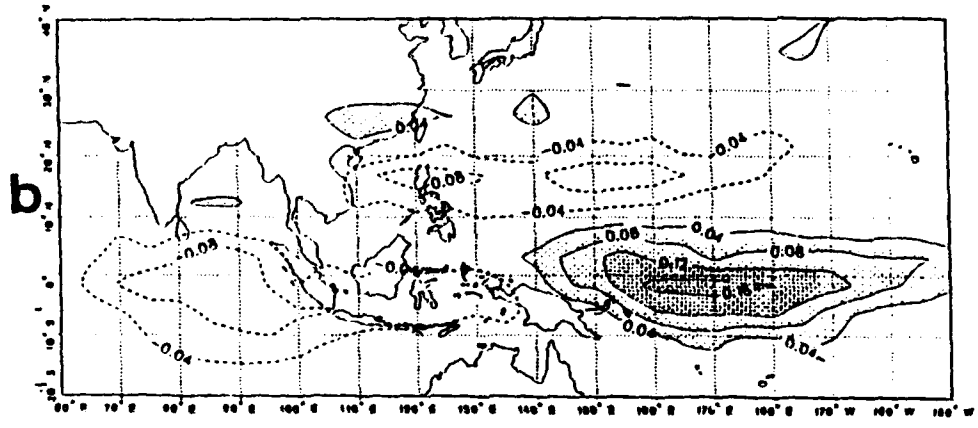


OLR EOF NO. 3

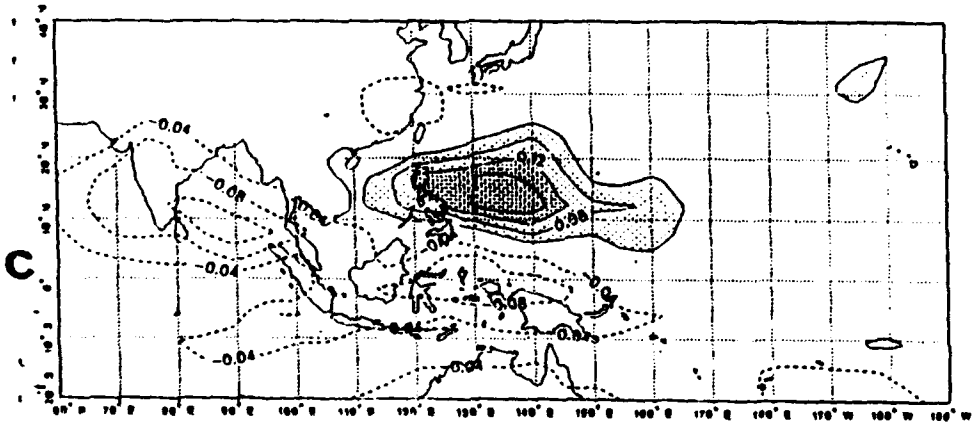


**Fig. 21(a)-(c)** The spatial structures associated with the first three OLR EOFs. Units are nondimensional. Positive contours greater than 0.04 are shaded and negative contours are dashed.

OLR EOF NO. 4

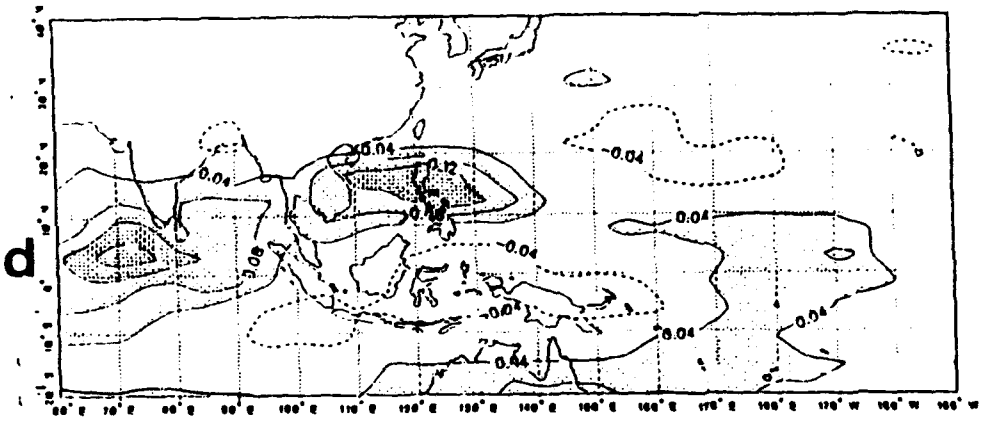


OLR EOF NO. 5

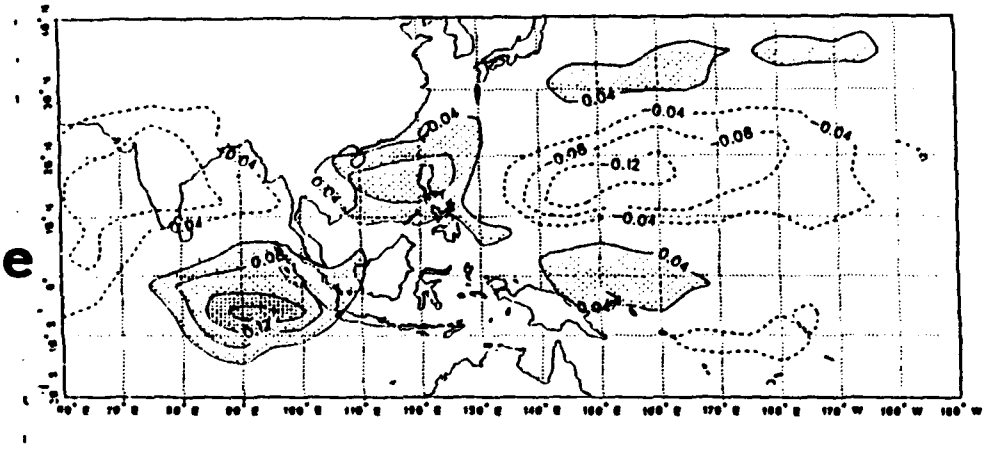


**Fig. 21(d)-(e)** As in Fig. 21, except for the fourth and fifth OLR EOFs.

the same manner as the examination of the zonal wind EOF coefficients. During a SM period that transitions to another west pattern (Table 4), the first OLR EOF contributes to the total variance in a negative sense (Fig. 22a), which indicates enhanced convection extending over the entire South China Sea and Philippine Sea region. The second OLR pattern also contributes to the total variance in a negative sense after -14 days (Fig. 22b). This orientation describes reduced convection between 10°-20°N over both the South China Sea and Philippine Sea, which is superposed on the northern portion of enhanced convection described by the negative orientation of EOF 1. The positive orientation of EOF 3 (Fig. 22c) implies active monsoon trough convection that is climatologically oriented from northwest to southeast, and a region of reduced convection over the northern portion of the Philippine Sea. The combination of the EOF 1 and 3 contributions suggests a region of enhanced convection extending from the Indian subcontinent through Indonesia and over the tropical WPAC. The orientations of EOFs 2 and 3 indicate that reduced convection is over the northern Philippine Sea, which would be consistent with a strong subtropical ridge that accompanies straight-moving tropical cyclones. The combined contributions to the total variance by these three EOF patterns remains nearly constant during the transition to another westerly pattern (i.e., recurve-south or transient-west). The fourth EOF pattern does not significantly contribute to the variance associated with the straight-moving to west transition.

During a persistent SM pattern that transitions to an easterly pattern, the positive contribution from EOF 3 dominates all other EOF contributions (Fig. 23c). This EOF describes enhanced convection in a northwest to southeast oriented monsoon trough with reduced convection over the northern Philippine Sea, which again would be consistent with

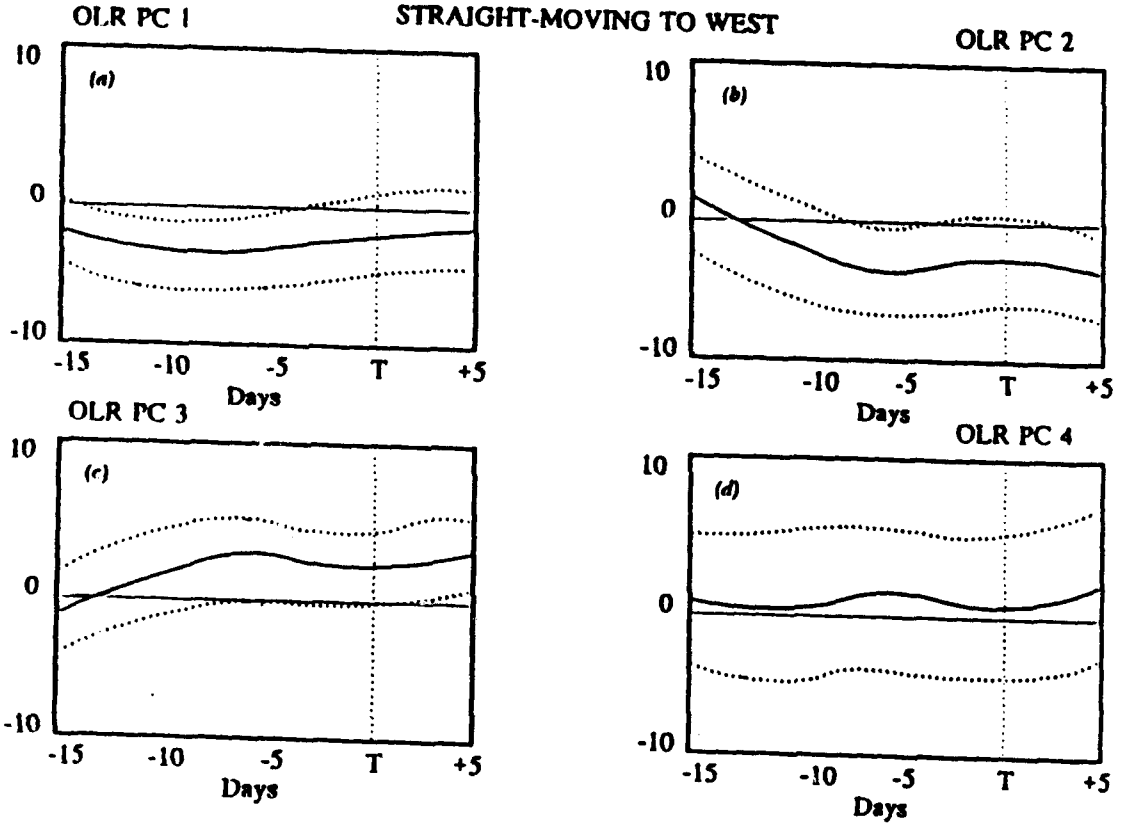


**Fig. 22** Variability of each of the leading four OLR EOF principal components related to the transition from the straight-moving tropical cyclone-based anomaly pattern to any west pattern. The abscissa defines the time (days) relative to the time of the transition, which is marked by the T. Principal component units are W $m^{-2}$.

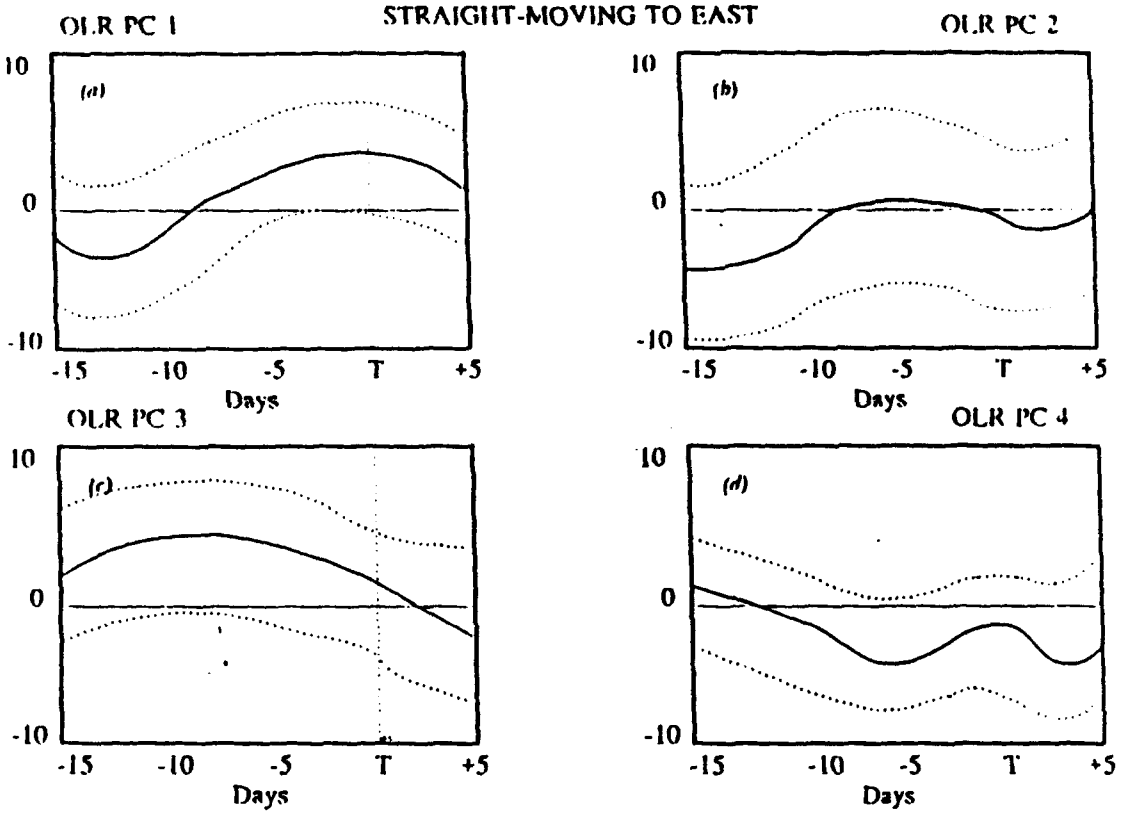


**Fig. 23** As in Fig. 22, except for the transition from the straight-moving tropical cyclone-based pattern to any east pattern.

straight-moving tropical cyclone characteristics. As the transition to an easterly pattern is approached, the contribution from EOF 3 is reduced while the EOF 1 coefficient becomes more positive and the EOF 4 coefficient becomes more negative. These changes signify an increase in convection over the equatorial Indian Ocean and a reduction in convection over the tropical WPAC.

Except for a slightly larger magnitude, the variability of the first EOF pattern during a RS to west period (Fig. 24a) is similar to the variability during a straight-moving to west period (Fig. 22a). However, large differences in the variabilities are found for the second and third EOFs. Five days before the transition to another westerly pattern, the contribution of EOF 2 to the total variance becomes oriented in a more positive sense. This indicates an increase in convection between 10°-20°N over the Philippine Sea. Prior to the transition time, the orientation of the third EOF during the RS to west period (Fig. 24c) is opposite to the orientation during a SM to west period (Fig. 22c). Therefore, enhanced convection is found over the northern portion of the Philippine Sea (PC 1 negative, PC 3 negative) during the persistent RS period.

The major difference between the RS-to-west and RS-to-east transition is contained in the contribution of the first EOF to the total variance (Figs. 24a, 25a). At -10 days during the RS-to-east transitions, the EOF 1 contribution changes from negative to positive, which indicates that enhanced convection conditions over the South China Sea and Philippine Sea change to reduced convection. The opposite change in convective activity occurs along the equator at 80°E (Fig. 21a). Compared with the recurve-south to west periods (Fig. 24c), the

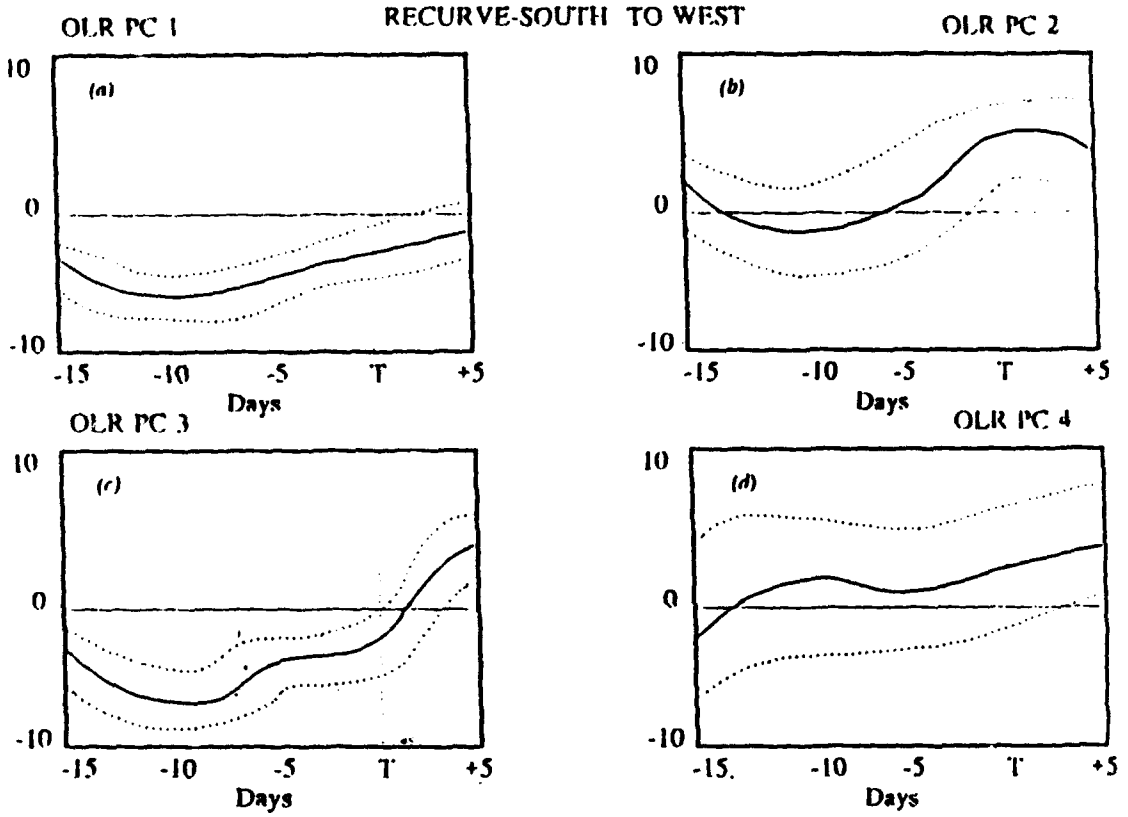


**Fig. 24** As in Fig. 22, except for the transition from the recurving-south tropical cyclone-based pattern to any other west pattern.

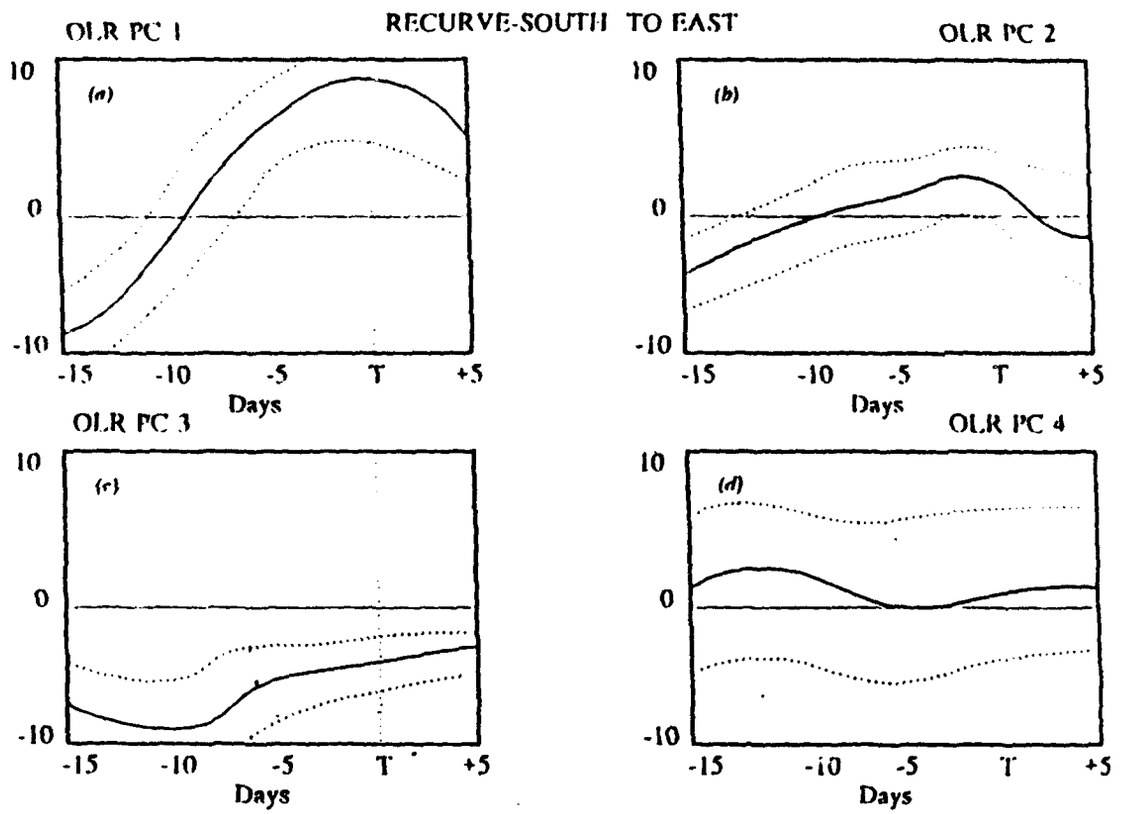


**Fig. 25** As in Fig. 22, except for the transition from the recurving-south tropical cyclone-based pattern to any east pattern.

negative orientation of the third EOF is slightly larger during the recurve-south to east periods (Fig. 25c).

Persistent RN periods that transition to other easterly patterns are dominated by a negative orientation of EOF 3 (Fig. 26c). This indicates a reduction in convection over the climatological monsoon trough region and increased convection over the northern Philippine Sea.

Ten days prior to the transition of a persistent RN pattern to a westerly pattern (Fig. 27), the maximum in the positive contribution of EOF 2 indicates enhanced convection between 10°-20°N over the Philippine Sea. These conditions are reinforced by the negative sense of EOF 3 prior to -10 days, which suggests that convection is reduced over the typical monsoon trough region, but enhanced over the northern Philippine Sea (Fig. 21c). Prior to the transition time, the orientation of EOF 3 changes from negative to positive while EOF 1 changes from positive to negative. Furthermore, the relative variance contribution by EOF 2 is reduced. These changes signify a reduction in convection over the Philippine Sea and an increase over the Indian Ocean and Indonesia, which is physically consistent with a change to a western regime.

Persistent inactive periods that transition to other easterly patterns are dominated by the positive contribution of EOF 1 to the total variance (Fig. 28a). At -5 days, the contribution of EOF 1 changes from positive to negative, which indicates a weakening of the inactive pattern (i.e., transition to another easterly pattern). The contributions to the total variance by the EOF three and four patterns are small compared to the contribution of EOF 1.

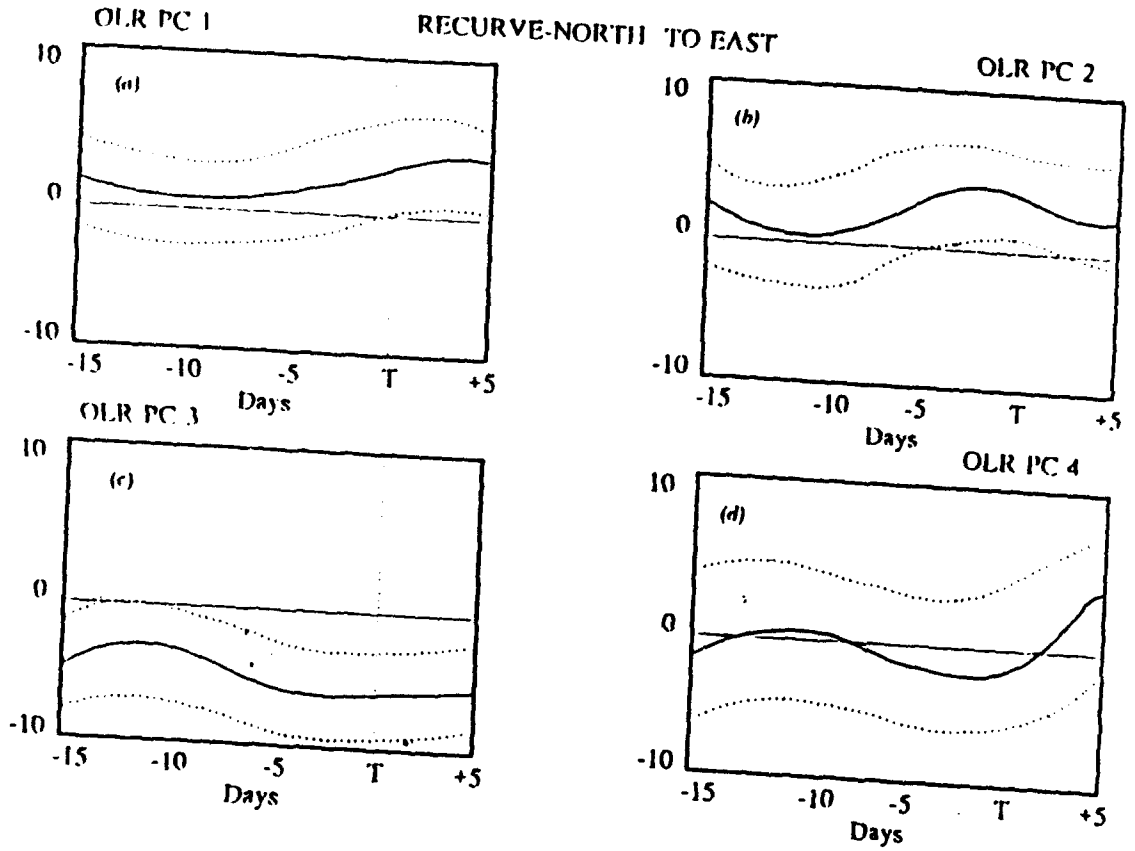


**Fig. 26** As in Fig. 22, except for transitions from the recurve-north tropical cyclone-based pattern to any other east pattern.

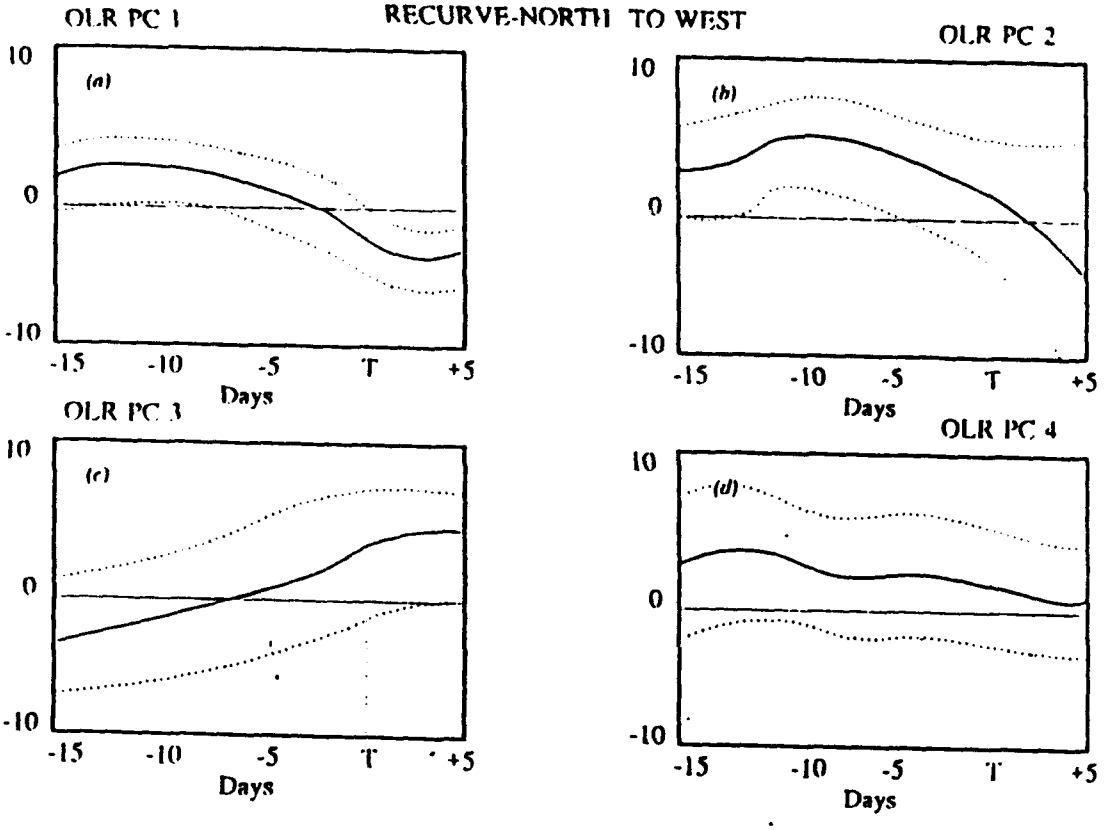


**Fig. 27** As in Fig. 22, except for transitions from the recurve-north tropical cyclone-based pattern to any east pattern.

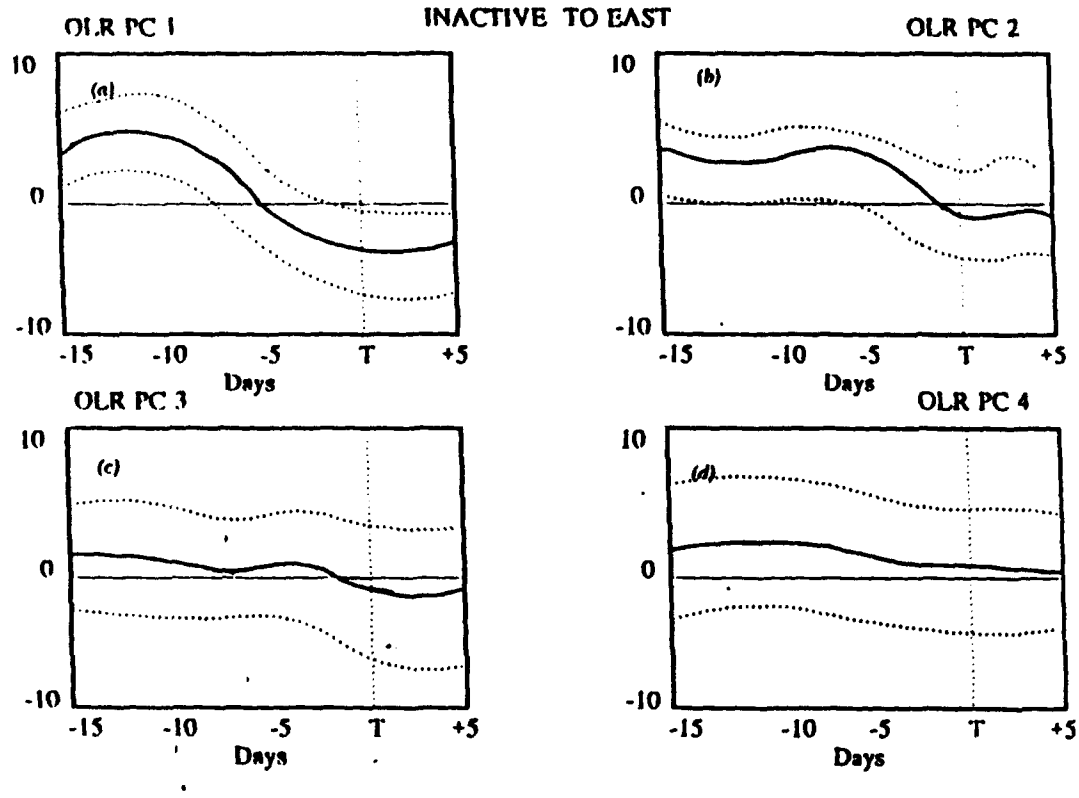


**Fig. 28** As in Fig. 22, except for the transitions from the inactive tropical cyclone-based anomaly pattern to any other east pattern.

Similar to the RS-to-east periods, the IN-to-west periods are dominated by EOF 1 and EOF 3, but in an opposite sense (Figs. 29a,c). Prior to -10 days, the positive contributions of EOF 1 and EOF 3 indicate a reduction in convection over the tropical western Pacific, with an increase in convection over the Indian Ocean. Between -10 and -5 days, the positive contributions by EOFs 1 and 3 are reduced, but the negative contribution by EOF 2 is a maximum. This change indicates an increase in convection along the equator between 150°E and 170°E. The remainder of the IN-to-west period is dominated by the negative contribution of EOF 1 and the change from negative to positive in the EOF 2 contribution. Both of these changes signify increased convection over the South China Sea and Philippine Sea, which is consistent with a change from an inactive to west period.

These comparisons between tropical cyclone-based patterns and the intrinsic variability in the large-scale OLR anomalies are similar to the comparisons with the zonal wind EOFs. That is, physically coherent variabilities of the large-scale OLR anomalies are associated with periods when the tropical cyclone-based anomalous large-scale circulation features are persistent or transitioning between patterns. Similar to the findings with respect to the zonal wind EOF patterns, the OLR EOF patterns describe variabilities that are on larger scales than the tropical cyclone-based patterns. In the next subsection, the associations between large-scale OLR anomalies and the large-scale anomalous wind circulations will be examined with respect to a more general description of the intrinsic variabilities of the anomalous tropical WPAC circulations.

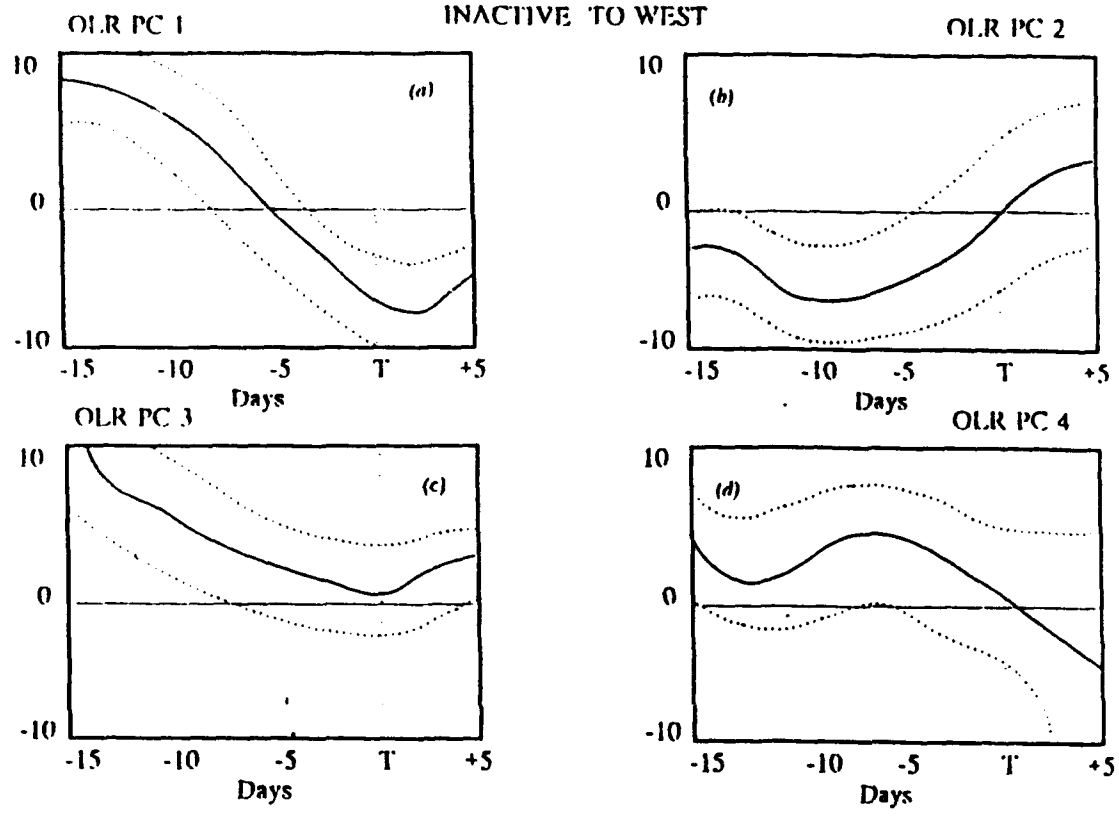


**Fig. 29** As in Fig. 22, except for the transitions from the inactive tropical cyclone-based anomaly pattern to any west pattern.

## C. VECTOR EOF ANALYSIS OF THE ANOMALOUS TOTAL WINDS

Similar to the EOF analysis applied to the anomalous zonal winds in Section A, the majority of EOF analyses in the meteorological sciences have been conducted on scalar data fields. For example, investigations of midlatitude variability typically utilize EOF analyses of height data at various levels in the vertical. Because of the weak height gradients in the tropics, wind data are preferable for identifying variability of tropical circulation features. A scalar EOF analysis of wind data is constrained to evaluate the zonal and meridional wind components separately (Pazan et al. 1982; Wylie et al. 1985; Schott et al. 1987). Some other investigations have utilized a vector EOF (VEOF) analysis to examine the complete wind vector (Hardy 1977; Hardy and Walton 1978; Legler 1983). Klink and Wilmott (1989) compared scalar EOF analyses of separate wind components with VEOF analyses of the total wind field and showed that separate analyses of the wind components may lead to biased results. Based upon these results, and recognition of the importance of both wind components for a complete description of both large- and synoptic-scale tropical circulation variability, the 1979-1987 GBA anomalous 700 mb wind data are re-analyzed utilizing a VEOF analysis of the total wind vector. Although EOF analysis is a widely used statistical procedure in meteorology, a brief description of VEOF with special emphasis to vector wind data based on Hardy (1977) is provided.

Utilizing exponential notation, the wind speed (s) and direction ($\theta$) are represented by a complex number as

$$v = se^{i\theta}.$$

The observations at N locations (i.e., grid points) are represented as a complex vector of N elements. At a time t, a vector $\mathbf{V}_t$ contains a complex element $v_{kt}$ at the $k^{th}$ grid point. The complete set of observations over T time units is then a N x T rectangular matrix, **V**. As in scalar EOF analysis, the eigentechnique is applied to an appropriate similarity matrix usually chosen as either a covariance or correlation matrix. Applied to vector data, a matrix **C** is defined as

$$C = V^{*}V/N$$

where $\mathbf{V}^{*}$ is the complex conjugate transpose of **V**. By definition, **C** is a N x N Hermitian matrix containing real values (variances) on the diagonal and complex values (covariances) off the diagonal. Similar to scalar EOF analysis, VEOF solves the equation

$$|C - \lambda I| = 0,$$

where $\lambda$ represents the eigenvalues of **C**, and **I** is the identity matrix. Because **C** is Hermitian, the eigenvalues are real and non-negative. The N orthogonal eigenvectors associated with the eigenvalues are defined from

$$CE = E\Lambda,$$

where $\mathbf{\Lambda}$ is the N x N diagonal matrix containing the N real eigenvalues, and **E** is a N x N complex matrix containing the N complex eigenvectors.

For a given eigenvector $\mathbf{E}_j$, the $k^{th}$ element is associated with the $k^{th}$ grid point. The $k^{th}$ complex element of the $j^{th}$ eigenvector may be written as

$$\epsilon_{k,j} = a_{k,j}\exp(i\alpha_{k,j}),$$

where $a_{k,j}$ defines the EOF representation of the wind speed and $\alpha_{k,j}$ represents the wind direction. These parameters may be used to plot a two-dimensional vector at the $k^{th}$ grid point location. As in a scalar EOF analysis, the units are relative.

Two factors utilized in scalar EOF analysis directly apply to VEOF analysis. The eigenvalues scaled by the trace of the covariance matrix can be used to determine the percentage of the total variance explained by the corresponding eigenvector. Similarly, the relative contribution of each eigenvector to the total field variance at a particular time can be computed as a coefficient associated with each eigenvector at each time. These coefficients are computed as

$$\boldsymbol{S} = \boldsymbol{EV},$$

where **V** is the original data matrix. For vector data, the coefficients are complex numbers that are represented by an amplitude and phase angle. As in scalar analysis where numerical eigenvector solutions differ from one another by an arbitrary sign, vector solutions differ by an arbitrary phase angle.

The percentage of variance explained by each of the first four VEOFs and the associated standard deviation is provided in Table 6. These four VEOFs explain 37.4% of the total variance. Because the convergence of the VEOF expansion is slightly faster than the scalar EOF expansion of the anomalous zonal wind components, the first four VEOFs will be analyzed whereas the first five scalar EOFs were investigated.

**TABLE 6** PERCENT OF THE TOTAL VARIANCE EXPLAINED BY EACH VEOF. The standard deviation is computed from the estimated error associated with each eigenvalue.

| VEOF NUMBER | PERCENT VARIANCE | STD. DEVIATION |
|---|---|---|
| 1 | 13.1 | 1.2 |
| 2 | 9.1 | 1.0 |
| 3 | 8.0 | 0.7 |
| 4 | 7.2 | 0.4 |

The arbitrary phase angles associated with the VEOF expansion can obscure the interpretation of the spatial patterns. A compositing technique is used to facilitate interpretation of the VEOF spatial patterns. The amplitude mean and standard deviation of each coefficient series is computed. The phase angles associated with all times with amplitudes larger than the mean plus one standard deviation are noted to determine the preferred phase angles associated with large amplitude coefficients (Fig. 30). The phase angles are defined in octants arranged clockwise from 0° (12 o'clock) to 360°. For each VEOF, a composite 700 mb wind anomaly chart is calculated for each octant that contains significantly large coefficient amplitudes. Additionally, a composite OLR anomaly chart is computed to compare the anomalous wind circulations with the anomalous convective activity.

### 1. VEOF Structures

During times when the first VEOF significantly contributes to the total variance of the anomalous large-scale tropical WPAC circulation, it is either oriented at 0° or 180° (Fig. 30a). Composite anomalous 700 mb winds and OLR indicate that a 0° orientation

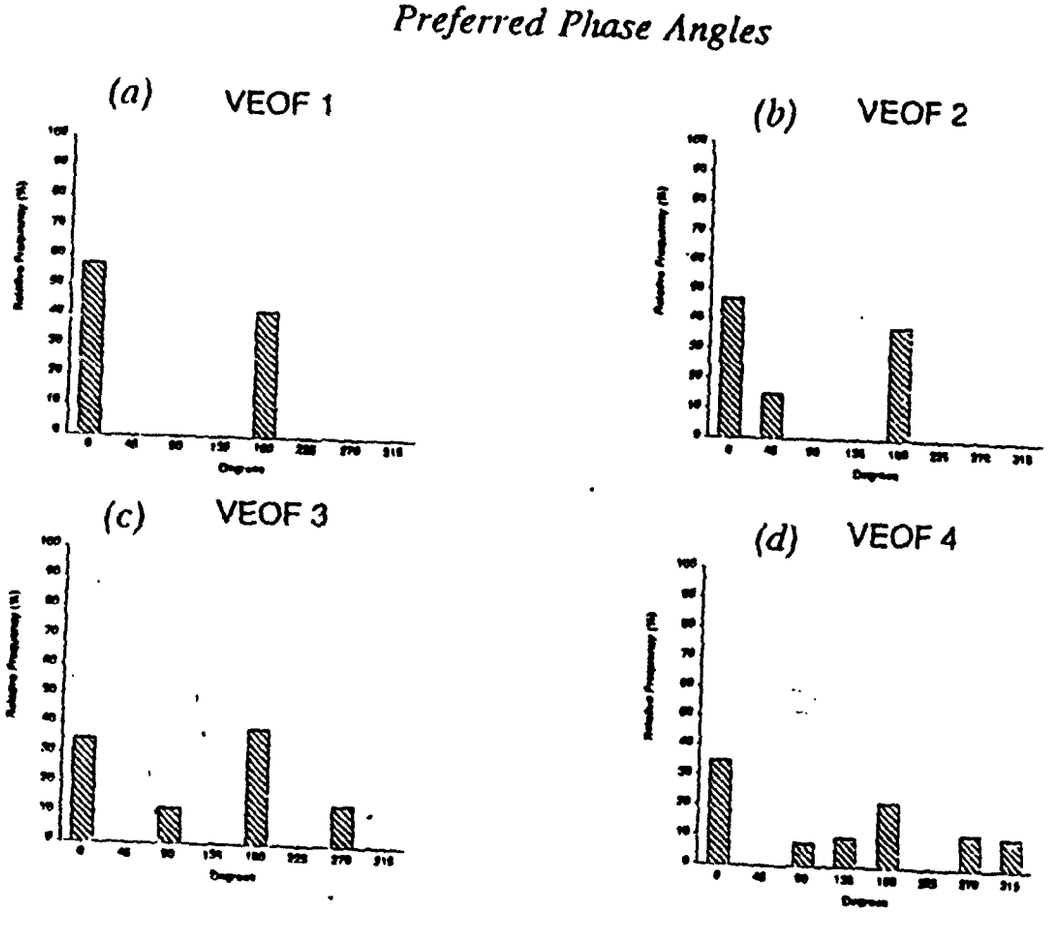


**Fig. 30** Preferred phase orientations of the leading four principal components computed from the VEOFs of the anomalous 700 mb winds.

describes an active monsoon trough with anomalous cyclonic circulations over India and the Bay of Bengal, the South China Sea, and the Philippine Sea (Fig. 31a). The anomalous trough is oriented from the northwest to the southeast, and enhanced convection is found throughout the monsoon trough region that extends to the central Pacific. The anticyclonic circulation anomaly centered at 27°N, 130°E indicates that the western portion of the subtropical ridge is stronger than normal. Opposite conditions are described by a 180° orientation of VEOF 1 (Fig. 31b). Anomalous large-scale anticyclonic circulations between 80°-140°E and the equator and 20°N suggest that the monsoon trough is very weak. Furthermore, the amount of convection over the monsoon trough region is below normal. A large region of enhanced convection is found over the equatorial Indian Ocean centered at 80°E.

The second VEOF is oriented towards 0°, 45°, or 180° when contributing a significant amount to the total variance of the anomalous 700 mb circulation (Fig. 30b). The composites of 700 mb anomalous winds and of anomalous OLR indicate that independent of phase angle, the second VEOF predominantly describes the variability of the subtropical ridge (Fig. 32). When oriented toward 0°, the VEOF 2 pattern depicts a weak ridge. The primary cyclonic anomaly over the subtropical WPAC is centered near 25°N, 165°E, and enhanced convective activity is associated with this 700 mb cyclonic anomaly. Furthermore, reduced convection is centered over a large area along 10°N between 65°E and 160°E. When oriented toward 180° (Fig. 32b), VEOF 2 describes a strong subtropical ridge with a large anomalous 700 anticyclonic circulation centered at 25°N and 150°E. This also is an area of reduced

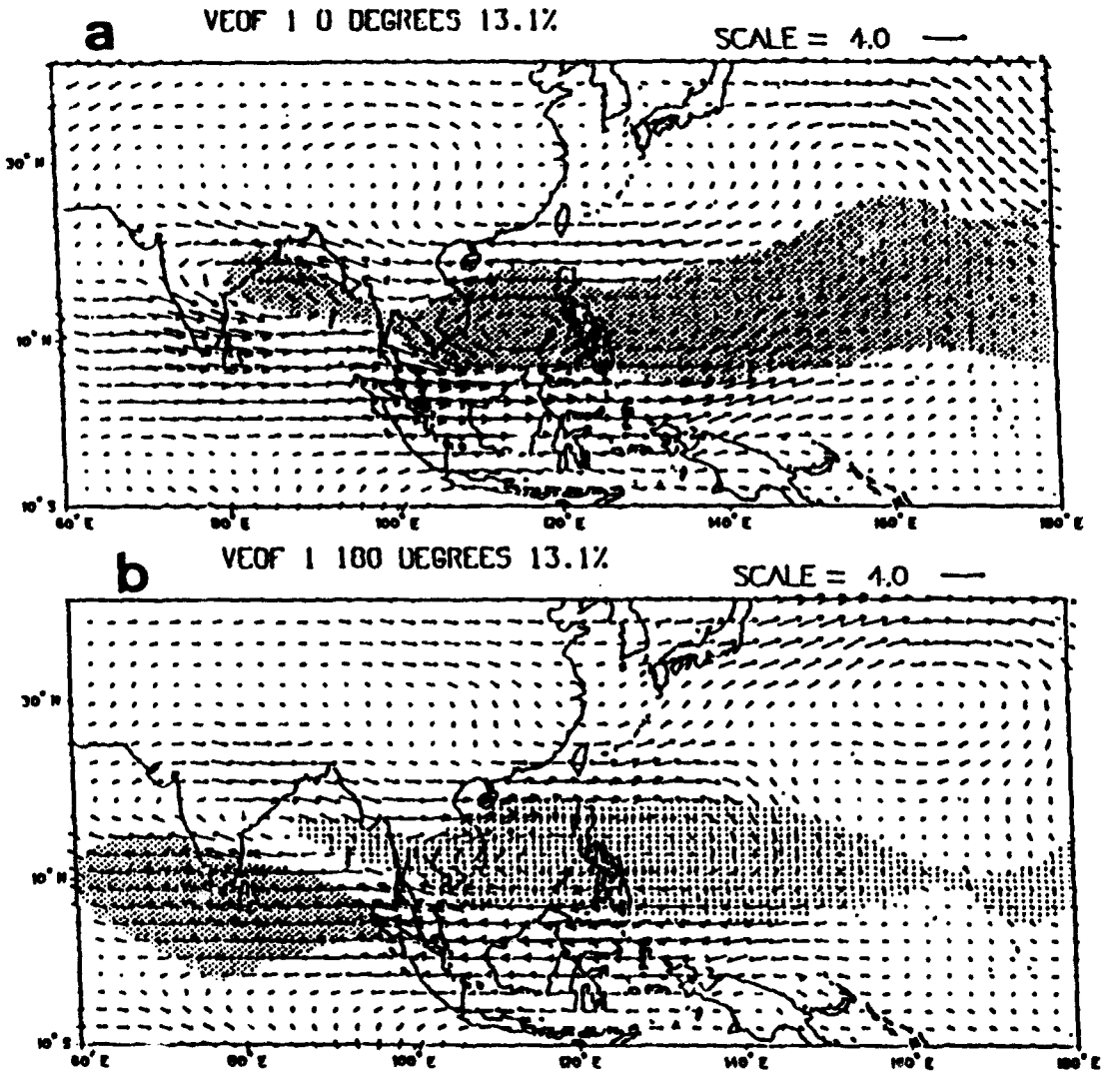


**Fig. 31** Composite of 700 mb wind anomalies for all times when the amplitude of the VEOF 1 principal component is larger than its mean plus one standard deviation, and (a) the phase orientation is toward 0°, or (b) the phase orientation is 180°. Vector units are m $s^{-1}$. Dense shading marks enhanced convection regions with OLR anomalies less than -5 W $m^{-2}$. Light shading marks below average convection regions with OLR anomalies greater than 5 W $m^{-2}$.

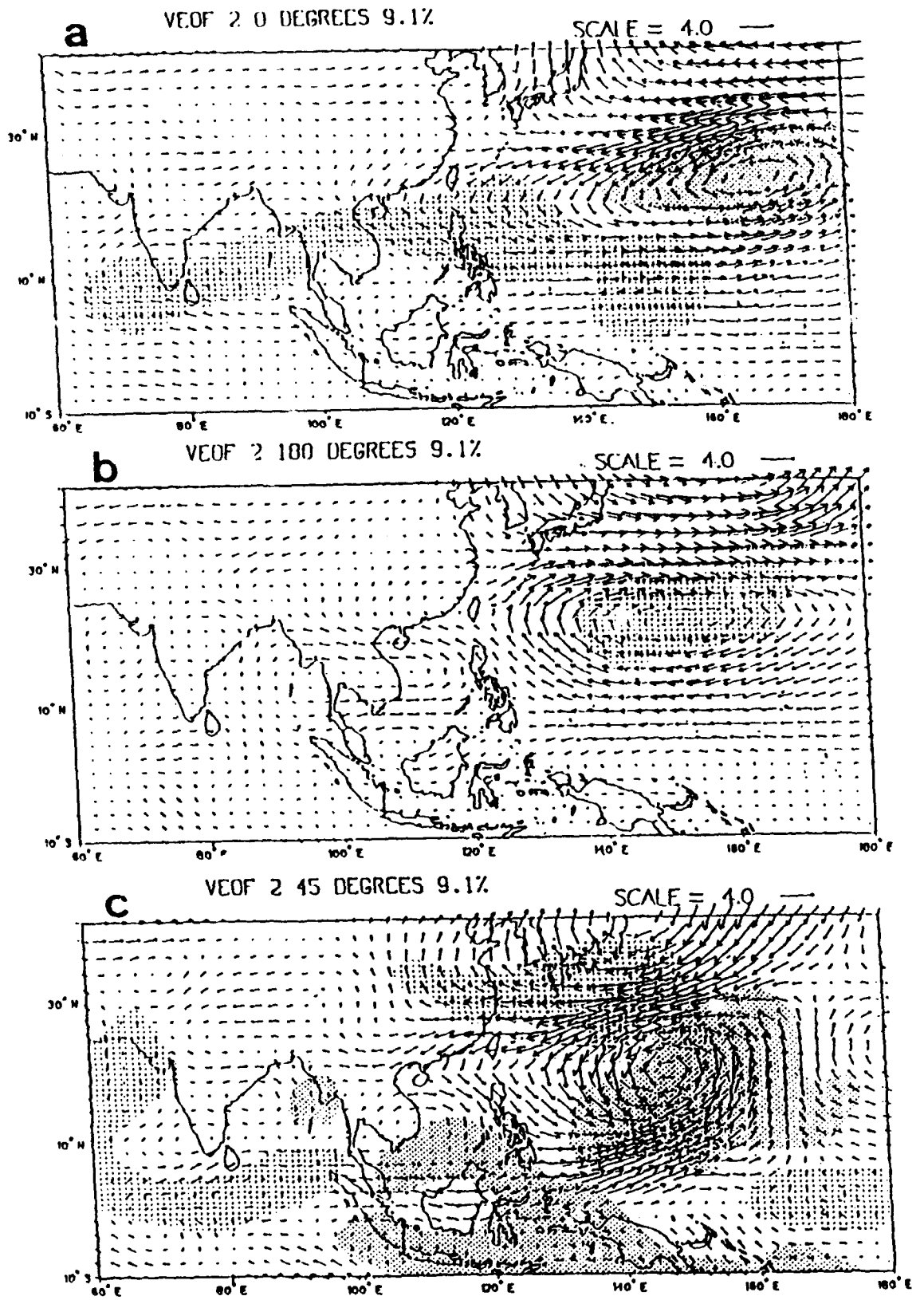


**Fig. 32** As in Fig. 31, except for the VEOF 2 structure oriented at **(a)** 0°, **(b)** 180°, and **(c)** 45°.

convection. The second VEOF also described a weak subtropical ridge when the coefficients are oriented toward 45° (Fig. 32c). However, the location of the anomalous 700 mb cyclonic circulation is shifted towards the southeast relative to the cyclonic circulation associated with a 0° orientation (Fig. 32a). The anomalous cyclonic circulation in Fig. 32c is also associated with enhanced convection.

The spatial patterns of anomalous 700 mb circulations for each orientation of the second VEOF suggest a coupling between the subtropical ridge anomalies with midlatitude circulation anomalies east of Japan. The midlatitude anomaly is always in an opposite sense to the subtropical anomaly. This aspect of the VEOF 2 spatial pattern resembles the western Pacific teleconnection described by Wallace and Gutzler (1981).

The preferred phase orientation of VEOF 3 is spread over four octants: 0°, 180°, 90°, and 270° (Fig. 30c). The large-scale 700 mb anomalous circulation pattern in Fig. 33 oriented at 0° (180°) describes an anticyclonic (cyclonic) center near 20°N, 140°E that is coupled to a cyclonic (anticyclonic) center near 35°N, 170°E. The OLR anomalies indicate reduced convection with anticyclonic anomalies and enhanced convection with the cyclonic anomalies. These anomaly patterns are similar to observational studies of anomalous weather conditions near Japan that are related to variations in tropical heating over the Philippine Sea (Gambo and Kudo 1983; Kurihara and Tsuyuki 1987; Nitta 1987, 1990). Furthermore, the anomaly pattern is qualitatively similar to the Rossby wave-like response to a tropical heat source defined by Hoskins and Karoly (1981).

The orientations of VEOF 3 towards 90° and 270° describe two centers of variability (Figs. 33c,d). The largest 700 mb anomalies are associated with midlatitude

circulations that are oriented west to east along 40°N over the western North Pacific. The second center of variability is located over the Indian subcontinent where an anomalous anticyclonic (cyclonic) circulation and reduced (enhanced) convection are found when the third VEOF is oriented toward 90° (270°).

The number of preferred directions associated with significant coefficients increases as the percent of variance associated with the VEOF decreases. For example, six preferred octants are associated with significant VEOF 4 coefficients (Fig. 30d). The orientations of VEOF 4 along 0° and 180° also represent a Rossby wave-like pattern (Figs. 34a,b) that begins near 20°N, 120°E and proceeds northeastward into the midlatitudes. The convection (OLR) anomalies are physically consistent with the circulation anomalies. The orientation towards 180° describes an active monsoon trough with increased convection over the Indian subcontinent that is oriented through Indonesia and into the equatorial WPAC. The primary difference between the VEOF 3 and 4 patterns seems to be the location of the start of the Rossby wave-like pattern, which appears to be tied also to the location of the convection anomalies. For the VEOF 3 patterns, the primary convection anomalies are located over the WPAC with little connection to the anomalies over the Indian Ocean. Consequently, the circulation anomalies tend to occur farther east over the subtropical WPAC. The primary convection anomalies associated with VEOF 4 are located over the climatological location of the monsoon trough with the circulation anomalies occurring over the Philippines.

The orientations of VEOF 4 towards 135° and 315° define a pattern that is dominated by a large-scale anomalous dipole pattern between the Indian subcontinent and the Philippine Sea (Figs. 34c,d). An anomalous anticyclonic (cyclonic) circulation over the

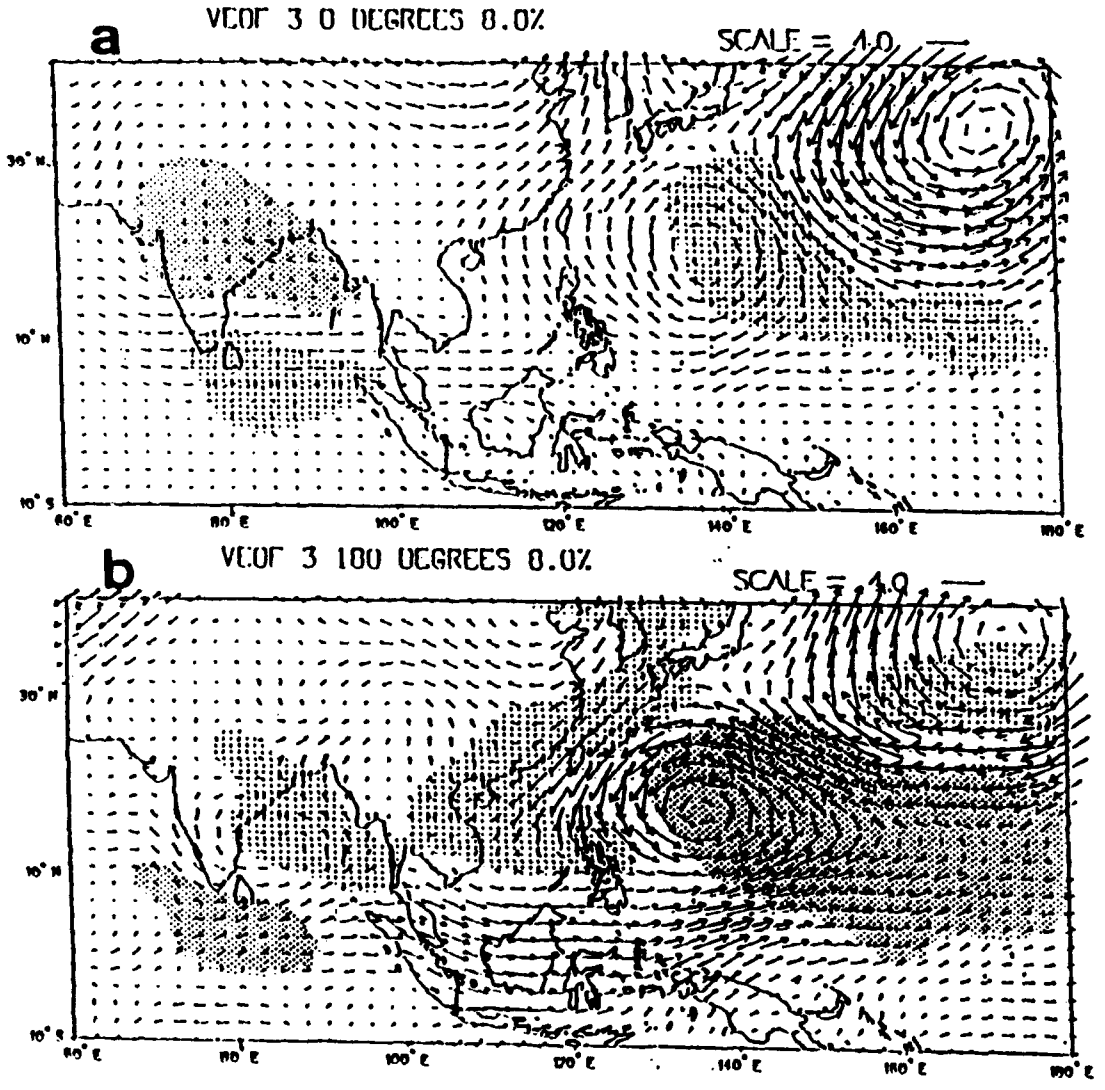


**Fig. 33** As in Fig. 31, except for the VEOF 3 structure oriented at **(a)** 0°, **(b)** 180°,**(c)** 90° and **(d)** 270°.

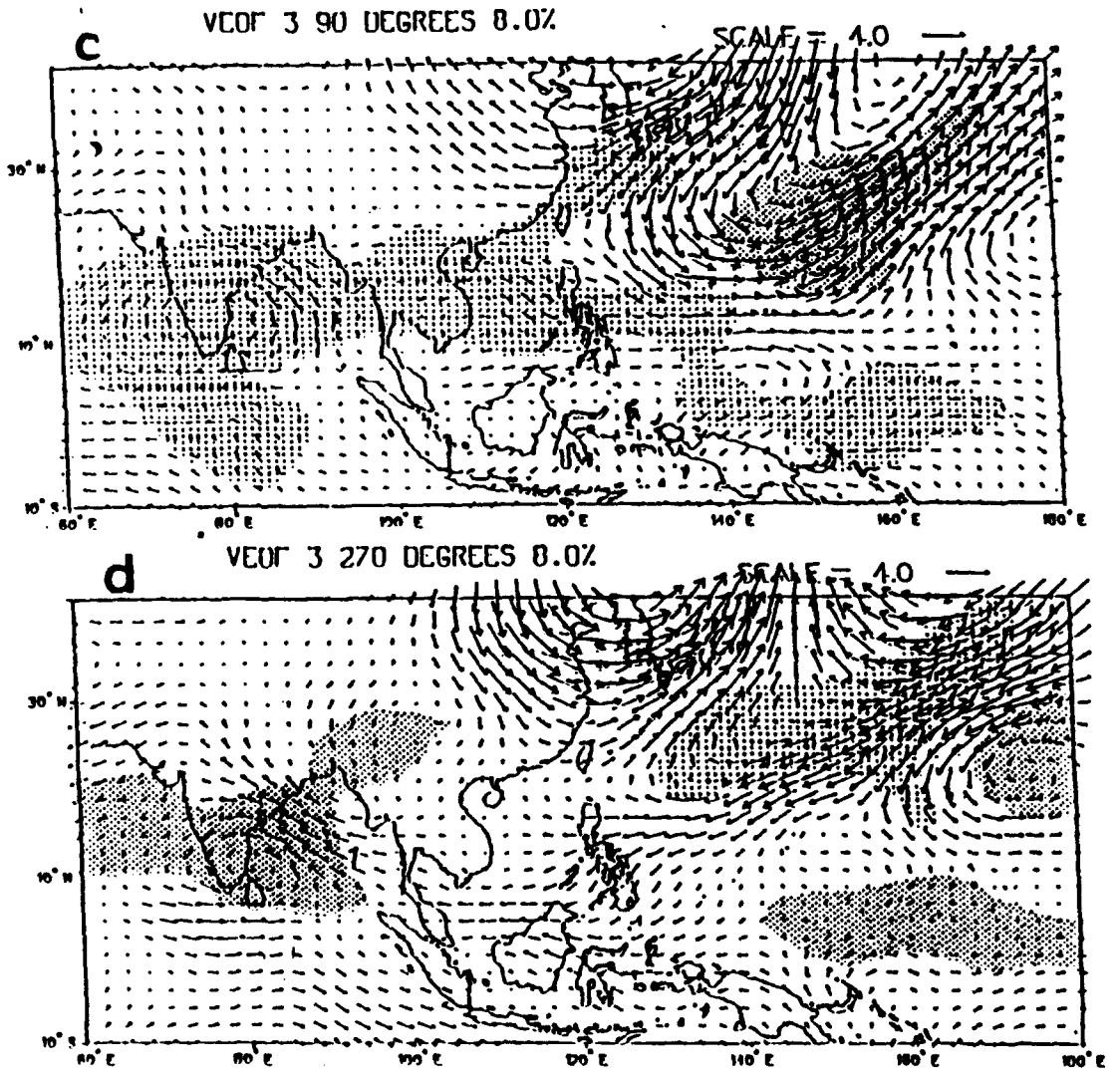


**Fig. 33** (continued)

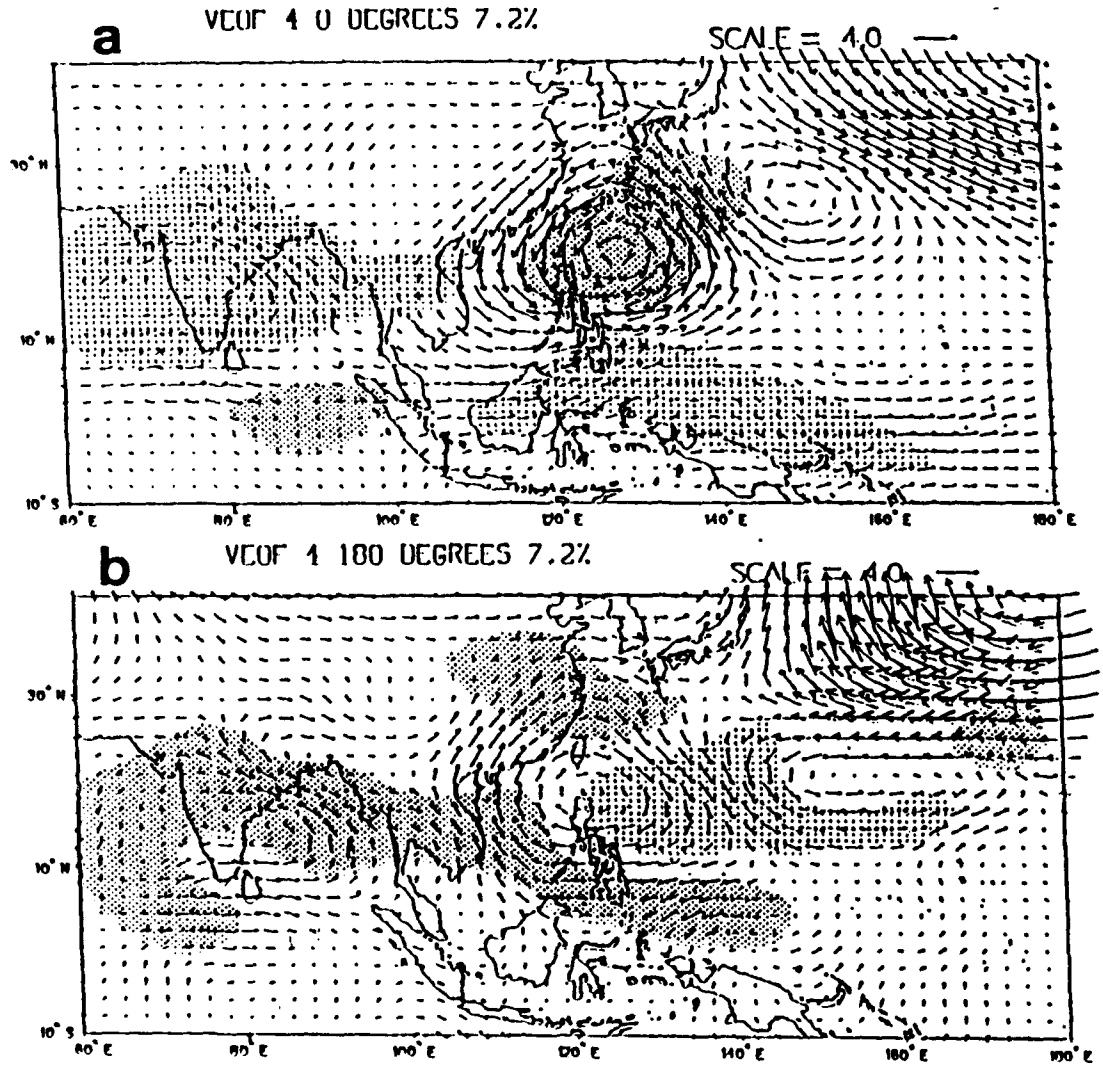


**Fig. 34** ...s in Fig. 31, except for the VEOF 4 structure oriented at **(a)** 0°, **(b)** 180°, **(c)** 135° and **(d)** 315°.

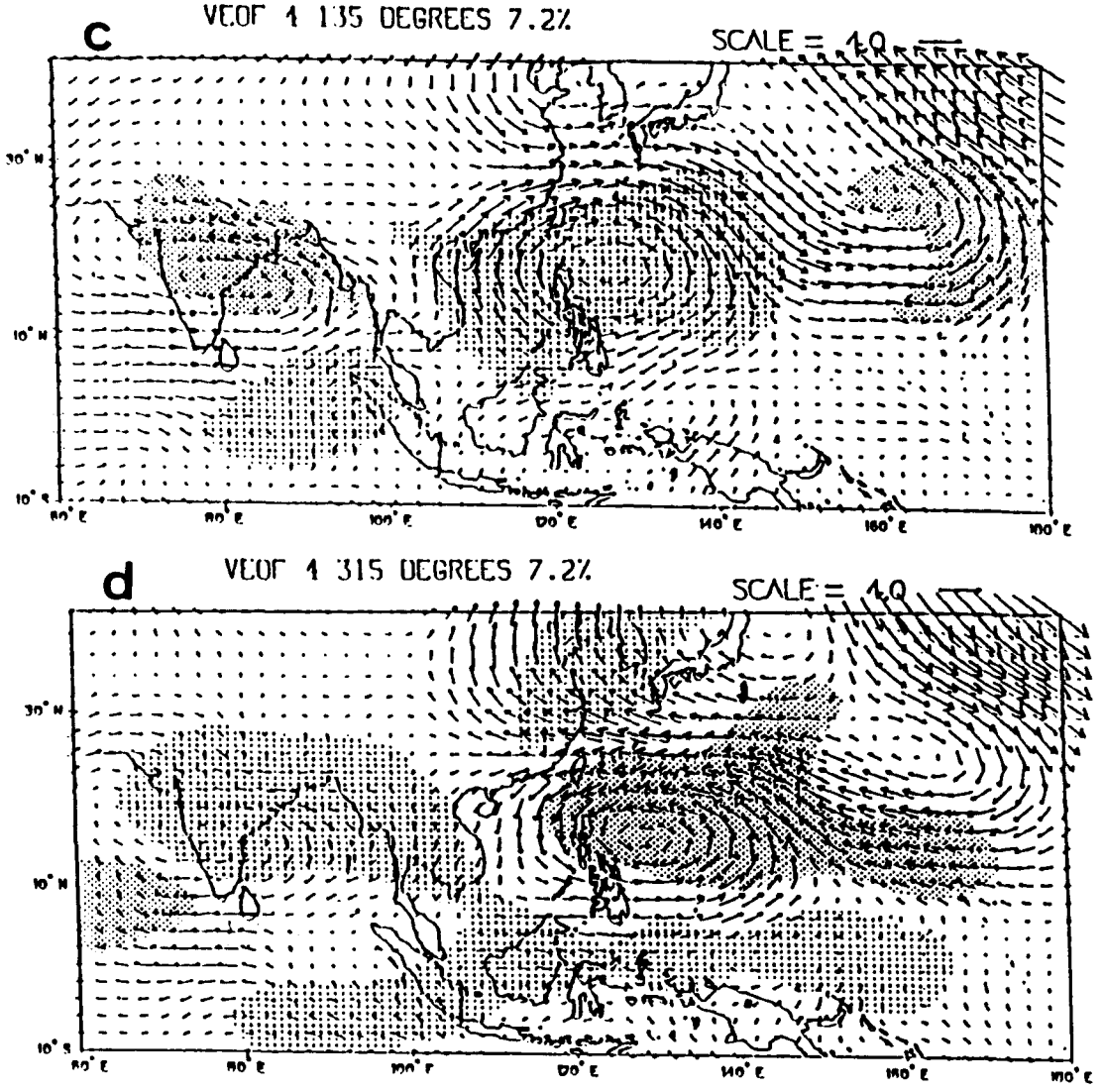


**Fig. 34** (continued).

Philippine Sea and a cyclonic (anticyclonic) circulation over India correspond to an orientation of 135° (315°). Enhanced (reduced) convection anomaloies are found with anomalous cyclonic (anticyclonic) circulations. An indication of Rossby wave-like patterns is also found extending over the western North Pacific.

In summary, the spatial patterns of anomalous 700 mb large-scale circulations defined by the first four VEOFs may divided into two groups. The first group contains VEOF 1 and 2 that describe the variability associated with the monsoon trough and the subtropical ridge. The second group consisting of VEOF 3 and 4 describe smaller-scale anomalous circulations that are primarily concentrated over the western Pacific. The anomalous circulation patterns seem to represent the atmospheric response to tropical heating with differences between the two VEOFs being due to the locations of the anomalous convection and circulation centers.

The composite anomalous convection anomalies based on the OLR data that are associated with each VEOF are physically consistent with the anomalous circulation anomalies. Anomalous cyclonic circulations are typically regions of enhanced convection, and reduced convection occurs with anticyclonic anomalies.

### 2. Variability of the VEOF Structures

The time variability of the VEOF patterns, which is identified by the coefficients associated with each spatial pattern, is examined with respect to periods of persistent and transitioning tropical cyclone-based patterns. The method used to examine the zonal wind component and OLR EOFs is repeated with these VEOF patterns.

During a SM to west period, the orientation of the VEOF 1 PC values toward 0° (Fig. 35a) and the VEOF 2 PC values toward 180° (Fig. 35b) indicates that the monsoon trough is active and the subtropical ridge is stronger than usual. These conditions prevail through the transition time to another westerly pattern. A strong subtropical ridge is also defined by the 0° orientation of VEOF 3 (Fig. 35c) and the 180° orientation of VEOF 4 (Fig. 35d), which both indicate anticyclonic anomalies over the subtropical WPAC (Figs. 33a, 34b). The transition from the persistent SM pattern to another westerly pattern is marked by a fluctuation in the VEOF 3 PCs, which become more oriented toward 90° after -5 days (Fig. 35c). This VEOF 3 orientation indicates a large anomalous cyclonic circulation associated with a midlatitude feature extending over the subtropical WPAC, which may account for a reduction in the strength of the subtropical ridge and a change in the tropical cyclone-based pattern.

The change from a persistent SM pattern to an easterly pattern seems to be reflected in all of the first four VEOFs, but at different times. Near -5 days, the rotations of the VEOF 1 PC values from 0° to 180° (Fig. 36a) and VEOF PC 2 from 180° to 0° (Fig. 36b) denote a change from an active to inactive monsoon trough, and a change from a strong to a weak subtropical ridge. A change in the VEOF 3 PCs to 180° (Fig. 36c), which occurs at -13 days, and the change in VEOF 4 PCs to 0° at -1 day both indicate a weakened subtropical ridge. The combination of all these changes also indicates a shift in the regions of enhanced convection from the monsoon trough region to the subtropical WPAC. The coincident timing of the phase changes in VEOFs 1 and 2 at -5 days indicates that the

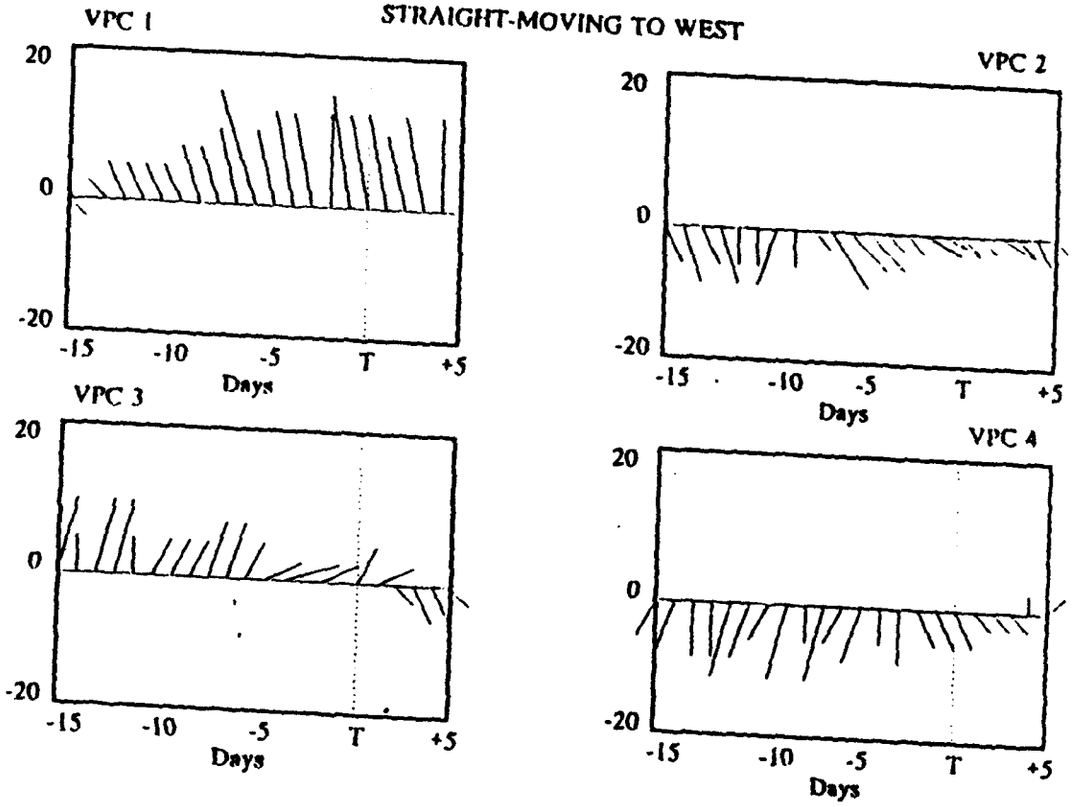


**Fig. 35** Variability of the VEOF principal components associated with a change in the tropical cyclone-based patterns from straight-moving to another west pattern. Abscissa scales are as defined in Fig. 13. Phase angles of the vectors are oriented such that 0° points to 12 o'clock and the rotation is clockwise.

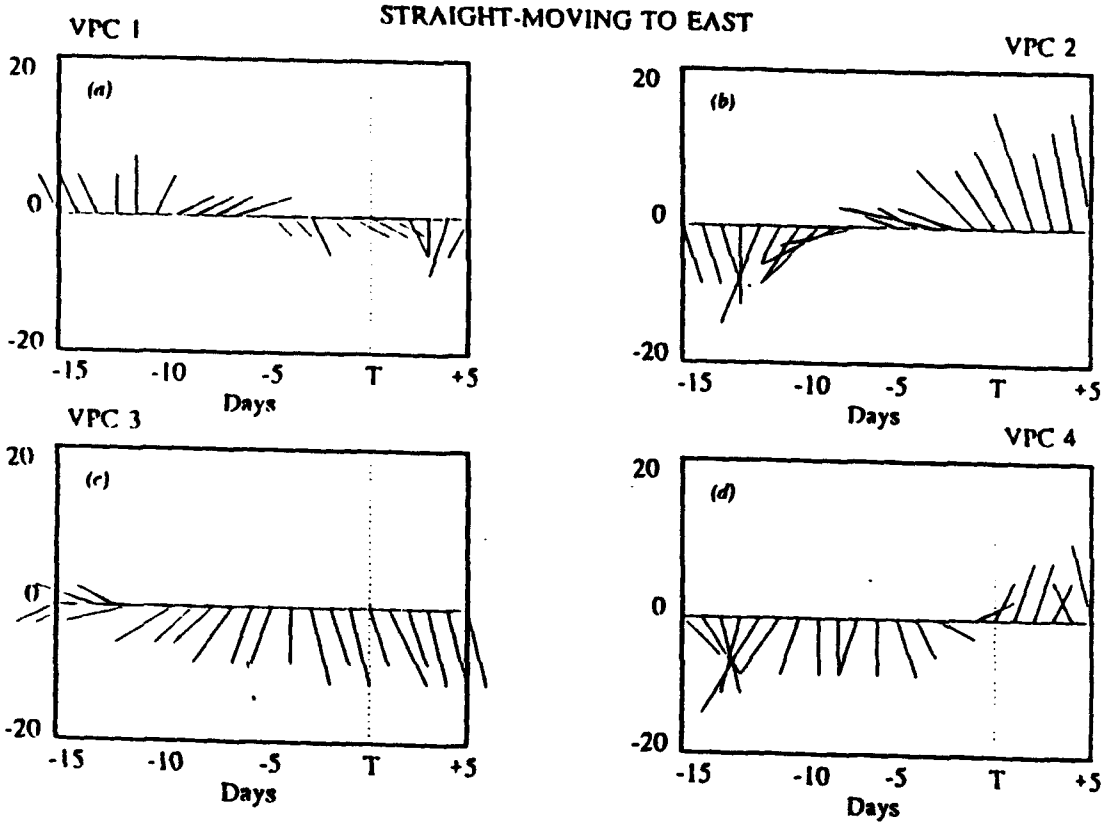


**Fig. 36** As in Fig. 35, except for transitions from the straight-moving tropical cyclone-based pattern to an east pattern.

changes in the monsoon trough and subtropical ridge may be coupled. Because of the Rossby wave-like patterns of VEOF 3 and 4, the timing of the changes in their coefficients may be due to the atmospheric response to the anomalous conditions during the persistent SM period (VEOF 3 at -13 days), and after the large-scale changes in the monsoon trough and subtropical ridge (VEOF 4 at -1 days).

The orientation of the VEOF 1 PCs remains consistently oriented towards 0° during RS periods that change to other westerly patterns (Fig. 37a). These alignments indicate an active monsoon trough with a weak subtropical ridge (Fig. 31). These anomalous conditions are also indicated by the orientation of the VEOF 3 PCs towards 180° (Fig. 37c). The amplitudes of the VEOF 4 coefficients are all small compared to the other PCs. This is probably due to the dipole patterns of the fourth VEOF (Fig. 37), which describe opposite anomalous conditions between the monsoon trough and subtropical ridge. By contrast, the first three VEOF coefficients describe similar anomalous conditions associated with these two large-scale features. The orientations of the VEOFs remain consistent throughout the RS period and the change to another westerly pattern.

At 5 days prior to a change from a persistent RS pattern to an easterly pattern, the rotation of the VEOF 1 PC values from 0° to 180° (Fig. 38a) signifies a change from an active to inactive monsoon trough. The rotation of the PC vectors is counter-clockwise, which is opposite to the clockwise rotation during a SM to east period (Fig. 36a). The VEOF 2 PC vectors rotate from 0° to 180° (Fig. 38b), which indicates a change from a weak to strong subtropical ridge. This change does not occur until the transition time. The 90°

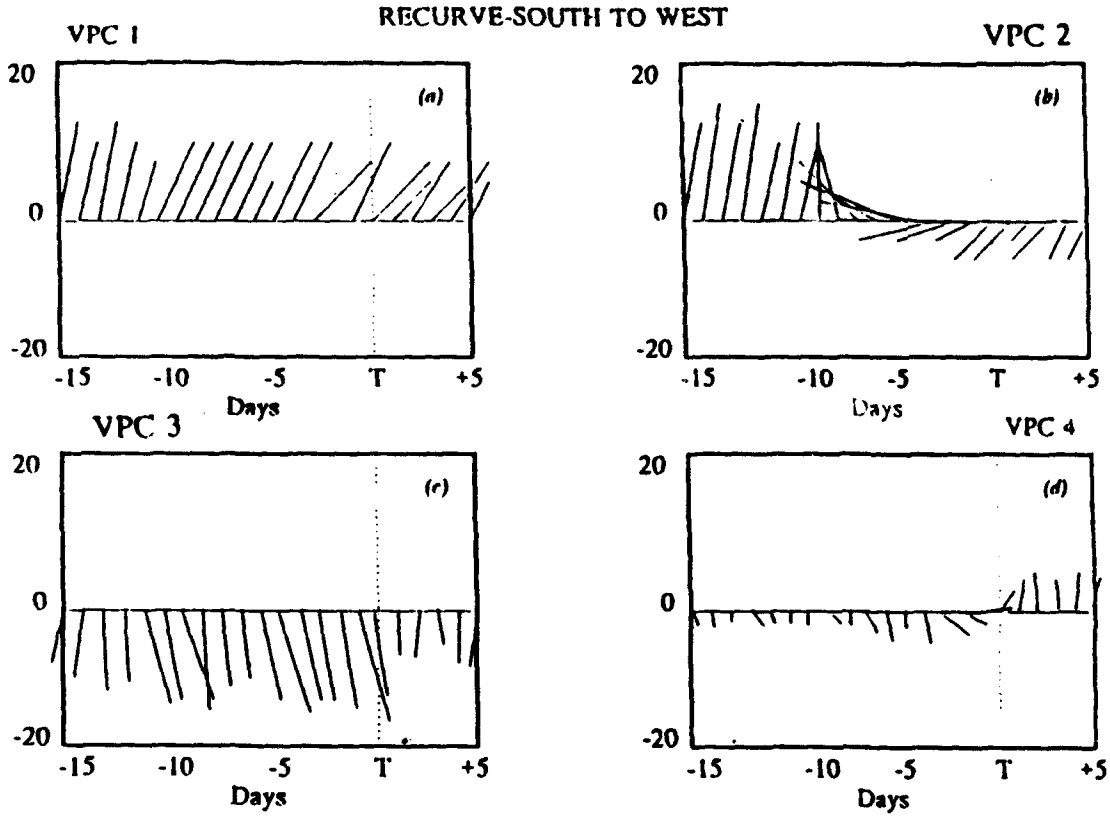


**Fig. 37** As in Fig. 35, except for transitions from the recurve-south tropical cyclone-based pattern to another west pattern.

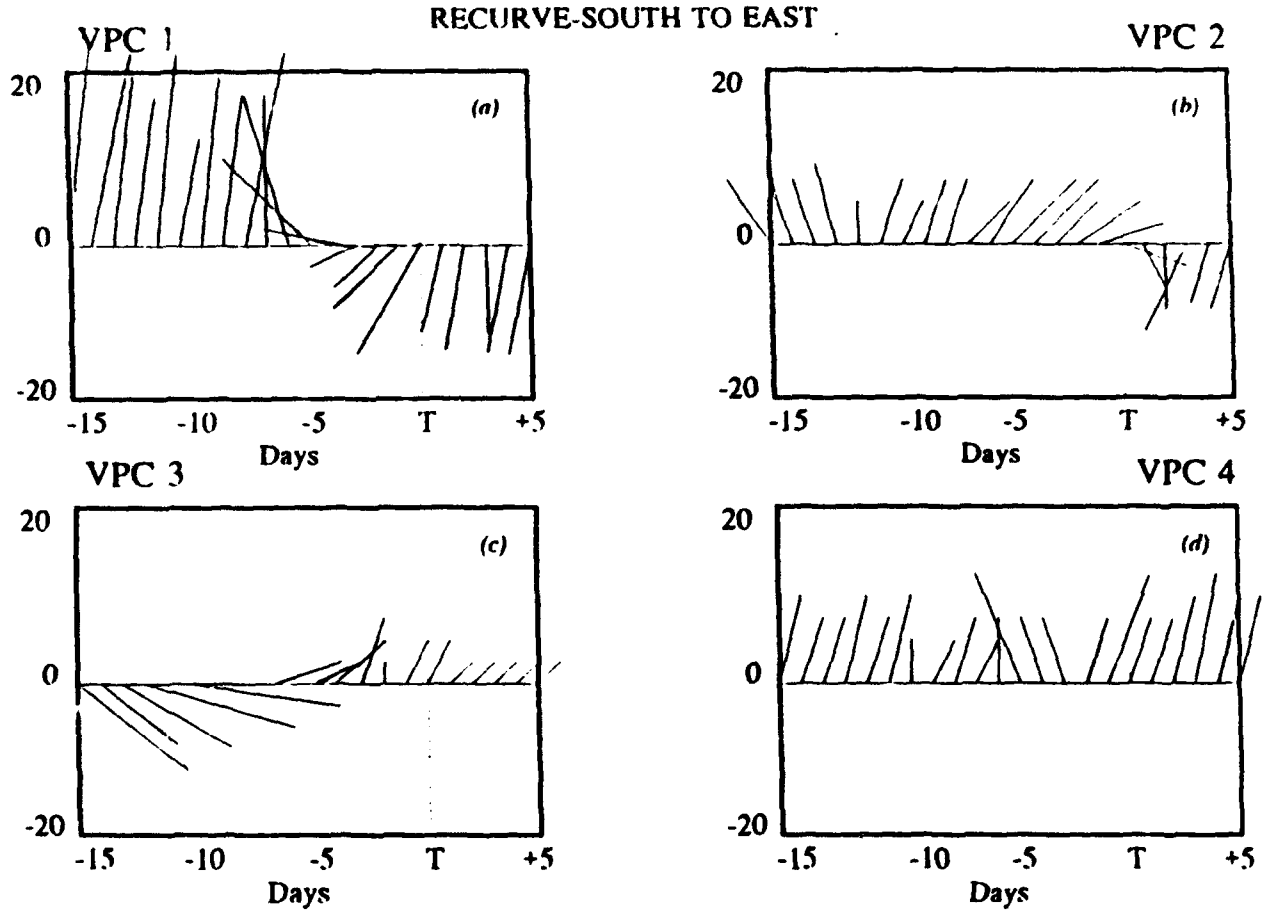


**Fig. 38** As in Fig. 35, except for transitions from the recurve-south tropical cyclone-based pattern to an east pattern.

orientation of the VEOF 3 coefficients (Fig. 38c) indicates a weakening of the monsoon trough, and reduced convection extending from India towards the South China Sea and over the Philippine Sea. The subtropical WPAC is dominated by the cyclonic anomalies associated with a midlatitude feature, and a region of enhanced convection that is oriented from the northeast to the southwest near 25°N, 155°E. The magnitudes of the VEOF 3 PC values indicate that these conditions are prevalent prior to 10 days before the transition to the easterly pattern. The orientation of the VEOF 4 coefficients remains consistently towards 0° throughout the RS transition to an easterly period (Fig. 38d). This orientation also describes a weak monsoon trough with reduced convection over India, and an anomalous cyclonic circulation and enhanced convection over the northern Philippine Sea. The combination of the various contributions to the total variance by the first four VEOFs during a RS to easterly transition describes a change from an active to inactive monsoon trough that begins five days prior to the transition. Closer to the transition time, a change from a weak to strong subtropical ridge occurs. OLR anomalies suggest that the region of enhanced convection associated with the weak subtropical ridge becomes oriented from the northeast to the southwest during the transition time.

Similar to the SM to west and RS to west transitions that are changes from one westerly pattern to another, the PC coefficients of the first four VEOFs do not appreciably change during the transition from the easterly RN pattern to another easterly pattern. The orientation of VEOF 1 coefficients toward 180° after -10 days (Fig. 39a) indicates a weak monsoon trough. The VEOF 2 coefficients are oriented between 0° and 45° (Fig. 39b), which

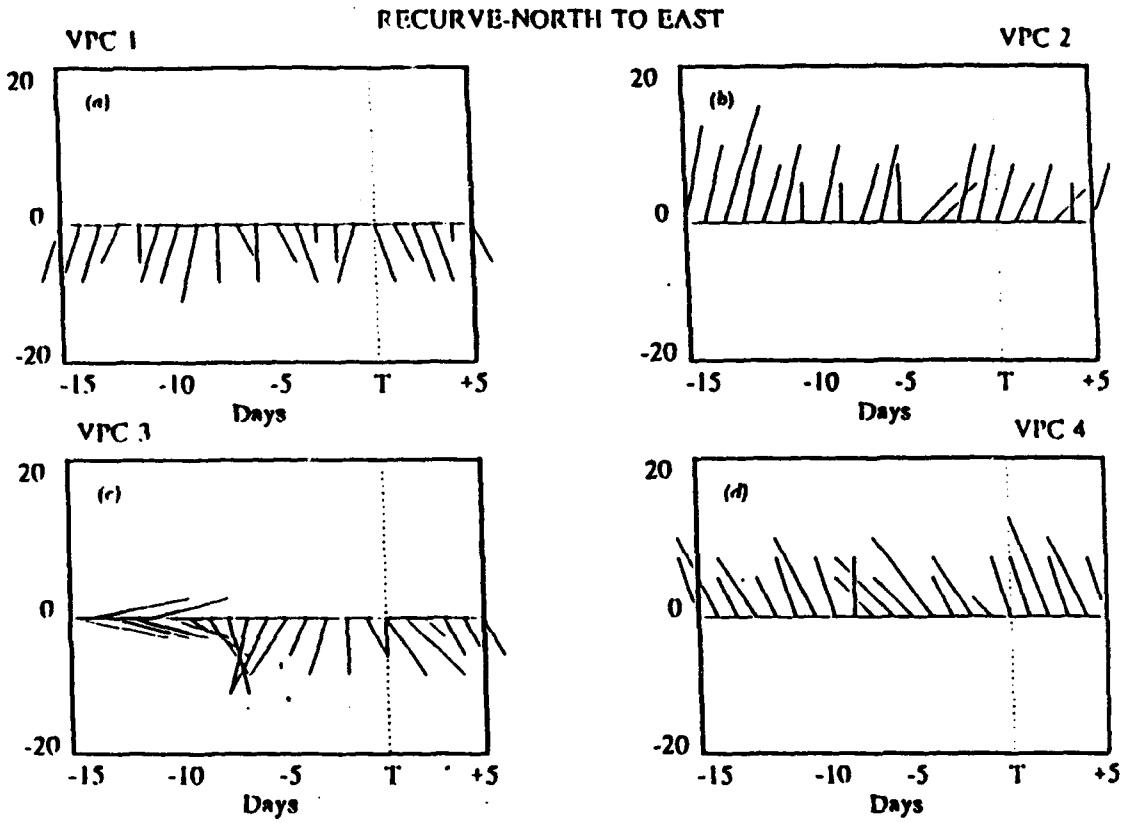


**Fig. 39** As in Fig. 35, except for transitions from the recurve-north tropical cyclone-based pattern to another east pattern.

indicates a weak subtropical ridge. The VEOF 3 PC vectors are oriented towards 180° after 10 days (Fig. 39c), which also suggests that the subtropical ridge is anomalously weak with enhanced convective activity over the western Pacific between 135°-180°E and 5°-25°N. The orientation of the VEOF 4 coefficients towards 315° also indicates a weak subtropical ridge and a weak monsoon trough.

The change in the VEOF 1 coefficients during a RN to westerly transition is similar, but with an opposite sign, to the SM to easterly and the RS to east transitions. Near -5 days, the rotation of the VEOF 1 PCs from 180° to 0° (Fig. 40a) signifies a change from an inactive to active monsoon trough. Also at -5 days, a change from a weak to strong subtropical ridge is denoted by the rotation from 0° to 180° of the VEOF 2 PC (Fig. 40b). The amplitudes of the VEOF 3 coefficients are small until about five days prior to the transition time (Fig. 40c). At this time, VEOF 3 is oriented towards 270°, which describes a weak cyclonic circulation over India with enhanced convection. Anomalous anticyclonic anomalies extend into the subtropical western Pacific from the midlatitudes. During the persistent RN period prior to -10 days, the fourth VEOF is oriented towards 315° (Fig. 40d), which describes a dipole anomaly pattern with cyclonic anomalies and enhanced convection over the subtropical western Pacific, and anticyclonic anomalies with reduced convection over the Indian subcontinent (Fig. 34f). As the transition to a westerly pattern approaches, the VEOF 4 PC values rotate to a 180° orientation (Fig. 40d). This pattern describes an active monsoon trough with enhanced convection and a strong subtropical ridge, which would be representative of a change from the easterly RN pattern to a westerly pattern.

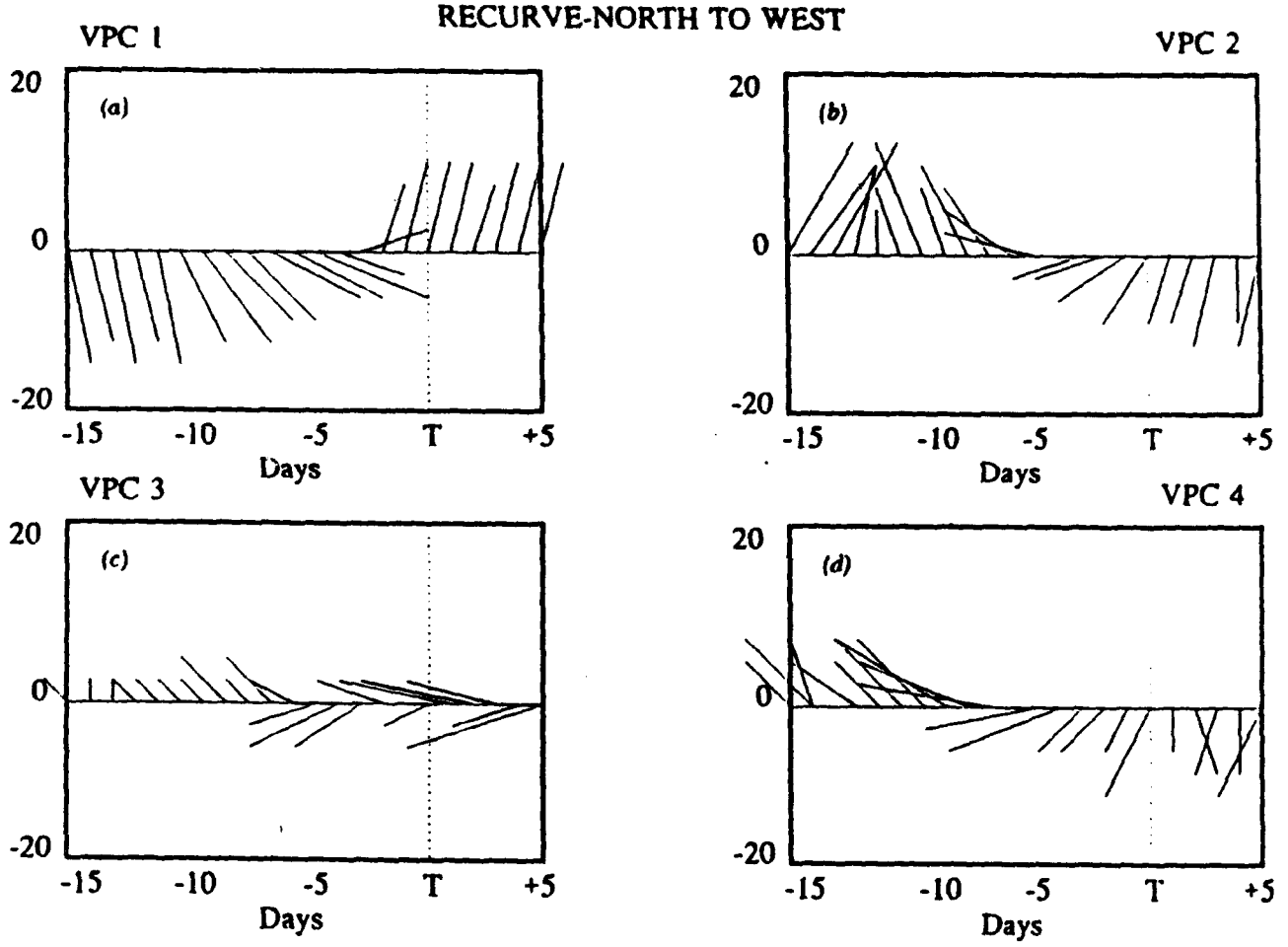


**Fig. 40** As in Fig. 35, except for transitions from the recurve-north tropical cyclone-based pattern to a west pattern.

During an IN to easterly transition, both the VEOF 1 and VEOF 2 PC values are consistently oriented towards 180° (Figs. 41a,b), which signifies a weak monsoon trough and a strong subtropical ridge with reduced convection anomalies over both regions. The PC values associated with the remaining VEOF patterns have much smaller amplitudes than the VEOF 1 and 2 values.

During the IN to westerly transitions, the variations in the VEOF 1, 3, and 4 PC vectors (Figs 42a,c,d) are similar to the changes during a RN to westerly transitions (Figs. 40a,c,d). The VEOF 2 PC values are consistently oriented towards 180° during the IN to west periods with the amplitudes decreasing as the transition approaches.

## D. SUMMARY

The purpose of applying the EOF technique to the anomalous tropical circulation and OLR data is to examine how representative the tropical cyclone-based anomalous circulation patterns are of the intrinsic variability of the large-scale circulation over the tropical WPAC. The EOF analysis was applied to three sets of meteorological variables as a type of cross-validation of the physical consistency identified by the EOF analyses. This is particularly true for the OLR data, which are based solely on satellite measurements and not tied to the GBA analysis system. A basic result of all three EOF analyses is that the intrinsic modes of variability in both circulation and OLR contain larger-scale features than identified with the tropical cyclone-based patterns. In all cases, the leading EOF patterns describe coherent features that spanned both the Indian Ocean and the tropical western Pacific. Furthermore, the variations of the leading EOF circulation and OLR modes during periods of persistent and transient tropical cyclone-based patterns are physically consistent with the tropical

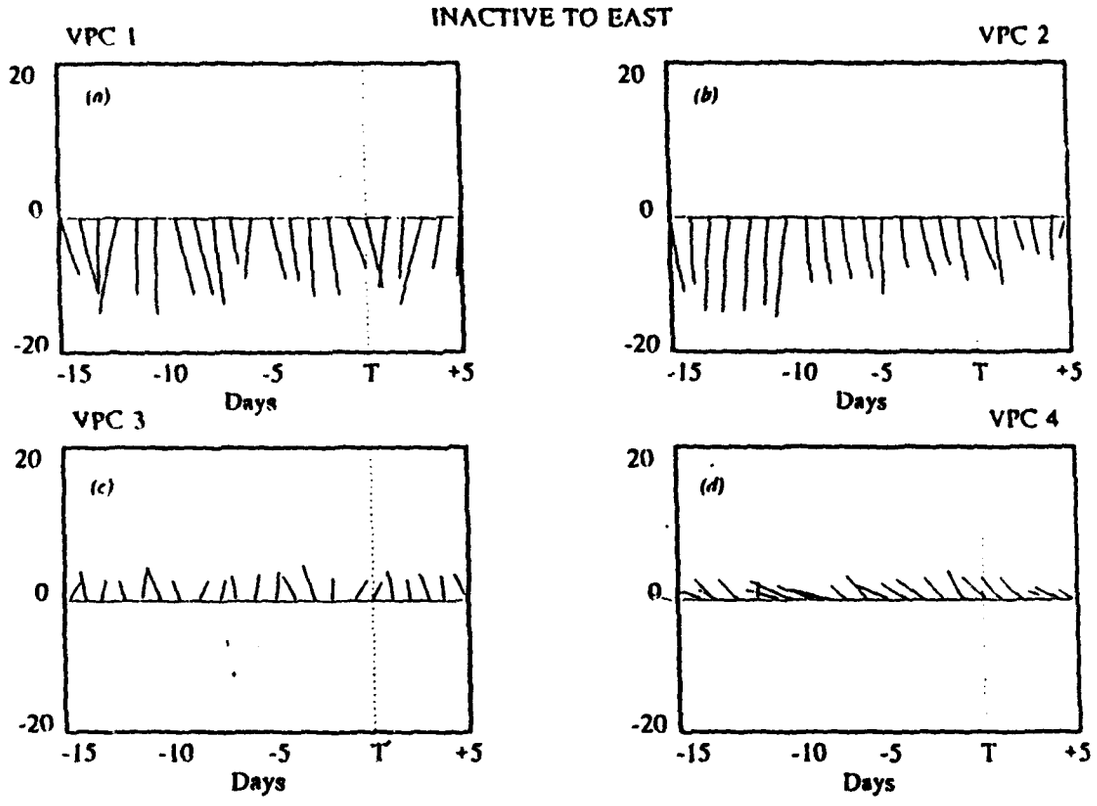


**Fig. 41** As in Fig. 35, except for transitions from the inactive tropical cyclone-based pattern to an east pattern.

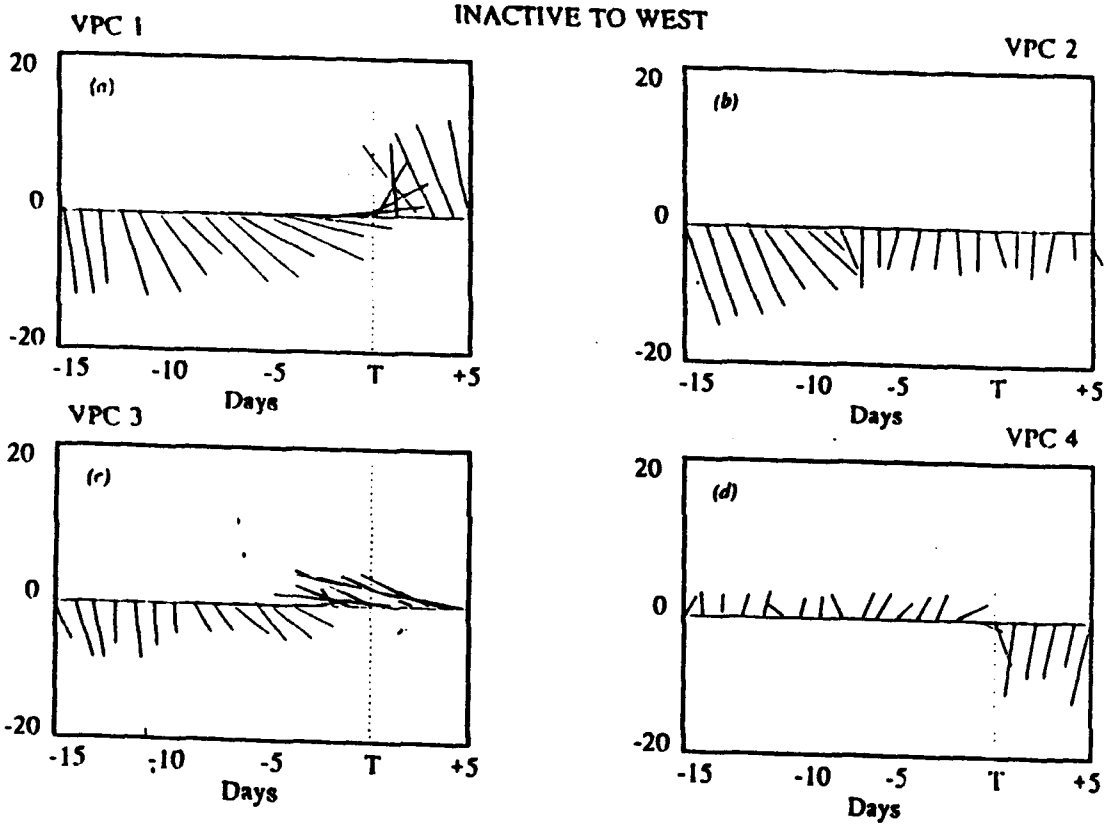


**Fig. 42** As in Fig. 35, except for transitions from the inactive tropical cyclone-based pattern to a west pattern.

cyclone-based patterns. This leads to the conclusion that the large-scale anomalous circulation features based on tropical cyclone track types and inactive periods have smaller scales, but are directly related to the basic variability of the large-scale circulations.

Earlier discussions in this Chapter highlighted the importance of an expression of the important physical aspects of the large-scale circulation variability related to tropical cyclone characteristics. The spatial patterns of large-scale variability described by the EOFs can be considered to be the result of a spatial filtering that highlights the statistically dominant features of the anomalous large-scale circulation. The relationships between these statistical depictions of atmospheric modes of variability and the primary dynamical characteristics of the atmosphere have been examined by Mo and Ghil (1987). They applied the EOF technique to a long integration of a simple, nonlinear deterministic barotropic model that allowed explicit identification of the dynamical features. Comparison of the EOFs with the dynamics of the model indicated that the EOFs were statistical expressions of the primary dynamical aspects of the model.

Although the EOF patterns describe the intrinsic modes of anomalous large-scale circulation variability, a goal of this research is to identify and classify circulation patterns that are related to tropical cyclone characteristics that are likely to be persistent and/or recurrent. The rather clear identification of the various EOF modes with physical components of the large-scale circulations of the tropical western Pacific suggest that the EOFs would provide a comprehensive basis for the classification of persistent and/or recurrent circulation patterns.

# IV. ANOMALOUS LARGE-SCALE FLOW PATTERNS OVER THE TROPICAL WESTERN NORTH PACIFIC

The observed low-frequency variability associated with tropical cyclone characteristics was discussed in Chapter I (Fig. 1). Active tropical cyclone periods may be dominated by one particular track type; different track types may occur during separate intervals within the active periods; or combinations of track types may occur throughout the active period. In Chapter I, the reasoning was that the reappearance of similar tropical cyclone characteristics suggests that recurrent anomalous large-scale circulation patterns may exist. Furthermore, the observation that recurring tropical cyclone attributes may also be persistent suggests that the recurrent anomalous large-scale circulation patterns may also be persistent. However, recurrent tropical cyclone characteristics, or anomalous large-scale circulation patterns connected with recurrent tropical cyclone characteristics, are not necessarily required to be persistent. This is a rather different condition from investigations of low-frequency variability of large-scale midlatitude circulations in which persistence was the primary criterion for classification of circulation patterns (Horel 1985a,b; Mo 1986; Vautard 1990).

The hypothesis investigated in this chapter is that the basic structure of the variability of the anomalous large-scale circulations over the tropical western North Pacific may be characterized by recurrent patterns that may also be persistent. The VEOFs defined in Chapter III identify the basic structure of the anomalous large-scale circulation variability over the tropical western North Pacific. These structures, or combinations of these structures, will be used as the basis for identification of recurrent patterns.

The VEOF decomposition of the anomalous 700 mb wind data allows the time series of anomaly fields to be expanded as a product of the EOFs (spatial patterns) and the principal components (time coefficients). The expansion is written as

$$V(\vec{x}, t) = \sum_{v=1}^{v_o} A_v(t) E_v(\vec{x}),$$

where the vector **x** represents the spatial data, $E_v$ is the vth EOF and $A_v(t)$ is the corresponding principal component, which is a function of time t. The summation of the product of principal components and EOFs begins with the first eigenvalue and proceeds in decreasing order of explained variance to an appropriate truncation $v_o$. Setting $v_o = 4$ provides an expansion that explains 37.4% of the total variance contained within the anomalous 700 mb large-scale wind data (Table 6). This rather slow convergence of the VEOF expansion is due to the large spatial domain of the analysis, which includes large variances associated with the midlatitude regions and the area over the Asian continent. The convergence of the expansion is much more rapid if a limited region only covering the tropical Indian Ocean and the tropical western North Pacific between the equator-30°N is considered (Table 7). The large gap between the variance explained by VEOF 2 and 3 indicates that an adequate depiction of the variance in the 700 mb anomalous large-scale circulation over the tropical and subtropical regions may be explained by only the first two VEOFs. This is consistent with the interpretation of these two EOFs as descriptions of the variability associated with the monsoon trough and subtropical ridge as in Chapter III. Therefore, the structure of the anomalous large-scale circulation variability described by the combination of the first two VEOFS will be used as the basis for identification of recurrent

patterns. By implication, the Rossby wave-like features present in VEOFs 3 and 4 are omitted. However, it will be shown that these features are important components of transitions between periods with recurrent circulation patterns.

TABLE 7 PERCENT OF THE TOTAL VARIANCE EXPLAINED BY EACH VEOF OVER THE TROPICAL INDIAN OCEAN, TROPICAL AND SUBTROPICAL WESTERN NORTH PACIFIC.

| VEOF NUMBER | PERCENT VARIANCE |
|---|---|
| 1 | 32.3 |
| 2 | 28.4 |
| 3 | 16.2 |
| 4 | 12.4 |

The use of EOFs to reduce the dimension of the phase space of atmospheric variability is consistent with many investigations of midlatitude circulations (Barnston and Livezey 1987; Mo and Ghil 1987; Molteni et al. 1990). Specifications of recurrent midlatitude flow patterns were initially based upon probability density estimates of the reduced-dimension phase space (Sutera 1987; Hanson and Sutera 1986; Molteni et al. 1990). Indications that the probability density estimate of the low-dimensional phase space is non-normal would indicate that portions of the phase space tend to recur more than others. The most simple representation is a bimodal distribution that is associated with blocked and zonal flow patterns (Mo and Ghil 1988). Based upon the observed bimodality of low-dimensional phase space representations of midlatitude flow variations, various cluster analysis techniques were used to identify more detailed characteristics of recurrent flow patterns (Legras et al. 1987; Mo and Ghil 1988;

Molteni et al. 1990). A cluster analysis of the reduced-dimension phase space of 700 mb anomalous large-scale circulation variability defined by the two leading VEOFs will be used to identify the recurrent flow patterns over the tropical Indian Ocean and western North Pacific Ocean.

## A. CLUSTER ANALYSIS

The two leading VEOFs of anomalous 700 mb large-scale circulations provide a two-dimensional phase space that simplifies the basic structure of the variability of the entire data set while preserving as much of the original structure as possible. Recurrent circulation patterns are defined as clusters within this two-dimensional depiction of the anomalous circulation.

Clustering techniques are generally classified as either a partitioning or hierarchical method. Hierarchical methods may be agglomerative, in which each point is initially treated as an individual cluster, and clusters are merged to satisfy an optimization criterion. By contrast, divisive hierarchical methods begin with all points belonging to one cluster and then proceed to split the cluster. In contrast to hierarchical methods that define clusters throughout the analysis, partition methods construct a specified set of k clusters. These clusters are defined to satisfy certain requirements of a partition such as each partition must contain at least one object and each object must belong to exactly one partition. The two types of clustering methods differ in that partition methods define the best distribution of the data within k groups whereas hierarchical methods define the number of groups as the analysis proceeds.

As the choice of clustering methods can be subjective, comparisons between different algorithms are valuable for determining the method best suited for a particular type of data or problem (Kaufman and Rousseeuw 1990). Therefore, results from a hierarchical and a partition method applied to the two leading VEOF coefficients are compared as a background for the definition of the clustering method used throughout the remainder of the analysis. The average linkage hierarchical method (Kalkstein et al. 1987) and the k-means partition method (Anderberg 1973) are compared. Kalkstein et al. (1987) compared three popular clustering methods that were all hierarchical and agglomerative and concluded that the average linkage method was superior for meteorological applications. This method compares the squared Euclidean distances between all pairs of observations with one observation from each cluster. The average squared Euclidean distance determines the similarity that is required to define cluster members. Mo and Ghil (1988) used a variant of the k-means partition method to determine clusters of Northern Hemisphere midlatitude circulations. The k-means method assigns each data point to that cluster (k clusters total) with the nearest centroid or mean.

One quite subjective aspect of cluster analysis is the number of clusters to be retained. Thus, a procedure is followed in which each method is repeatedly applied while adding one cluster each step. The iterations are stopped when the additional cluster either represents a subset of extreme cases taken from a previously defined cluster, or the number of members of the new clusters is less than 10% of the next smallest cluster. The number of clusters is the same in each comparison between the average linkage and k-means method.

A partition method is particularly effective when applied to a data set that tends to form natural groupings (Kalkstein et al. 1987). The concentration of the leading vector EOF

coefficients along distinct phase orientations (Fig. 30) suggests that this data set may be well suited to a partition cluster analysis. Comparisons between the k-means and average linkage methods indicate that the average linkage method tends to form one central large cluster with several peripheral clusters that are much smaller. These smaller clusters are primarily composed of extreme cases of anomalous large-scale circulations. The k-means method results in clusters that are more aligned with the original phase orientations of the VEOF coefficients. Based on these initial comparisons, the k-means method is chosen to identify the recurrent patterns of the 700 mb anomalous large-scale circulation.

The k-means algorithm satisfies the two requirements of a partition defined above, i.e., each cluster must contain at least one member, and each data object must belong to exactly one group. The second criterion is typically refered to as "hard clustering" since rigid decisions are made regarding each point's membership in a cluster. Relaxation of this criterion results in "fuzzy clustering" since some degree of uncertainty is incorporated into the definition of the cluster membership. In this fuzzy cluster analysis, membership coefficients define the degree to which a data point belongs to each cluster. Normally, the assignment of sequences of circulation anomalies to a particular cluster identifies patterns that are nearly constant. However, the fuzzy analysis allows identification of sequences that may contain attributes of several clusters. These may be associated with slowly varying circulation features that may identify mechanisms that cause a circulation pattern to change from one cluster to another. Outlines of both the hard and fuzzy cluster algorithms are provided before specific results from the application of the cluster analysis to the leading VEOF coefficients are discussed.

## 1. Hard Clusters

A generalization of many clustering methods that minimize the product of the determinants of the scatter or covariance matrices are based on the maximum likelihood principle (Scott and Symons 1971; Bock 1987). In this subsection, the hard cluster version of the k-means method is defined in the maximum likelihood context following Bock (1987). A fuzzy version of the k-means method is defined in the following section.

A sample of n observations $(\mathbf{x}_1,\mathbf{x}_2,\ldots,\mathbf{x}_i,\ldots\mathbf{x}_n)$ is to be partitioned into k clusters. Each observation $\mathbf{x}_i$ is defined by p variables such that $\mathbf{x}_i=(x_{i1},x_{i2},\ldots,x_{ij},\ldots,x_{ip})$. The approach taken to solve this problem is to assume that each observation is independent and originates from a multivariate normal distribution defined as $N(\boldsymbol{\mu}_t, \boldsymbol{S}_t)$, where $\boldsymbol{\mu}_t$ is the mean vector and $S_t$ is the covariance matrix of the distribution associated with cluster t. The independence constraint requires special attention, which is addressed in the description pertaining to the design of the algorithm in subsection 2. By definition, $S_t$ is a symmetric positive definite matrix. If the observation i is contained in the cluster t, then the index i is contained within the set $C_t$ and the density of $\mathbf{x}_i$ is defined as

$$\frac{1}{(2\pi)^{p/2}\left|\boldsymbol{S}_t\right|^{1/2}} e^{-(\mathbf{x}_i-\boldsymbol{\mu}_t)^T\boldsymbol{S}_t^{-1}(\mathbf{x}_i-\boldsymbol{\mu}_t)/2}, \qquad (1)$$

where the notation $()^T$ denotes a transpose of a matrix or vector. Notice that the cluster mean $\boldsymbol{\mu}_t$ and the covariance $S_t$ are unknown along with the members of the set $C_t$.

The likelihood function is defined as the product of (1) for all observations i as

$$L = \prod_{t=1}^{k} \prod_{i \in C_t} \frac{1}{(2\pi)^{p/2} |\Sigma_t|^{1/2}} e^{-(x_i - \mu_t)^T \Sigma_t^{-1} (x_i - \mu_t)/2}. \quad (2)$$

The most likely values for the unknown index array $C_t$, mean vector and covariance matrix can be defined by maximizing L. It is more convenient to maximize the log-likelihood function defined as

$$\Phi = -\frac{1}{2} np \log(2\pi) - \frac{1}{2} \sum_t \left( \sum_i u_{it} \right) \log |S_t| - \frac{1}{2} \sum_t \sum_i u_{it} (x_i - \mu_t)^T S_t^{-1} (x_i - \mu_t) \quad (3)$$

where $u_{it} = 1$ when i is contained in $C_t$ and $u_{it} = 0$ otherwise. The $u_{it}$ are subject to the constraint

$$\sum_{t=1}^{k} u_{it} = 1, \quad i = 1, \ldots, n.$$

The cluster mean is defined by setting the first derivative of (3) with respect to $\mu_t$ equal to zero, which yields

$$\mu_t = \frac{\sum_{i=1}^{n} u_{it} x_i}{\sum_{i=1}^{n} u_{it}}. \quad (4)$$

Setting the first derivative of (3) with respect to $S_t$ to 0 and solving for $S_t$ yields

$$S_t = \frac{\sum_{i=1}^{n} u_{it} (x_i - \mu_t)(x_i - \mu_t)^T}{\sum_{i=1}^{n} u_{it}}. \quad (5)$$

Both of these expressions require that cluster t is not empty. Substituting (5) into (3) results in

the third term of (3) also being a constant, as is the first term. Therefore, optimization of the log-likelihood function requires only that the second term of (3) be optimized to define $u_{it}$. That is, the minimization criterion is

$$\frac{1}{2}\sum_{t=1}^{k}\left(\sum_{i=1}^{n} u_{it}\right)\log|S_t|. \tag{6}$$

Various special cases of the above have been considered. The first case assumes that all covariances are equal (i.e., $S_t = S$ for = 1,...,k). The expression (5) now becomes

$$S = \frac{1}{n}\sum_{i=1}^{n}\sum_{t=1}^{k} u_{it}(x_i-\mu_t)(x_i-\mu_t)^T, \tag{7}$$

and the objective criterion to be minimized becomes

$$\frac{1}{2} n \log|S|. \tag{8}$$

The k-means method is a special case of the above when S is reduced to a unity matrix multiplied by a constant factor such that

$$S=\sigma^2 I_p. \tag{9}$$

Introduction of this expression into the likelihood function defines a variance estimate as

$$\sigma^2=\frac{1}{np}\sum_{t=1}^{k}\sum_{i=1}^{n}\sum_{j=1}^{p} u_{it}(x_{ij}-u_{tj})^2. \tag{10}$$

The minimization criterion is then defined as

$$\frac{1}{2} np \log(\sigma^2). \tag{11}$$

As defined above, this expression indicates that the k-means method minimizes the distance between each data point and each cluster mean. The generalization of the k-means method defined by (6) allows each cluster to have its own covariance structure (i.e., shape). The second generalization defined by (7) specifies that each cluster has the same covariance structure, and the k-means generalization specifies that each cluster is spherical.

### 2. Fuzzy Clusters

The above formulation may be further generalized by relaxing the constraint on the $u_{it}$. That is, individual points do not need to belong to only one cluster, and the $u_{it}$ define the degree to which a point belongs to each cluster. The constraints on the $u_{it}$ are then

$$u_{it} \geq 0 \quad \textit{for all } i,t \ ,$$

and

$$\sum_{t=1}^{k} u_{it} = 1 \quad \textit{for all } i.$$

In the fuzzy case, the $u_{it}$ are called membership functions, and the above criteria imply that all $u_{it}$ are less than or equal to 1 for all i and t. Therefore, the primary difference between the fuzzy and hard clustering methods related to the log-likelihood function (3) is that the $u_{it}$ become continuous in the range [0,1]. Estimation of the $u_{it}$ based on the optimization of (3) must now take into account the above constraints. Examinations of the properties associated with these constraints have led to the recognition that truly fuzzy values of the $u_{it}$ can be obtained by squaring the different membership functions associated with terms specifying the distance between each point and the cluster center (Kaufman and Rousseeuw 1990). The linear term in (3) is replaced by a quadratic, but the $u_{it}$ remain equal to 0 and 1 at the

boundaries as defined by the above constraints. This specification allows minima to be reached at intermediate values of $u_{it}$ ($0 < u_{it} < 1$) in addition to values of 0 and 1. The modified log-likelihood function (3) is now written as

$$\phi = -\frac{1}{2}\sum_{t}\sum_{i}\left[u_{it}^{2}(x_i-\mu_t)^{T}S_t^{-1}(x_i-\mu_t)+u_{it}p\log(2\pi)+u_{it}\log|S_t|\right]. \quad (12)$$

This function can be differentiated with respect to the mean vector and covariance matrix to provide

$$\mu_t = \frac{\sum_{i=1}^{n} u_{it}^{2}x_i}{\sum_{i=1}^{n} u_{it}^{2}}, \quad (13)$$

and

$$S_t = \frac{\sum_{i=1}^{n} u_{it}^{2}(x_i-\mu_t)(x_i-\mu_t)^{T}}{\sum_{i=1}^{n} u_{it}}. \quad (14)$$

The objective function (12) can be rewritten by respectively collecting all terms that contain the square of the membership function and those that maintain an exponent equal to 1. The new form becomes

$$\phi = -\frac{1}{2}\sum_{t=1}^{k}\sum_{i=1}^{n}(u_{it}2A_{it} + u_{it}^{2}B_{it}), \quad (15)$$

where the $A_{it}$ contain the linear terms and the $B_{it}$ contain the quadratic terms. The combination of (15) with the constraints upon the $u_{it}$ can be rearranged to form a Lagrange

equation (Kaufman and Rousseeuw 1990). Setting the derivative of the Lagrange equation with respect to the $u_{it}$ equal to 0 and solving for the $u_{it}$ provides the optimal representation of the membership functions. These are defined as

$$u_{it} = \frac{1/B_{it}}{\sum_{t=1}^{k} (1/B_{it})} + \frac{1}{B_{it}} \left( \frac{\sum_{t=1}^{k} (A_{it}/B_{it})}{\sum_{t=1}^{k} (1/B_{it})} - A_{it} \right). \qquad (16)$$

Based on (12) and (15), the $B_{it}$ are defined as

$$B_{it} = (\boldsymbol{x}_i - \boldsymbol{\mu}_t)^T \boldsymbol{S}_t^{-1} (\boldsymbol{x}_i - \boldsymbol{\mu}_t). \qquad (17)$$

Therefore, the $B_{it}$ define the Mahalanobis distance between the observation $\mathbf{x}_i$ and the center of cluster t. This term will be equal to 0 if $\mathbf{x}_i$ is equal to the cluster center and infinity if $\mathbf{x}_i$ is an infinite distance from the center. Therefore, the first term of (16) varies between 0 and 1. Also from (12) and (15), the $A_{it}$ are defined as

$$A_{it} = \frac{1}{2} (p \log(2\pi) + \log|\boldsymbol{S}_t|). \qquad (18)$$

The first term in (18) is a constant and the second term contains the determinant of the covariance matrix associated with cluster t. Based upon (17) and (18), the specifications of the membership coefficients in (16) are assigned a value between 0 and 1 based on the distance between each point and the cluster centers, and then modified based upon the probability structure associated with each cluster. If all determinants of the covariance matrices are equal, then the second term of (16) would be equal to 0. Therefore, the

assignment of the membership coefficients would only be based upon the distance of each point to each cluster center. This condition corresponds to a fuzzy k-means algorithm.

### 3. Clustering Algorithm

In this section, the specific clustering algorithm is defined. A discussion of special considerations given to the sensitivity of the algorithm to the choice of seed points and the independence between observations follows from the algorithm definition. The fuzzy clustering method defined by (16), (17), and (18) is applied to the two leading VEOFs of the anomalous large-scale 700 mb circulations. Therefore, each $\mathbf{x}_i$ is composed of the two complex coefficients associated with the two leading VEOFs at time i (i.e., p = 2). Initially, the desired number of clusters, k, must be chosen. A random number generator is used to identify k seed points that define the initial centers of the clusters.

**Step 1:** Initial values of the membership coefficients are assigned to each observation based upon the distance to each seed point. The membership coefficient $u_{it}$ corresponding to the closest seed point t to observation $\mathbf{x}_i$ is set to 1, and all other membership coefficients for observation $\mathbf{x}_i$ are set to 0.

**Step 2:** For each cluster t, the mean vector and covariance matrix are calculated using (13) and (14).

**Step 3:** The new membership coefficients are evaluated using (16), (17), and (18). If no values of the new membership coefficients differ from the previous value by more than some small number, then stop the procedure; otherwise go to step 2.

Typically, the number of iterations required before the clustering algorithm converged is less than five for two clusters, and near 25 for 10 clusters.

The output of the clustering algorithm consists of a set of k membership coefficients for each observation (i.e., the $u_{it}$, for i = 1,2,...,n and t = 1,2,...,k), which define the degree to which an observation belongs to each cluster. An observation will be assigned to a cluster t if the membership coefficient for that cluster is at least twice as large as any other membership coefficient. If no membership coefficient satisfies this criterion, then the observation belongs to a diffuse cluster that may represent a transition between clusters.

An iterative procedure is followed to examine any sensitivity of the resultant groupings to the choice of seed points and the independence of the observations. For each choice of k clusters, repeated applications of the algorithm described above are begun by randomly choosing k different seed points. The first seed point is chosen from the entire set of 2754 observations (sample of 9 years with 306 12-h analyses between 00 UTC 1 June and 12 UTC 31 October). Beginning with this first seed point, every tenth observation going back to the start of the data set, and forward to the end of the data set is chosen to compose a reduced data set from which the remaining k-1 seed points are defined. That is, the independence between observations is simulated by the choice of every tenth observation, which corresponds to every fifth day. The cluster algorithm is then applied to the reduced data set. Because of the rapid convergence of the clustering algorithm, this procedure was repeated 100 times for each choice of k clusters. The stability of the final definition of clusters was examined using the mean and standard deviations of the cluster centers computed from the 100 reduced samples. Large standard deviations associated with the cluster centers indicate excessive sensitivity to the choice of seed points, or lack of independence between observations. However, the variability between cluster centers from the 100 reduced samples

is more a function of the number of clusters k than of the seed points or reduced sample. For values of k that are too small to adequately define the natural partitioning within the data set, the standard deviations associated with the cluster centers indicate a large amount variability among the 100 iterations. For larger values of k, very small standard deviations indicate that the cluster algorithm could consistently identify the primary partitions within the leading VEOF coefficients regardless of seed points and reduced sample size.

The final aspect of the clustering method to be examined concerns the number of clusters to be retained. Results of the stability analysis defined above indicate that stability of the cluster algorithm increases as the number of clusters increases. However, the number of realistic clusters within the data set must be estimated. Therefore, the procedure defined above is followed to determine the optimal number of clusters to be retained. That is, the number of clusters is increased until the additional cluster either represents a subset of extreme cases from a previously defined cluster, or the number of members within the new cluster is less than 10% of the next smallest cluster.

## B. CLUSTERS OF THE ANOMALOUS 700 MB LARGE-SCALE CIRCULATION

Results of the examinations regarding the number of clusters to retain and the sensitivity of the analysis to seed points or independence between observations indicated that six clusters provide an optimal partitioning of the two leading VEOF coefficients. Small standard deviations associated with cluster centers based on the 100 reduced samples and random seed points indicated no overlap between the centers. As a final step, the clustering algorithm is applied to the entire set of 2754 observations. The final set of cluster centers is well within one standard deviation of the mean cluster centers defined by the 100 reduced

samples. The cluster centers defined as an amplitude and phase angle for both leading VEOF coefficients, and the number of members in each cluster are provided in Table 8. Cluster 7 is the diffuse cluster containing observations with no dominant membership coefficients.

A schematic representation of the cluster results is provided in Fig. 43. The preferred phase orientations of VEOF 1 are 0° and 180° (Fig. 30). VEOF 1 is oriented towards 0° in clusters 1, 2 and 6, and towards 180° in clusters 3, 4, and 5. The preferred phase orientations of VEOF 2 are 0°, 45°, and 180°. VEOF 2 is oriented towards 0° in cluster 4 and 5; towards 180° in clusters 1, 2, and 3; and towards 45° in cluster 6. Therefore, the cluster analysis correctly identifies the major partitions within the separate components of the two leading VEOFs.

The VEOF analysis identified the basic modes of the variability of the anomalous 700 mb large-scale circulation. The cluster analysis is applied to the two leading VEOFs to identify the basic circulation patterns that could be composed of combinations of the two leading modes of variability. The schematic representation of the cluster centers (Fig. 43) suggests a rather symmetric structure to the partitioning of the variability of the anomalous large-scale circulations. The phase orientations of VEOF 1 in clusters 4, 5, and 6 are directly opposite to the orientations in clusters 1, 2, and 3. The orientations of VEOF 2 in clusters 1 and 2 are directly opposite to the orientations in clusters 4 and 5. The orientation of VEOF 2 in cluster 6 is shifted about 90° from the orientation in cluster 3. The symmetric structure of the cluster definitions seems similar to the symmetric structure of the tropical cyclone-based circulation transition patterns depicted in Fig. 11.

**TABLE 8** CLUSTER CENTERS. Centers are defined as the average amplitude and phase angle of the two leading VEOFs. The number of members within each cluster was determined from the membership coefficients. Cluster 7 represents the diffuse cluster containing observations that have no dominant membership coefficients. Amplitudes are nondimensional.

| | VEOF 1 | | VEOF 2 | | |
|---|---|---|---|---|---|
| | Amplitude | Phase | Amplitude | Phase | Members |
| Cluster 1 | 22.5 | 4.6° | 10.3 | 200.9° | 408 |
| Cluster 2 | 6.2 | 11.2° | 7.5 | 195.1° | 272 |
| Cluster 3 | 15.2 | 185.2° | 5.5 | 185.7° | 251 |
| Cluster 4 | 21.2 | 187.3° | 9.2 | 13.1° | 194 |
| Cluster 5 | 3.0 | 189.6° | 4.6 | 24.9° | 714 |
| Cluster 6 | 15.8 | 4.4° | 9.9 | 14.0° | 187 |
| Cluster 7 | - | - | - | - | 728 |

The amplitudes associated with cluster 5 are much smaller than the amplitudes associated with the other clusters. Cluster 5 also contains more members than any other cluster except for the diffuse cluster 7. These characteristics suggest that members of cluster 5 contain small anomalies with circulation patterns that are close to the climatological mean. The significance of such a cluster has been discussed by Molteni et al. (1990) with regard to nonlinear aspects of low-frequency dynamics associated with midlatitude circulation regimes. Linear models of atmospheric variability result in symmetric modes about the mean state of the system because the linear dynamical equations are symmetric with respect to the sign of the perturbation imposed on the basic state.

Nonlinear models of circulation variability identify asymmetric modes that have been described as transitions between a number of attractors (Lorenz 1963; Legras and Ghil 1985;

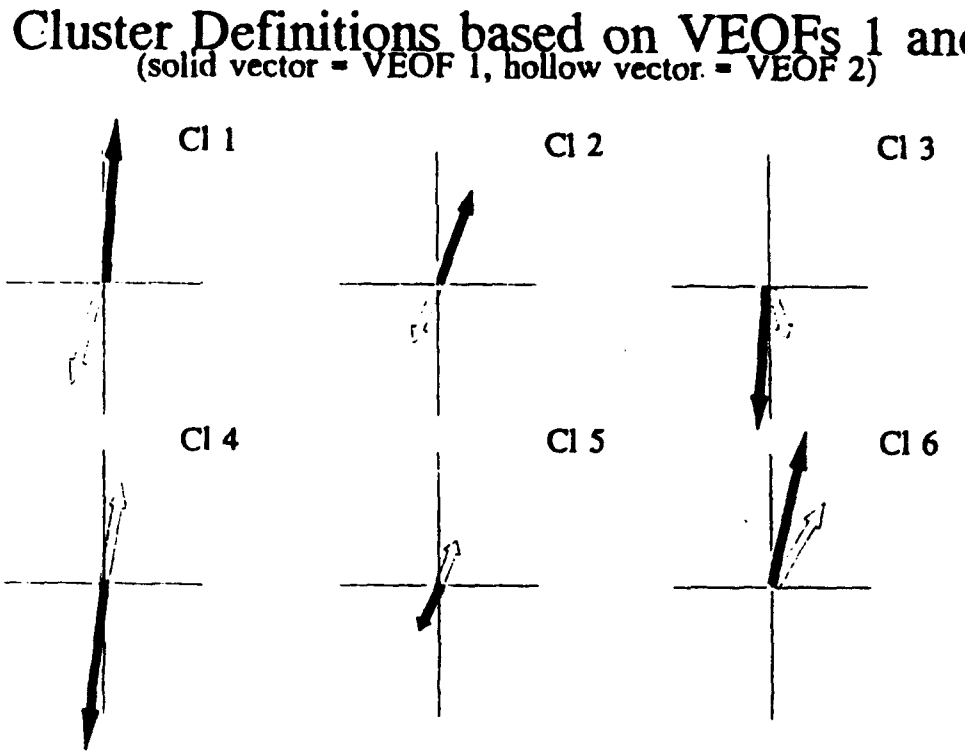


**Fig. 43** Schematic depiction of the orientation of the leading two VEOFs for each cluster. Phase angle is such that 0° is at the 12 o'clock position and increases clockwise. The length of each vector is proportional to the amplitude of the VEOF coefficient.

Mo and Ghil 1988). Therefore, the non-normal probability density estimates (e.g., bimodal distributions associated with blocking and zonal flow patterns) of atmospheric parameters reflect the dominance of nonlinear interactions within the atmospheric dynamical system. This can be interpreted as the self-interaction of an anomaly with itself, which tends to feed back onto the anomaly amplitude. The cluster analysis of Molteni et al. (1990) also includes a large cluster that lies close to the climatological mean. Based upon the above arguments, Molteni et al. conclude that this large cluster that straddles the mean state represents the portion of atmospheric variability where linear interactions are dominant. In their cluster analysis of midlatitude flow patterns based upon anomaly correlations, Mo and Ghil (1988) specifically require the existence of such a cluster. The existence of this cluster as determined by the fuzzy cluster algorithm applied to the leading VEOFs is solely determined by the internal distribution of the data, as was the cluster defined by the method employed by Molteni et al. (1990).

In the following subsections, the cluster patterns and relationships to tropical cyclone characteristics and large-scale circulation features are examined. The anomalous 700 mb large-scale circulation patterns and OLR anomalies associated with each cluster are defined by compositing all members of each cluster. The number of fields contained in each composite is defined by the number of members in each cluster provided in Table 8. The circulation pattern associated with each cluster is also compared to the tropical cyclone-based circulation patterns to identify relationships between the clusters and tropical cyclone track types. In the second subsection, the relationship between each cluster and tropical cyclone track types is quantified using a contingency table analysis. In the final section, the anomalous global 200

mb and 700 mb streamfunction and velocity potential will be described to provide a more complete depiction of the large-scale circulation patterns associated with each cluster.

### 1. 700 mb Circulation and OLR Anomalies Associated with Each Cluster

Cluster 1, which is defined by a 0° orientation of VEOF 1 and a 180° orientation of VEOF 2, is dominated by an active monsoon trough at 700 mb (Fig. 44a). Anomalous cyclonic circulations define the extent of the monsoon trough, which is oriented from central India to the Philippine Sea. Negative OLR anomalies representing enhanced convection exist along the axis of the large-scale region of cyclonic anomalies. Anticyclonic anomalies along 20°N between 110°-160°E indicate that the subtropical ridge is stronger than normal. However, no large positive OLR anomalies are associated with this anomalous ridge circulation. Cyclonic anomalies are found east of Japan between 30°-40°N. These anomalies seem to be coupled with the tropical cyclonic and subtropical anticyclonic anomalies to the southwest, which is suggestive of a Rossby wave-like pattern that may be tied to the large region of enhanced convection associated with the monsoon trough. Examination of the 200 mb and 700 mb streamfunction anomalies will be used later to confirm this relationship.

The circulation patterns associated with cluster 1 resemble the straight-moving tropical cyclone-based circulation pattern (Fig. 3a). The enhanced monsoon trough, which is distinguished by the large cyclonic anomalies and negative OLR anomalies, suggests that cluster 1 would be associated with active tropical cyclone periods. Because of the strong subtropical ridge, cluster 1 would be identified with straight-moving tropical cyclones.

The orientation of each VEOF in cluster 2 is similar to the orientations defined with cluster 1, but the amplitudes of the vectors are smaller (Fig. 43). Similarly, the cluster 2

anomalies (Fig. 44b) are also smaller than the cluster 1 anomalies. Although the strength of the anomalous monsoon trough in cluster 2 is smaller than cluster 1, the subtropical anomalous anticyclonic circulation in cluster 2 covers a larger area than the corresponding feature in cluster 1. Large positive OLR anomalies are coincident with the anticyclonic anomalies over the subtropical western Pacific, which indicates less convection than normal. Thus, cluster 2 seems to have a stronger subtropical ridge. Although the cluster 2 circulation pattern is dominated by the strong subtropical ridge, the cyclonic anomalies and negative OLR anomalies over the monsoon trough region suggest cluster 2 would also be associated with tropical cyclone activity. Furthermore, the strong ridge suggests straight-moving tracks would be most likely.

Cluster 3 is defined by a 180° orientation of VEOF 1 and 2 (Fig. 43). Anticyclonic anomalies cover the entire region of the monsoon trough from central India through the South China Sea (Fig. 44c). These anticyclonic circulations are connected to a large anomalous anticyclonic circulation between 10°-30°N and 125°E-180°E that has a southwest-to-northeast orientation. Less convection than normal is found over this entire region (Fig. 44c). A small cyclonic anomaly in the vicinity of Taiwan has a corresponding region of negative OLR anomalies (i.e., enhanced convection). A large region of enhanced convection is centered on the equator near 90°E. The OLR anomaly pattern associated with this cluster is similar to one branch of an observed seesaw in large-scale convection between the equatorial Indian Ocean and the tropical western North Pacific (Weickmann and Khalsa 1990). The dominance of anticyclonic anomalies over both the region of the monsoon trough

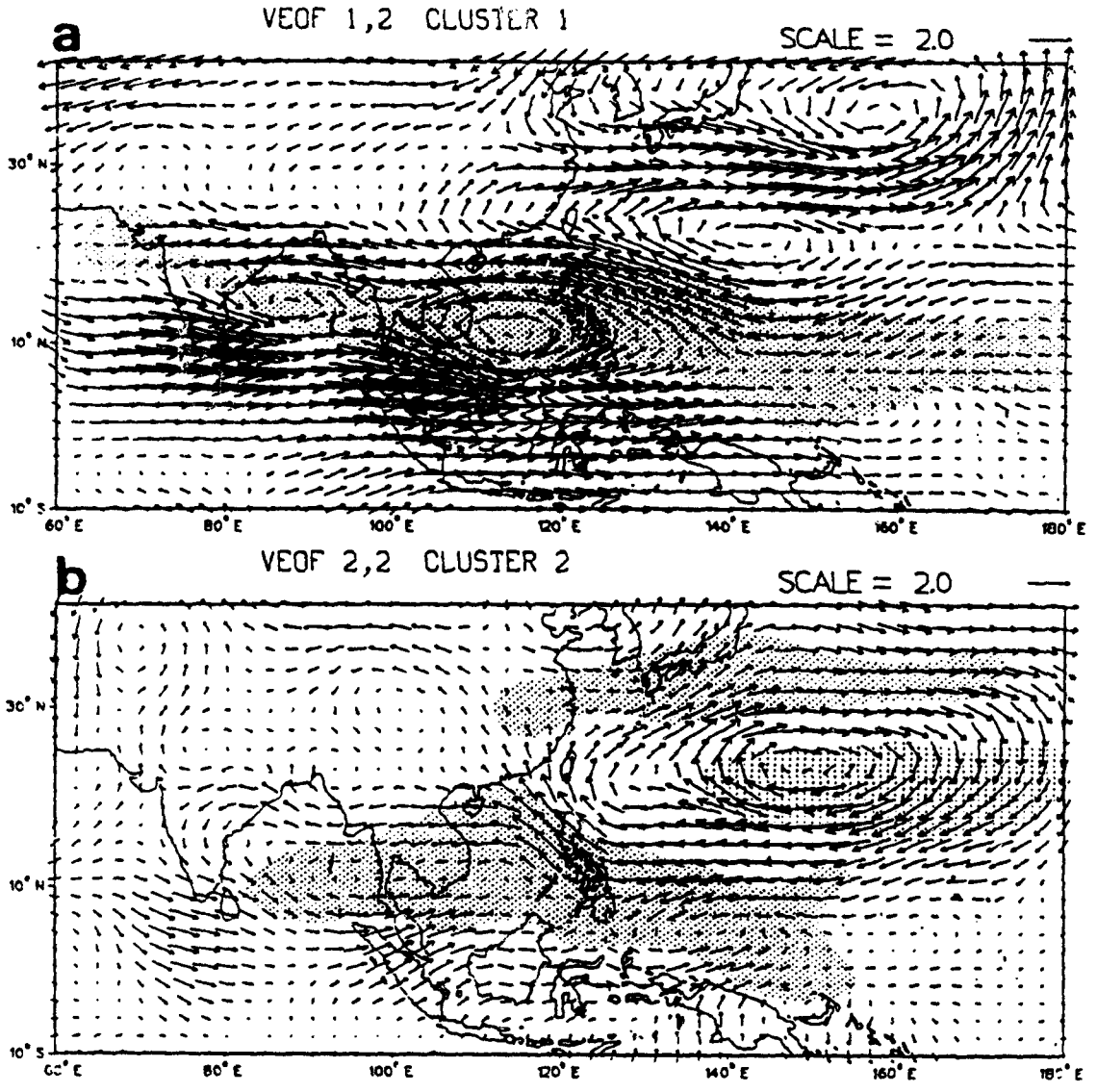


**Fig. 44** Composite of 700 mb wind anomalies (m $s^{-1}$) based on each of the six cluster centers. Dense shading denotes areas where the OLR anomalies are below -5 W $m^{-2}$. Light shading denotes enhanced convective areas where the OLR anomalies are greater than 5 W $m^{-2}$.

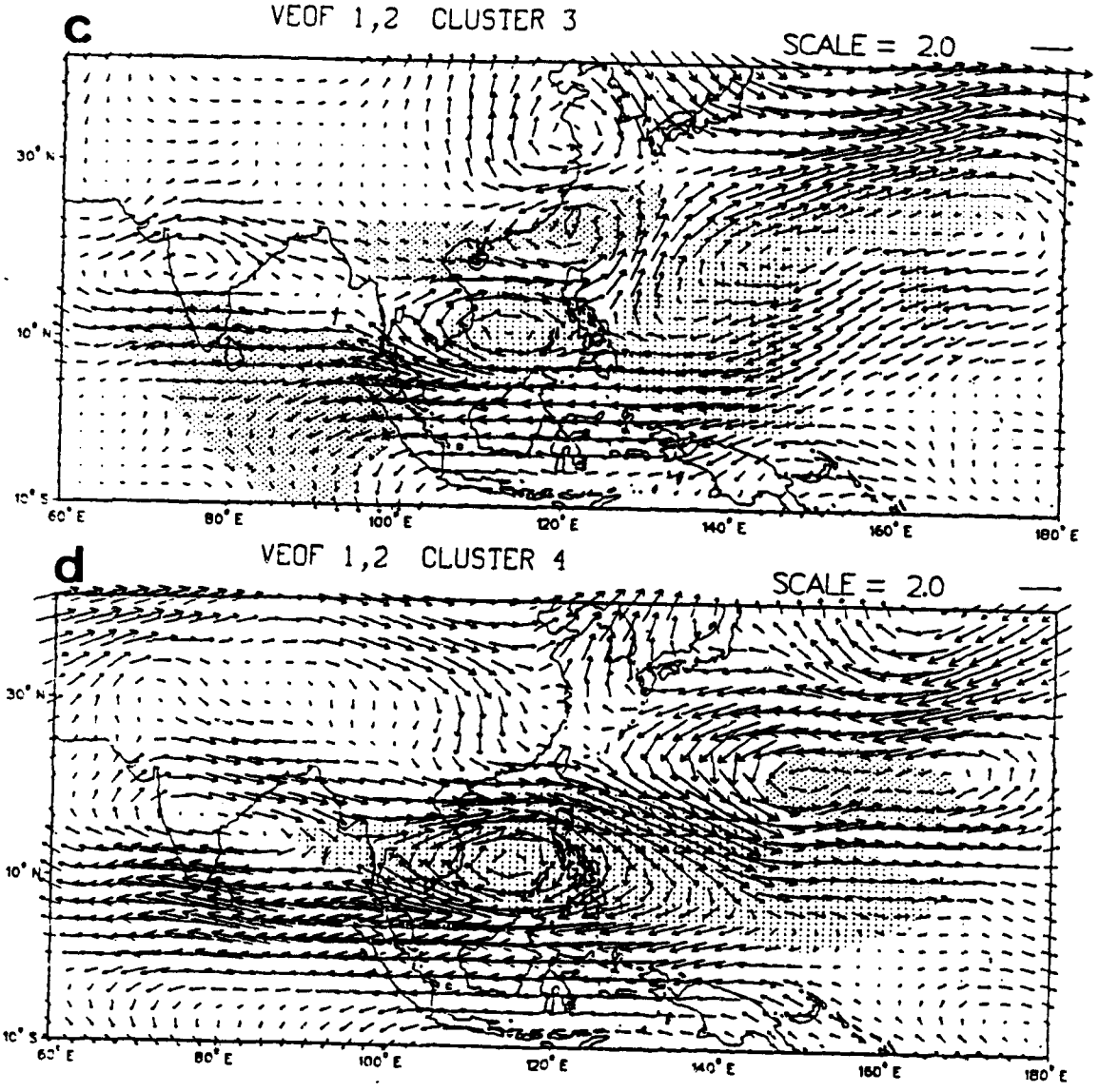


**Fig. 44** (continued).

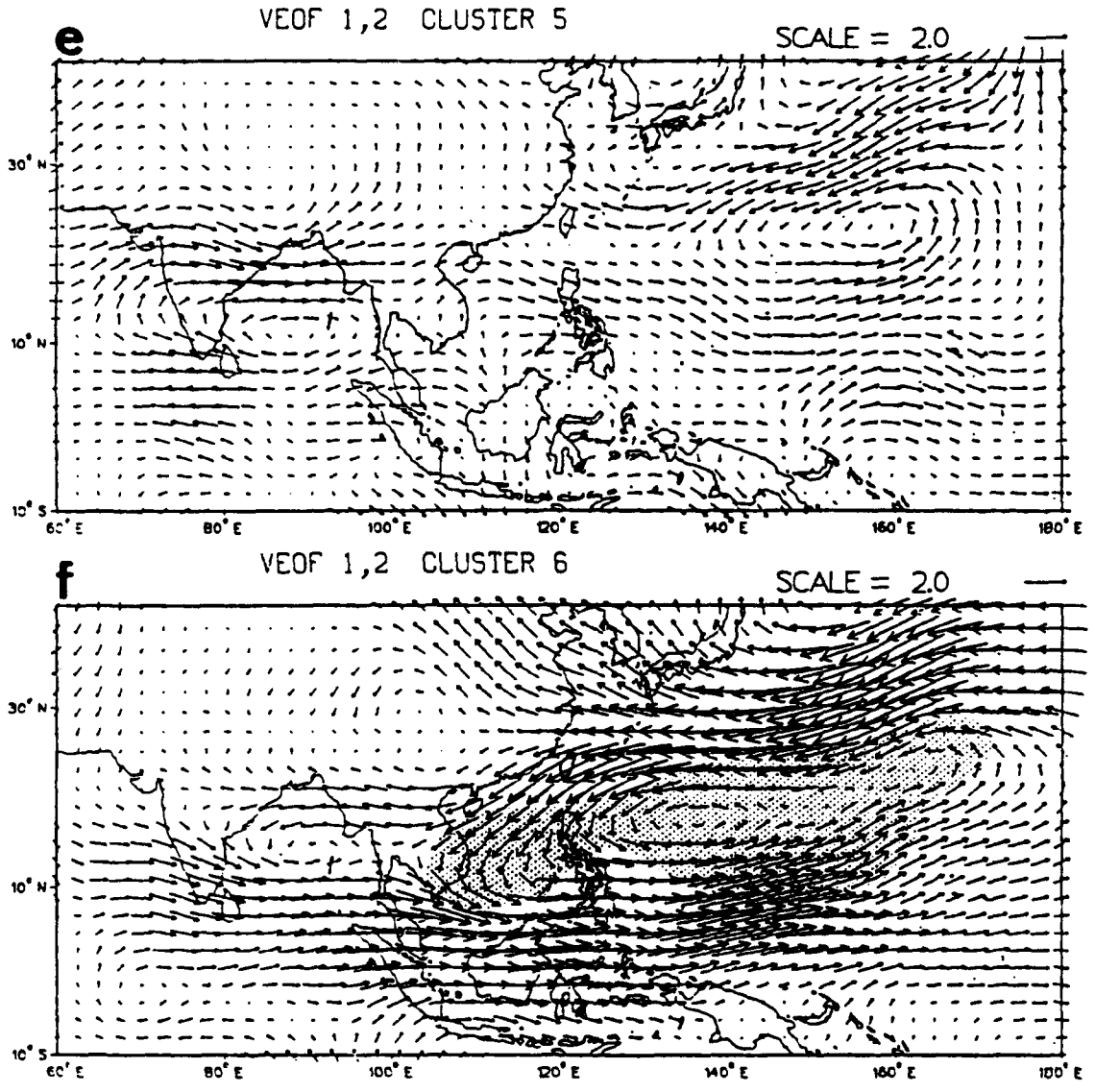


**Fig. 44** (continued).

and subtropical ridge suggest that cluster 3 would be associated with inactive periods of tropical cyclones.

The orientations of each VEOF in cluster 4 are opposite to the orientations in cluster 1. Consequently, the anomalous 700 large-scale circulations and OLR anomalies associated with cluster 4 (Fig. 44d) are opposite to the patterns of cluster 1 (Fig. 44a). Anticyclonic anomalies extend from central India to the South China Sea and Philippine Sea, which indicates a weak monsoon trough. Positive OLR anomalies, which indicate reduced convection, are coincident with the anticyclonic circulation anomalies. A large cyclonic anomaly along 25°N between 130°E-180°E indicates that the subtropical ridge is weaker than normal. Negative OLR anomalies associated with enhanced convection are found within the center of this large anomalous cyclonic circulation. Anticyclonic anomalies also occur at 40°N to the east of Japan. Therefore, the three primary circulation features present in cluster 1 are also present in cluster 4, but in the opposite sense.

The cluster 4 circulation pattern is very similar to the recurving-north tropical cyclone-based pattern (Fig. 4). A weak monsoon trough and weak subtropical ridge suggests that tropical cyclogenesis would tend to occur at higher latitudes over the subtropical western North Pacific, and recurving tracks would be most likely.

The amplitudes associated with the VEOFs describing cluster 5 are much smaller than the other clusters (Fig. 43, Table 8). Although the anomalous 700 mb circulation pattern has a cyclonic anomaly centered at 20°N and 160°E and an anticyclonic anomaly over the Bay of Bengal, the amplitudes of the anomalies associated with cluster 5 are small (Fig. 44e). Furthermore, no regions of significant negative or positive OLR anomalies are present.

The small wind and OLR anomalies associated with cluster 5 are consistent with the interpretation that this cluster straddles the climatological mean state over the tropical Indian Ocean and western Pacific. Because of the small wind and OLR anomalies associated with the cluster 5 circulation patterns, it is not possible to estimate whether cluster 5 would be associated with active or inactive periods or whether a specific track type would be preferred. It will be shown below that cluster 5 is associated with periods containing variable activity and track types, which is also consistent with the interpretation of this cluster's relationship with the climatological mean state.

Cluster 6 represents an active monsoon trough plus a weak subtropical ridge (Fig. 44f). Cyclonic anomalies are oriented east/west from central India to the Philippine Sea. These anomalies associated with the monsoon trough are connected to cyclonic anomalies that are oriented from the southwest to the northeast over the subtropical western Pacific. The largest negative OLR anomalies (enhanced convective clouds) are located with the subtropical cyclonic anomalies.

The circulation pattern associated with cluster 6 suggests a combination of the recurving-south and recurving-north tropical cyclone-based patterns (Figs. 3, 4). The enhanced monsoon trough is associated with tropical cyclone activity over lower latitudes, and the weak subtropical ridge is identified with recurving-south tracks. Furthermore, the extent of the weak ridge, and the negative OLR anomalies extending over the subtropical western Pacific are suggestive of tropical cyclogenesis over the subtropical latitudes, which would be a recurving-north track.

Although the clusters are defined from the basic structure of the anomalous 700 mb large-scale circulation, many of their qualities are similar to the tropical-cyclone based anomalous large-scale patterns. The relationships between tropical cyclone characteristics and the cluster patterns will be examined below, after more complete physical descriptions of the cluster patterns are defined.

### 2. Large-scale Streamfunction and Velocity Potential Anomalies Associated with Each Cluster

A more complete description of the physical characteristics associated with each cluster may be obtained by examining the anomalous 700 mb and 200 mb streamfunction and velocity potential anomalies for each cluster. The streamfunction ($\psi$) and velocity potential ($\chi$) are defined as

$$\nabla^2\chi = \delta, \qquad \nabla^2\psi = \zeta,$$

where the divergence ($\delta$) and relative vorticity ($\zeta$) are defined

$$\delta = \frac{\partial u}{\partial x} + \frac{\partial v}{\partial y}, \qquad \zeta = \frac{\partial v}{\partial y} - \frac{\partial u}{\partial x}.$$

These quantities are computed on the Global Band Analysis Mercator grid using the appropriate map factor, and Method II of Shukla and Saha (1974). The velocity potential equation is solved by setting the north/south boundary values to 0. The computed values of the velocity potential are then used to determine boundary conditions for the streamfunction. The north/south boundaries (60°N and 40°S respectively) are sufficiently far from the tropical latitudes to avoid any irregularities over that region. The anomalies are computed using the same method as for the 700 mb wind components.

### *a. Streamfunction Anomalies*

Comparisons between the 700 mb and 200 mb streamfunction anomalies and the 700 mb anomalous circulations for each cluster (Fig. 44) will help clarify the large-scale features associated with the cluster patterns. A global domain is examined to identify any characteristics that are larger in scale than the Indian Ocean and western North Pacific regions. The anomalous streamfunction and velocity potential patterns associated with each cluster are defined by the same compositing procedure used to derive the anomalous 700 mb winds and the anomalous OLR patterns. Again, the number of fields in each composite is equal to the number of members in each cluster (Table 8).

The 700 mb streamfunction anomaly pattern for cluster 1 is dominated by the cyclonic anomalies associated with the enhanced monsoon trough (Fig. 45b). Small anticyclonic anomalies near 25°N, 140°E are related to the strong subtropical ridge (Fig. 44a). The cyclonic anomalies east of Japan in the cluster 1 pattern (Fig. 44a), which were suggestive of a Rossby wave-like pattern seem more representative of a midlatitude anomaly feature in the anomalous 700 mb streamfunction field (Fig. 45b). This is also suggested by the 200 mb streamfunction field (Fig. 45a) in which the cyclonic anomalies over the Sea of Japan are more representative of a midlatitude feature.

The dominance of the anomalous subtropical ridge in cluster 2 is emphasized over the subtropical western North Pacific at 700 mb (Fig. 46b). However, the most dominant feature at 200 mb is a Rossby wave-like pattern that begins over the central North Pacific and extends southeastward to the Gulf of Mexico, with a hint of a second arch-like pattern over the North Atlantic (Fig. 46a). Wave-like patterns are also evident (although

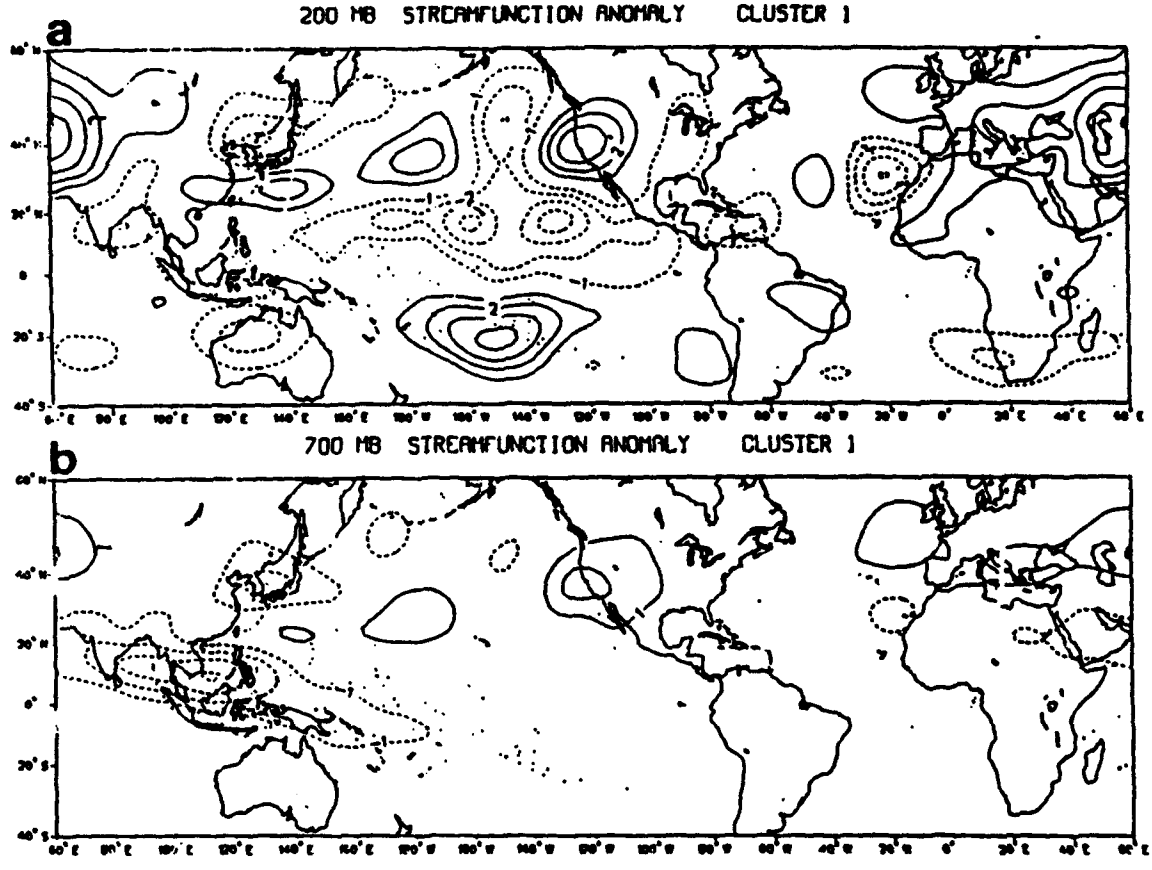


**Fig. 45** Streamfunction anomalies at (a) 200 mb and (b) 700 mb associated with cluster 1. The contour interval is 1 x $10^6$ $m^2$ $s^{-1}$.

weaker) in the 700 mb anomalous streamfunction data, which implies an equivalent barotropic structure associated with the wave pattern. The curious aspect of this pattern is that it does not seem to emanate from a tropical source as described by many theoretical (Hoskins and Karoly 1981; Simmons et al. 1983; Sardeshmukh and Hoskins 1988) and observational (Kurihara and Tsuyuki 1987; Lau and Phillips 1986; Kiladis and Weickmann 1992) studies of Rossby wave-like features. Rather, the wave train could be related to orographic forcing within the midlatitudes (Charney and DeVore 1979; Hoskins and Karoly 1981) that is occurring consistently when the tropical circulation features are represented by cluster 2.

No anomalies are found over the Southern Hemisphere associated with this cluster and most of the other clusters. This is most likely due to the lack of data over the Southern Hemisphere, which would tend to force the Global Band Analysis to a near-climatological state.

The 700 mb streamfunction anomalies associated with cluster 3 are dominated by the large anticyclonic circulation that exists over the South China Sea and extends northeastward over the subtropical western Pacific (Fig. 47b). The large 200 mb anticyclonic anomalies over the subtropical North Pacific indicate that the northernmost portion of the anticyclonic anomalies in cluster 3 exhibit an equivalent barotropic structure. However, a baroclinic structure is evident over the South China Sea with upper-level cyclonic anomalies overlying the 700 mb anticyclonic anomalies. No other coherent anomaly patterns are associated with cluster 3 over the remainder of the globe.

The 700 mb streamfunction anomalies associated with cluster 4 (Fig. 48b) are very similar to the 700 mb vector anomalies (Fig. 44d). The only dominant features

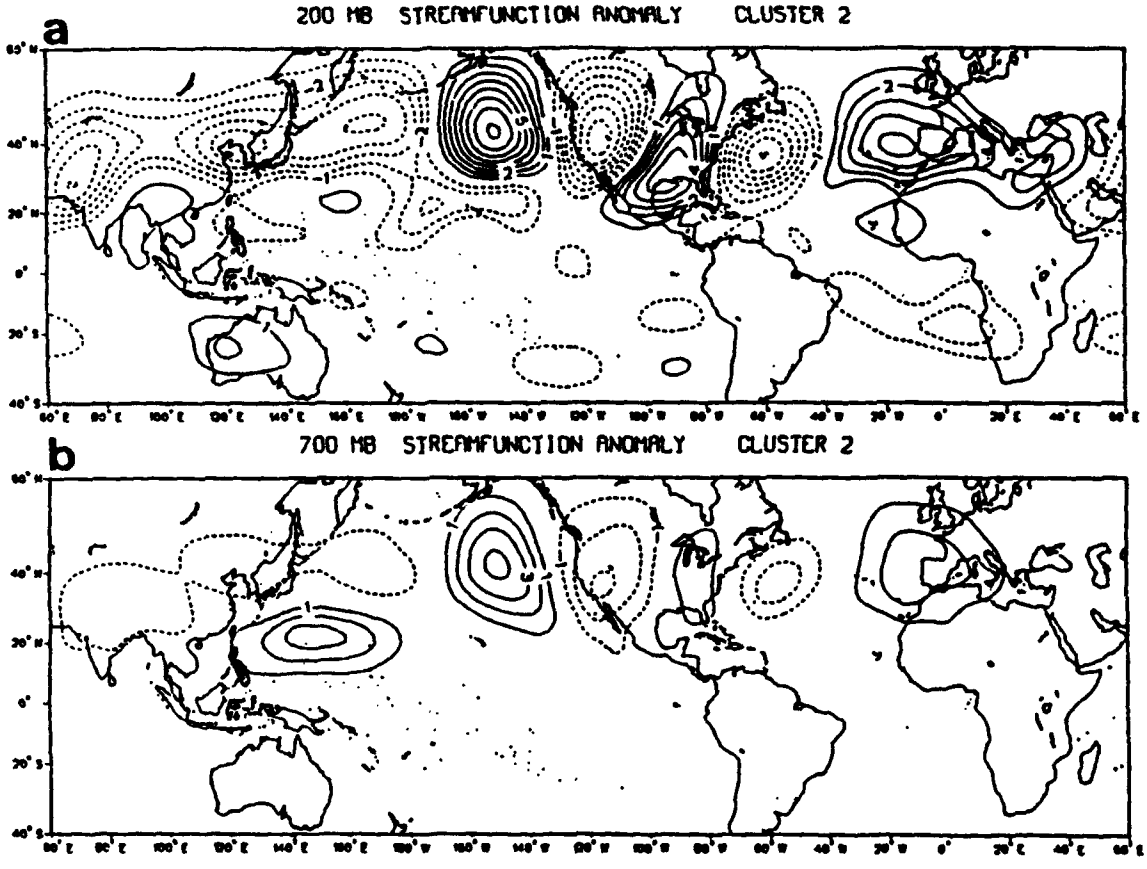


**Fig. 46** As in Fig. 45, except for cluster 2.

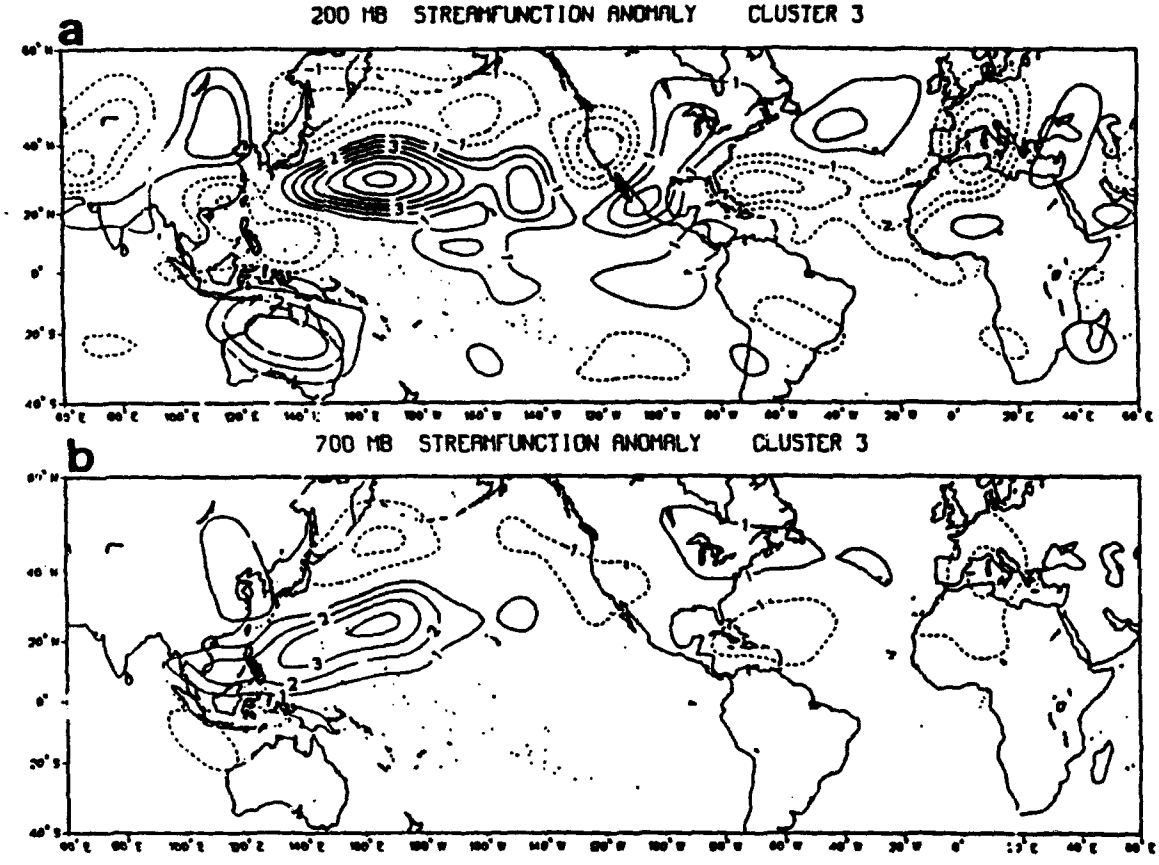


**Fig. 47** As in Fig. 45, except for cluster 3.

are over the Indian Ocean and the western Pacific. Anticyclonic anomalies over central India and the South China Sea and cyclonic anomalies over the subtropical Pacific indicate a weak monsoon trough and a weak subtropical ridge. The 200 mb anomalies suggest that the anomalies associated with the subtropical ridge are equivalent barotropic while the anomalies associated with the monsoon trough are baroclinic. The coupling of the anticyclonic anomalies over the subtropical Pacific and cyclonic anomalies immediately to the north is similar to the West Pacific teleconnection pattern identified by Wallace and Gutzler (1981).

No appreciable 700 mb or 200 mb streamfunction anomalies over the Indian Ocean or western Pacific are associated with cluster 5 (Figs. 49a,b). This is expected given the small amplitudes of VEOF 1 and 2 in cluster 5 and the vector wind fields in Fig. 44e.

The anomalous 700 mb streamfunction (Fig. 50b) associated with cluster 6 is consistent with the large cyclonic anomalies connecting an active monsoon trough and a weak subtropical ridge (Fig. 44f). The anticyclonic anomalies east of Japan at 150°E suggest that the subtropical ridge is displaced northward by a monsoon trough that protrudes eastward and northward over the subtropical North Pacific. The anomalies associated with the active monsoon trough exhibit a baroclinic structure south of 20°N (Fig. 50a). The small 200 mb cyclonic anomalies over the East China Sea suggest a change to an equivalent barotropic structure north of 20°N. The coupling of 200 mb anticyclonic anomalies over the South China Sea and Philippine Sea with cyclonic anomalies over the East China Sea and cyclonic anomalies over the midlatitudes northeast of Japan is suggestive of a Rossby wave-like pattern emanating from the region of enhanced convection over the western Pacific (Fig. 44f). Also

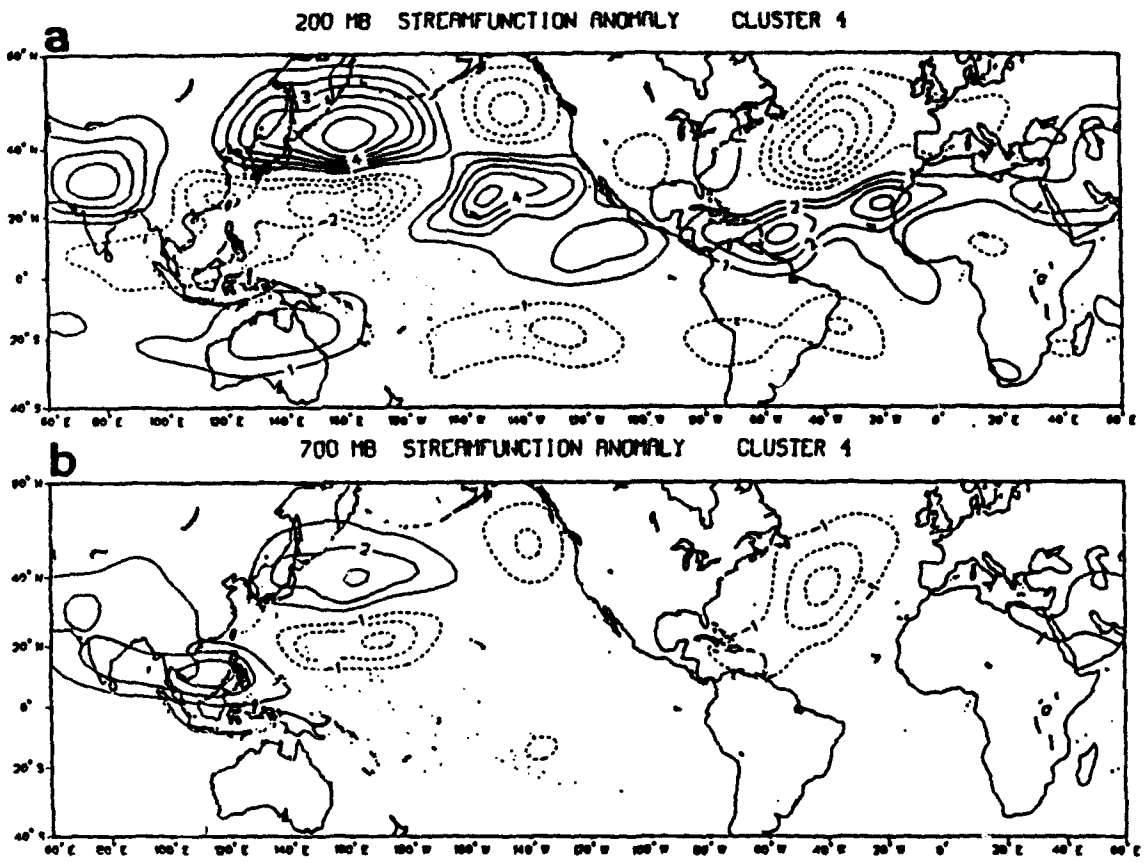


**Fig. 48** As in Fig. 45, except for cluster 4.

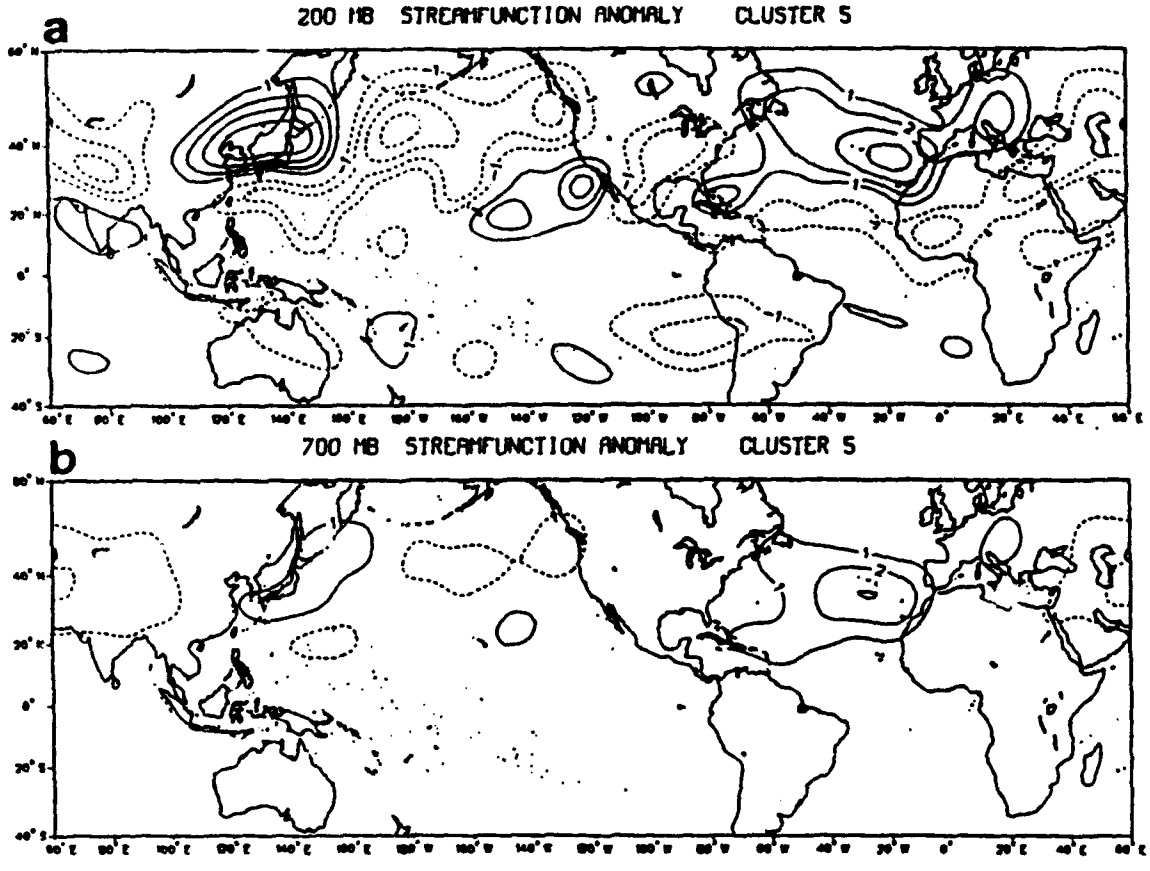


**Fig. 49** As in Fig. 45, except for cluster 5.

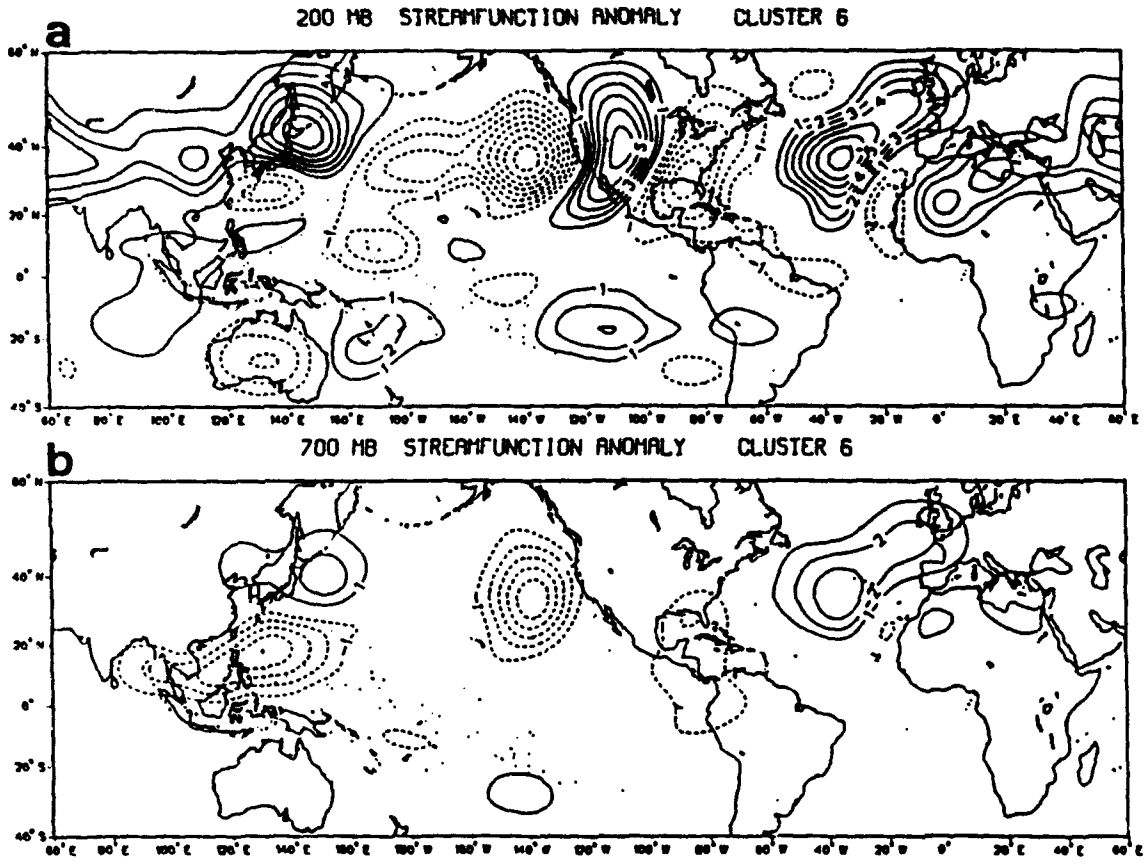


**Fig. 50** As in Fig. 45, except for cluster 6.

an indication of a 200 mb wave-like feature is present over North America (Fig. 50a) which does not seem to be directly related to the western Pacific circulation or heating anomalies.

### *b. Velocity Potential Anomalies*

. The anomalous velocity potential illustrates regions of anomalous convergence and divergence with the irrotational flow defined by the velocity potential directed perpendicular to th : contours from positive to negative values. Comparisons between the 200 mb and 700 mb convergence and divergence patterns provide a qualitative estimate as to the sense of the vertical motion between these levels.

A large region of anomalous convergence (divergence) at 700 mb (200 mb) over the maritime continent is associated with cluster 1 (Fig. 51). This irrotational flow pattern is consistent with the active monsoon trough and the large area of enhanced convection in Fig. 44a. Although the negative OLR anomalies indicate enhanced convection over the Bay of Bengal and central India (Fig. 44a) and anomalous divergence at 200 mb is present over these regions, the primary region of 700 mb convergence is concentrated east of 100°E. An opposite velocity potential pattern exists over the eastern equatorial Pacific where anomalous divergence (convergence) occurs at 700 mb (200 mb). The vertical motion suggested by the dipole in velocity potential anomalies between the western and eastern equatorial Pacific implies that an anomalous Walker circulation exists with the primary upward branch over Indonesia and the downward branch over the Eastern Pacific. In general, the anomalous velocity potential appears as a global zonal wavenumber 1 feature with the ascent branch over the maritime continent and the descent branch over the remainder of the equatorial regions analogous to a winter season Walker circulation.

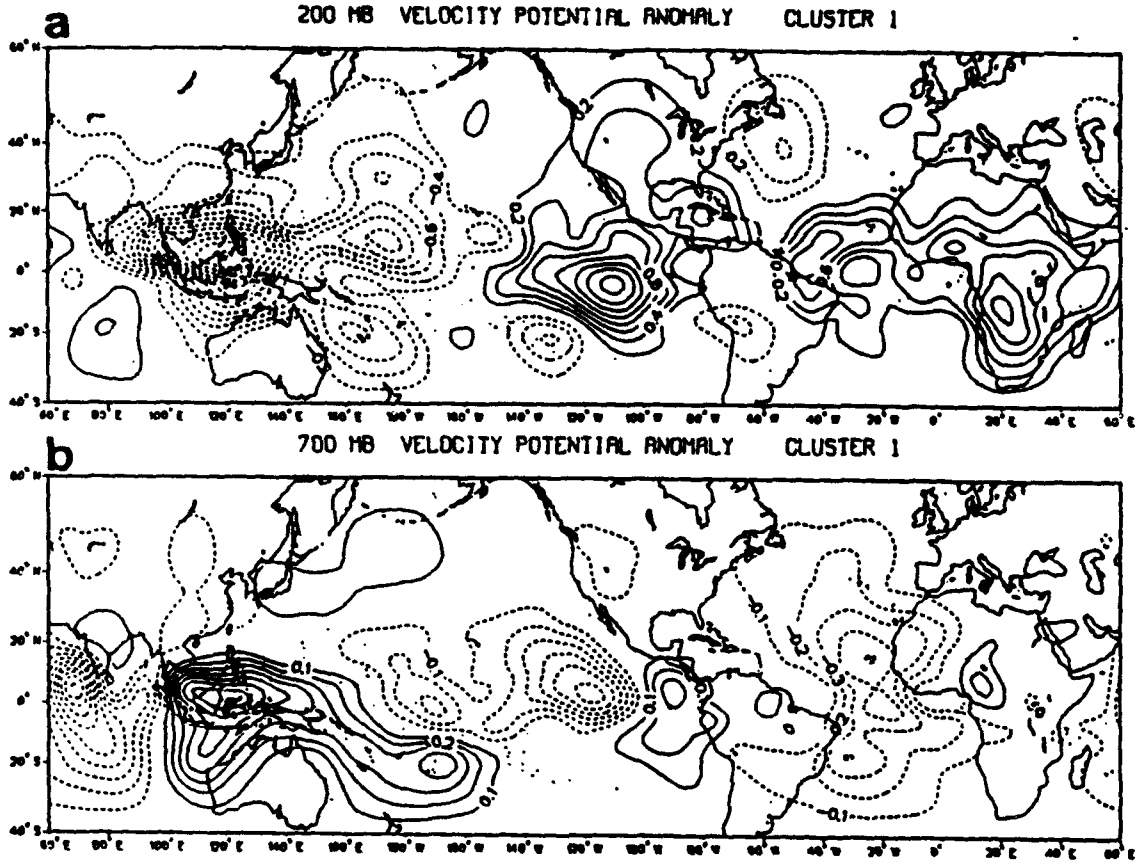


**Fig. 51** Velocity potential anomalies at **(a)** 200 mb and **(b)** 700 mb associated with cluster 1. The contour interval is 0.2 x $10^6$ $m^2$ $s^{-1}$ at 200 mb, and 0.1 x $10^6$ $m^2$ $s^{-1}$ at 700 mb.

The velocity potential anomalies over Indonesia associated with cluster 2 (Fig. 52) are similar to the anomalies identified with cluster 1, and consistent with the enhanced monsoon trough and convection over this region (Fig. 44b). The magnitudes of the anomalous 700 mb convergence and 200 mb divergence are smaller for cluster 2, which is consistent with the cluster definition (Fig. 44).

The velocity potential anomalies for cluster 2 (Fig. 52) appear as a zonal wavenumber 2 pattern with the primary ascent branches over the maritime continent, and the Central American monsoon and Amazon basin regions. The primary descent branch associated with the maritime continent ascent region is located over the subtropical Central Pacific, which is consistent with the anomalous 700 mb subtropical ridge described by cluster 2 (Fig. 44b). These anomalous convergence-divergence pattern and inferred vertical motions are similar to descriptions by Magana and Yanai (1991) of fluctuations in the tropical upper-tropospheric trough (TUTT) associated with convection over the maritime continent. The descent regions associated with the convection over Central and South America are also located adjacent to these ascent regions. The differences between the wavenumber 1 pattern associated with cluster 1 and the wavenumber 2 pattern of cluster 2 may be due to the strength of the convection (upward branch) over the maritime continent, which contributes to the Walker circulation exhibiting a larger influence on the global-scale circulation. However, more regional features in cluster 2 are evident when the convection over Indonesia is weakened.

In association with cluster 3 (Fig. 53), large-scale anomalous divergence (convergence) is found at 700 mb (200 mb) over the South China Sea and subtropical western

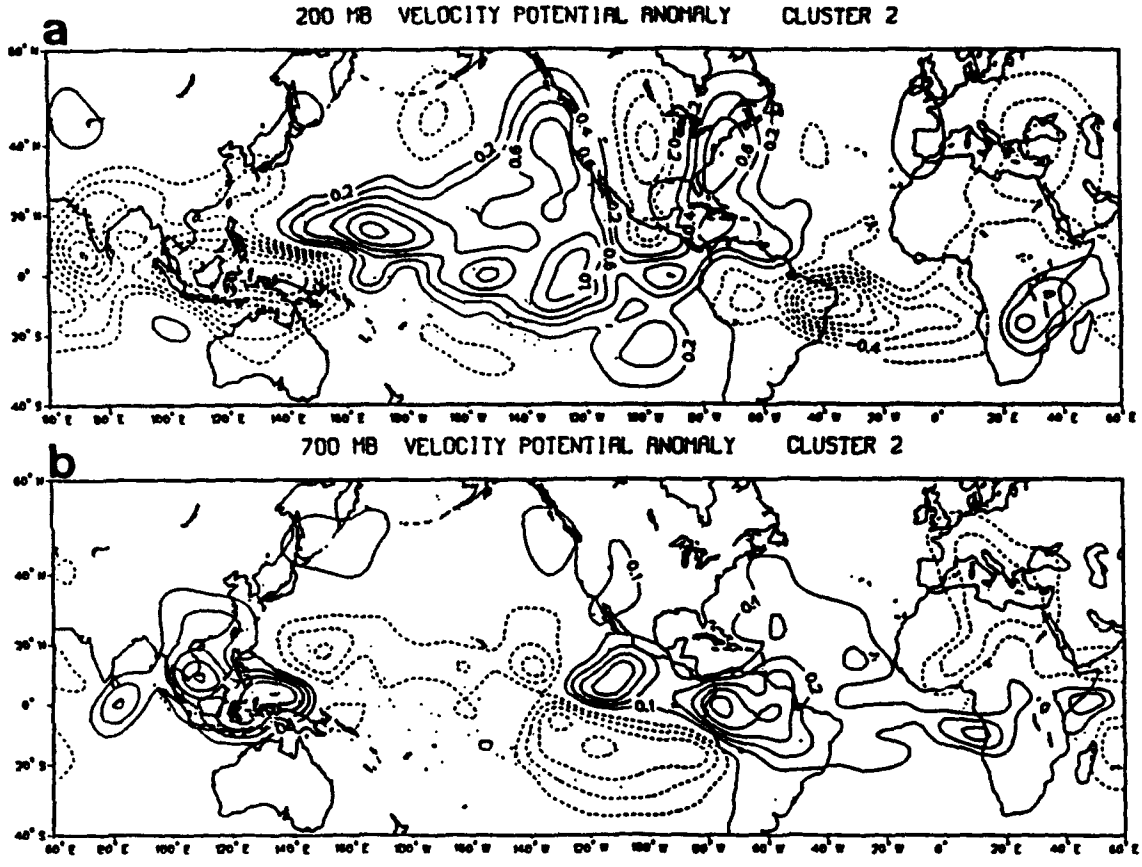


**Fig. 52** As in Fig. 51 except for cluster 2.

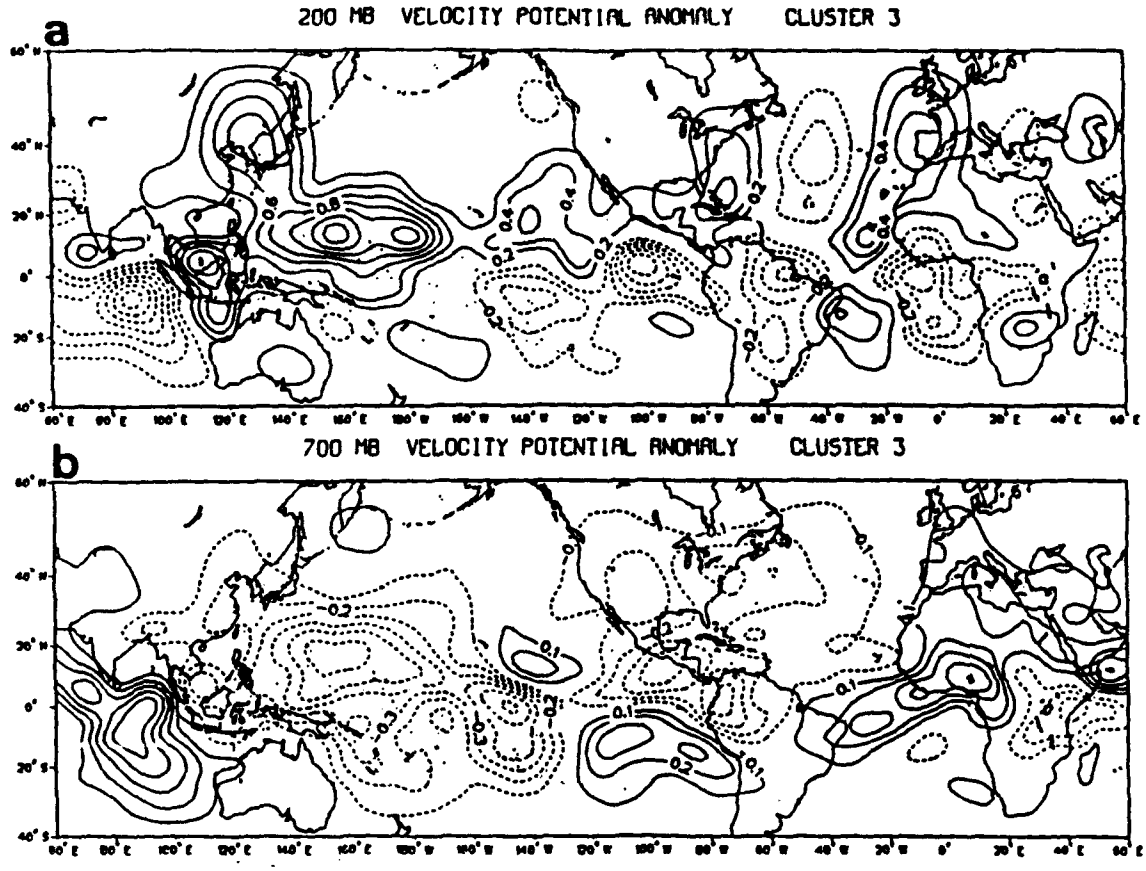


Fig. 53 As in Fig. 51, except for cluster 3.

North Pacific. This pattern may be identified with large-scale anomalous sinking motion over this region, which would be consistent with 700 mb anticyclonic anomalies and positive OLR anomalies (Fig. 44c). The region of enhanced convection identified in Fig. 44c by the negative OLR anomalies along the equator between 80°-100°E is associated with anomalous divergence (convergence) at 200 mb (700 mb).

The anomalous 200 mb velocity potential identified with cluster 4 has a global zonal wavenumber 1 structure (Fig. 54a) that is almost opposite to the cluster 1 anomalies (Fig. 51a). The primary anomalous convergent cell of this wavenumber 1 pattern is centered over the South China Sea. Anomalous divergence is found at 700 mb over the same region (Fig. 54b). This anomalous 700 mb (200 mb) divergence (convergence) pattern over the tropical western Pacific is consistent with the inactive monsoon trough and positive OLR anomalies over that region (Fig. 44d).

No coherent large-scale velocity potential anomalies are associated with cluster 5 (Fig. 55). This is consistent with the vector wind and OLR composites (Fig. 44e) and the small amplitudes of the VEOF components (Fig. 43e). The absence of coherent anomalies is also consistent with the previous interpretation that cluster 5 is associated with the climatological tropical pattern.

The anomalous 200 mb velocity potential identified with cluster 6 also appears as a global zonal wavenumber 1 pattern (Fig. 56a). The primary divergent region at 200 mb is located over the South China Sea and Philippine Sea. The southwest to northeast orientation of the large-scale divergence anomaly is consistent with a similar orientation in the

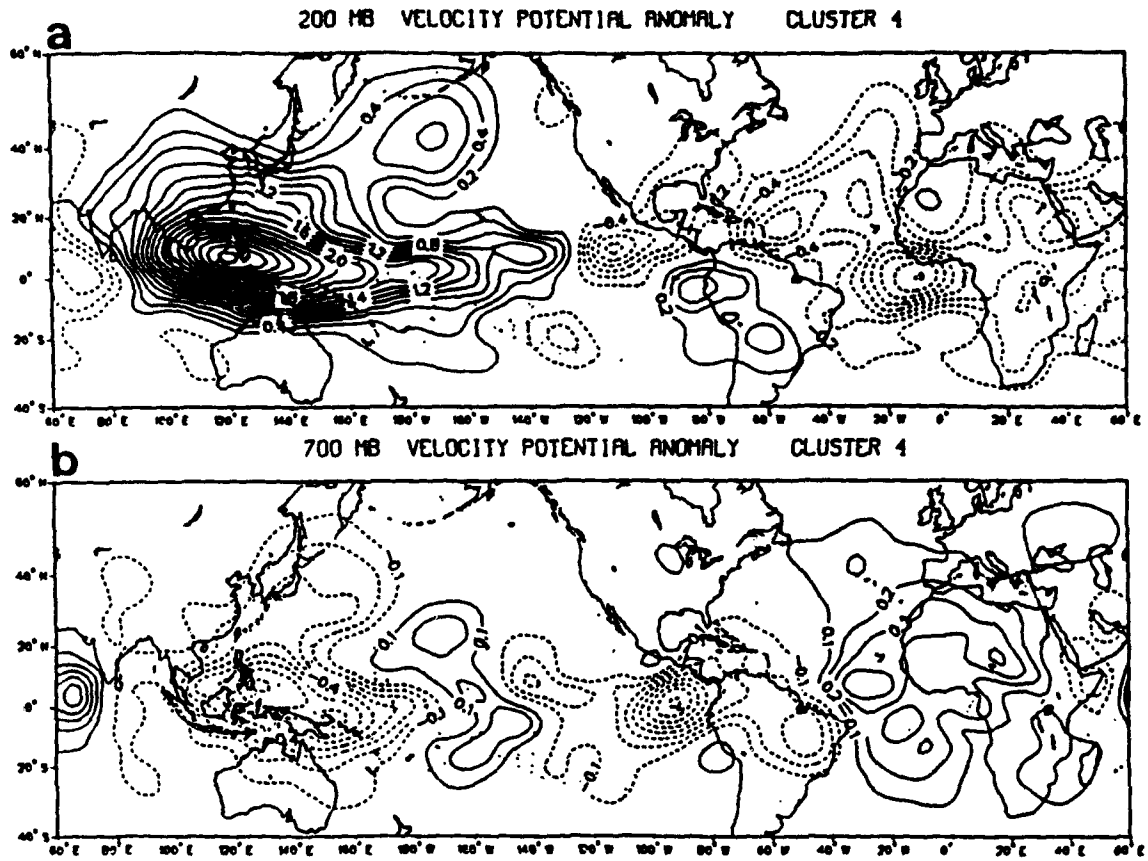


**Fig. 54** As in Fig. 51, except for cluster 4.

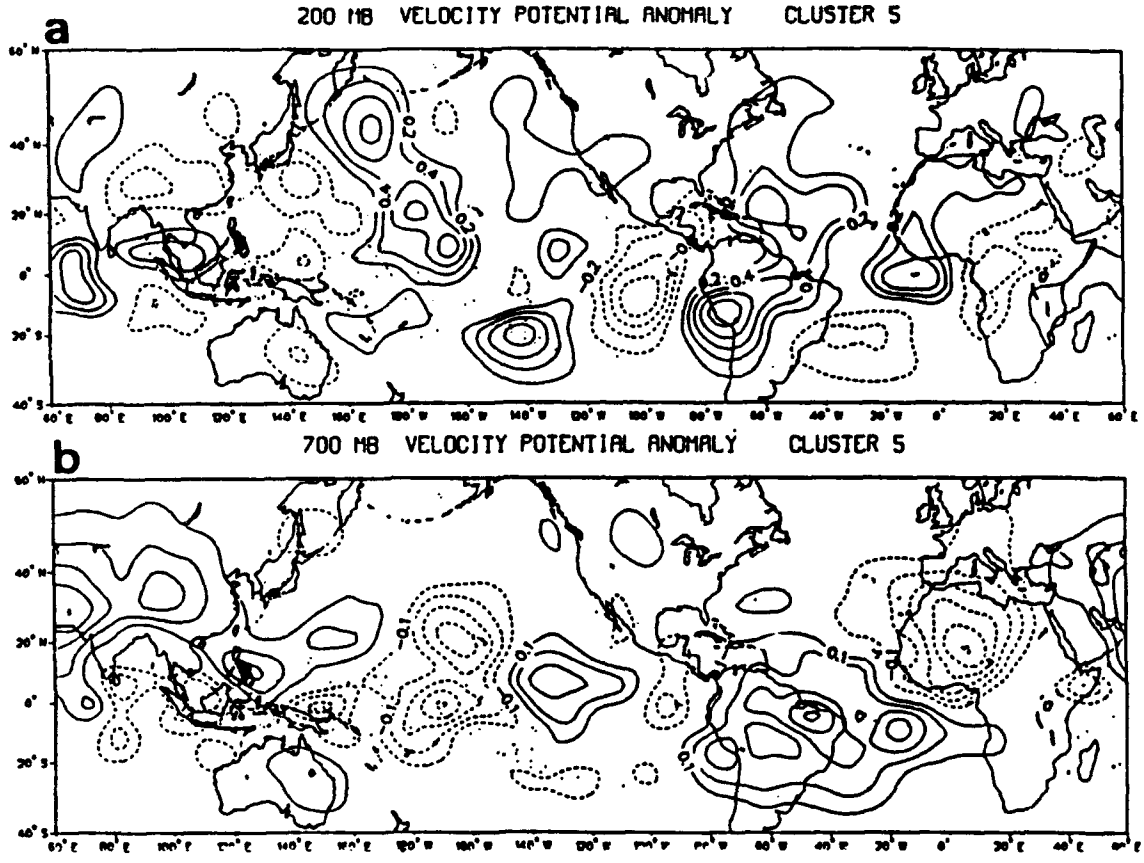


**Fig. 55** As in Fig. 51, except for cluster 5.

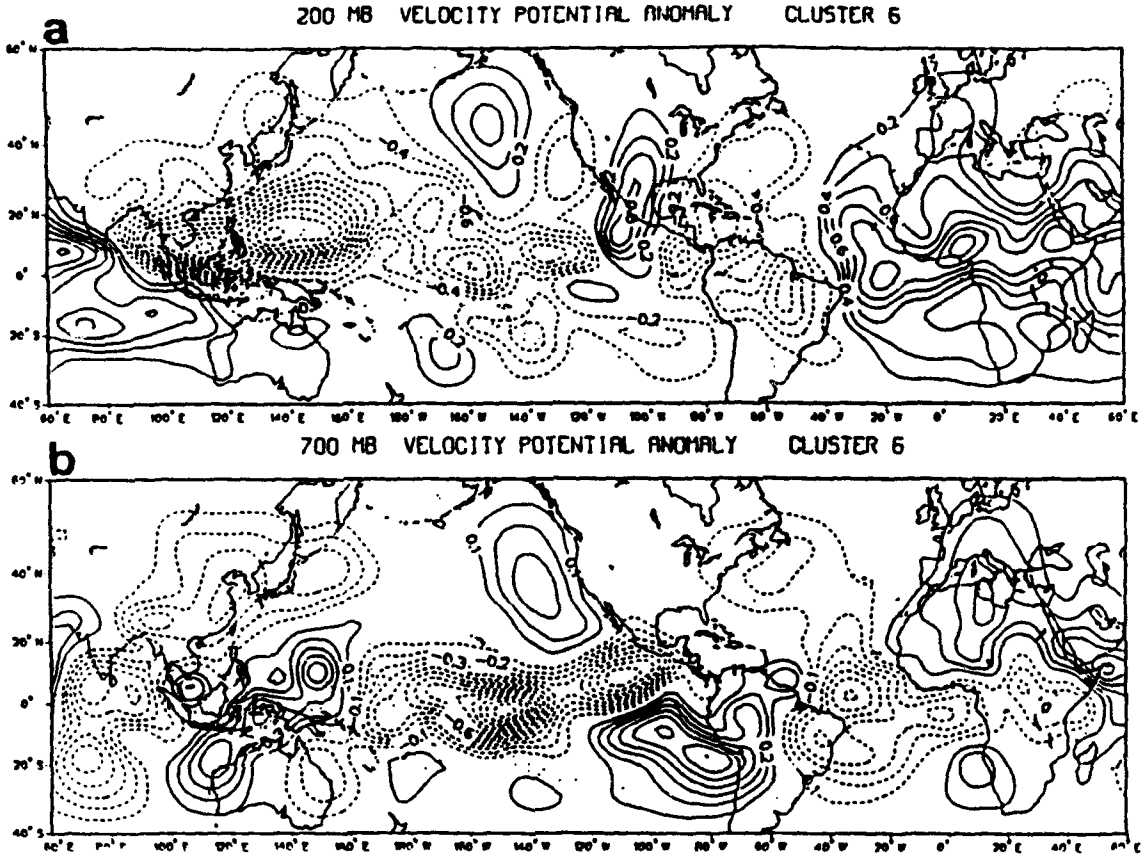


**Fig. 56** As in Fig. 51, except for cluster 6.

anomalous 700 mb winds and anomalous OLR (Fig. 44f). The anomalous 700 mb velocity potential (Fig.56b) contains more small-scale features than the 200 mb velocity potential anomaly patterns.

### 3. Clusters and Tropical Cyclone Characteristics

The relationship between the clusters and tropical cyclone track characteristics is examined by constructing a contingency table of the numbers of cyclones with each track type that occur during periods when the anomalous 700 mb large-scale circulation pattern belonged to each cluster (Table 8). The tropical cyclones occurring between 1 June and 31 October 1979-87 are used. The assignment of a particular track to a cluster is based upon the cluster that exists at the time when the tropical cyclone reaches tropical storm intensity (35 kt). Tropical cyclone track types are defined as straight-mover, recurve-south, recurve-north, and South China Sea.

Although this is concurrent with the time period used to define the clusters, the clusters are derived from the internal large-scale circulation variability within the entire data set that contains many more analyses without tropical cyclones than with cyclones. Therefore, this comparison does not represent a true independent data set. It is also not a true dependent data set since the circulation patterns are not directly derived from tropical cyclone-based criteria, as were the patterns defined by Harr and Elsberry (1991).

The contingency table relating cluster number to track type during 1979-87 is provided in Table 9. Because of the similarity in circulation patterns associated with clusters 1 and 2, and also clusters 4 and 6, these clusters are grouped together for purposes of classifying the track types with each cluster. A hypothesis test using a chi-square criteria

(Freund 1971) is applied to examine whether a null relationship exists between track type and cluster number. The chi-square value at the 0.05 significance level with 12 degrees of freedom (5 by 4 table) is 21.03. Because the test statistic computed from Table 9 is 41.55, the hypothesis that there is no relationship between track type and cluster number is not accepted. Furthermore, the significance level in this test actually exceeds 0.001 (chi-square value of 32.91), This cluster-based classification also exceeds the significance level based upon the relationship between track types and the tropical cyclone-based circulation patterns defined by Harr and Elsberry (1991).

The majority of straight-moving tracks are associated with clusters 1 and 2, and the majority of recurving tracks are associated with clusters 4 and 6. Ten of the 13 recurving-south cyclones associated with clusters 1 and 2 occurred concurrently with existing straight-moving cyclones. Similarly, four of the six straight-moving cyclones associated with clusters 4 and 6 occurred when one or more recurving cyclones also existed. These cases that do not fit the dominant track type tend to be associated with changing cluster patterns, which is also implied by the large number of recurving-south tracks occurring in cluster 7 (transition periods). Therefore, there are nearly an equal number of cyclones following recurving-south tracks in clusters 4 and 6 as are associated with changing patterns in clusters 1, 2 and 7. This implies that the predictability of recurving-south tracks may be less than the predictability associated with the other track types.

The numbers of tropical cyclones occurring over the South China Sea are nearly equal for clusters 1,2 and 4,6. In this case, the combination of clusters 4 and 6 is misleading, since all the South China Sea cyclones are associated with cluster 6. The equal

**TABLE 9** TROPICAL CYCLONE TRACK TYPES AND CLUSTER NUMBERS. Summary of the numbers of tropical cyclones following each track type identified with each cluster number.

| | CLUSTER NUMBER | | | | |
|---|---|---|---|---|---|
| | 1,2 | 3 | 5 | 4,6 | 7 |
| Straight-mover | 31 | 1 | 9 | 6 | 6 |
| Recurve-south | 13 | 1 | 8 | 25 | 12 |
| Recurve-north | 2 | 4 | 7 | 19 | 4 |
| South China Sea | 6 | 2 | 1 | 9 | 6 |

distribution of South China Sea cyclones between clusters 1,2 and 6 is consistent with the 700 mb cyclonic anomalies over that region (Figs. 44a,b,f).

The relatively few occurrences of tropical cyclones associated with cluster 3 is consistent with the large region of 700 mb anticyclonic anomalies (Fig. 44c) and the large-scale descent associated with the 200 mb and 700 mb velocity potential anomalies. The nearly equal distribution of track types associated with cluster 5 is also consistent with the previous interpretation of cluster 5 being related to the climatological mean. Although the large-scale 700 mb circulation anomalies reside in cluster 5, a large portion of the time (Table 9) there are significantly fewer occurrences of tropical cyclones following any of the four track types. This suggests that the tropical cyclone genesis, or intensification to tropical storm intensity, may be less likely (but still possible) when the large-scale circulation is near the climatological mean.

## C. DISCUSSION AND SUMMARY

A fuzzy clustering algorithm has been applied to the coefficients of the two leading VEOFs of the anomalous 700 mb large-scale circulation over the Indian Ocean and western

North Pacific Ocean. Based upon a series of procedures designed to estimate the stability of the cluster algorithm, a set of six clusters have been defined, and a large diffuse seventh cluster has been defined to contain observations that do not clearly belong to one of the six primary clusters. The cluster analysis captures the basic partitioning of the anomalous circulation variability since the cluster means are composed of the preferred phase angles of the leading two VEOFs.

The clusters are shown to be associated with physically consistent patterns by compositing the anomalous 700 mb winds, OLR, 700 mb streamfunction and velocity potential, and 200 mb streamfunction and velocity potential. Cyclonic anomalies at 700 mb are typically coincident with enhanced convection, anomalous convergence at 700 mb and anomalous divergence at 200 mb. Anticyclonic anomalies at 700 mb are typically coincident with reduced convection, 700 mb anomalous divergence and 200 mb anomalous convergence. The large-scale circulation anomalies that are south of 20° N have a baroclinic structure, and circulation anomalies north of 20°N have an equivalent barotropic structure.

The 200 mb large-scale velocity potential anomalies associated with clusters 1, 4 and 6 exhibit a global zonal wavenumber 1 pattern. Because of this pattern, it is interesting to compare these clusters with the global-scale 30-60 day oscillation originally observed by Madden and Julian (1972) and identified with global wavenumber 1 upper-tropospheric divergent circulations (Lorenc 1984; Krishnamurti et al. 1985). The large-scale velocity potential anomalies associated with these three clusters may be qualitatively compared with the phases of this global oscillation. Clusters 1 and 4 represent opposite phases of the large-scale oscillation. Cluster 1 is similar to the active phase of the oscillation that has enhanced

convection over Indonesia, which occurs when the large-scale upper-level divergent anomaly is positioned over Indonesia (Fig. 51). Cluster 4 is similar to the inactive phase with reduced convection associated with the large-scale, upper-level convergent portion of the wavenumber 1 pattern (Fig. 54a). Cluster 6 is similar to a transition phase between the patterns identified with clusters 1 and 4. The anomalous large-scale, upper-level divergent anomalies in cluster 6 are concentrated over the subtropical western North Pacific (Fig. 56a), which is slightly north and east of the primary cluster 1 features (Fig. 51a). The leading edge of the large-scale 200 mb convergent anomaly in cluster 6 extends over most of the Indian Ocean in conjunction with the eastward shift of the anomalous 200 mb divergent anomalies. This cluster representation is similar to descriptions of changes in the large-scale circulations associated with the evolution of the 30-60 day oscillation during the Northern Hemisphere summer (Knutson and Weickmann 1987). Furthermore, the lack of clear global wavenumber 1 patterns at 700 mb for clusters 1, 4, and 6 is consistent with the observation that the primary large-scale signal associated with the global oscillations exists in the upper troposphere (Knutson and Weickmann 1987; Rui and Wang 1990). Of course, these descriptions are based solely on static depictions of the variability of the anomalous large-scale circulations over the Indian Ocean and western Pacific, rather than more continuous representations of the phases of the oscillation.

A comparison between observed tropical cyclone track characteristics and the cluster definition at the time a tropical cyclone intensifies to tropical storm strength identifies a significant relationship between the track type and cluster number. This relationship is more

statistically significant than the one identified by Harr and ELsberry (1991) between track type and tropical cyclone-based anomaly patterns.

These clusters have been defined in terms of the variance of the anomalous 700 mb large-scale circulation. By definition, they define recurrent patterns. Based upon physically consistent relationships found in the other tropical circulation variables, it may be concluded that the clusters identify the basic structure of the large-scale circulation variability over the tropical western North Pacific region. Furthermore, these basic structures are related to tropical cyclone occurrence and track type.

The relationships between the tropical cyclone characteristics and the clusters, which define a more complete structure of large-scale circulation variability, provide a more comprehensive demonstration that many aspects of tropical cyclone characteristics are controlled by the large-scale circulation. The velocity potentials especially suggest that these clusters are related to global-scale tropical circulation features.

One specific utility of the fuzzy clustering technique is the specification of the large-diffuse cluster, which may represent observations that are transitions between the six primary clusters. Further examination of the properties of the clusters, and the transitions between the clusters, in the next chapter will lead to a more complete depiction of the variability of the large-scale circulation over the tropical western Pacific. If specific sequences or evolutions between the recurrent cluster patterns could be identified, then the relationships with tropical cyclone characteristics could be utilized as a potential prediction tool for tropical cyclone activity and track type.

# V. CHARACTERISTICS OF THE RECURRENT ANOMALOUS LARGE-SCALE CIRCULATION PATTERNS

In Chapters III and IV, a logical process was followed to generalize the procedure used in Harr and Elsberry (1991) and summarized in Chapter II. This process led to the following:

- The basic structures of the anomalous large-scale 700 mb circulation were identified.
- The dominant structures were combined to identify the most recurrent patterns of the anomalous large-scale 700 mb circulation.
- Examination of other parameters such as large-scale convection, and upper-level convergence-divergence anomalies identified physically consistent relationships with the recurrent 700 mb patterns.
- Tropical cyclone occurrence and track types were shown to be statistically and physically related to the recurrent 700 mb patterns.

The combination of these points demonstrate that many aspects of tropical cyclone characteristics are controlled by large-scale circulation patterns. Therefore, the remaining questions to be investigated are related to the characteristics of the recurrent patterns, the relationships between the patterns, and the preferred transitions.

By construction, the patterns defined by the cluster analysis are constrained to be recurrent. Although the analysis in Chapter IV clearly demonstrated the physical significance of the instantaneous patterns, their relative contribution to the total variability of the large-scale circulation must be established. As a first step, the internal consistency of the recurrent patterns is identified. If a particular pattern exists, this step addresses whether there is less

fluctuation in the large-scale circulation than would occur normally. A second characteristic to be examined is the fraction of the anomalous large-scale circulation variability explained by each pattern. Although the VEOF analysis identifies the amount of variance associated with each basic structure, the leading structures have been combined in an optimal manner, which results in a repartitioning of the variance distribution.

The relationships among the individual clusters are defined by examining the transitions between them. Given the relationships between tropical cyclone characteristics and the cluster patterns, if specific sequences or evolutions between the recurrent patterns exist, they could be used to forecast tropical cyclone activity. Physical descriptions of the primary transition paths are used to identify factors that influence the establishment, maintenance and transitions of the recurrent patterns.

## A. INTERNAL VARIABILITY OF THE RECURRENT CIRCULATION PATTERNS

This section examines the relationship between internal fluctuations associated with a particular recurrent pattern and the total variability in the 700 mb wind anomaly data set. This analysis identifies the circulation features that remain consistent for a given recurrent pattern without regard to the length of time that the pattern may persist. The sensitivity of the cluster definitions, which were based upon whether a particular membership coefficient was at least twice as large as all other membership coefficients, is also examined. If this specification is too general, then the within-cluster variances will be large. If the within-cluster variance equals the climatological variance, then the clusters do not contain any features that fluctuate less than would be expected from climatology. The opposite situation

occurs if a particular map is only assigned to a cluster if the membership coefficient is equal to one.

The internal consistency of each cluster is defined by the ratio of the within-cluster variance to the total climatological variance. For a cluster L, the mean pattern is specified as C(L), which are the patterns defined in Fig. 44. The total climatological mean is specified as T, which is computed from the complete 1979-87 data. The within-cluster variance is computed as

$$\sigma^2(L) = \sum_{i=1}^{N} u(i,L) \left| M_i - C(L) \right|^2, \qquad (19)$$

where N is the length of the total data set, $M_i$ is the 700 mb anomaly map at time i, and u(i,L) is the membership coefficient pertaining to cluster L at time i. The climatological variance is computed as

$$\sigma^2(C) = \sum_{i=1}^{N} \left| M_i - T \right|^2. \qquad (20)$$

The ratio between the within-cluster variance and the total variance is evaluated for each wind component separately.

The variance ratio associated with the cluster 1 zonal wind (Fig. 57a) indicates that the anomalous westerly winds that define the equatorward portion of the active monsoon trough fluctuate much less than the climatological variability (values << 1). The zonal wind anomalies associated with the strong subtropical ridge also fluctuate less than average, but not to the degree associated with the equatorial wind anomalies. Although the cluster 1 pattern contains a stronger ridge than normal (Fig. 44a), it is not as consistent a feature as the

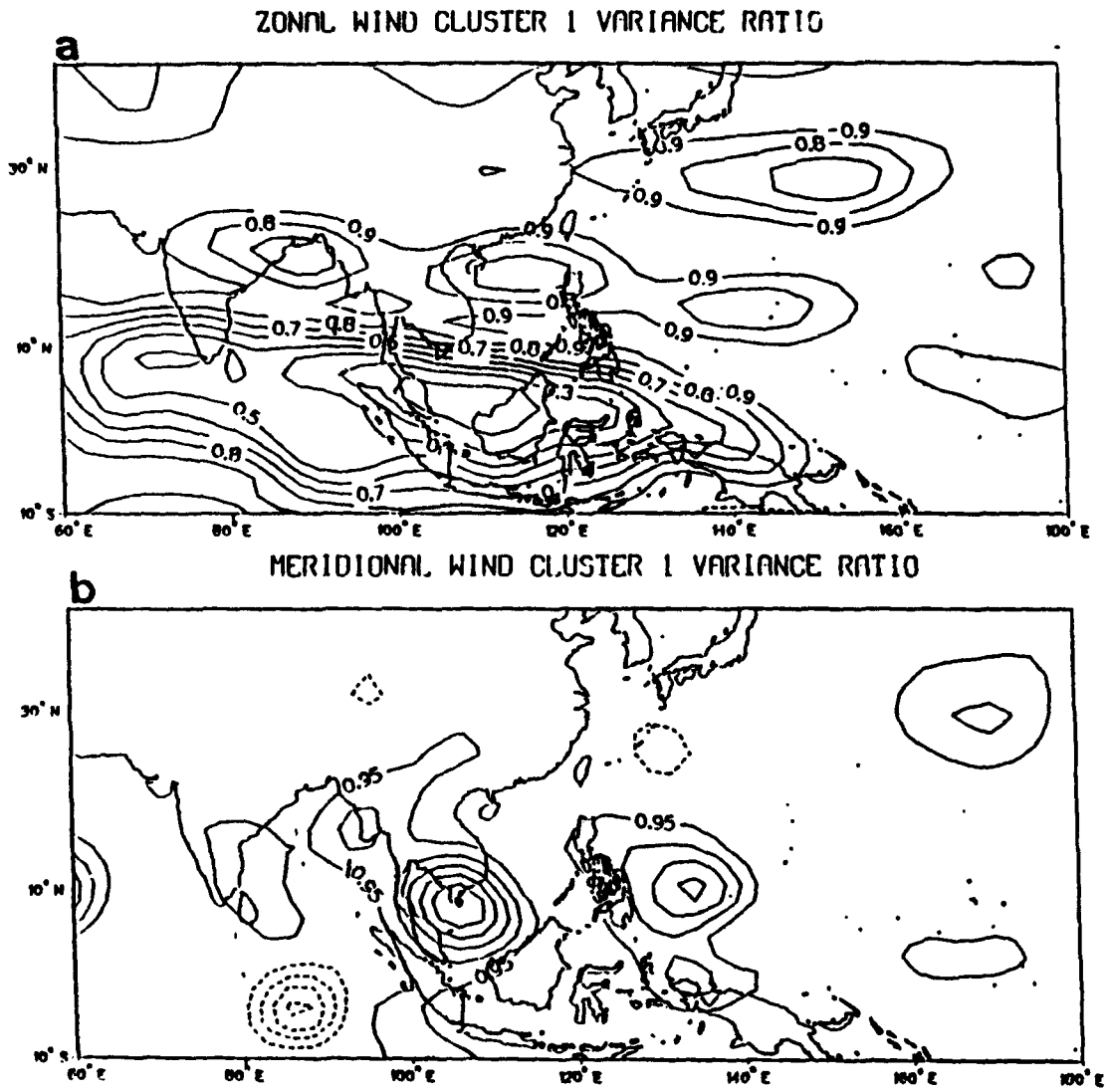


**Fig. 57** Ratio of the within-cluster 1 variance to the total climatological variance for the 700 mb anomalous **(a)** zonal wind, and **(b)** meridional wind components. The contour interval for the zonal wind in 0.1, and for the meridional wind the contour interval is 0.05. Units are nondimensional.

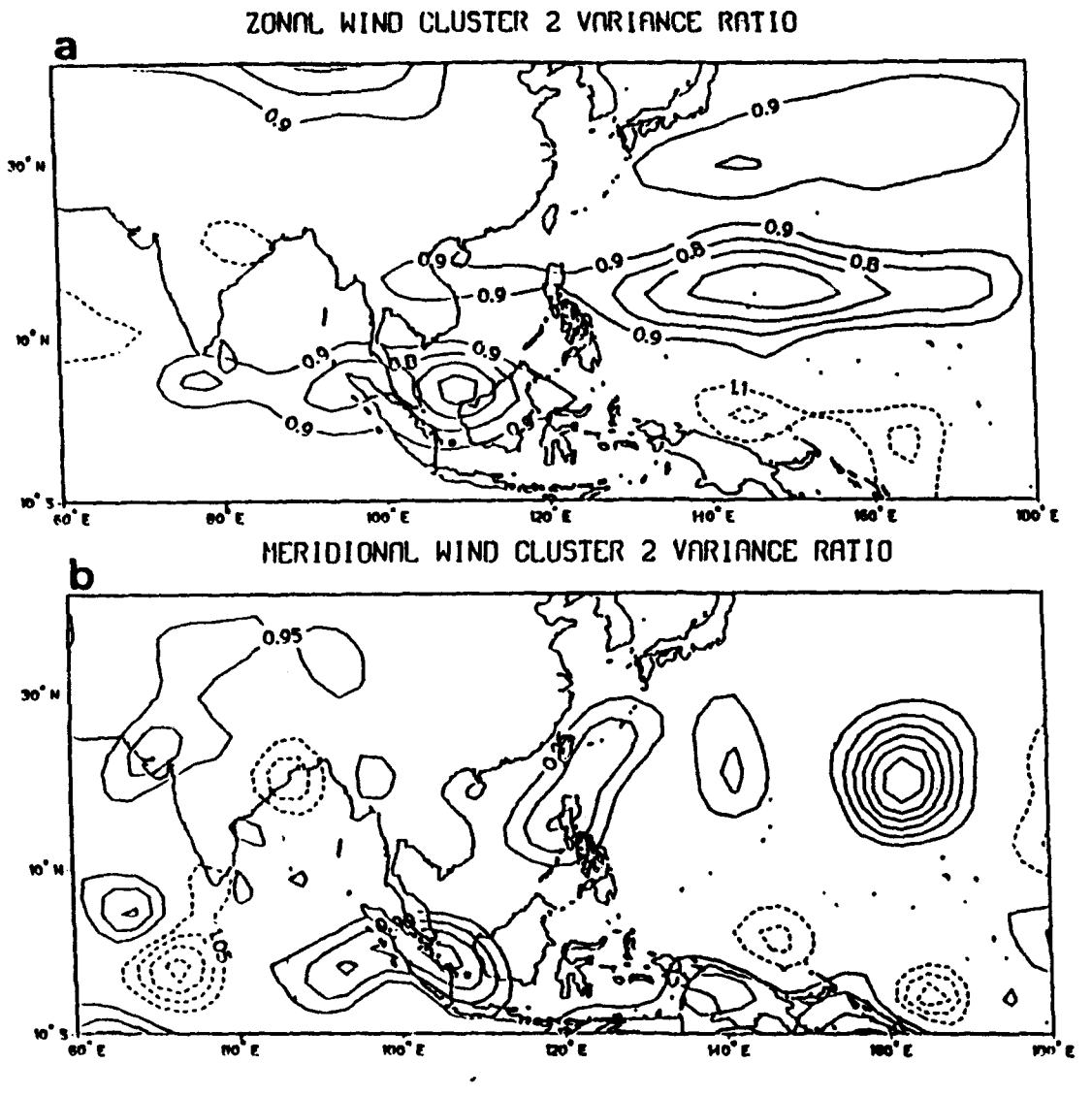


**Fig. 58** As in Fig. 57, except for cluster 2.

monsoon trough. The only regions in which the meridional winds fluctuate less than normal (Fig. 57b) are associated with the cyclonic anomalies along the enhanced monsoon trough in cluster 1 (Fig. 44a).

The zonal wind anomalies associated with the strong subtropical ridge in cluster 2 exhibit a smaller variance than normal (Fig. 58a). A small portion of the zonal winds along the equatorward side of the active monsoon trough fluctuate less than the climatological variation. However, the variance ratio is not nearly as small as the cluster 1 ratio in the monsoon area. The cluster 2 meridional wind variance ratio is also dominated by the circulation associated with the strong subtropical ridge (Fig. 58b). Some indication of persistent cross-equatorial winds is found over Indonesia.

The variance ratios of the cluster 1 and 2 wind components provide further interpretations regarding the relationships between the cluster patterns and tropical cyclone track types. Although these cluster patterns define a strong subtropical ridge, the variability of this feature within the cluster is about 80% of the climatological variability. This is in contrast to the very small fluctuations of the monsoon trough circulation anomalies (cluster 1). Therefore, tropical cyclone genesis, which is more tied to the active monsoon trough, would be better associated with these clusters (in particular cluster 1) than would track type, which is more tied to the subtropical ridge.

The small fluctuations associated with the anomalous easterly zonal wind anomalies between the equator and 10°N in cluster 3 dominate the variance ratio patterns (Fig. 59a). The meridional winds associated with anomalous anticyclonic circulations over Indonesia exhibit less variability compared to climatology. A region of meridional wind variability that

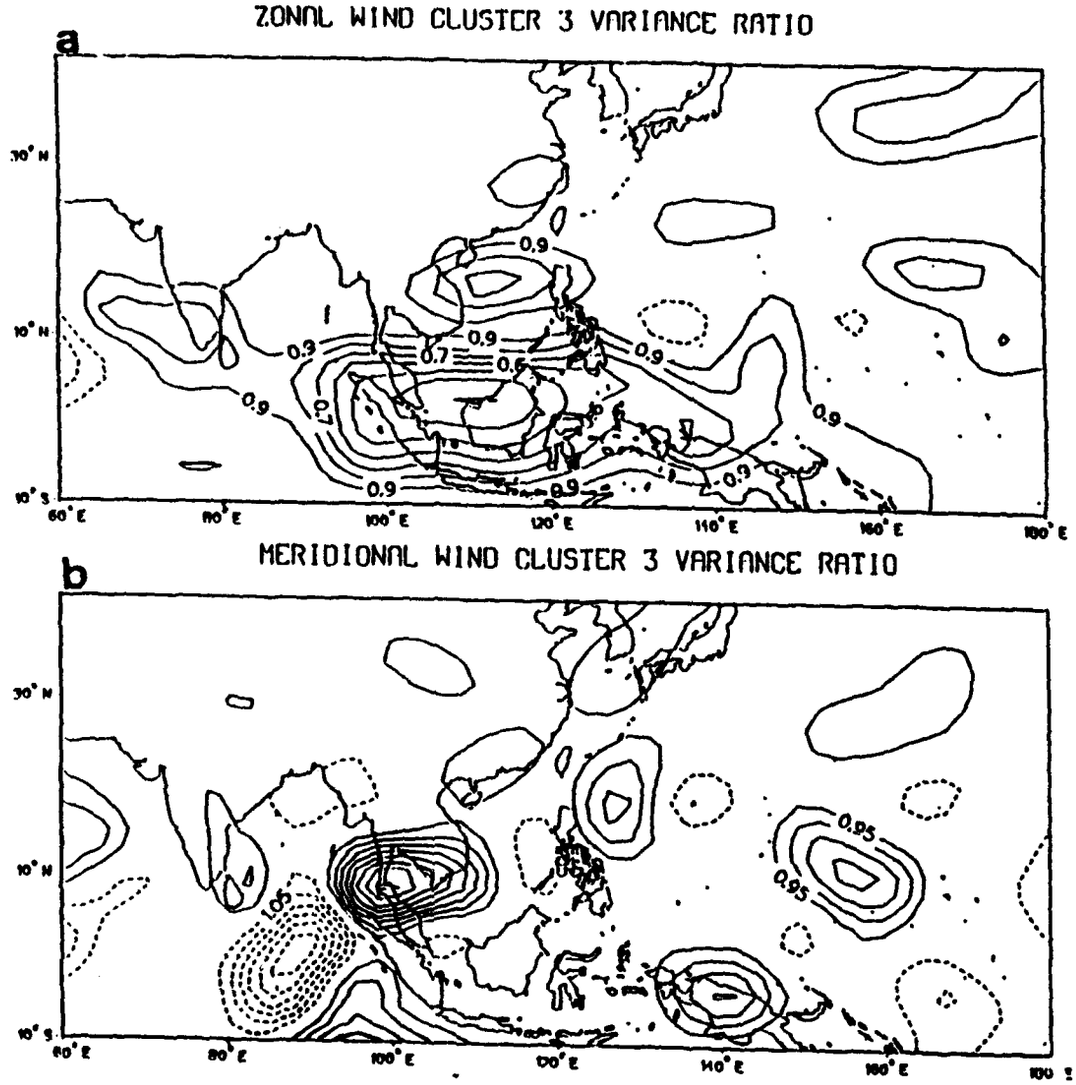


**Fig. 59** As in Fig. 57, except for cluster 3.

is larger than the climatological variation is found along the equator near 90°E (Fig. 59b), which is located in a region of large positive OLR anomaly (Fig. 44c).

The variance ratio patterns for both the zonal wind and meridional wind components of cluster 4 (Fig. 60) are very similar to the cluster 1 patterns (Fig. 57). However, the equatorial zonal wind anomalies are easterly, and the subtropical anomalies are associated with a weak subtropical ridge (Fig. 44d). The persistent meridional winds (Fig. 60b) are associated with anomalous anticyclonic circulations within the inactive monsoon trough. The anomalous subtropical westerlies on the southern branch of the weak subtropical ridge in cluster 4 are much more consistent than the corresponding easterlies associated with the strong subtropical ridge in cluster 1. This suggests that a weak subtropical ridge anomaly, when present, may be a more consistent pattern than the strong ridge anomaly. This is also suggested by the tropical cyclone track characteristics in Table 8, which have a statistically significant relationship between the occurrence of tropical cyclones following recurve-north tracks and the circulation pattern associated with cluster 4.

The internal variabilities of the zonal and meridional wind components of cluster 5 are equal to the climatological variability over all regions (Fig. 61). This is consistent with the interpretation that cluster 5 represents the variability about the climatic mean.

The extension of large westerly zonal wind anomalies over the South China Sea and Philippine Sea along the equatorward side of an active monsoon trough dominates the variance ratios of the cluster 6 zonal wind components (Fig. 62a). A major portion of the pattern of consistent meridional wind anomalies is oriented from the southeast towards the northwest (Fig. 62b), which is associated with the reverse orientation of the active monsoon

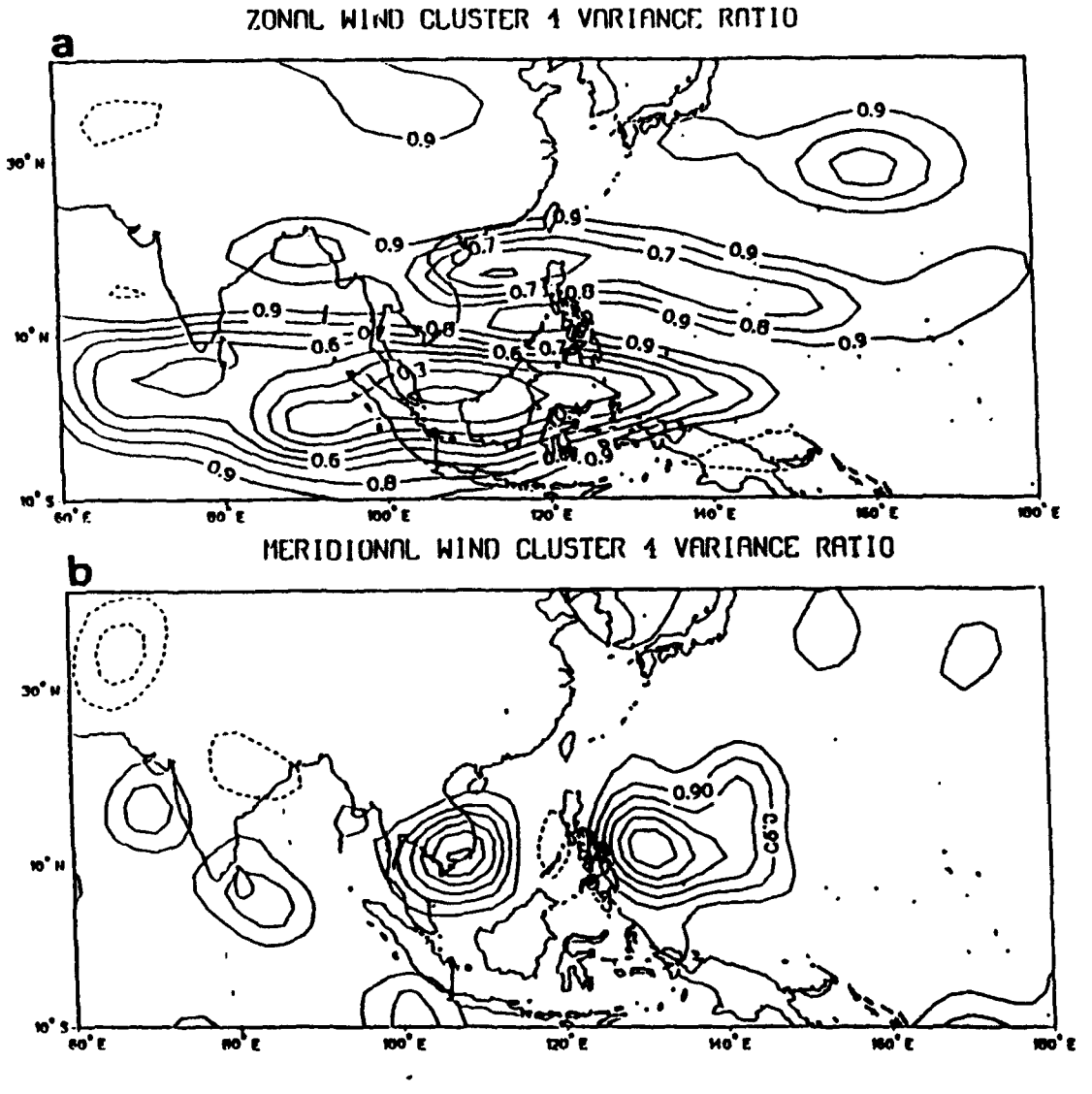


**Fig. 60** As in Fig. 57, except for cluster 4.

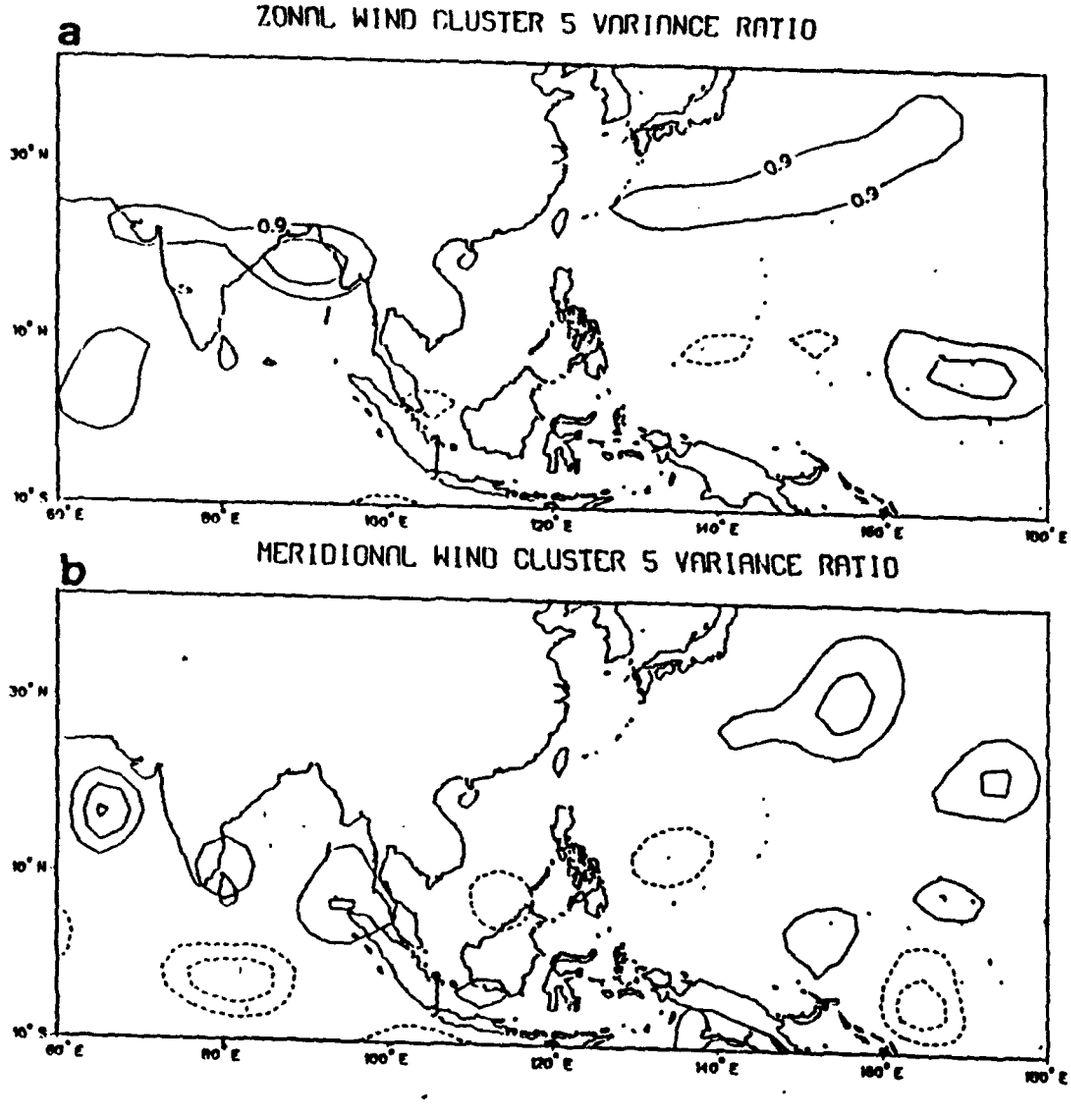


Fig. 61 As in Fig. 57, except for cluster 5.

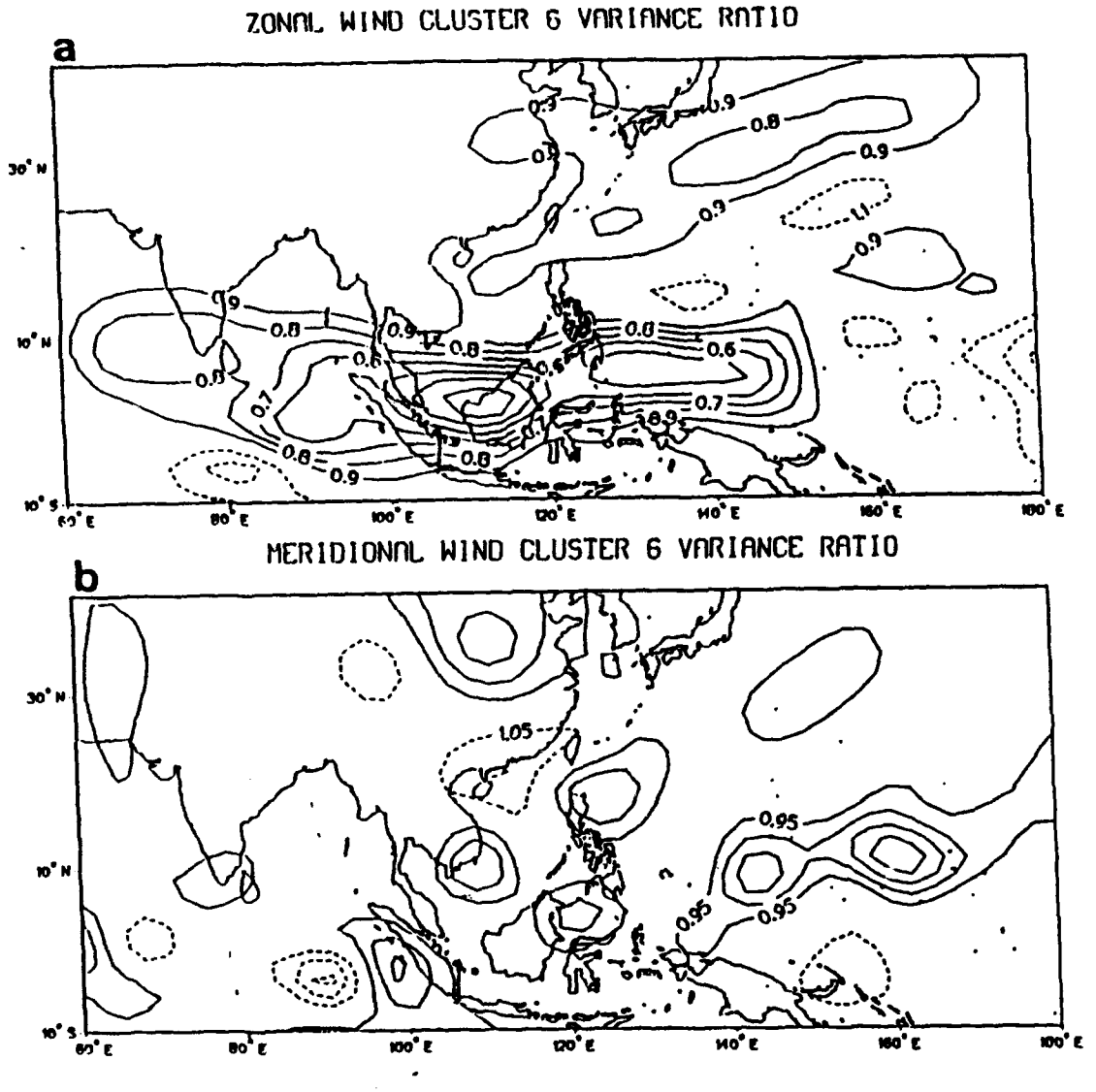


**Fig. 62** As in Fig. 57, except for cluster 6.

trough from the South China Sea to the subtropical western North Pacific (Fig. 44f). The pattern of consistent meridional winds is similar to the orientation of 850 mb vorticity anomalies that are described by Lau and Lau (1990, 1992) as northwestward propagating synoptic-scale disturbances. These features are consistent with the 700 mb cyclonic anomalies and negative OLR anomalies over the South China Sea and Philippine Sea in cluster 6 (Fig. 44f). Lander (1993) discusses the relationship between northwestward- or northward-moving tropical cyclones and a reverse-oriented monsoon trough as indicated by cluster 6.

The variance ratio pattern associated with cluster 7 (not shown), which contains all maps that were evenly distributed among all clusters, contains no features that were large enough to appear on the contour map using the same interval as clusters 1-6. This is consistent with the interpretation of cluster 7 as representing transient fluctuations between the six primary clusters.

The depictions of the variance ratios for all the clusters are consistent with the interpretation that the zonal wind component over the tropics is considered to be representative of large-scale circulations and the meridional wind component is considered representative of disturbances exhibiting shorter space and time scales. Only those features associated with large-scale zonal wind anomalies have consistently smaller fluctuations than the climatological average. The most internally consistent meridional wind fluctuations are generally between 70-80% of the climatological variability.

The most consistent anomaly features are associated with the depiction of the monsoon trough. Anomalies denoting a strong subtropical ridge fluctuate more than anomalies that

identify a weak subtropical ridge. These aspects may indicate that the inherent predictability of tropical cyclone occurrence, if it is based only on large-scale circulations as defined by the cluster patterns, may be larger than the predictability of track type. This is because track type depends upon the state of the subtropical ridge, which exhibits fluctuations that approach the climatological variability. Finally, only features associated with the primary large-scale circulations of each cluster, as defined in Chapter IV, exhibit any reduction in variability compared to the climatological variance.

## B. RELATIONSHIPS BETWEEN THE CLUSTER PATTERNS AND THE TOTAL VARIABILITY OF LARGE-SCALE CIRCULATIONS

The amount of the variance in the total 700 mb wind anomaly data set explained by each VEOF is defined in Table 6. The cluster analysis defines the most recurrent large-scale circulation anomalies as combinations of the two leading modes. The amount of total sample variance explained by the six cluster patterns is described in this section.

A variance ratio is again used to define the proportion of the total variance represented by each cluster pattern. Since the clusters are defined as combinations of the leading two VEOF modes, these modes are used to partially reconstruct the 700 mb wind anomalies as

$$\mathbf{V}(\boldsymbol{x}, t) = \sum_{v=1}^{2} \alpha_v(t) E_v(\boldsymbol{x}),$$

where $\mathbf{x}$ represents the spatial grid, and $\alpha_v(t)$ is the vth principal component associated with the eigenvector $E_v$ at time t. For a cluster L, the mean pattern as defined by the partially reconstructed anomalies is defined as $C(L^*)$. The within-cluster variance is then defined as

$$\sigma^2(L^*) = \sum_{i=1}^{N} u(i,L)\,|M_i - C(L^*)|^2, \qquad (21)$$

where each symbol is defined with reference to (19). The climatological variance remains as defined by (20). Now the ratio of the within-cluster variance to the total variance defines the fraction of the total variance represented by the combination of the leading two VEOF modes in each cluster.

The westerly anomalies along the equatorward side of the active monsoon trough in cluster 1 contain nearly all of the climatological variance over that region (Fig. 63a). The zonal wind anomalies in cluster 1 associated with the subtropical ridge represent a much smaller portion of the total field variance. This is consistent with the internal consistency of the cluster 1 anomalies defined in Fig. 57a. The only appreciable amount of total variance represented by the meridional winds of cluster 1 are associated with the anomalous cyclonic circulations within the active monsoon trough (Fig. 63b).

The easterly anomalies associated with the strong subtropical ridge in cluster 2 explain a large fraction of the total variance between 10°-20°N and 100°-140°E (Fig. 64a). The westerly anomalies along the equatorward side of the monsoon trough (Fig. 64a) represent a much smaller portion of the total variance than similar anomalies in cluster 1 (Fig. 63b). Meridional anomalies associated with the western portion of the anomalous subtropical ridge represent a fair amount of the total variance (Fig. 64b). Also, the meridional winds associated with cross-equatorial flow near Indonesia represent nearly 40% of the total variance. The amounts of explained variance associated with the anomalies representing the monsoon trough are consistent with previous interpretations regarding the relationships between clusters 1 and

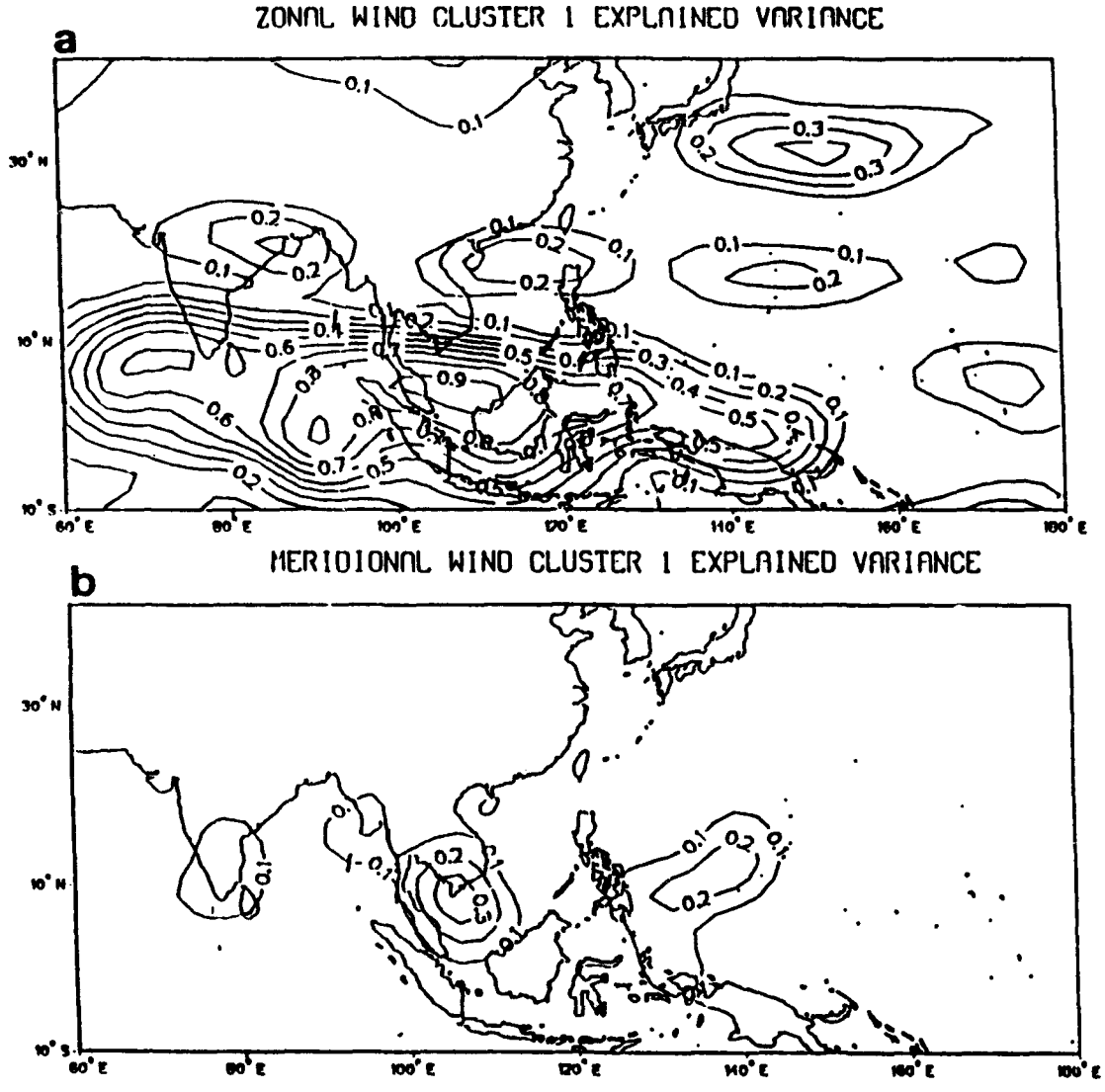


**Fig. 63** The fraction of the total climatological variance represented by the variance within cluster 1 for the 700 mb anomalous (**a**) zonal wind component and (**b**) meridional wind component. The contour interval is 0.1 for both the zonal and the meridional wind components. Units are nondimensional.

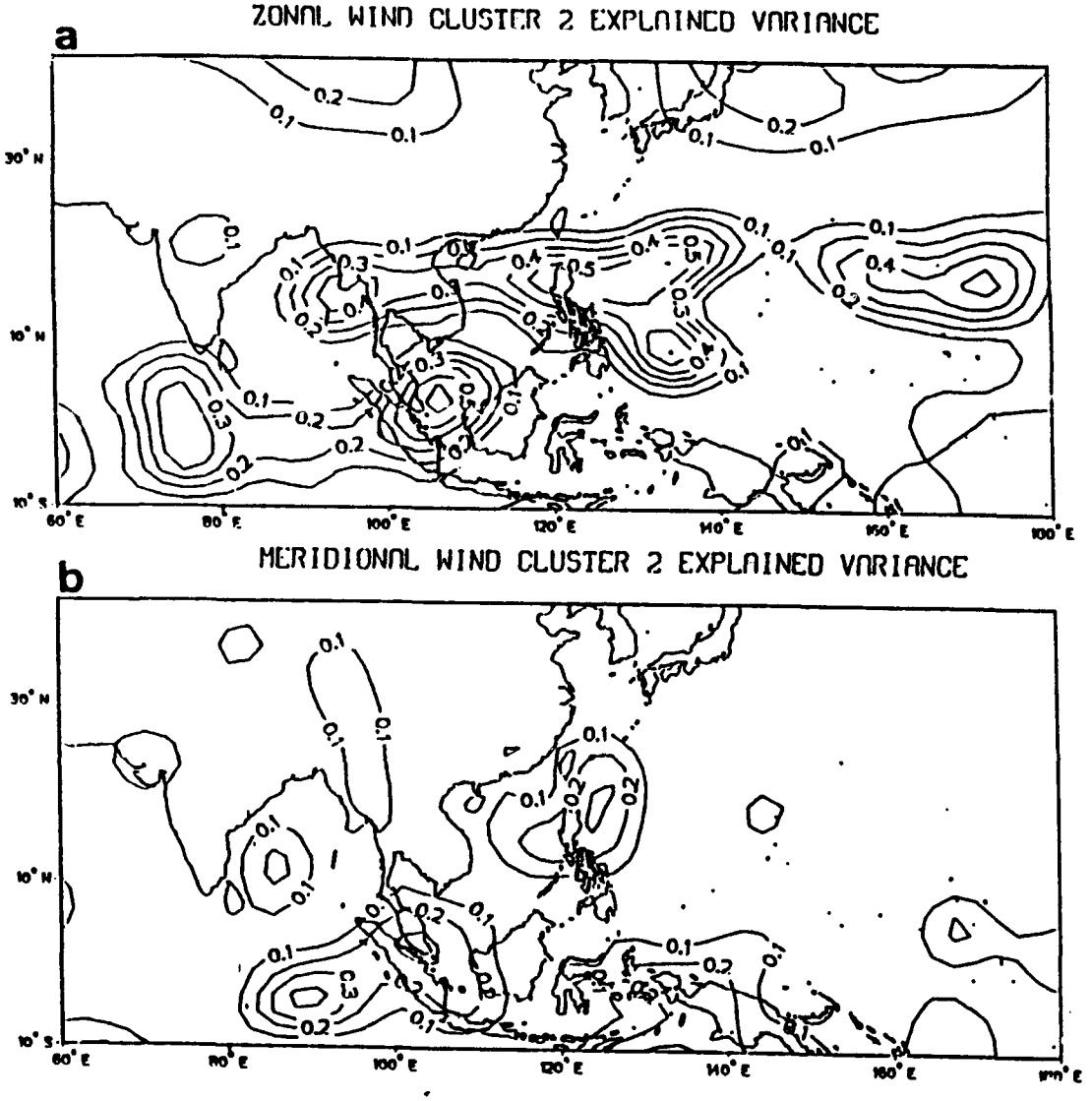


**Fig. 64** As in Fig. 63, except for cluster 2.

2, and tropical cyclone occurrence over the monsoon trough region. Furthermore, the reduction in variance represented over the subtropical ridge is consistent with the interpretation that the relationship between track type and clusters 1 and 2 is more variable than the relationship with genesis.

The zonal wind anomalies associated with the inactive monsoon trough in cluster 3 (Fig. 44c) represent a large portion of the overall variance (Fig. 65a). The zonal wind anomalies associated with the anomalous subtropical anticyclonic circulation also represents a large portion of the climatological variance. Meridional components over Southeast Asia, which represent anomalous anticyclonic anomalies within the monsoon trough, also explain a large portion of the climatological variance (Fig. 65b).

The pattern of the amount of explained variance in cluster 4 is similar to the cluster 1 pattern for both zonal (Fig. 66a) and meridional (Fig. 66b) winds. The zonal wind anomalies associated with the southern edge of the inactive monsoon trough anomaly represent nearly all of the total field variance. The only meridional wind component anomalies that explain more than 10% of the total variance are associated with anomalous anticyclonic circulations within the inactive monsoon trough (Fig. 66b).

Easterly anomalies associated with a weak anticyclonic anomaly centered over the Bay of Bengal in cluster 5 (Fig. 44e) do represent about 20% of the total variance (Fig. 67a). No coherent meridional wind component anomalies are found in cluster 5 that represent more than 10% of the total variance (Fig. 67b). The extension of westerly anomalies between the equator and 10°N and between 100°-140°E in cluster 6 represents a large portion of the total variance (Fig. 68a). The zonal wind anomalies along the northern portion of the cyclonic

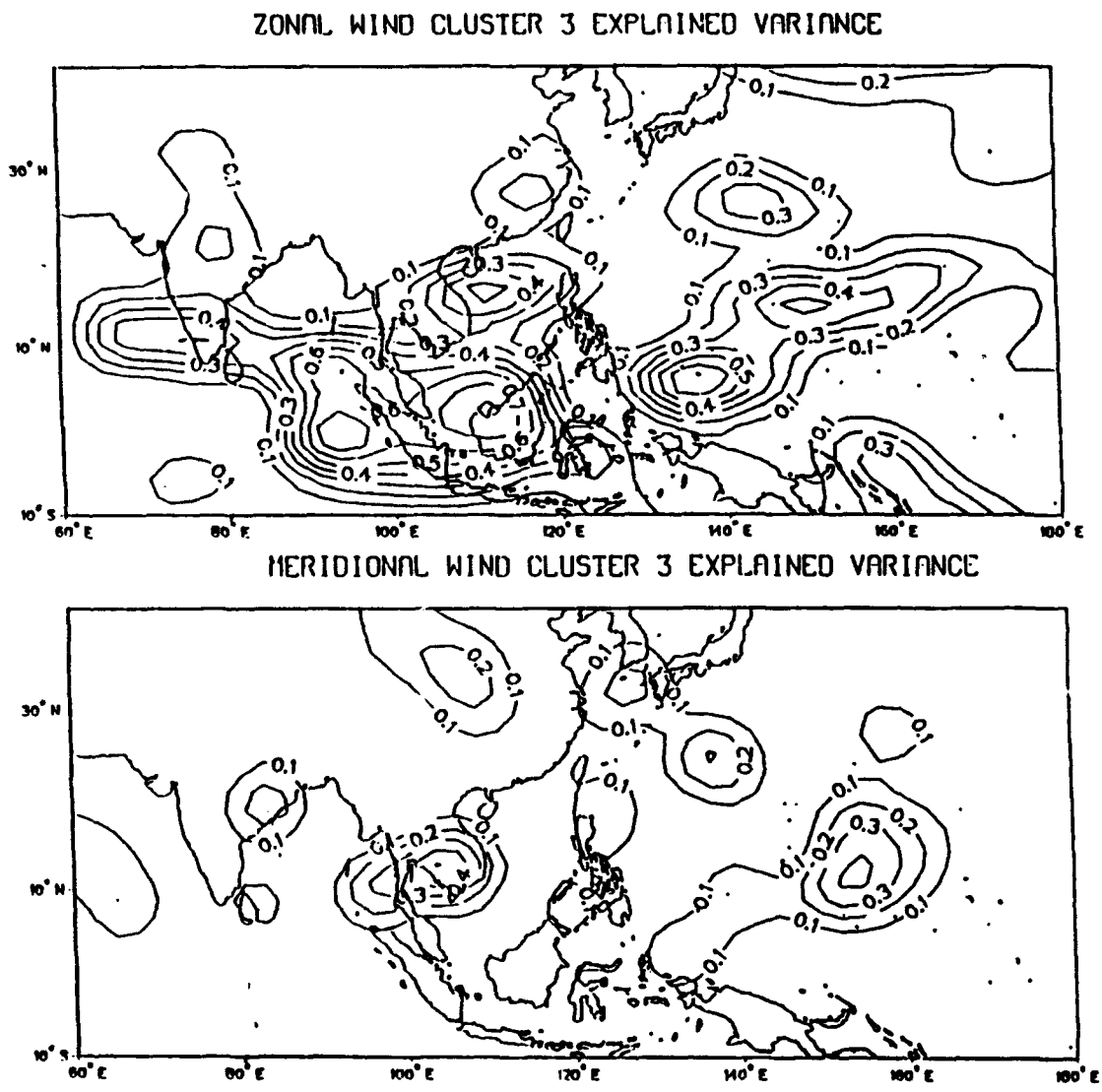


**Fig. 65** As in Fig. 63, except for cluster 3.

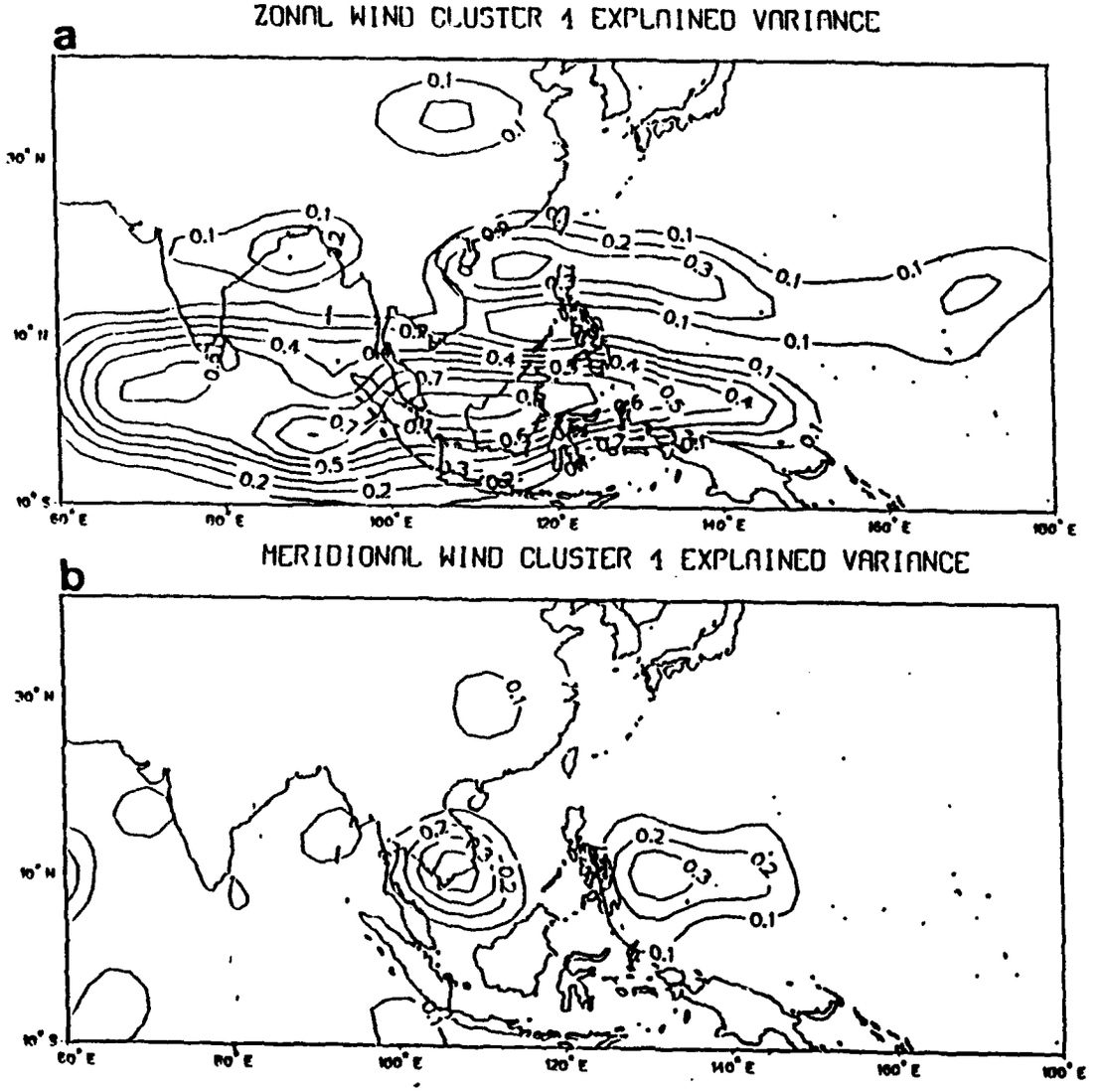


**Fig. 66** As in Fig. 63, except for cluster 4.

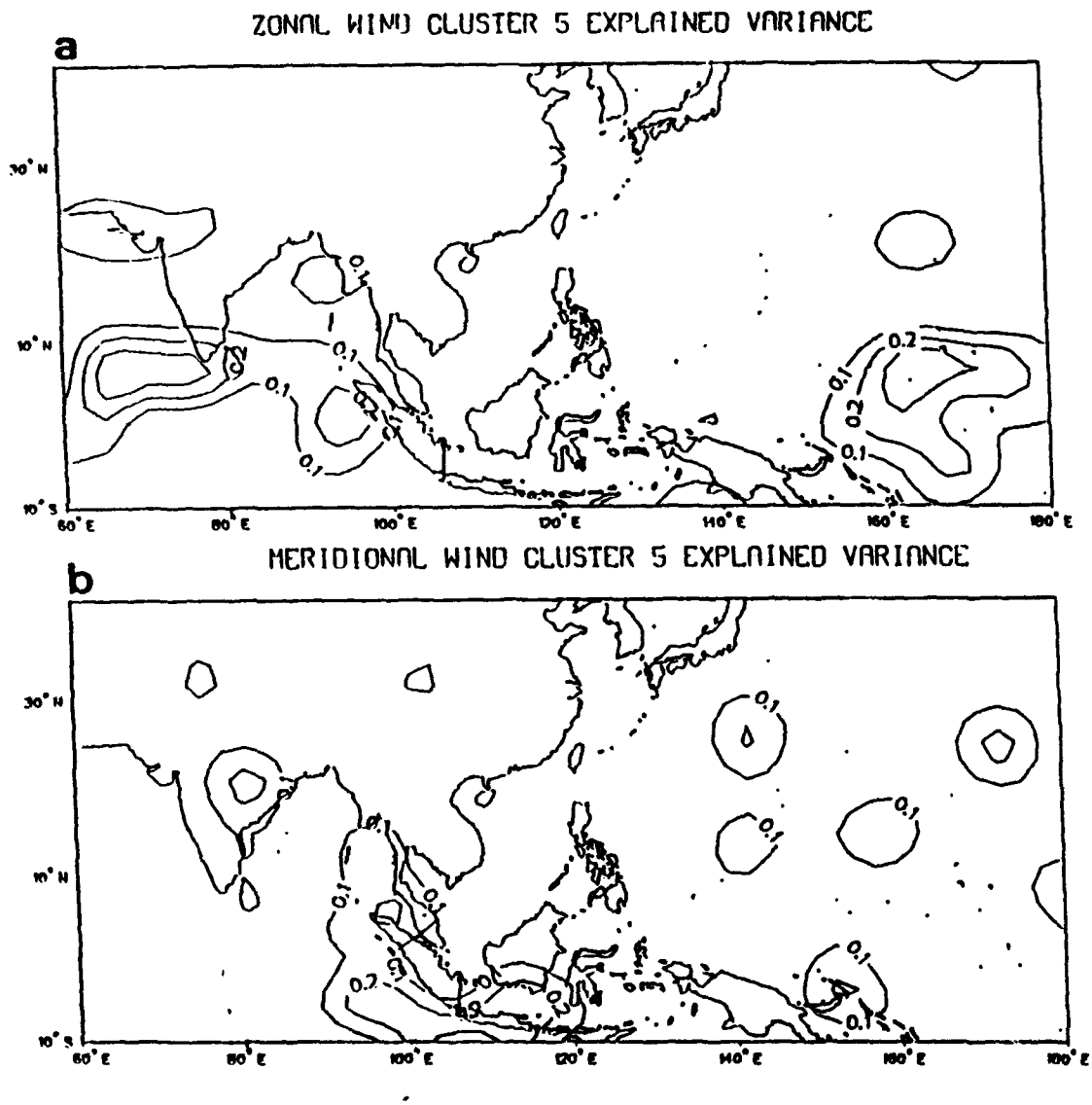


**Fig. 67** As in Fig. 63, except for cluster 5.

anomaly that is associated with a reverse-oriented monsoon trough (Fig. 44f) also represent much of the total variance (Fig. 68a). Meridional wind component anomalies associated with this feature represent about 10%-20% of the total field variance (Fig. 68b).

No zonal or meridional wind component anomalies associated with cluster 7 represent more than 10% of the total variance (not shown). This is consistent with cluster 7 containing those anomaly patterns that are not representative of any of the six primary cluster patterns.

Generally, the portions of each cluster pattern that explain a large amount of total variance are also portions that fluctuate less than average. These portions are always related to the primary large-scale circulation features that the cluster pattern is describing, which are also the primary physical attributes of each cluster that are related to tropical cyclone characteristics.

*The descriptions of the variance ratios and the amounts* of total variance represented by each cluster indicate that the clusters are internally consistent, and that the clusters capture the optimal partition of the variability of the anomalous 700 mb large-scale circulation. Descriptions of the relationships between the clusters and the physical aspects of these relationships will provide a complete representation of the variability of the large-scale 700 mb circulation.

## C. CLUSTER STATISTICS

In Chapter IV, descriptions of the physical characteristics of the clusters, and their relationships to other tropical circulation variables and features, defined the physical representations of each cluster pattern. The analysis of the internal characteristics and their relationship to the total variance of the large-scale 700 mb wind anomalies provide further

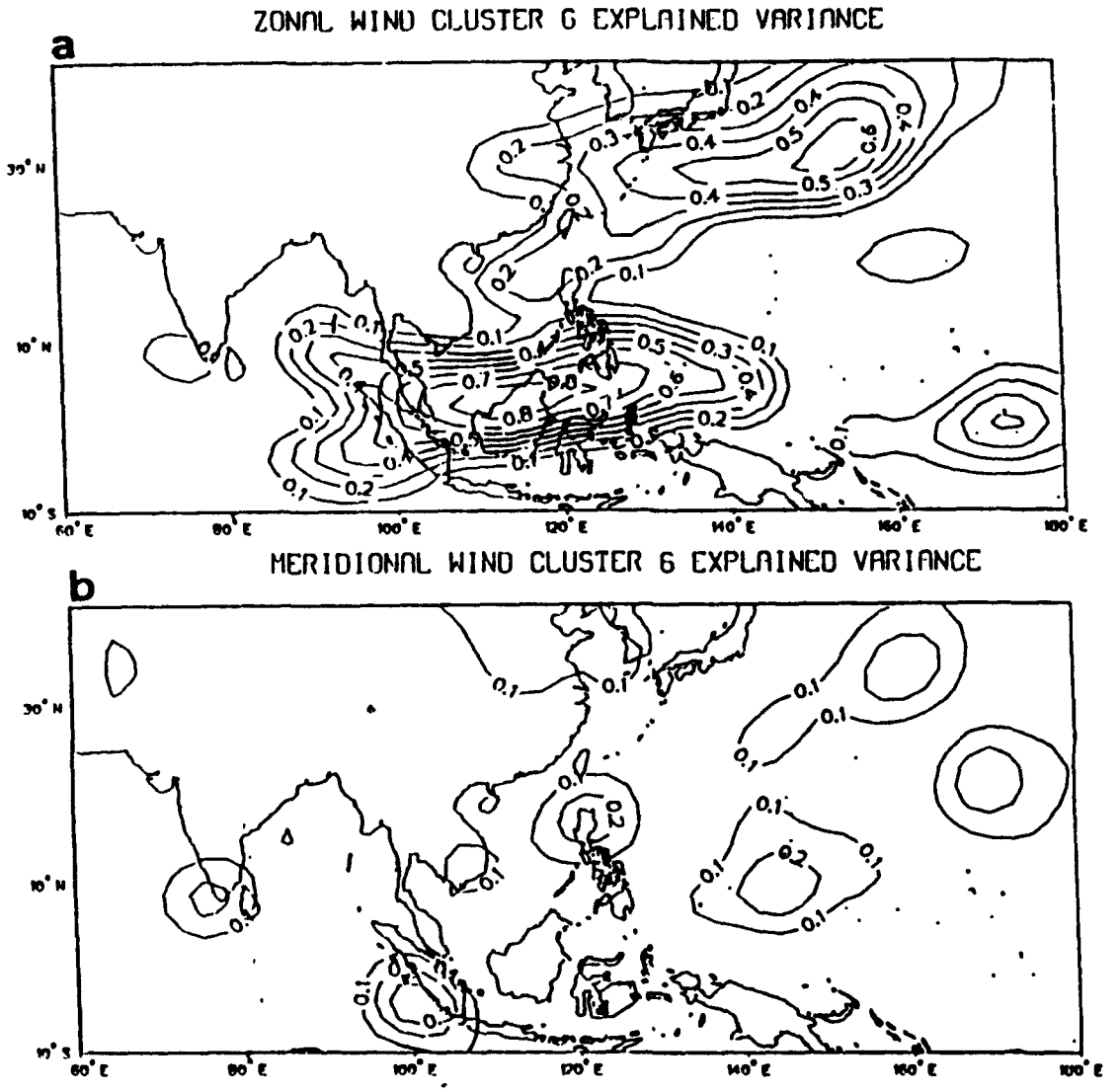


**Fig. 68** As in Fig. 63, except for cluster 6.

evidence of the physical significance of the cluster patterns. In this section, the statistical characteristics of the cluster patterns are described.

The average duration of a passage through each cluster is shown in Table 10. Cluster 7 is not included since it is defined by the collection of maps that do not represent any specific type of anomaly pattern. Although cluster 5 has the largest number of members excluding the diffuse cluster 7 (Table 8), the amount of time spent in it during each passage is the smallest of any cluster, which is consistent with the interpretation of cluster 5 as representing small anomalies about the climatological mean. The average duration of a passage through cluster 2 is also small, which is related to its proximity in the VEOF framework to cluster 5. As described in Chapter IV, cluster 2 may be a transition cluster through which anomalies pass while heading to cluster 1, which has a larger average duration time. The average duration of passages through clusters 1 and 4 are longest, which is consistent with the large areas of persistent anomalies (Figs. 57, 60) that represent most of the total variance (Figs. 63, 66). Large standard deviations associated with the average passage times within each cluster indicate a broad distribution of durations.

**TABLE 10** AVERAGE DURATION OF PASSAGES THROUGH EACH CLUSTER.

| CLUSTER NUMBER | AVERAGE DURATION (Days) | STANDARD DEVIATION (Days) |
|---|---|---|
| 1 | 5.4 | 3.9 |
| 2 | 2.7 | 2.6 |
| 3 | 4.5 | 2.0 |
| 4 | 5.8 | 4.7 |
| 5 | 2.1 | 1.5 |
| 6 | 4.2 | 2.7 |

## D. TRANSITIONS BETWEEN CLUSTERS

The concept of transitions between multiple planetary flow regimes was introduced by Mo and Ghil (1987) using a pattern correlation method to define the circulation regimes. Mo and Ghil (1988) re-examined the transitions between flow regimes by using a variation of the k-means cluster algorithm.

The numbers of transitions between the six primary clusters of the 700 mb wind anomalies are given in Table 11. Transitions to cluster 7 are not counted because cluster 7 contains anomaly patterns that are not directly related to any of the six primary clusters. Intermediate steps during transitions between clusters, e.g., cluster 1 to cluster 7 and then to cluster 6, are ignored so that this sequence is recorded as a transition from 1 to 6. A transition from a cluster to cluster 7 that is then followed by a transition back to the original cluster is recorded as a transition from one cluster to itself.

Several appealing attributes are readily apparent in this transition matrix (Table 11). Notice that many cells have no observed transitions, which indicates that transitions between several of the clusters never occurred during the nine-year sample. Therefore, transitions are limited to occur between distinct pairs of clusters.

Transitions between the tropical cyclone-based circulation patterns (Figs. 10, 11) were analyzed using an equiprobability model to identify the significant transitions. Identification of significant transitions was necessary to highlight the important transitions, since transitions were observed in every cell of the transition matrix. The transition matrices of Mo and Ghil (1988) and Molteni et al. (1990) also contained entries in every cell. Therefore, the lack of observed direct transitions between many of the six clusters in Table 11 is a significant result,

which indicates that the cluster analysis successfully isolates the most physically significant transitions occurring within the data set.

**TABLE 11** TRANSITIONS BETWEEN PAIRS OF CLUSTERS. Transition numbers enclosed in parentheses are significant as determined by the equiprobability model described in Chapter II.

| FROM | TO | | | | | |
|---|---|---|---|---|---|---|
| | 1 | 2 | 3 | 4 | 5 | 6 |
| 1 | 3 | (6) | 0 | 0 | 0 | (15) |
| 2 | (15) | 5 | 0 | 0 | 6 | (11) |
| 3 | 0 | (8) | 0 | 5 | (12) | 0 |
| 4 | 0 | 0 | (7) | 0 | (13) | 0 |
| 5 | 0 | (14) | (19) | 8 | 0 | 10 |
| 6 | 7 | 3 | 0 | 4 | (21) | 0 |

The transition matrix may also be depicted by the schematic diagram in Fig. 69. All transitions are shown in this diagram. The circle size associated with each cluster is proportional to the number of members in each cluster. The sign of the VEOF 1 coefficient associated with each cluster may be used to classify the clusters into two groups. Clusters 3 and 4 are contained in the inactive group, which refers to the inactive monsoon trough and the lack of tropical cyclones over the monsoon trough region (i.e., negative VEOF 1). Clusters 1, 2 and 6 are then classified in the active group (i.e., positive VEOF 1). Cluster 5, which represents the small anomalies about the climatic mean, does not belong to either group.

Based upon these classifications, the transitions between the clusters are also grouped into two sets. One set includes transitions that occur between clusters within the active or

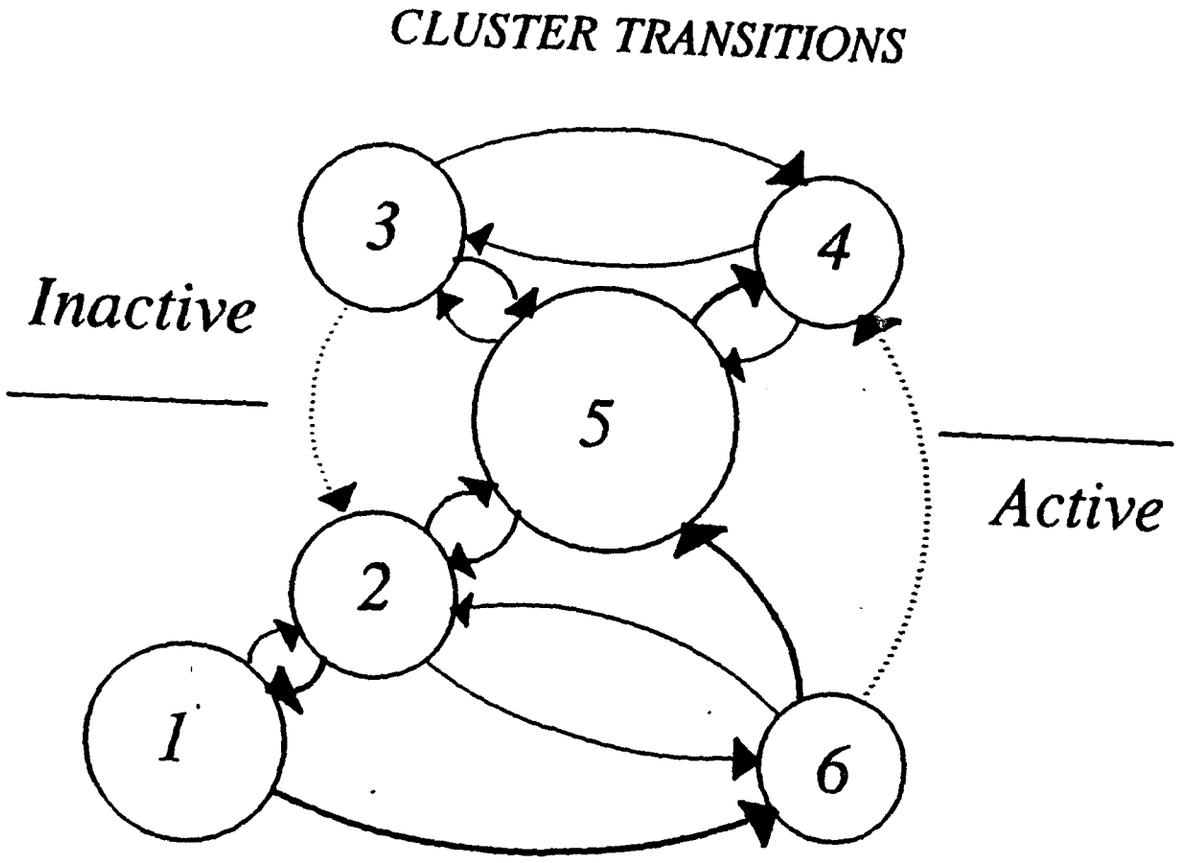


**Fig. 69** Schematic diagram indicating the transition paths between the six clusters. The circle size is proportional to the number of members in each cluster. Transitions represented by dashed lines are taken less frequently than transitions represented by thick lines. All transitions observed to occur are shown. Active/inactive refers to the state of the monsoon trough (see text for details).

inactive group exclusively (e.g., transitions between clusters 1 and 2, 2 and 6, or 3 and 4). The second group contains transitions that lead to a crossing of the boundary between the active and inactive clusters. As illustrated in Fig. 69, these transitions may pass through the small-anomaly cluster 5. Emphasis is placed upon this second set of transitions, because they result in major circulation changes over the tropical western North Pacific and associated changes in tropical cyclone characteristics.

Transitions that lead to a change from active to inactive clusters are shown in Fig. 70a. Thick arrows between clusters represent transitions that occur more frequently than transitions depicted with thin or dashed arrows. The primary transitions between active to inactive clusters pass through cluster 6. The transition from cluster 6 primarily passes to cluster 5 and then to cluster 4, or less frequently to cluster 3. However, some direct transitions from cluster 6 to cluster 4 occur. These transitions from active to inactive clusters via cluster 6 usually begin in cluster 1.

It is of interest to examine Fig. 70a in relation to the total number of transitions in Table 11. Although the transition from cluster 5 to cluster 4 is a major link in the change from active to inactive clusters (Fig. 70a), this transition path is not significant in the context of all possible transitions (Table 11). However, all eight of the transitions from cluster 5 to 4 defined in Table 11 are a part of the more general 1-6-5-4 transition path shown in Fig. 70a. The opposite situation pertains to the minor transition between clusters 5-3 in Fig. 70a. In this case, the transition from cluster 5 to cluster 3 is statistically significant in the context of all possible transitions. However, only four of the 19 transitions from cluster 5 to cluster 3 are associated with a 6-5-3 change from active to inactive clusters. The remaining 15

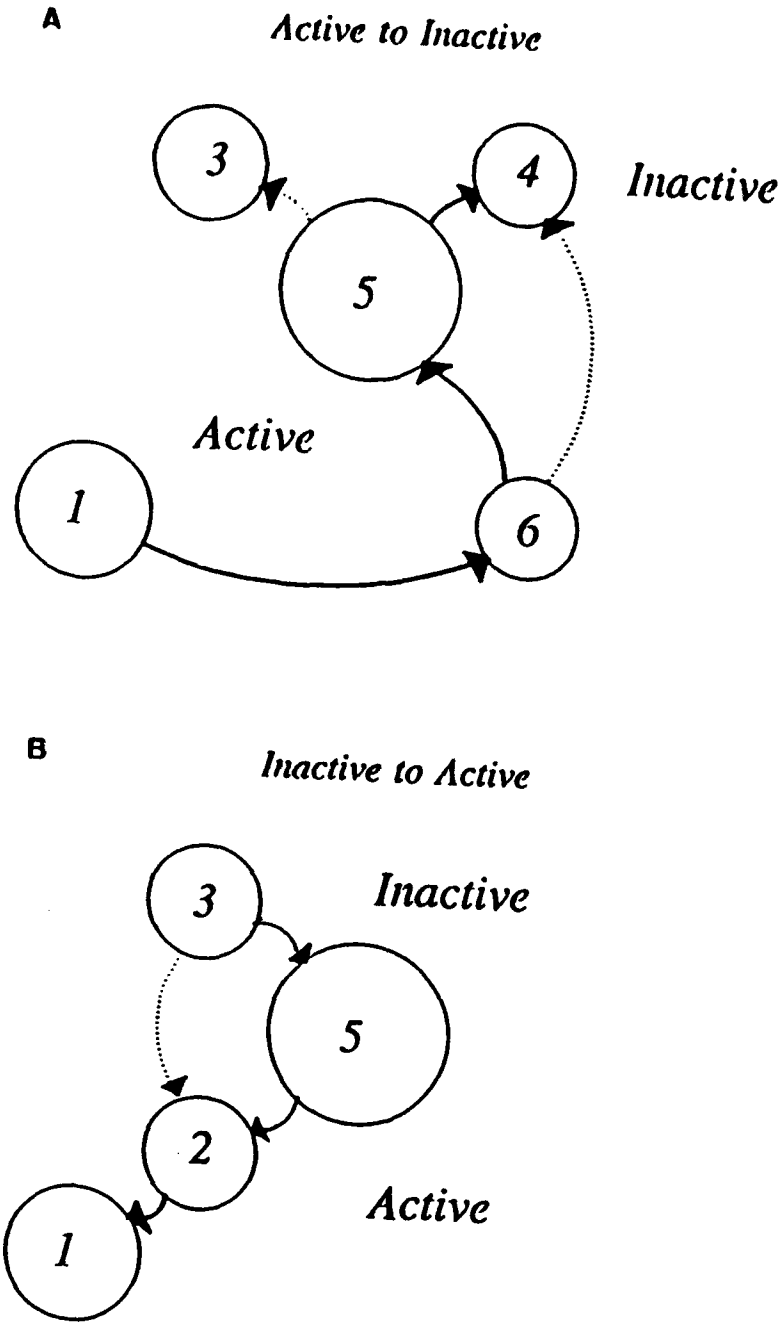


**Fig. 70** Schematic diagram as in Fig. 69, except indicating only the preferred transition paths leading from (a) active to inactive clusters, and (b) inactive to active clusters.

transitions are associated with passages from the inactive clusters to the small-anomaly cluster and then to cluster 3 (i.e., transitions 4-5-3 or 3-5-3).

Transitions that lead from inactive clusters to active clusters pass through cluster 3 (Fig. 70b). Although transitions from cluster 3 primarily pass through cluster 5 before proceeding to cluster 2, some direct transitions between clusters 3 and 2 occur. This portion of the transition from inactive to active clusters is symmetric with the transitions from active to inactive clusters via clusters 6-5-4 or clusters 6-4. However, no transition paths are found that proceed from clusters 3-5-6, which would be symmetric with the observed transition path between clusters 6-5-3. Rather, the transition from inactive to active clusters generally proceeds through cluster 2 to cluster 1. This is consistent with the interpretation of cluster 2, which is dominated by a strong subtropical ridge and a slightly active monsoon trough (Fig. 44b), while cluster 1 contains a very active monsoon trough and a mildly strong subtropical ridge. It is also consistent with the short durations of passages through cluster 2 (Table 11).

The transitions between active and inactive clusters represent the most dramatic transformations of the large-scale tropical circulation over the western North Pacific. Based upon the relationships between the clusters and tropical cyclone characteristics, these transitions would have large impacts upon tropical cyclone genesis and motion. The following subsections will provide physical descriptions pertaining to the primary transition paths between active and inactive clusters. These descriptions are based upon composites of anomalous 700 mb winds, OLR, 700 mb streamfunction and velocity potential, and 200 mb streamfunction and velocity potential. Composites are constructed relative to the entrance time (denoted as day 0) into the cluster contained in the opposite group (i.e., during a

transition between clusters 6-5-4, day 0 is the time of entrance into cluster 4). The composites begin 15 days prior to day 0 (i.e., -15 days) and proceed to 2 days after day 0 (i.e., +2 days). Representative composites are used to describe the evolution of the anomalous large-scale tropical circulation during the transition between the active and inactive cluster groups.

### 1. Transition 1-6-5-4

There are 16 instances of a cluster transitions that began in cluster 1, proceeded through cluster 6, and then either transitioned directly to cluster 4, or indirectly transitioned to cluster 4 via cluster 5. The average time required to complete this series is 12.3 days with a standard deviation of 6.4 days. The composite procedure described above is applied to each of the tropical circulation variables, and the results are compared to several tropical circulation characteristics in the final subsection.

#### *a. 700 mb Wind Anomalies and OLR Anomalies*

At -15 days, weak 700 mb cyclonic circulation anomalies centered over the Indian subcontinent and the South China Sea are associated with a mildly active monsoon trough and areas of enhanced convection (Fig. 71a). A region of enhanced convection extends beyond 160°E along 5°N, and a weak cyclonic anomaly at 5°N, 140°E. A large anticyclonic anomaly centered near 25°N, 150°E indicates that the subtropical ridge is stronger than normal.

At -12 days (Fig. 71b), the anomalies associated with the active monsoon trough increase, and the extension of the trough to 160°E is more pronounced. Enhanced convection is associated with cyclonic anomalies at the eastern end of the extended

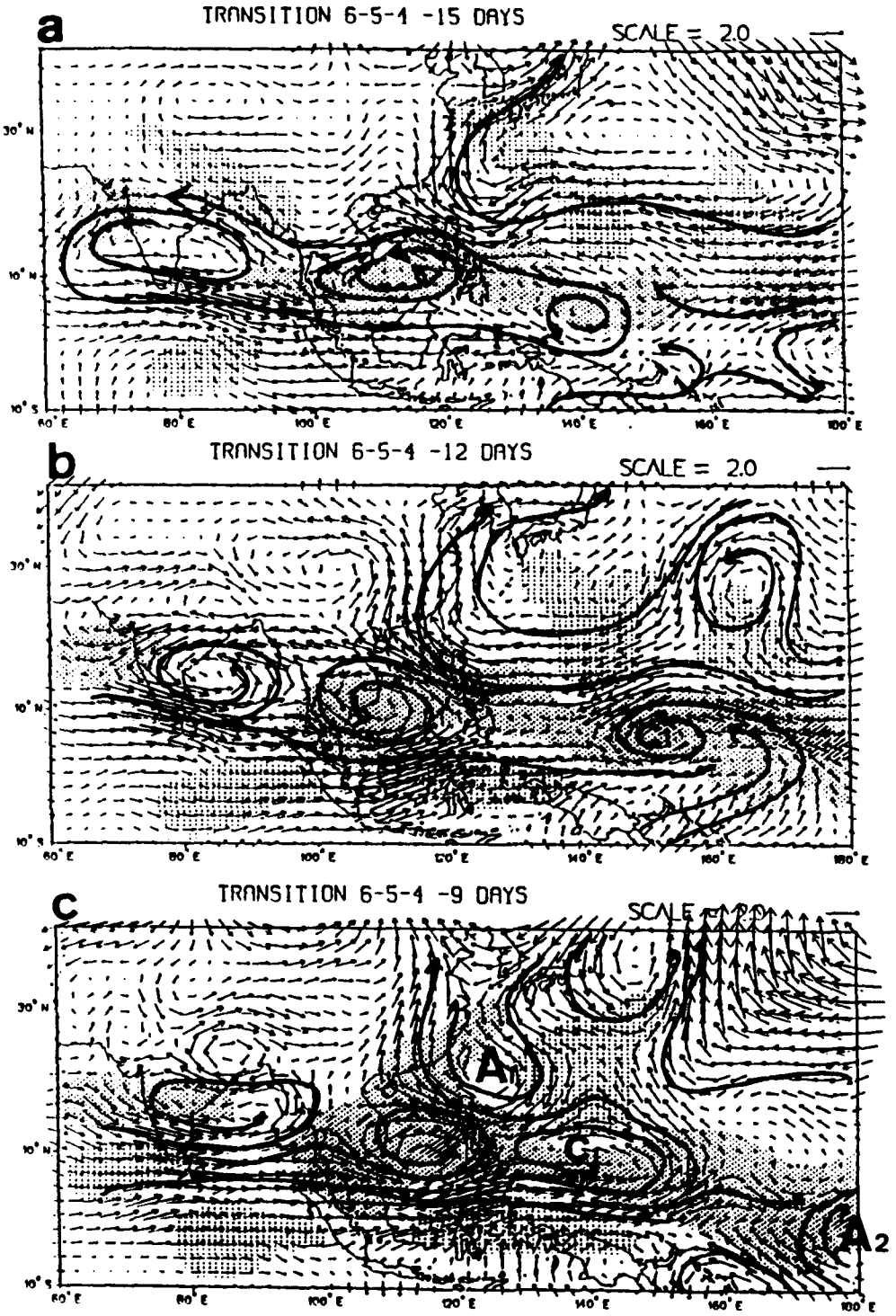


**Fig. 71** Composite for 700 mb wind anomalies and OLR anomalies for the 1-6-5-4 transition path at (**a**) -15 days, (**b**) -12 days, (**c**) -9 days, (**d**) -5 days, (**e**) -2 days and (**f**) 0 days prior to the entrance into cluster 4. Vector units are m $s^{-1}$. Dense shading marks enhanced convection regions with OLR anomalies less than -5 W $m^{-2}$. Light shading marks below average convection regions with OLR anomalies greater than 5 W $m^{-2}$.

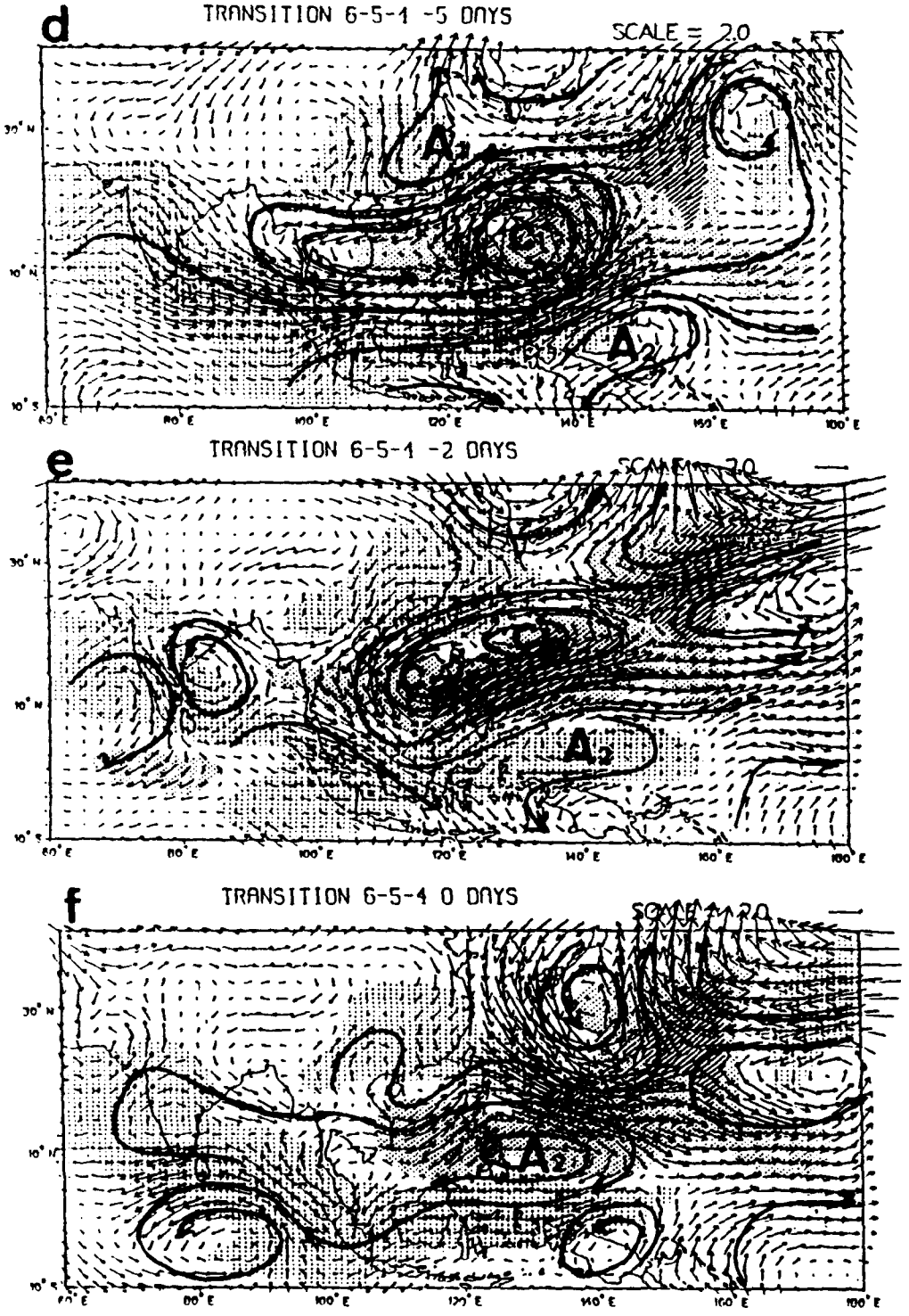


**Fig. 71** (continued).

monsoon trough (labeled C1 in Fig. 71b). In the more complete time sequence, the cyclonic circulations near 160°E appear to be associated with easterly waves that propagated westward from the central Pacific and have become part of the eastern extension of the monsoon trough. A large region of positive OLR anomalies (i.e., reduced convection) is centered on the equator at 80°E. The subtropical ridge remains stronger than normal, which indicates a cluster 1 anomaly pattern (Fig. 44a).

The strength of equatorial westerly anomalies between 100°E and 160°E at -9 days (Fig. 71c) is associated with continued intensification of the monsoon trough extension over the western Pacific and the absorption of C1, which has continued to move westward. A clockwise circulation anomaly located on the equator at 175°E has entered the domain from the east (labeled A2). The most significant aspect of the changes evident at -9 days concerns a connection in both the wind and OLR fields between the circulation associated with the monsoon trough and a midlatitude cyclonic anomaly located east of Japan at 145°E. This connection has split the large anticyclonic anomaly circulation that is present in the day -12 composite, which leaves the western portion of the anomalous ridge near 20°N, 125°E (labeled A1 in Fig. 71c). The orientation of the anomalous monsoon trough has shifted to west-east with the connection to the midlatitude anomalous circulation.

During the succeeding days, the connection between the eastern extension of the monsoon trough and the midlatitude cyclonic anomaly becomes stronger as the anomalous monsoon trough becomes oriented from the southwest to the northeast (Fig. 71d). C1 has moved northwestward and become the primary circulation associated with the reverse-oriented monsoon trough. The circulation A2 has also become oriented from

southwest to northeast, and has continued to move westward as if coupled to C1. The region of enhanced convection associated with the anomalous monsoon trough has also moved northward and westward in conjunction with the anomalous circulations. An elongated region of reduced convection extends along the equator between 90° and 160°E. This region of positive OLR anomalies can be traced to an eastward shift in the anomalies located along the equator at 80°E at -12 days.

The wind and OLR anomaly patterns described at -5 days are well represented by the cluster 6 pattern. Furthermore, the evolution of the anomalies via northwestward propagation of anomalous circulation features is similar to northwestward-moving synoptic-scale features over the western North Pacific identified by Lau and Lau (1990, 1992) and Liebmann and Hendon (1990). However, the connection to the anomalous midlatitude circulation was not observed in these previous studies.

At day -2 (Fig. 71e), the primary circulation of C1 has been split into two smaller circulations located over the South China Sea (labeled C1A) and at 20°N, 130°E (labeled C1B). These circulations continue to have a southwest to northeast orientation, and have a connection with the anomalous cyclonic circulation near 30°N, 175°E The circulation associated with A2 and the area covered by positive OLR anomalies have expanded over the western Pacific.

At day 0, circulation C1A has weakened over the South China Sea and C1B has continued to move north-northeastward (Fig. 71f). The circulation of A2 has now become the dominant feature over the Philippine Sea, with anticyclonic circulation anomalies and positive OLR anomalies extending over the entire monsoon trough region, and even to

the Indian subcontinent. The combination of these anomaly patterns with the cyclonic anomalies located over the subtropical western Pacific are similar to cluster 4. Furthermore, the anomaly patterns at day 0 are almost exactly out of phase with the patterns at day -12 (Fig. 71b), which was identified with cluster 1. This is consistent with the out of phase relationships between clusters 1 and 4 discussed with respect to the anomalous wind, streamfunction and velocity potential patterns in Chapter IV.

### *b. Streamfunction Anomalies*

The evolution of the anomaly circulations described above may also be examined using the 200 mb and 700 mb streamfunction anomalies. At -15 days (Fig. 72a), weak cyclonic anomalies are found over the Philippine Sea, and anticyclonic anomalies exist east of Japan in association with a midlatitude ridge. At -12 days (Fig. 72b), the coupling of cyclonic anomalies to the north of Korea and anticyclonic anomalies over the East China Sea indicate an increase in the upper-level westerly flow over the east Asia coast. Approximately 60° long. downstream from these anomalous circulations, opposite anomaly patterns are found over the central North Pacific. The tilt of these circulations implies an extraction of energy from the westerly current, and the building of an anomalous mid-Pacific trough. Indeed, the anomalous 200 mb trough is deep enough to be associated with a 700 mb cyclonic circulation anomaly near 30°N, 165°E (Fig. 71b). This orientation of the 200 mb streamfunction anomalies as a meridional dipole over the western North Pacific and opposite circulations over the central North Pacific are similar to features described by Hsu et al. (1990) for a Northern Hemisphere winter case of a 30-60 day oscillation (Madden and Julian 1972). This

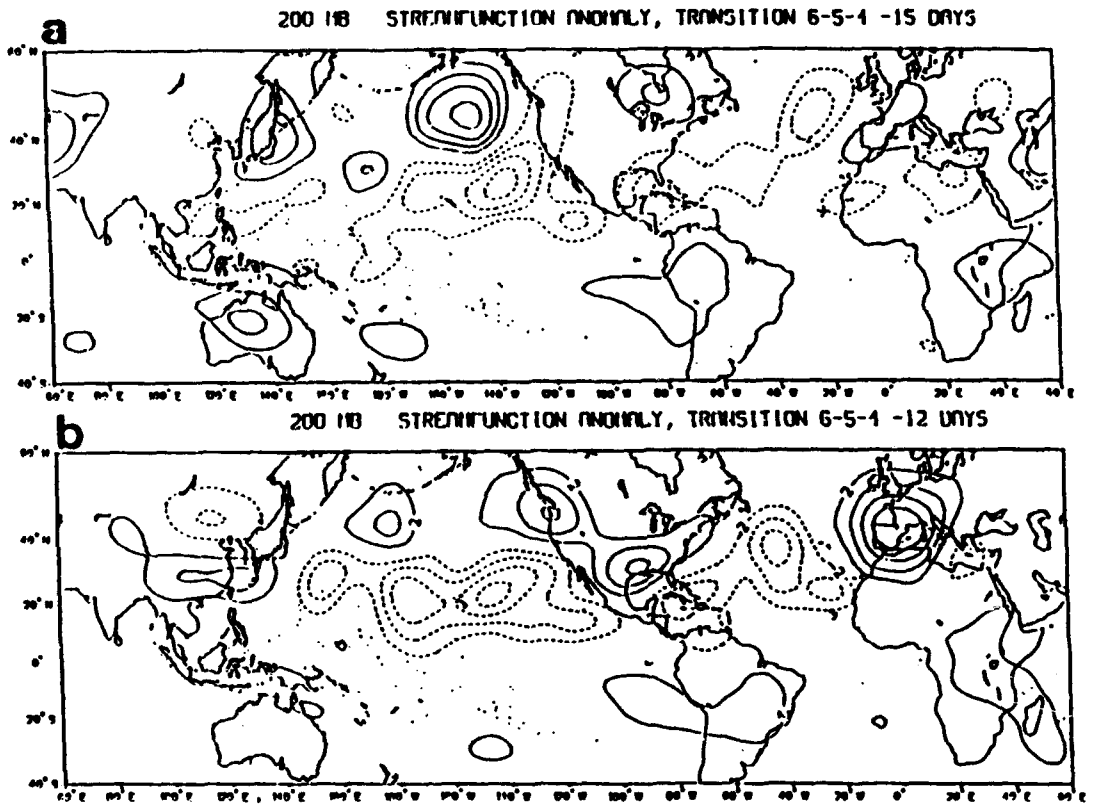


**Fig. 72** Composite for 200 mb wind streamfunction anomalies for the 1-6-5-4 transition path at **(a)** -15 days, **(b)** -12 days, **(c)** -9 days and **(d)** -5 days prior to the entrance into cluster 4. The contour interval is 2.0 x $10^6$ $m^2$ $s^{-1}$. Negative contours are dashed.

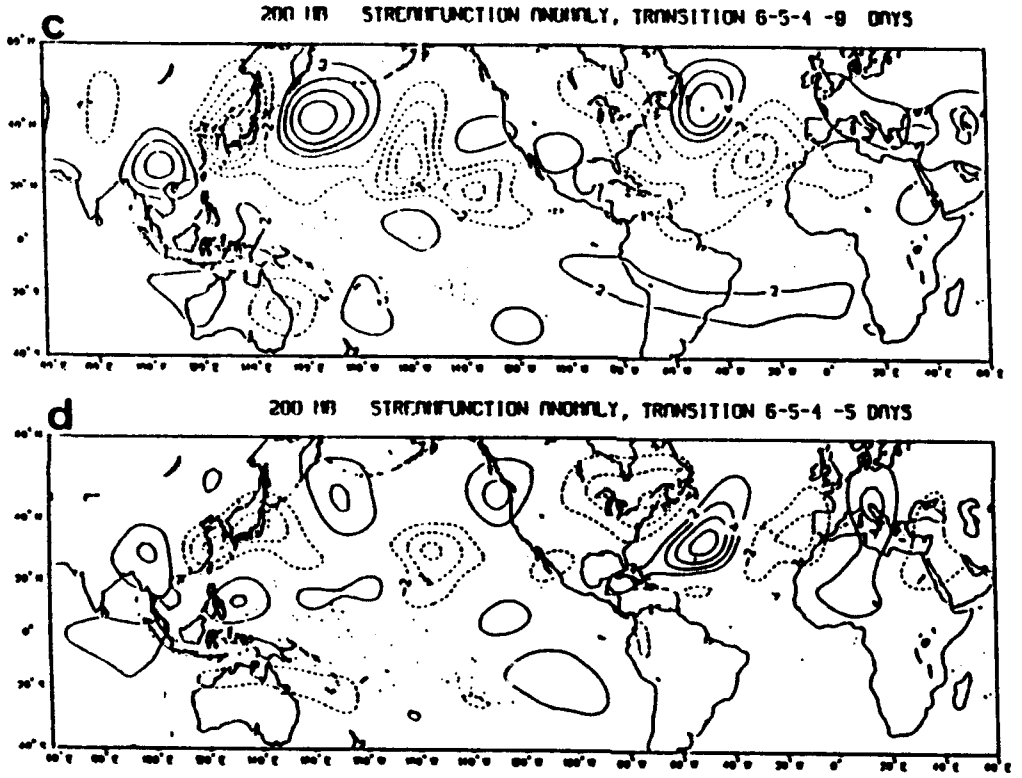


**Fig. 72** (continued).

pattern was also identified by Simmons et al. (1983) as one phase of the most unstable 40-day normal mode associated with the planetary circulations.

The 200 mb anomaly patterns at -12 days are also evident in the 700 mb streamfunction anomalies (Fig. 73b). Cyclonic anomalies over the equatorial Pacific eventually become identified with the eastward extension of the monsoon trough. The analysis of 700 mb circulation anomalies identified a connection between the eastern portion of the monsoon trough and a midlatitude circulation at -9 days (Fig. 71c). The 200 mb streamfunction anomalies undergo a transformation from a meridional dipole pattern over the western North Pacific and eastern Asia (Fig. 72b) to a Rossby wave-like pattern with the primary cyclonic circulation located immediately east of Japan (Fig. 72c). It is the 700 mb component of this midlatitude circulation that links with the monsoon trough. The upper-level wave pattern may be attributed to the enhancement of the convection within the anomalous monsoon trough (Fig. 71c) as described by Hoskins and Karoly (1981). The Rossby wave-like pattern is also present at 700 mb (Fig. 73c), which indicates an equivalent barotropic structure. The linkage between the anomalous cyclonic circulations of the monsoon trough and the anomalous midlatitude circulation east of Japan is very evident in the anomalous 700 mb streamfunction field (Fig. 73c) at -9 days.

At -5 days, the upper-level anomalous wave pattern has weakened considerably (Fig. 72d). As day 0 is approached (not shown), the pattern disappears and no other coherent large-scale features are evident in the 200 mb streamfunction anomalies. At -5 days, the anomalous cyclonic circulation associated with the monsoon trough is linked with cyclonic anomalies that cover much of the western and central North Pacific.

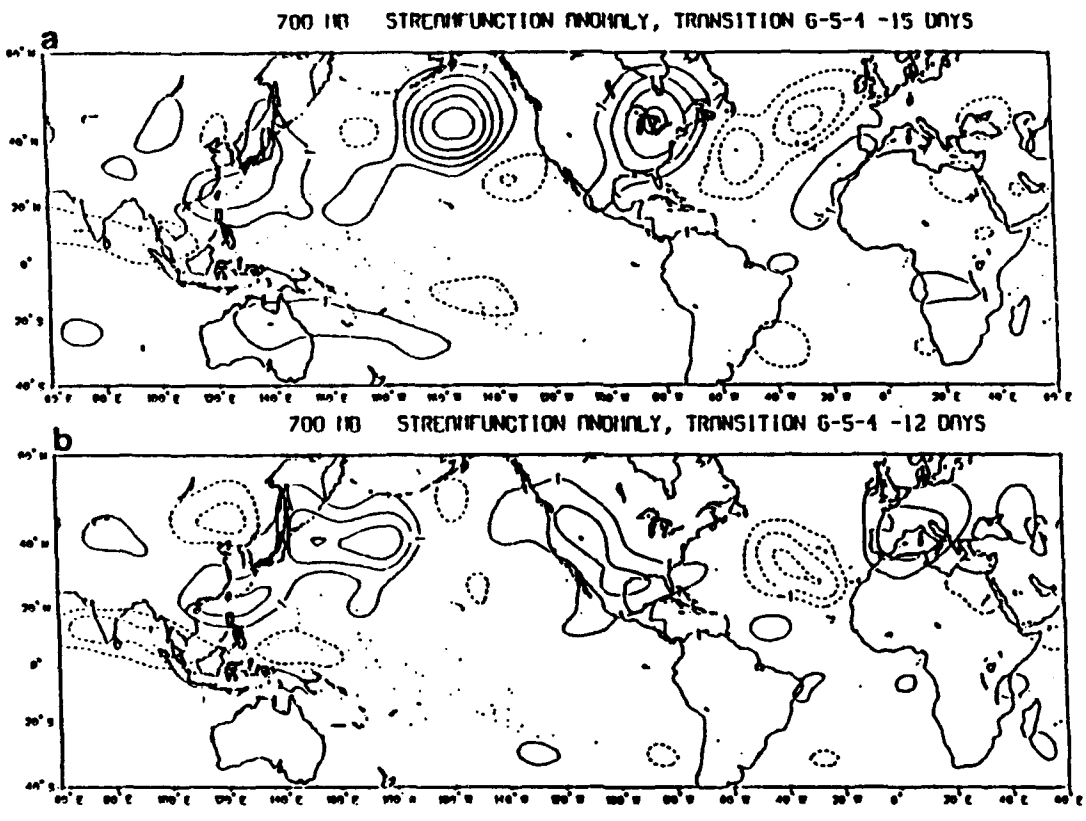


**Fig. 73** As in Fig. 72, except for 700 mb.

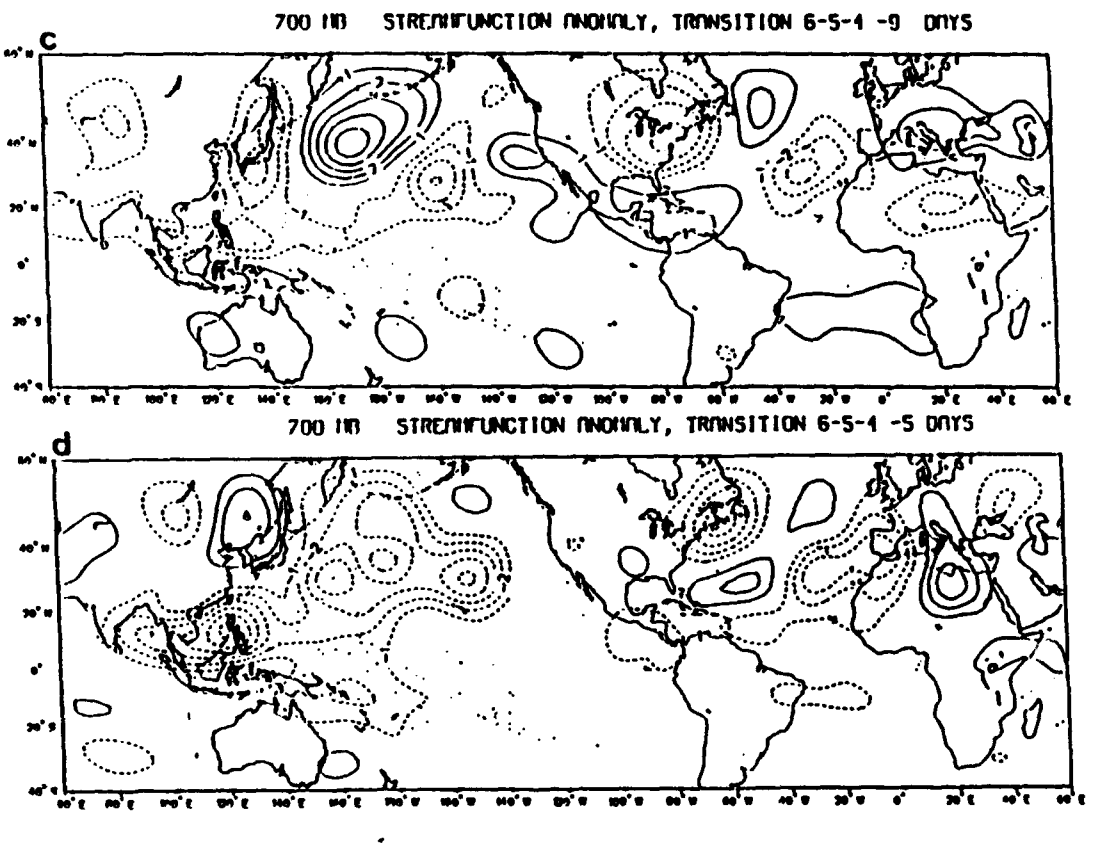


**Fig. 73** (continued).

### c. *Velocity Potential Anomalies*

At -15 days, the 200 mb (700 mb) velocity potential anomalies indicate large-scale divergence (convergence) associated with the active monsoon trough and enhanced convection (Figs. 74a, 75a). There is anomalous convergence at 200 mb (Fig. 74a) over the position of the 700 mb anomalous subtropical ridge. At -12 days, there is a 200 mb divergence center over Indonesia and a second divergence center over the equatorial central Pacific (Fig. 74b). At 700 mb, one large convergence center covers both of these regions (Fig. 75b). These convergence/divergence patterns are consistent with the extension of the anomalous monsoon trough over the western Pacific. Furthermore, the upper-level velocity potential anomalies represent a wavenumber one pattern, while the 700 mb anomalies appear to represent a weak wavenumber two pattern. Over the western and eastern Pacific, the 700 mb and 200 mb convergence and divergence patterns are oriented such that large-scale descent is implied over the eastern Pacific with ascent over the central Pacific and Indonesia. A region of descending air exists over the subtropical western Pacific that is straddled by the two primary ascent branches, and coincides with the strong subtropical ridge that is part of the cluster 1 pattern at -12 days.

Discussions in the previous subsections define the start of the reorientation of the anomalous monsoon trough at -9 days with the connection between the cyclonic anomalies associated with the trough and a midlatitude circulation that may be forced by a Rossby-like wave train emanating from the western Pacific. This connection is very evident in both the 200 mb and 700 mb velocity potential anomalies. Prior to -9 days, the 200 mb (700 mb) divergent (convergent) circulations were oriented along the equatorial

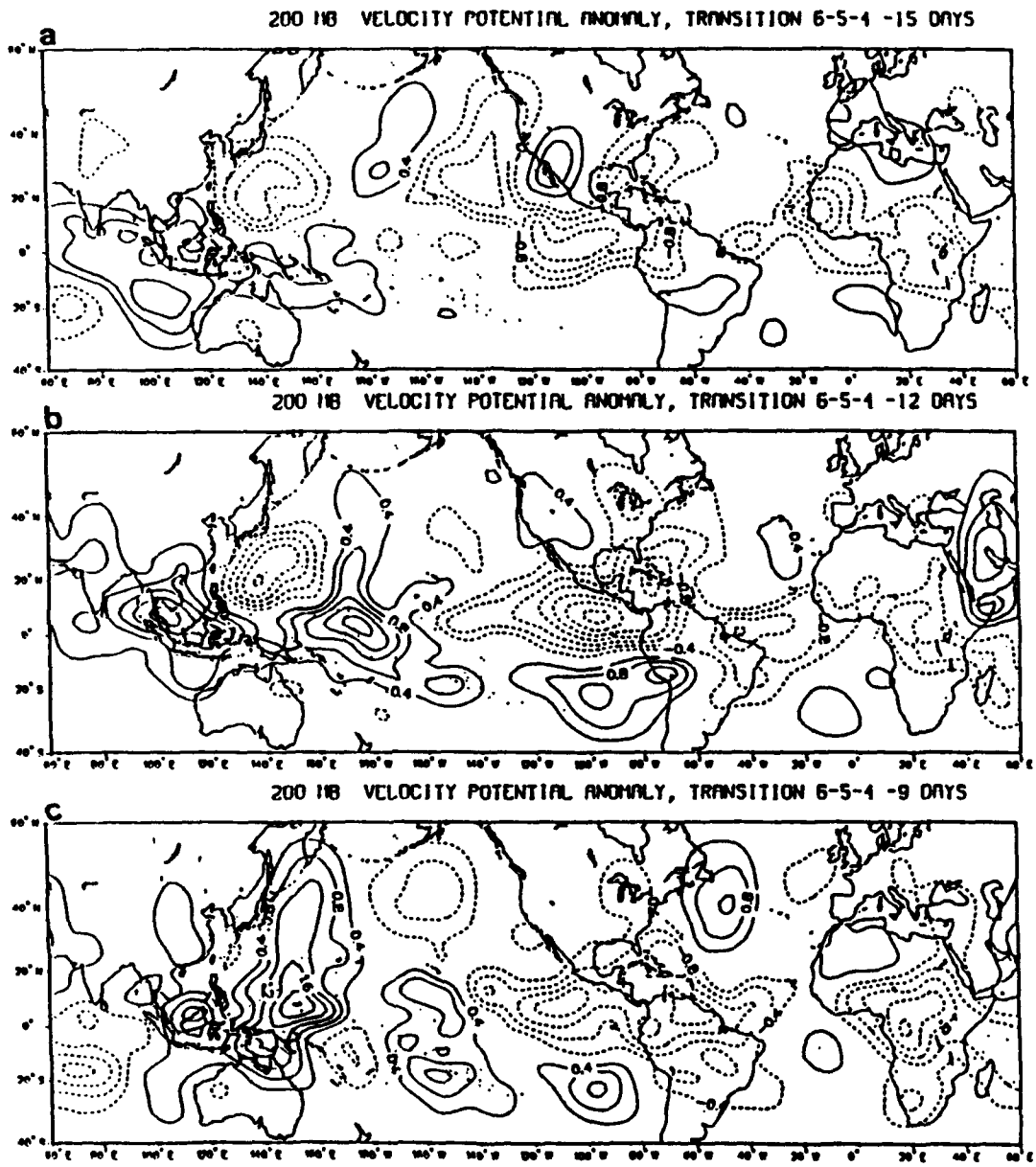


**Fig. 74** Composite for 200 mb wind velocity potential anomalies for the 1-6-5-4 transition path at (a) -15 days, (b) -12 days, (c) -9 days, (d) -5 days and (e) 0 days prior to the entrance into cluster 4. The contour interval is 0.2 x $10^6$ $m^2$ $s^{-1}$. Negative contours are dashed.

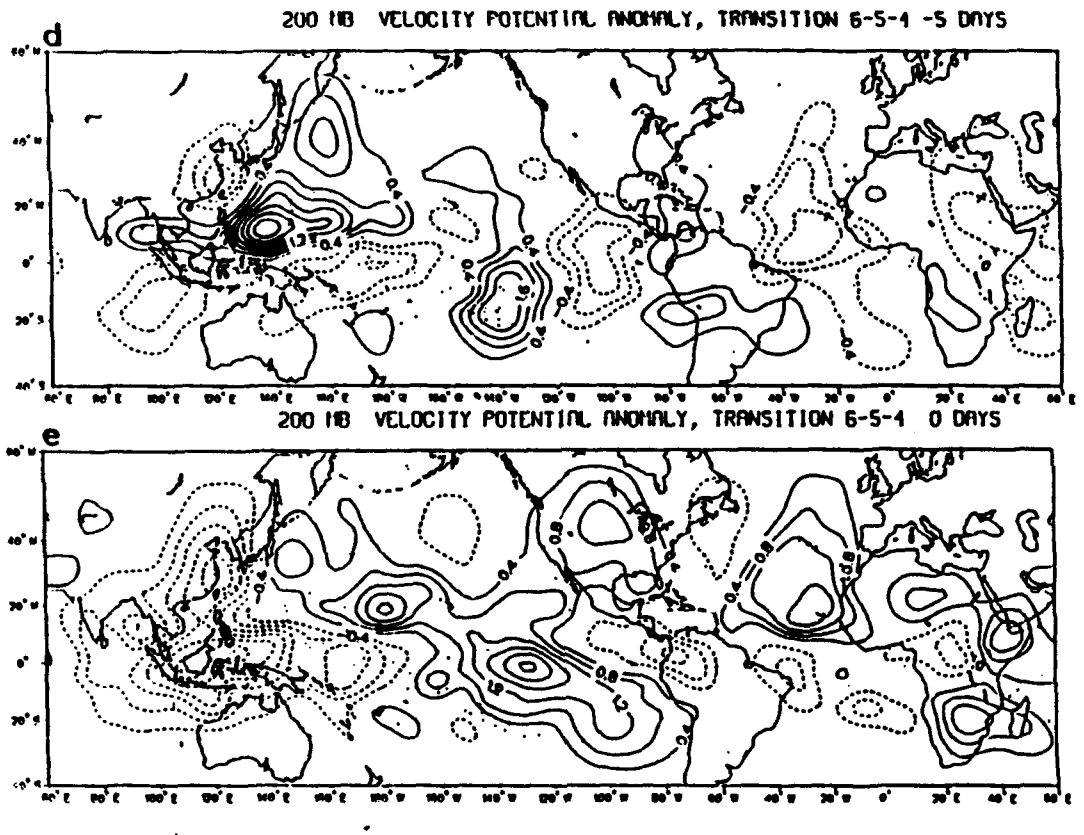


**Fig. 74** (continued).

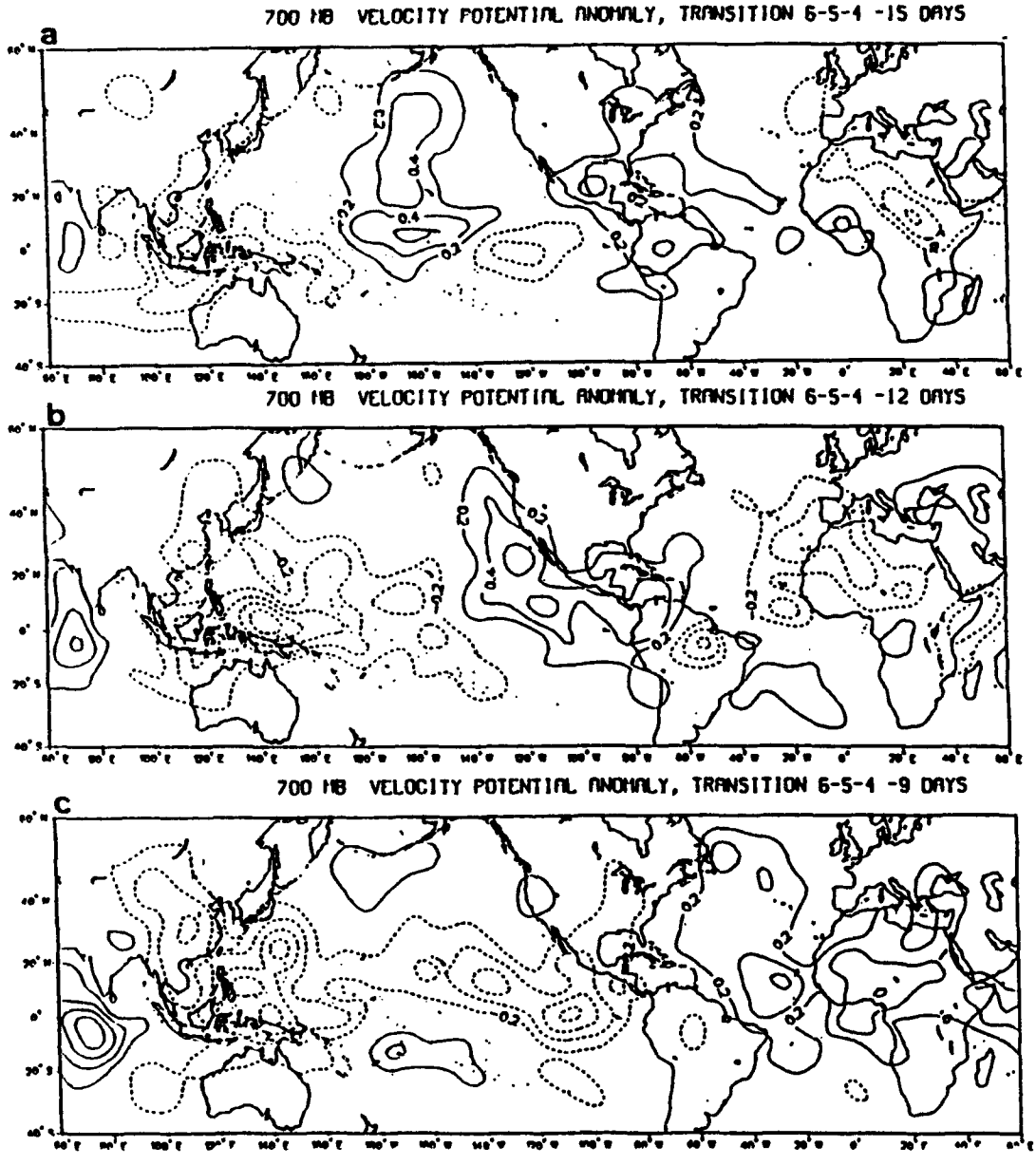


**Fig. 75** As in Fig. 74, except for 700 mb.

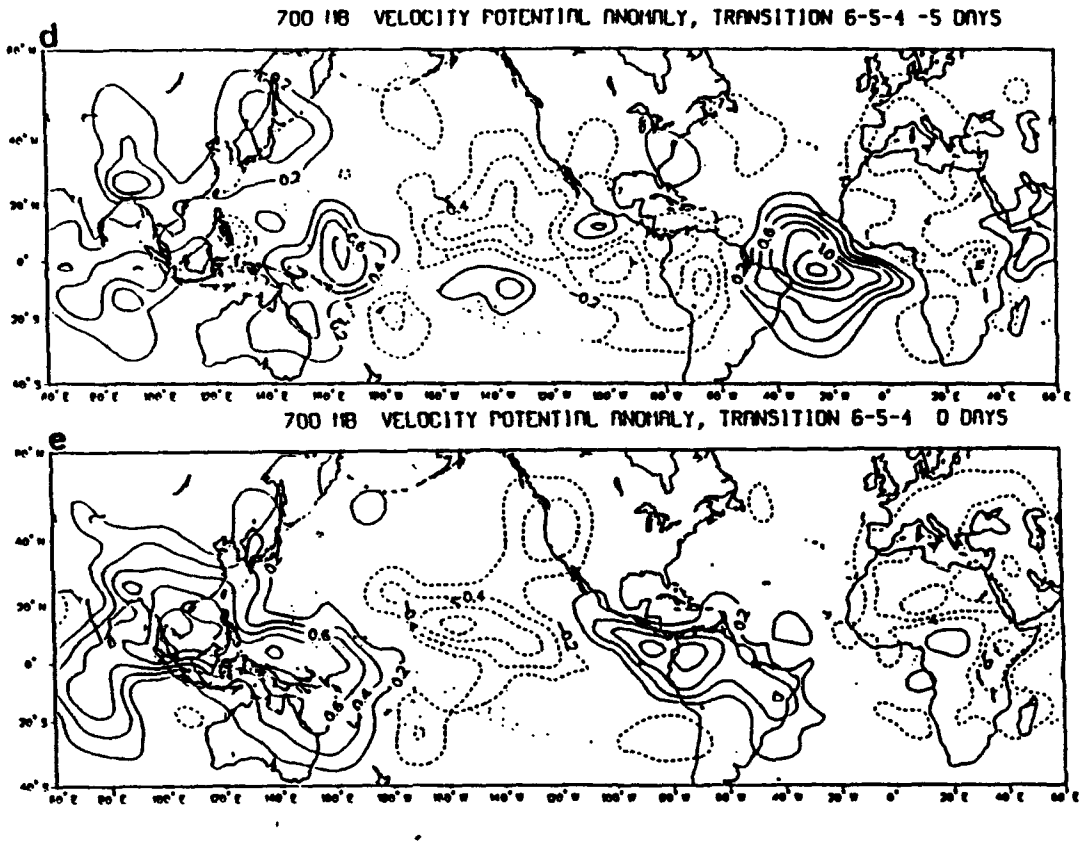


**Fig. 75** (continued).

latitudes. At -9 days, a large portion of the anomalies become meridionally oriented over the western North Pacific (Figs. 74c, 75c).

At -5 days, there is a concentrated band of 200 mb divergence associated with the anomalous monsoon trough that is oriented from the southwest to the northeast (Fig. 74d). There is still a connection between these divergent anomalies and 200 mb divergence associated with the midlatitude cyclonic circulation east of Japan. The 200 mb divergent anomalies associated with the monsoon trough and enhanced convection are straddled by a convergent anomaly to the south and a convergent anomaly to the northwest. These are related to the anticyclonic anomalies and lack of convection associated with the anticyclonic circulations A1 and A2 in Fig. 71d. There is some indication that the large-scale convergent anomaly that is south of the northward -moving monsoon trough may have propagated eastward between -9 days and -5 days. However, it is not possible to determine whether it is part of a global-scale propagating signal or whether it is locally forced by the concentrated zone of convection immediately to the north. The 700 mb velocity potential anomalies indicate a rather disorganized pattern over the western Pacific at this time (Fig. 75d).

As day 0 is approached, the velocity potential anomalies indicate large-scale 200 mb (700 mb) convergence (divergence) (Figs. 74e, 75e) over the western Pacific that would be associated with descending air and reduced convection, which is consistent with the transition to the inactive clusters.

The velocity potential anomalies complete a description of a three-dimensional evolution of anomalous patterns that indicate a strong coupling between the 200

mb and 700 mb circulations and large-scale convection during the 1-6-5-4 transition. A major component in the process is the linkage between the anomalous monsoon trough that extends well over the tropical western North Pacific with a midlatitude cyclonic circulation. .The presence of an enhanced 200 mb mid-Pacific trough may play an active role in this linkage. The enhanced trough is related to a large-scale upper-level dipole anomaly pattern, which represents energy input into the westerly current over the western North Pacific, and extraction of the energy within the mid-Pacific trough. The critical aspect of the transition seems to be the transformation of the upper-level dipole pattern to a Rossby-wave like pattern with a large cyclonic anomaly east of Japan. The lower-level circulation of this cyclonic anomaly becomes linked with the monsoon trough. Therefore, the entire process involves many scales of motion at upper and lower levels, plus involves both large-scale dynamical and diabatic processes.

The predominance of the global-scale 30-60 day oscillation is best identified as an upper-level wavenumber 1 divergent circulation. Because the 200 mb velocity potential anomalies do seem to propagate eastward during the 1-6-5-4 transition, a time-longitude depiction of the 200 mb velocity potential anomaly is examined during this transition (Fig. 76). The anomalies are averaged in a near equatorial band between 5°S-10°N over the longitudes 60°E-150°W. A combination of westward and eastward propagation of the large-scale velocity potential anomalies is evident between -15 and 0 days. The largest divergent anomalies exist over the equatorial western Pacific at -6 days, which seems to be a time and region where eastward- and westward-moving components merge. These may be associated with westward-moving easterly waves within the eastern extension of the

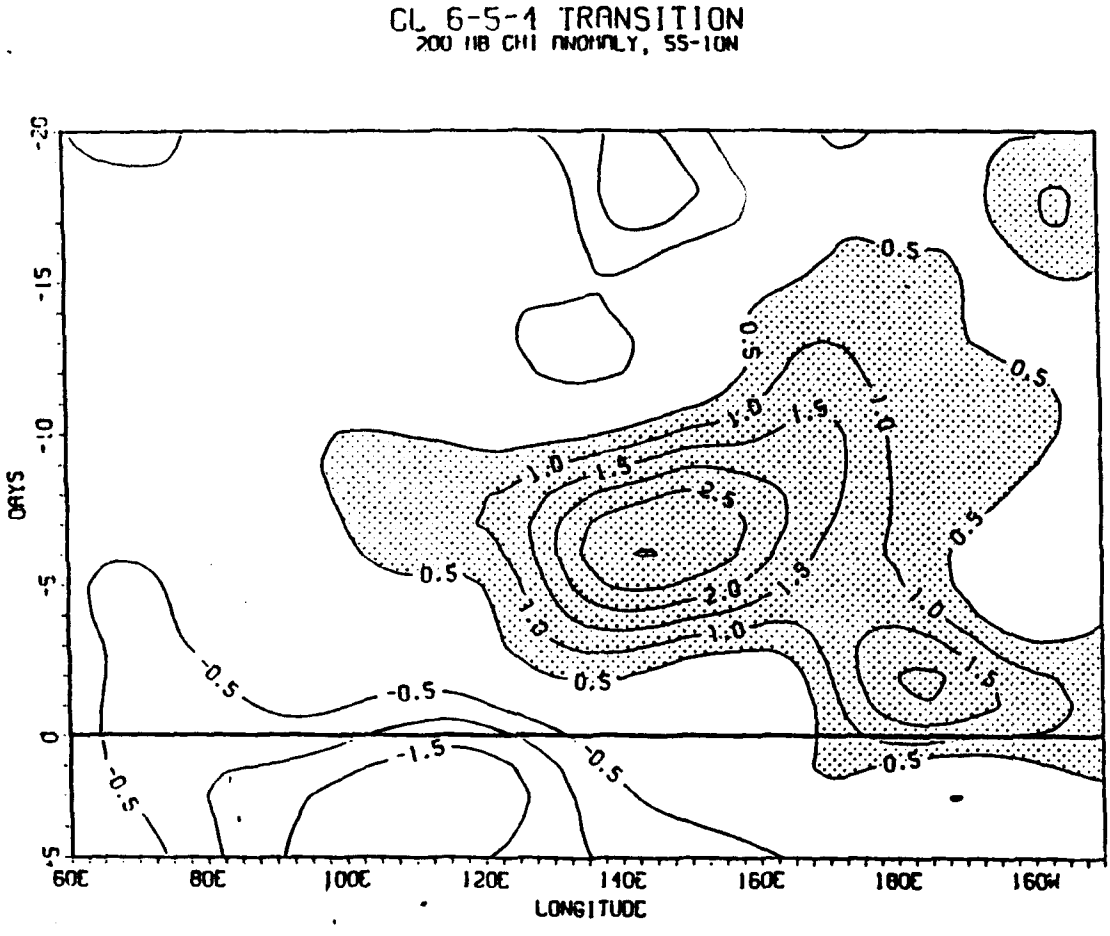


**Fig. 76** Time-longitude section (5°S - 10°N) of 200 mb anomalous velocity potential during the 1-6-5-4 transition path. Day 0 (thick horizontal line) marks the time of entrance into cluster 4. The contour interval is 0.5 x $10^{-6}$ $m^2$ $s^{-1}$. Positive contours are shaded.

anomalous monsoon trough and eastward-moving super cloud clusters associated with the 30-60 day oscillation.

### *d. Tropical Cyclone Characteristics*

Although the above discussion has concentrated on the evolution of the large-scale circulation features associated with the 1-6-5-4 transition, it is evident from the anomaly patterns that tropical cyclone characteristics may have both an active and passive role in the large-scale circulation transition. In a passive sense, the tropical cyclone genesis regions and track types will be altered by the transformation of the large-scale circulations throughout the transition period. Early in the period when cluster 1 is dominant, genesis would be more likely within the active monsoon trough over the South China Sea and Philippine Sea. The presence of a strong subtropical ridge at -15 and -12 days would suggest a preference for straight-moving tropical cyclones. This is consistent with the classification of the anomaly patterns into cluster 1, which is predominantly associated with straight-moving tropical cyclones (Table 9).

Tropical cyclones may also play a more active role in the transition process. During 12 of the 16 cases used to construct the 1-6-5-4 composites, the circulations C1A and C1B are associated with tropical cyclones. The cyclone associated with C1A is either a South China Sea storm, or a Philippine Sea storm that is following a straight-moving track. Cyclone C1B follows a recurving track type. The effect of these multiple cyclone situations upon the association of track types with cluster number was discussed earlier with respect to Table 9. Many of the recurving cyclones that are classified with clusters 1 or 2, and the straight-moving and South China Sea cyclones that are classified with clusters 4 and

6, are associated with this transition cycle. Therefore, the generation of cyclonic anomalies along the large-scale southwest to northeast oriented cyclonic circulation (C1 in Fig. 71), which is propagating northwestward, is associated with tropical cyclones. Furthermore, the combined effect of the multiple tropical cyclones may be to essentially complete the circulation transition by carrying the anomalous cyclonic circulation into the subtropical latitudes. One example of this scenario was associated with tropical cyclones Gerald, Frieda and Holly during 1987 (not shown).

*e. Relationships with Northwestward Propagating Synoptic-Scale Features*

It was mentioned above that the 700 mb wind anomaly patterns are similar to northwestward propagating synoptic-scale circulations over the western Pacific examined by Lau and Lau (1990, 1992) and Liebmann and Hendon (1990). Lau and Lau (1990) identified these features in an extended EOF analysis of 850 mb vorticity. The VEOF analysis here is calculated over a much larger domain than used by Lau and Lau and thus does not identify these local circulation features as one of the leading modes of variability. However, the 1-6-5-4 transitions described above indicate that large-scale northwestward propagating features play an integral role in the transitions of the large-scale circulations derived from this VEOF analysis.

A VEOF analysis of the 700 mb GBA wind anomalies from 1979-87 is also calculated over a smaller domain (5°S-30°N, 100°-150°E) to determine if the identification of the northwestward propagating features is dependent upon the domain. The three leading VEOFs (not shown) identify features that are similar to the leading three VEOFS of the large domain analysis. However, the fourth and fifth VEOF modes from the

smaller domain do describe a series of northwestward propagating circulations for phase orientations of 45° and 225°. These two modes, which explain 7.8% and 7.2% of the variance, are coupled with closely spaced eigenvalues and their spatial patterns are in quadrature, which is an EOF representation of a propagating signal. The spatial pattern associated with the 225° orientation of VEOF 4 is shown in Fig. 77. The mean and standard deviations of the VEOF 4 and 5 time coefficients are used to identify periods when these modes represent a significant amount of the circulation variance. During the 1979-87 June-October periods, the VEOF 4 and 5 modes were dominant in 47 cases. All 16 of the 1-6-5-4 transition periods are contained in this set. Furthermore, 87% of the 47 periods are associated with tropical cyclones over the western Pacific.

The evolution of the large-scale 700 mb and OLR anomalies during a period when the northwestward propagating features are dominant is investigated using a composite analysis similar to the analysis used to investigate the 1-6-5-4 transition. In this case, the last 12 h of a significant period is labeled as time 0, and composites for the 225° orientation are constructed from -7 days to +2 days. The average duration of these significant periods is 6.2 days with a standard deviation of 4.1 days. Note the 45° orientation pattern would be out of phase with the 225° orientation, and the VEOF 5 orientations would be in quadrature with the VEOF 4 patterns.

The composite evolution of 700 mb wind anomalies at -7 days has a strong anticyclonic anomaly over the South China Sea and the Philippine Sea that is associated with less convection than normal (Fig. 78a). However, a cyclonic anomaly and a region of enhanced convection are present to the southeast of the anticyclonic anomaly. At

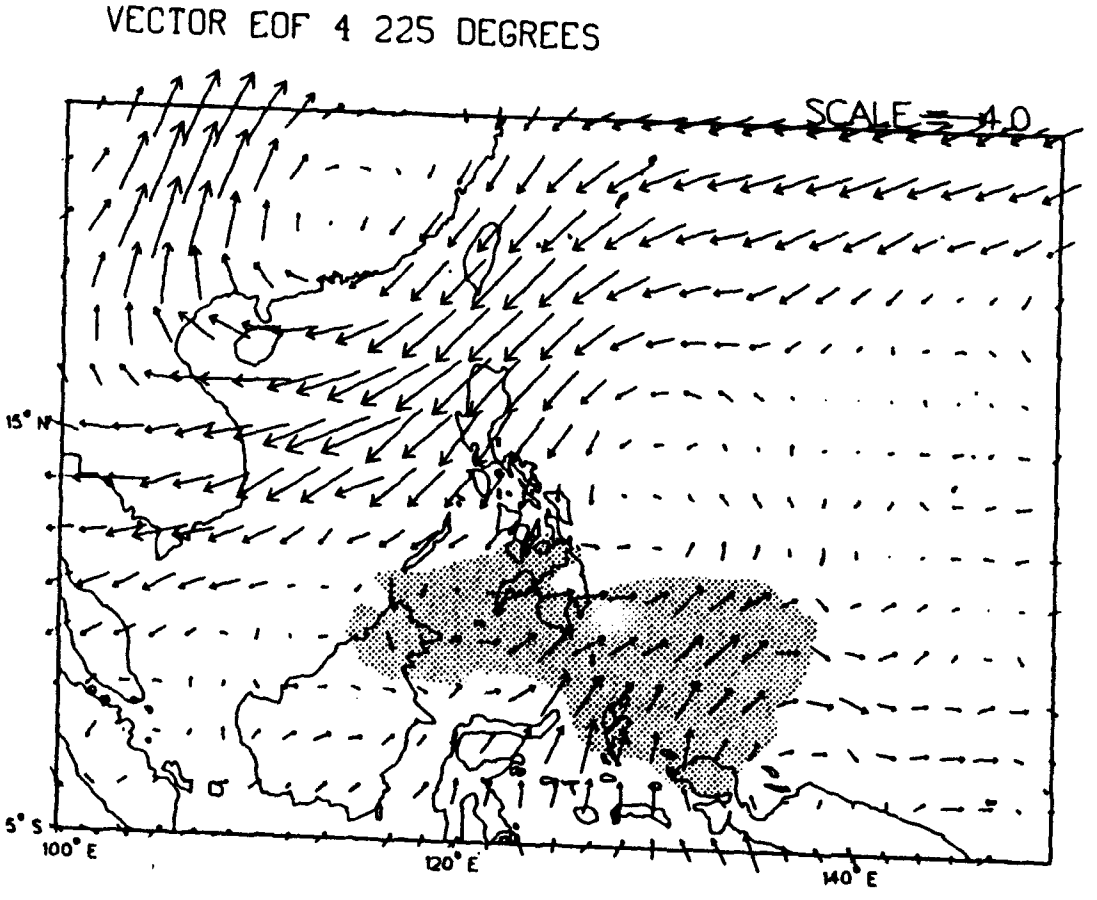


**Fig. 77** Structure of VEOF 4 computed over the smaller domain and oriented at 225°. Units are nondimensional.

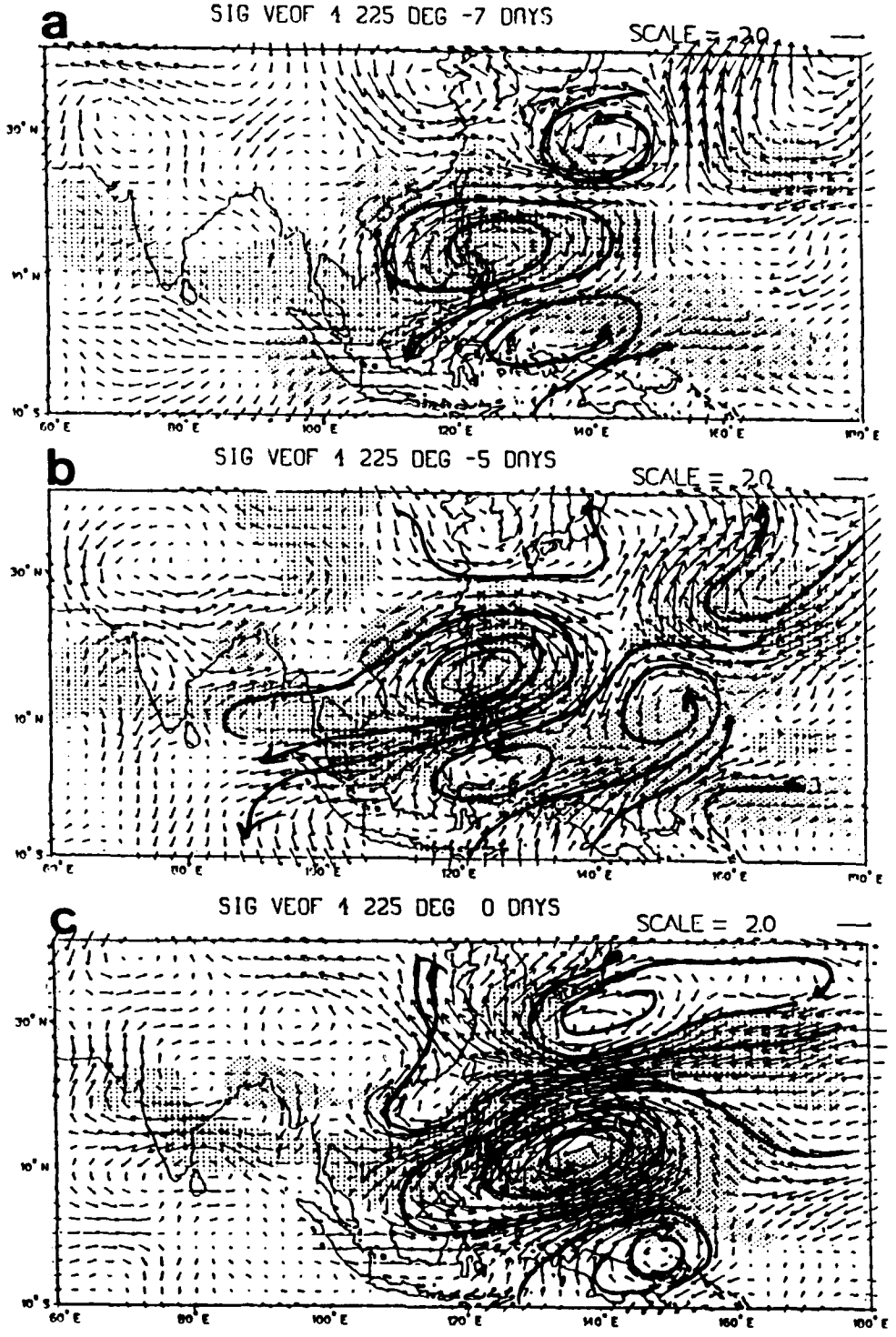


**Fig. 78** Composite for 700 mb wind anomalies and OLR anomalies for the variability of VEOF 4 during periods containing significant coefficients at **(a)** -7 days, **(b)** -5 days and **(c)** 0 days prior to the end of the period. Vector units are m $s^{-1}$. Dense shading marks enhanced convection regions with OLR anomalies less than -5 W $m^{-2}$. Light shading marks below average convection regions with OLR anomalies greater than 5 W $m^{-2}$.

-5 days (Fig. 78b), the anticyclonic circulation and the positive OLR anomalies are becoming elongated from the southwest to the northeast. The cyclonic anomalies to the southeast are more intense than at -7 days and are also oriented from the southwest to northeast. By day 0 (Fig. 78c), the anticyclonic anomaly has moved northwestward and weakened while the cyclonic anomalies to the southeast have intensified and cover the Philippine Sea. The OLR anomalies associated with the cyclonic anomalies indicate enhanced convection is occurring over the Philippine Sea. Therefore, the anomaly pattern is reversed during the 7-day period. In comparison of the anomalous circulation patterns during the 1-6-5-4 transition patterns defined above, these patterns are limited to circulation and convection anomalies over a smaller region of the western Pacific. When these northwestward propagation periods occur in connection with the transitions, these patterns are a subset of larger scale 1-6-5-4 anomalies over the Indian Ocean and the midlatitudes.

The evolution of the anomalous patterns associated with the smaller domain VEOF patterns are summarized using time-longitude diagrams (Fig. 79). Although the propagation of individual sets of meridional wind anomalies is westward, the evolution of the meridional wind anomalies exhibits an eastward group velocity with successive periods of northerly wind anomalies along the equator beginning farther to the east (Fig. 79a). The meridional wind anomalies reach a maximum at day 1, which is consistent with the definition of day 0 as the end of a dominant northwestward propagation period. Each occurrence of northerly anomalies along the equator is separated by approximately six days. The zonal wind anomalies also propagate westward along the equator (Fig. 79b). Because the zonal winds are more representative of the larger-scale circulations over the tropics, the evolution of the

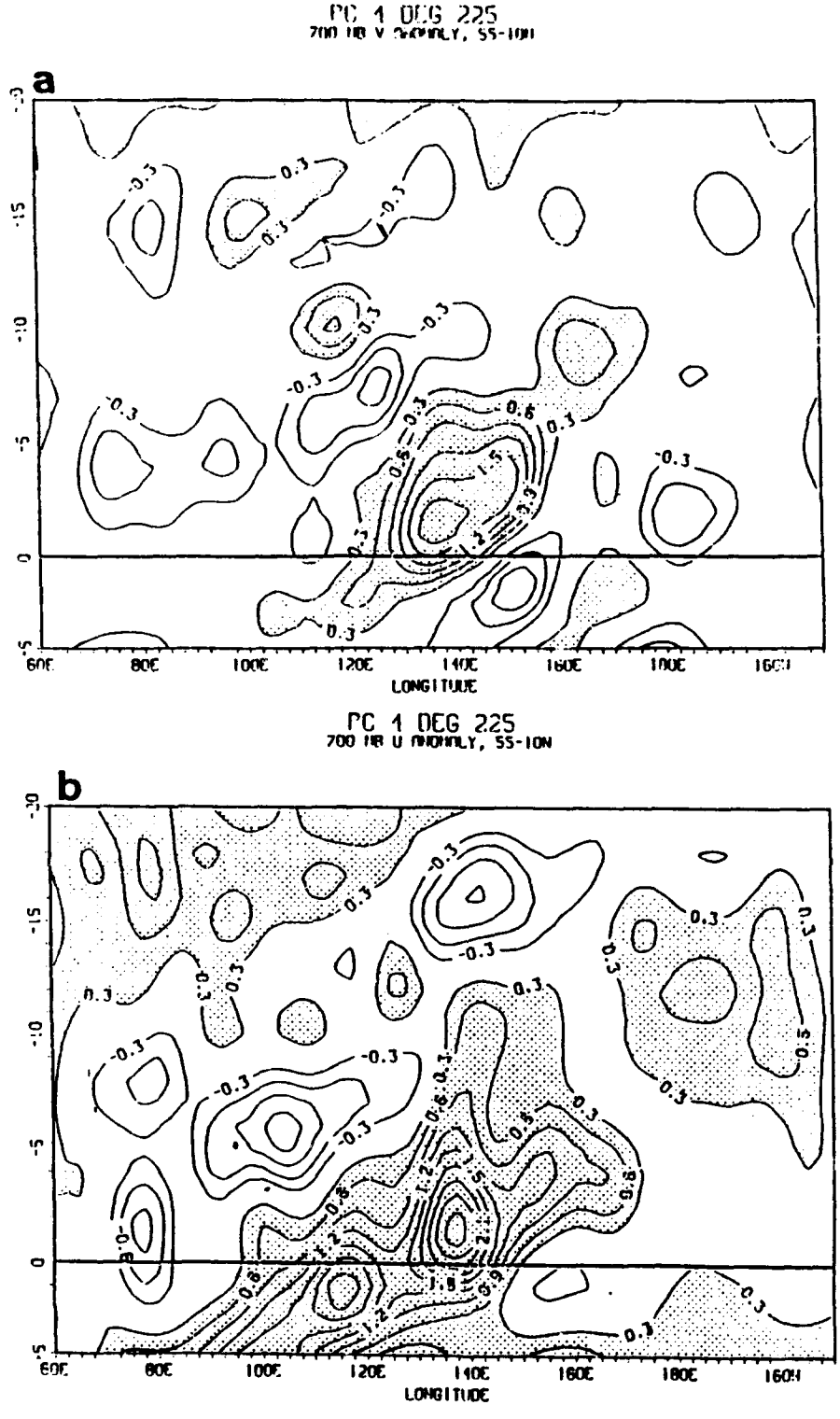


**Fig. 79** Time-longitude section of 700 mb anomalous (a) meridional wind and (b) zonal wind components averaged between 5°S-10°N during periods containing significant VEOF 4 coefficients. Units are m $s^{-1}$. Positive contours are shaded.

associated monsoon trough and subtropical ridge during these periods is examined on a latitude-time diagram (Fig. 80). Westerly anomalies over the equatorial western Pacific, coupled with easterly anomalies over the subtropical latitudes, define an active monsoon trough that has peak amplitude prior to -10 days. Comparison of Figs. 79 and 80 indicates that the amplitude in the meridional anomalies increases as the strength of the zonally oriented anomalous circulation weakens near -10 days. This is suggestive of an energy transfer from the zonal kinetic energy of the large-scale equatorial westerlies to eddies that are represented by the fluctuations in the meridional component. The average kinetic energy based upon the same composite definitions is shown by the solid line in Fig. 81. The zonal kinetic energy, which peaks near -15 days, gradually diminishes as the anomalous westerlies decrease and energy is transferred to the disturbance circulations, which is signified by the increase in the amplitude and organization of the meridional winds after -7 days.

The evolution of the zonal and meridional wind anomalies associated with the 1-6-5-4 transitions is compared with the above VEOF analysis of the smaller domain. The variability of the transition pattern meridional wind anomalies (Fig. 82) does not indicate a regular progression of wave disturbances as was found with the smaller domain VEOF 4 wind data. Rather, the 1-6-5-4 transition is dominated by the cyclonic zonal wind circulation associated with the enhanced monsoon trough (Fig. 83). The maximum westerly anomalies along the southern boundary of the anomalous monsoon trough are reached at -8 days. Whereas the circulation anomalies associated with the cluster 1-6-5-4 transitions are dominated by the zonal wind fluctuations, disturbances propagating northwestward over the western Pacific that are isolated by the VEOF analysis over the smaller domain are dominated

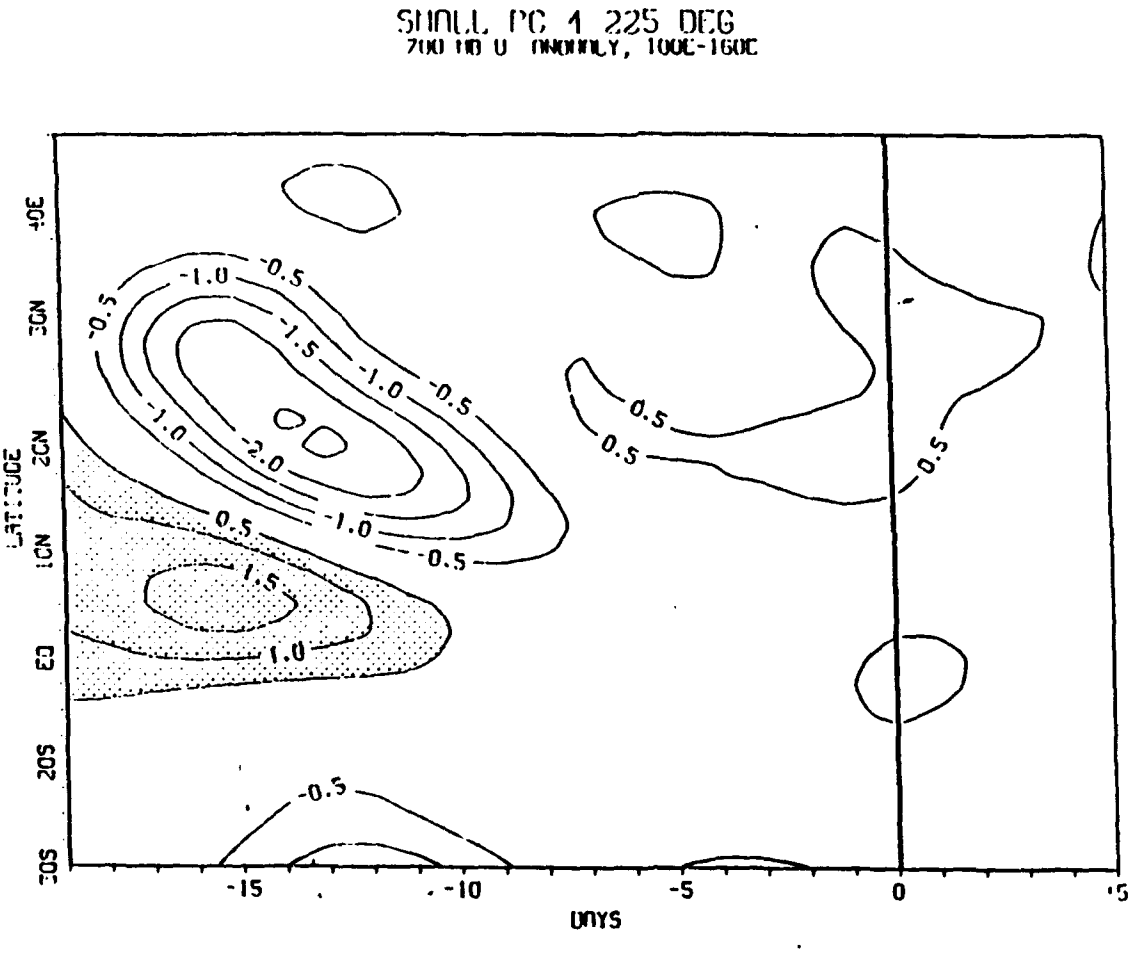


**Fig. 80** Latitude-time section of 700 mb anomalous zonal wind components averaged between 100°E-160°E during periods containing significant VEOF 4 coefficients. Units are m $s^{-1}$. Positive contours are shaded.

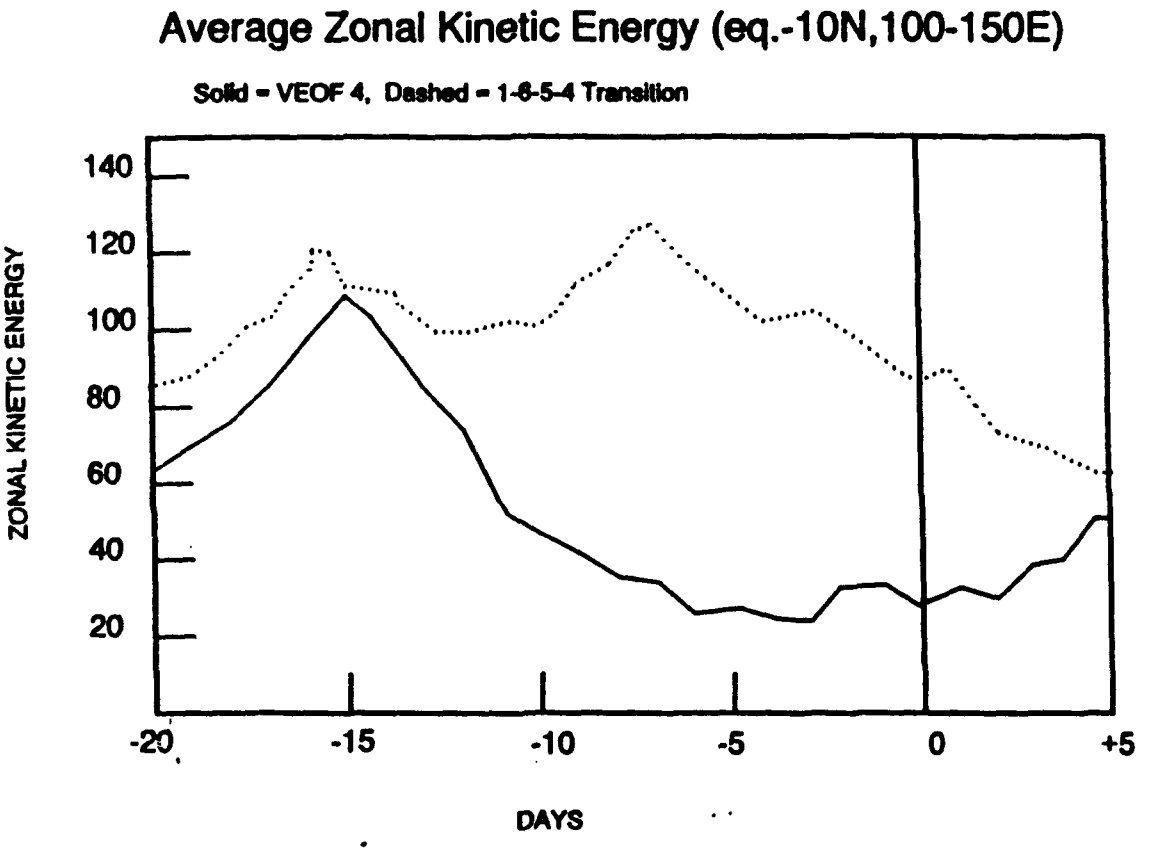


**Fig. 81** Area averaged (equator-10°N, 100°-150°E) values of zonal kinetic energy as a function of time along the 1-6-5-4 transition path (dashed line) and throughout periods of significant VEOF 4 coefficients (solid line).

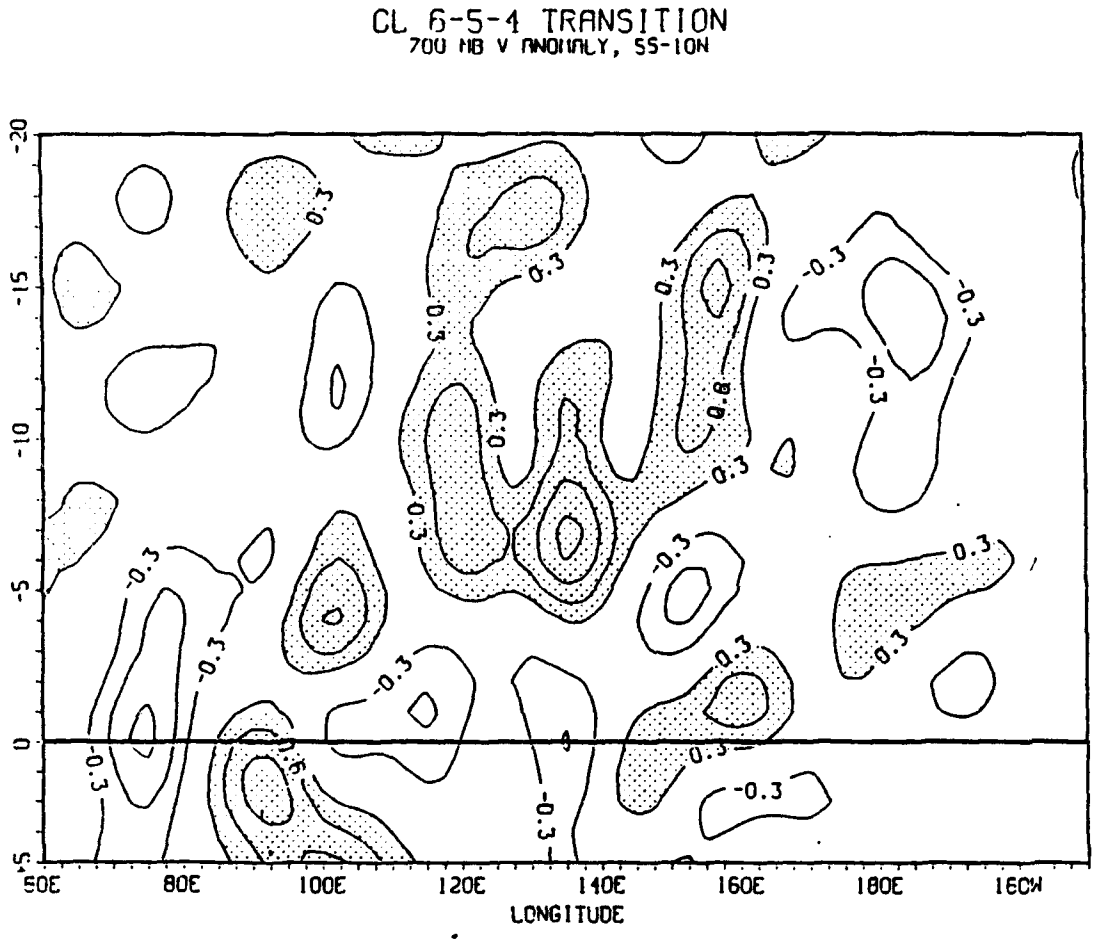


**Fig. 82** Time-longitude section of 700 mb anomalous meridional wind components averaged between 5°S-10°N during the 1-6-5-4 transition path. Units are m $s^{-1}$. Positive contours are shaded.

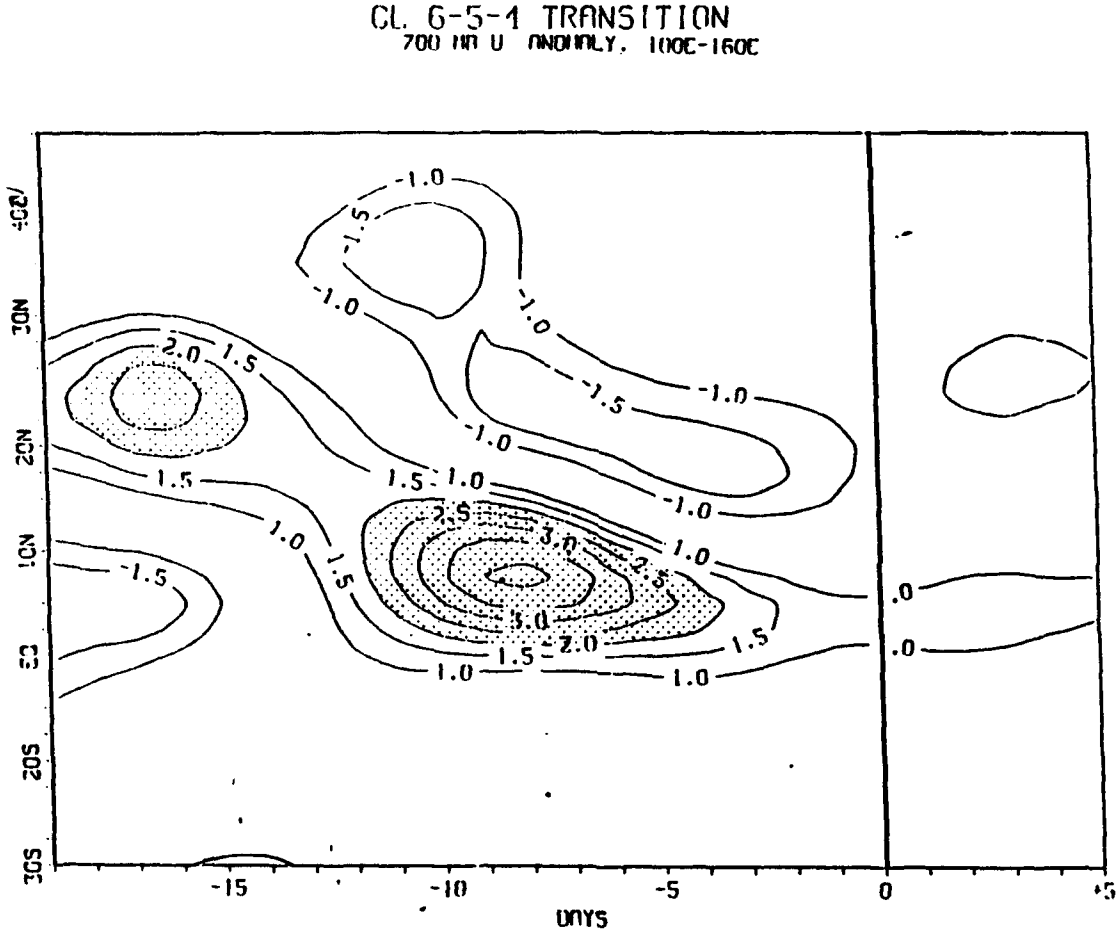


**Fig. 83** Latitude-time section of 700 mb anomalous zonal wind components averaged between 100°E-160°E during the 1-6-5-4 transition path. Units are m $s^{-1}$. Positive contours above 2 m $s^{-1}$ are shaded.

by the meridional wind variations. The reduction in zonal kinetic energy (dashed line in Fig. 81) after the peak in anomalous westerly winds is not as rapid as the reduction associated with the disturbances defined by VEOF 4. This suggests that the zonal kinetic energy representing the larger-scale circulation is not completely transferred to smaller-scale disturbances as suggested above in relation to the composites based on the VEOF 4 analysis. This is consistent with the anomaly pattern composites, which indicate that the cluster transition patterns are larger in scale and even have global circulation characteristics.

A final comparison is made between the 200 mb velocity potential anomalies associated with the cluster 1-6-5-4 transitions (Fig. 76) and the evolution based upon the composites of the 225° orientation of VEOF 4 (Fig. 84). The 200 mb velocity potential anomalies during the evolution of the VEOF 4 anomalies propagate westward between 180°-100°E. Upper-level convergence near 120°E at -7 days is associated with the anticyclonic anomalies and reduced convection over the Philippine Sea as indicated in Fig. 78a. As the anticyclonic anomaly moves northwestward, upper-level divergence anomalies, which are associated with the cyclonic circulation anomalies in Fig. 78, propagate westward over the Philippine Sea. These circulation patterns are quite different from the 1-6-5-4 transition patterns of 200 mb velocity potential, which contained both eastward and westward propagating components.

### *f. Summary*

Although the cluster 1-6-5-4 transition patterns appear similar to northwestward propagating disturbances defined by Lau and Lau (1990, 1992), they are a combination of large-scale components and interactions with smaller-scale features that are

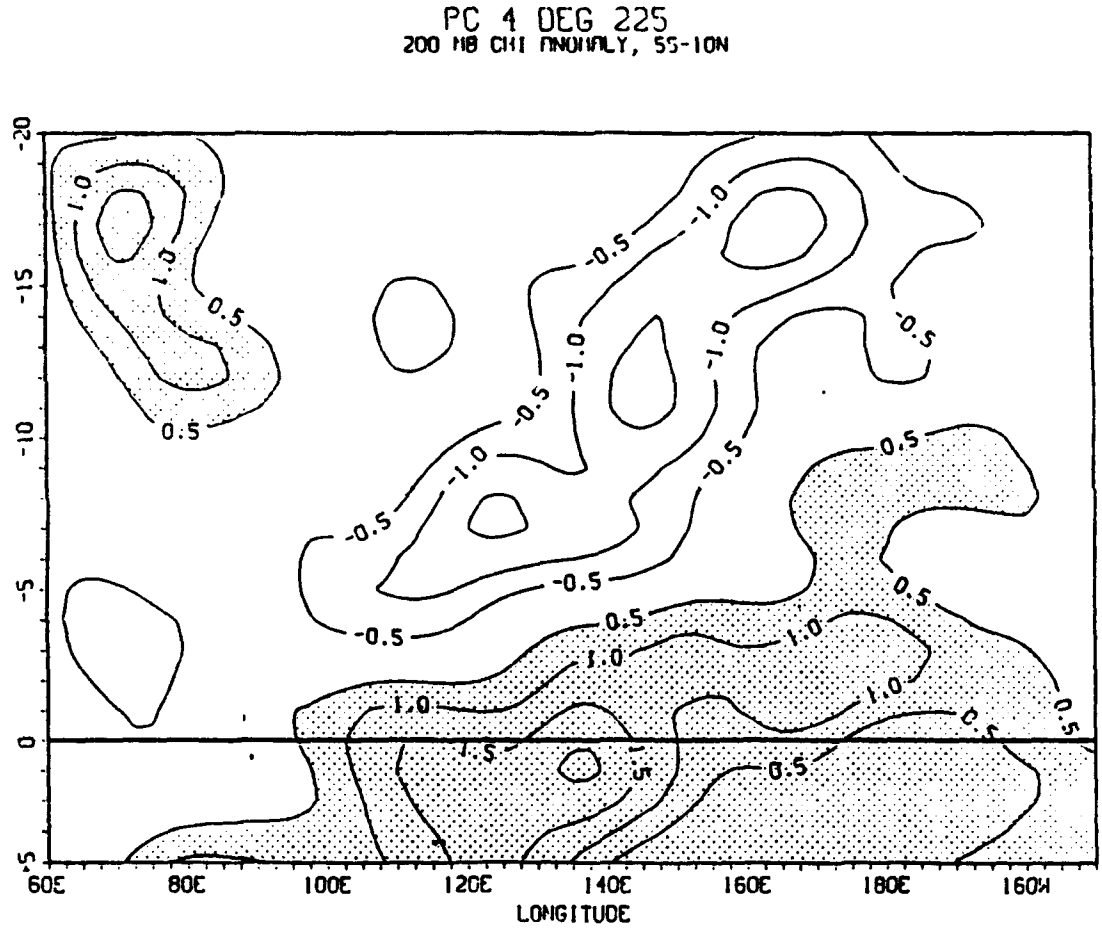


**Fig. 84** Time-longitude section of 200 mb velocity potential anomalies averaged between 5°S-10°N during periods of significant VEOF 4 coefficients. The contour interval is 0.5 x $10^{-6}$ $m^2$ $s^{-1}$. Positive contours are shaded.

related to the synoptic-scale circulations and also to tropical cyclones. The evolution of the zonal wind anomalies (Fig. 83) suggests that the large-scale circulations initiate the transition process via a build-up of zonal mean kinetic energy associated with an active monsoon trough. This kinetic energy is eventually transferred to disturbances within the trough. Although these disturbances start as rather large-scale features that essentially describe the anomalous monsoon trough circulation, they may evolve into smaller features similar to those described by Lau and Lau (1990, 1992). In many cases, they are associated with a western (eastern) tropical cyclone that follows a straight (recurve) track.

In terms of the cluster patterns, the 1-6-5-4 transition is characterized by a change in the monsoon trough orientation from northwest-southeast to southwest-northeast. This is related to two factors. The first is an interaction between the cyclonic circulations associated with the monsoon trough and midlatitude or subtropical circulations that act to begin the reorientation. The second factor is related to the formation of smaller circulation anomalies that seem to complete the reorientation and eventually leads to cyclonic anomalies over the subtropical western Pacific, which is indicative of the cluster 4 pattern. In the following section, a second transition path from active to inactive clusters is described that does not result in cyclonic anomalies over the subtropical western Pacific.

### 2. Transition 6-5-3

The transition path between clusters 6-5-3, which also leads to a change from active to inactive clusters occurs seven times over the nine-year data sample. The average time required to complete this transition is 10.7 days with a standard deviation of 7.2 days.

### *a. 700 mb Wind Anomalies and OLR Anomalies*

At -15 days, the monsoon trough is active with enhanced convection anomalies that extend along the trough from the Bay of Bengal through the Philippine Sea (Fig. 85a). The eastern portion of the trough is more intense than the western portion. A large cyclonic circulation anomaly near 25°N, 155°E is associated with a TUTT cell at 200 mb (not shown). This subtropical circulation is linked with the convection anomalies associated with the monsoon trough circulation. At -12 days (Fig. 85b), the eastern portion of the trough is still active with negative OLR anomalies (enhanced convection). The OLR anomalies have two distinct patterns. One region of convective activity is arranged in a typical northwest to southeast orientation from the South China Sea to the equator and 150°E. A second region is oriented from the southwest to the northeast in association with the cyclonic anomaly that is a downward reflection of the TUTT. The connection between the subtropical cyclonic anomalies and the monsoon trough is characteristic of a cluster 6 pattern.

At -9 days, the replacement of the western portion of the monsoon trough with anticyclonic anomalies has extended into the South China Sea along with positive OLR anomalies. The cyclonic circulations associated with enhanced portion of the trough and the TUTT have merged to form a large cyclonic anomaly over the Philippine Sea. At this time, the connection between the monsoon trough and a subtropical cyclonic circulation is similar to an intermediate step in the 1-6-5-4 transition path. However, a major difference here occurs when the subtropical cyclonic anomaly seems to move southwest to merge with the monsoon trough circulation. A large anticyclonic anomaly over Japan at -9 days may

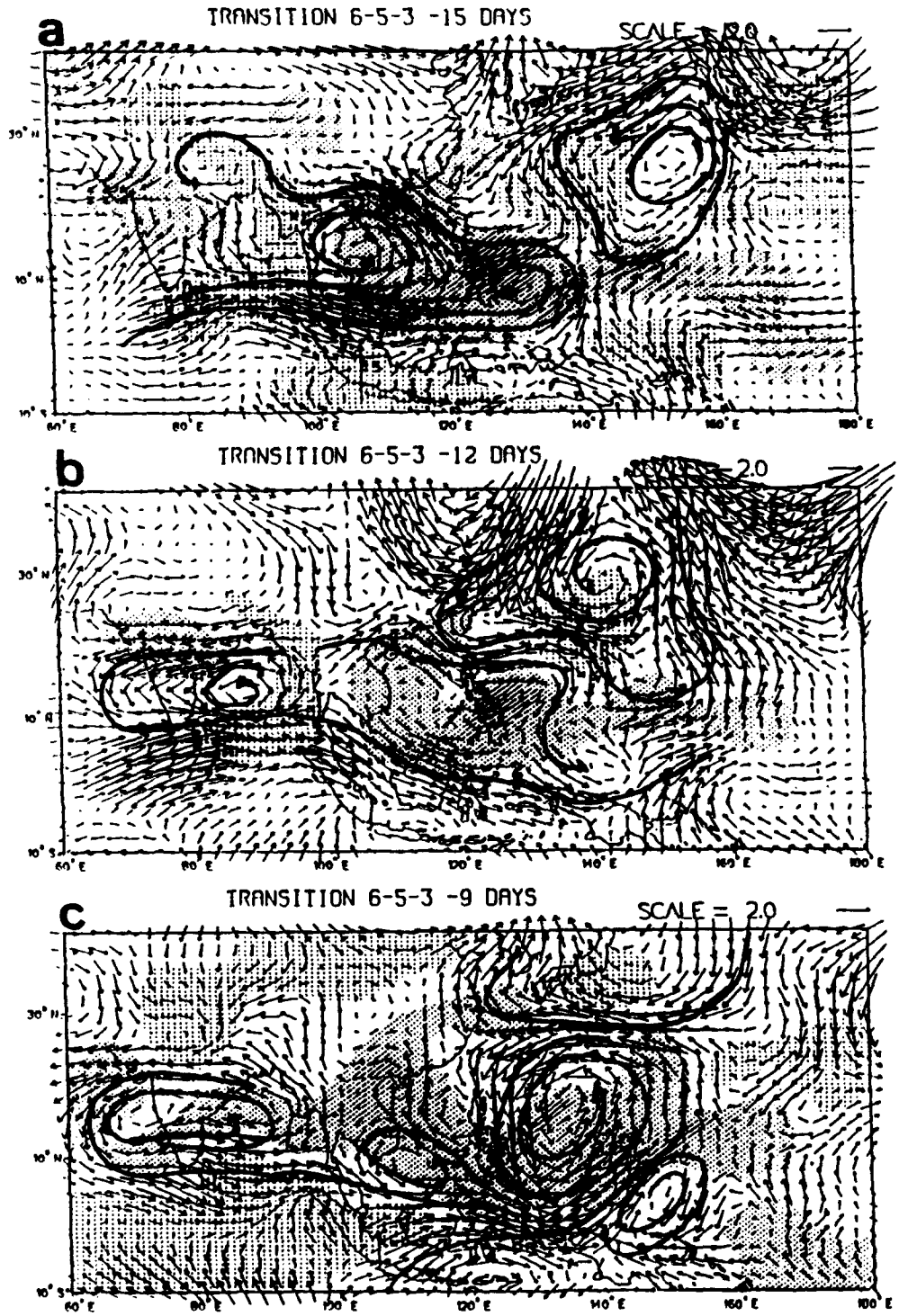


**Fig. 85** Composite for 700 mb wind anomalies and OLR anomalies for the 6-5-3 transition path at **(a)** -15 days, **(b)** -12 days, **(c)** -9 days, **(d)** -4 days and **(e)** 0 days prior to the entrance into cluster 3. Vector units are m $s^{-1}$. Dense shading marks enhanced convection regions with OLR anomalies less than -5 W $m^{-2}$. Light shading marks below average convection regions with OLR anomalies greater than 5 W $m^{-2}$.

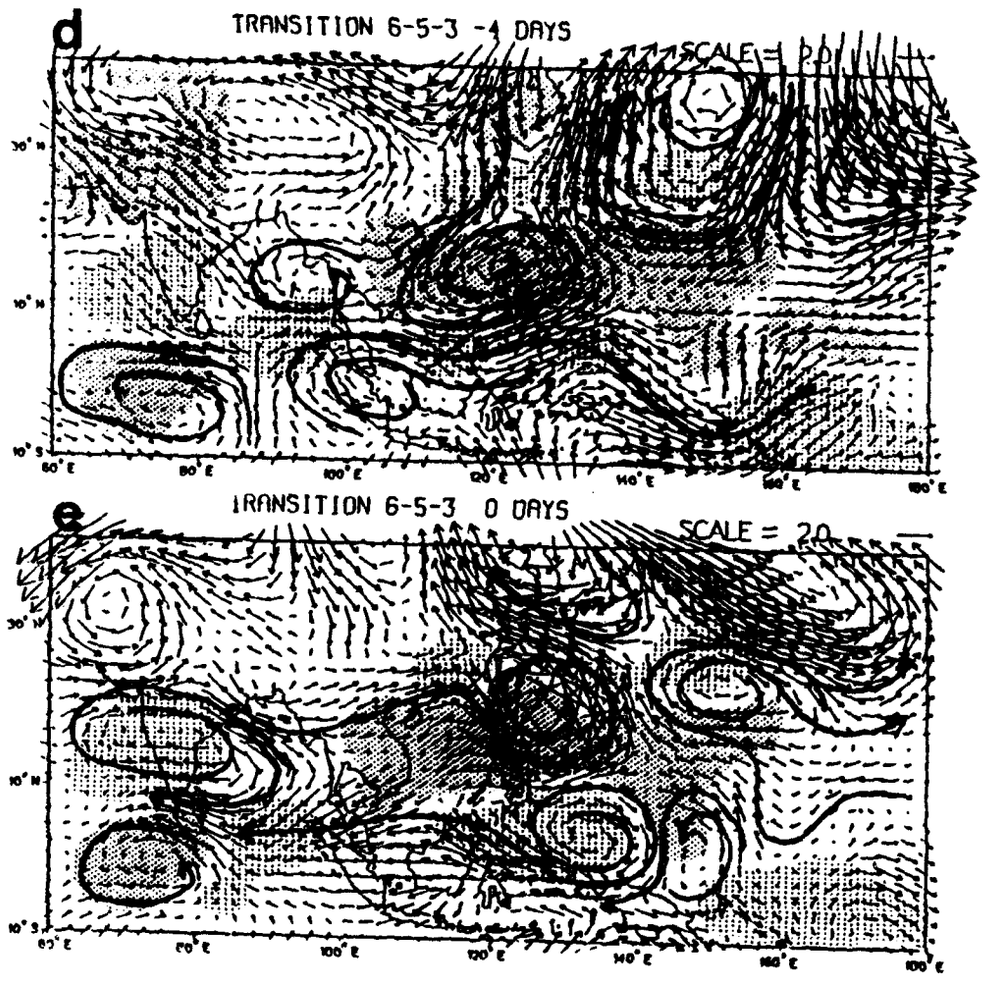


**Fig. 85** (continued).

block any northward movement of the anomalous circulations associated with the monsoon trough connection to the TUTT.

At -4 days (Fig. 85d), the cyclonic circulation over the Philippine Sea has consolidated and moved westward. Weakening of the monsoon trough convection over the tropical western Pacific has occurred, and has been replaced by anomalous ridging and associated positive OLR anomalies. The anomaly pattern over the Philippine Sea in Fig. 85 is again similar to the description of northwestward propagating features by Lau and Lau (1990, 1992) and Leibmann and Hendon (1990). However, a large region of anticyclonic anomalies associated with a circulation east of Japan extends southward over the subtropical western Pacific.

At day 0 (Fig. 85e), the northwestward-moving cyclonic circulation has intensified and in five of the seven cases is associated with a tropical cyclone. The anticyclonic anomaly to the southeast of the cyclonic anomaly also moved northwestward and becomes the eastern portion of an elongated area of anticyclonic anomalies over the climatological position of the monsoon trough. The positive OLR anomalies that were present along the equator at 80°E at -12 days appear to have propagated eastward along the equator to 120°E at day 0. The only region of enhanced convection along the equator now exists at 90°E. The entire subtropical western Pacific between 140°E-180°E is covered by an anticyclonic anomaly, which may have been enhanced via the southward extension of the midlatitude anomaly present east of Japan at -4 days. The combination of this subtropical anticyclonic anomaly and the weakened monsoon trough is representative of the cluster 3 anomaly pattern.

### *b. Streamfunction Anomalies*

At -15 days, an anomalous 200 mb cyclonic circulation that is associated with the TUTT is near 25°N, 150°E (Fig. 86a), which coincides with the 700 mb circulation described above (Fig. 85a). There is only a slight indication of this circulation in the 700 mb streamfunction anomalies (Fig. 87a). At -12 days (Fig. 86b), the 200 mb streamfunction anomaly pattern is similar to the -9 day pattern associated with the 1-6-5-4 transition path (Fig. 72c). That is, a Rossby-like wave pattern is present that seems to emanate from the regions of enhanced convection associated with the monsoon circulation. The phase of this wave pattern is such that there is an anomalous cyclonic circulation over Japan. In the 1-6-5-4 path, the cyclonic anomalies associated with the circulation over Japan connected with the monsoon trough circulation and this connection was evident at both 200 mb and 700 mb. In the 6-5-3 path, this cyclonic circulation over Japan does not connect with the monsoon trough circulation. Rather, the anticyclonic cell to the east of Japan appears to be more dominant than in the 1-6-5-4 case. Perhaps only the circulation anomalies at both 700 mb and 200 mb that are associated with the TUTT are connected to the circulation associated with cyclonic anomaly over Japan.

The 200 mb Rossby wave pattern at -12 days does not persist as it appears to retrograde as the anticyclonic anomaly to the east of Japan intensifies (Fig. 86c). Consequently, a large anticyclonic anomaly covers the majority of the subtropical western Pacific. This wave pattern is similar to a pattern identified by Lau and Phillips (1986) during Northern Hemisphere winter seasons, and to the Eurasian teleconnection pattern described by Wallace and Gutzler (1981). Lau and Phillips associated the wave pattern with anomalous

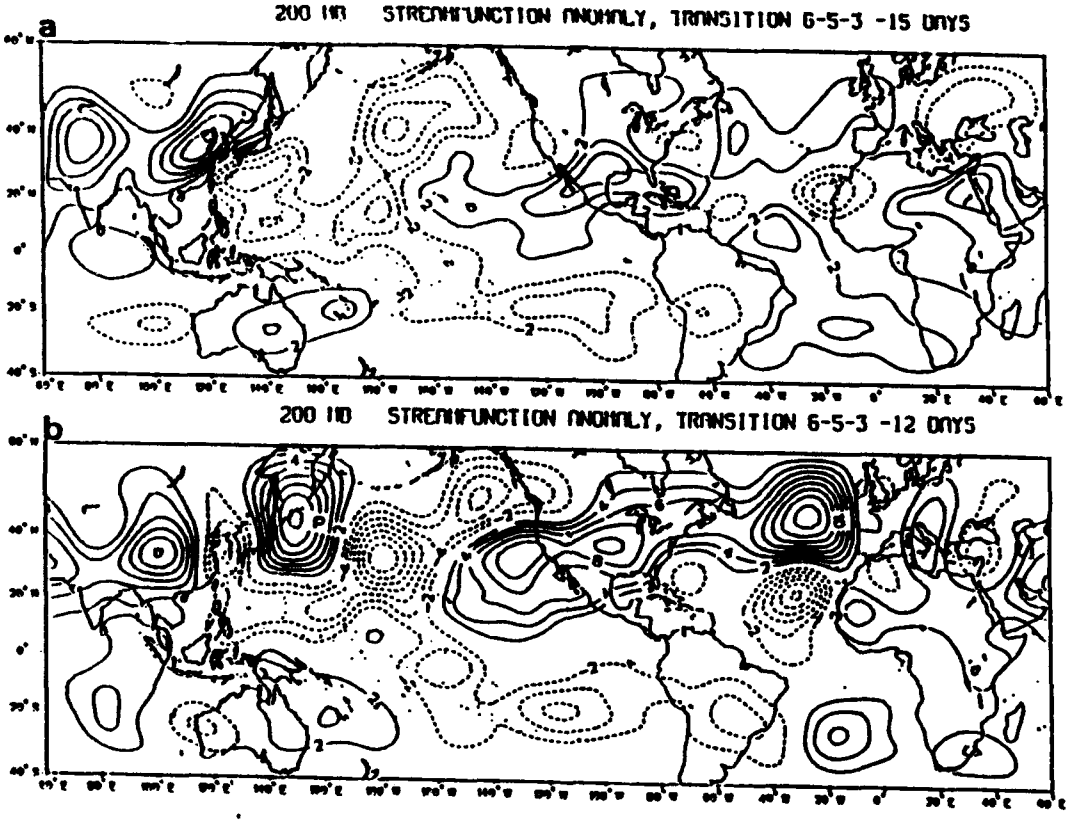


**Fig. 86** Composite for 200 mb wind streamfunction anomalies for the 6-5-3 transition path at (a) -15 days, (b) -12 days, (c) -9 days and (d) -4 days prior to the entrance into cluster 3. The contour interval is 2.0 x $10^6$ $m^2$ $s^{-1}$. Negative contours are dashed.

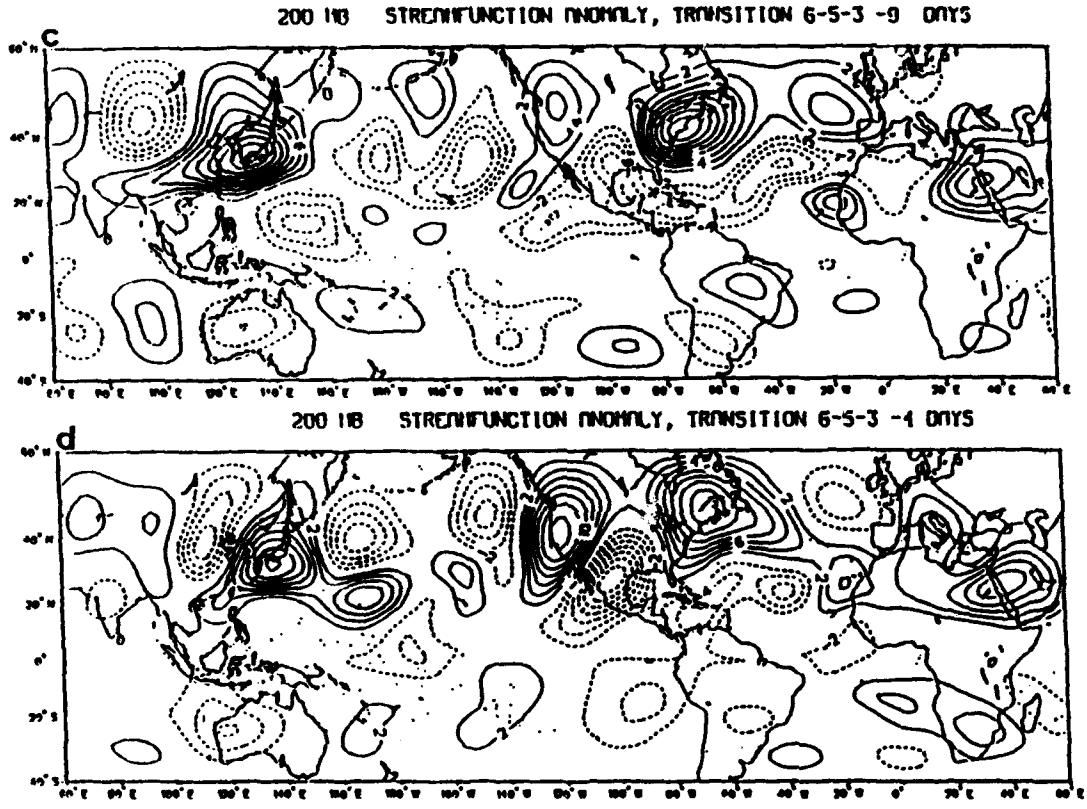


**Fig. 86** (continued).

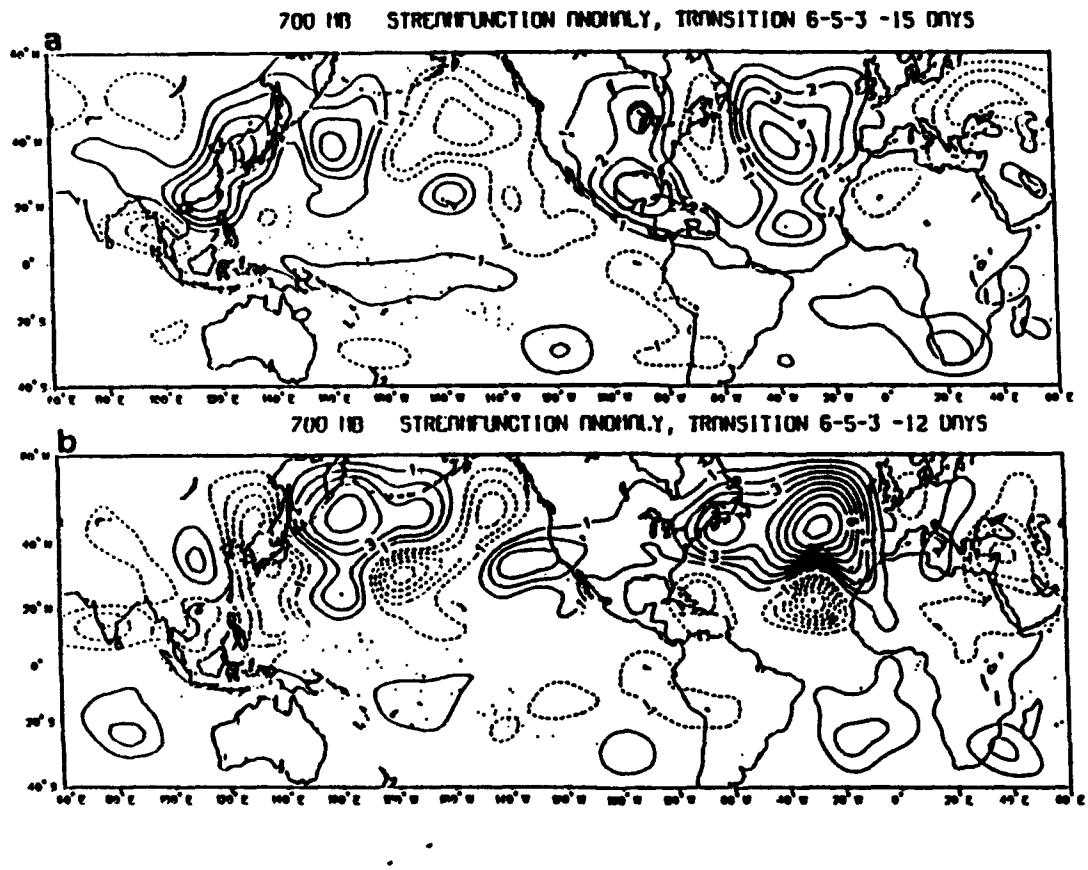


Fig. 87 As in Fig. 86, except for 700 mb.

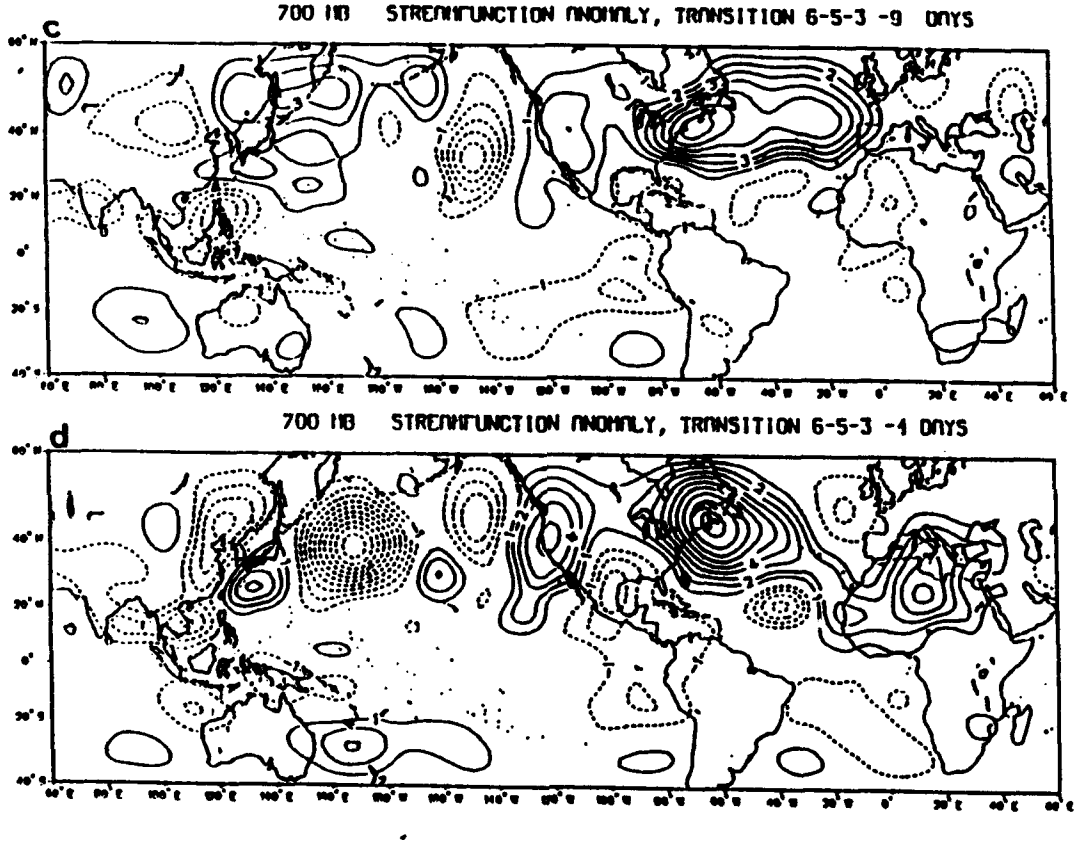


**Fig. 87** (continued).

equatorial heating over the equatorial western Indian Ocean. At -9 days, this pattern is not evident at 700 mb (Fig. 87c), but is found at -4 days (Fig. 87d). This pattern with the anticyclonic anomaly covering the western Pacific persists, which seems to effectively prevent the tropical circulation anomalies from moving northward.

### *c. Velocity Potential Anomalies*

At -15 days, the velocity potential anomalies at 200 mb (700 mb) indicate anomalous divergence (convergence) over the monsoon trough region (Figs. 88a, 89a), which is consistent with the anomalous enhanced convection associated with the active monsoon trough. A concentrated region of upper-level convergence is located near 30°N, 145°E, which is associated with the anomalous TUTT circulation discussed above (Fig. 86a). At -12 days, a connection seems to be established between the midlatitude and tropical divergent circulations at both 200 mb (Fig. 88b) and 700 mb (Fig. 89b), which is similar to the connection described with respect to the streamfunction anomalies. This connection between the divergent circulations is again limited to the circulation over the tropical western Pacific in which the negative OLR anomalies are found. The equatorial divergent circulations at 200 mb appear to have spread eastward from the maritime continent region between day -15 and day -12 (Fig. 88b). Thus, the divergent lobe with a center near 30°N, 150°E may be more related to the phasing of the midlatitude and the TUTT circulations, and may not involve any connection between the monsoon trough circulations and the midlatitude trough circulations (as in the 1-6-5-4 transition). At 700 mb (Fig. 89b), the merger of the convergence over the maritime continent and over the monsoon trough appears to be more connected with the 700 mb divergence anomaly along the equator at 140°W. Given the 200

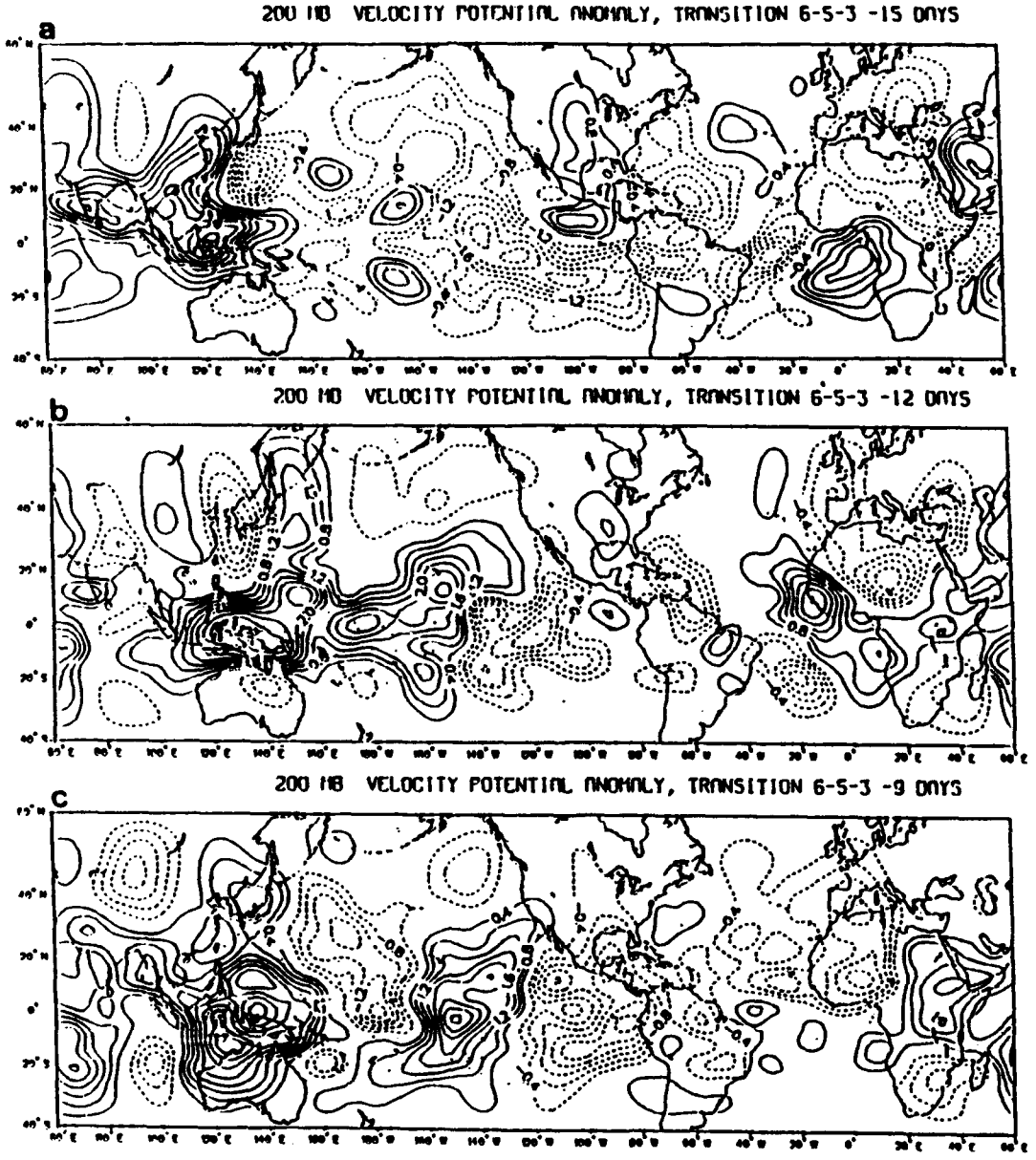


**Fig. 88** Composite for 200 mb wind velocity potential anomalies for the 6-5-3 transition path at **(a)** -15 days, **(b)** -12 days and **(c)** -9 days prior to the entrance into cluster 3. The contour interval is 0.2 x $10^6$ $m^2$ $s^{-1}$. Negative contours are dashed.

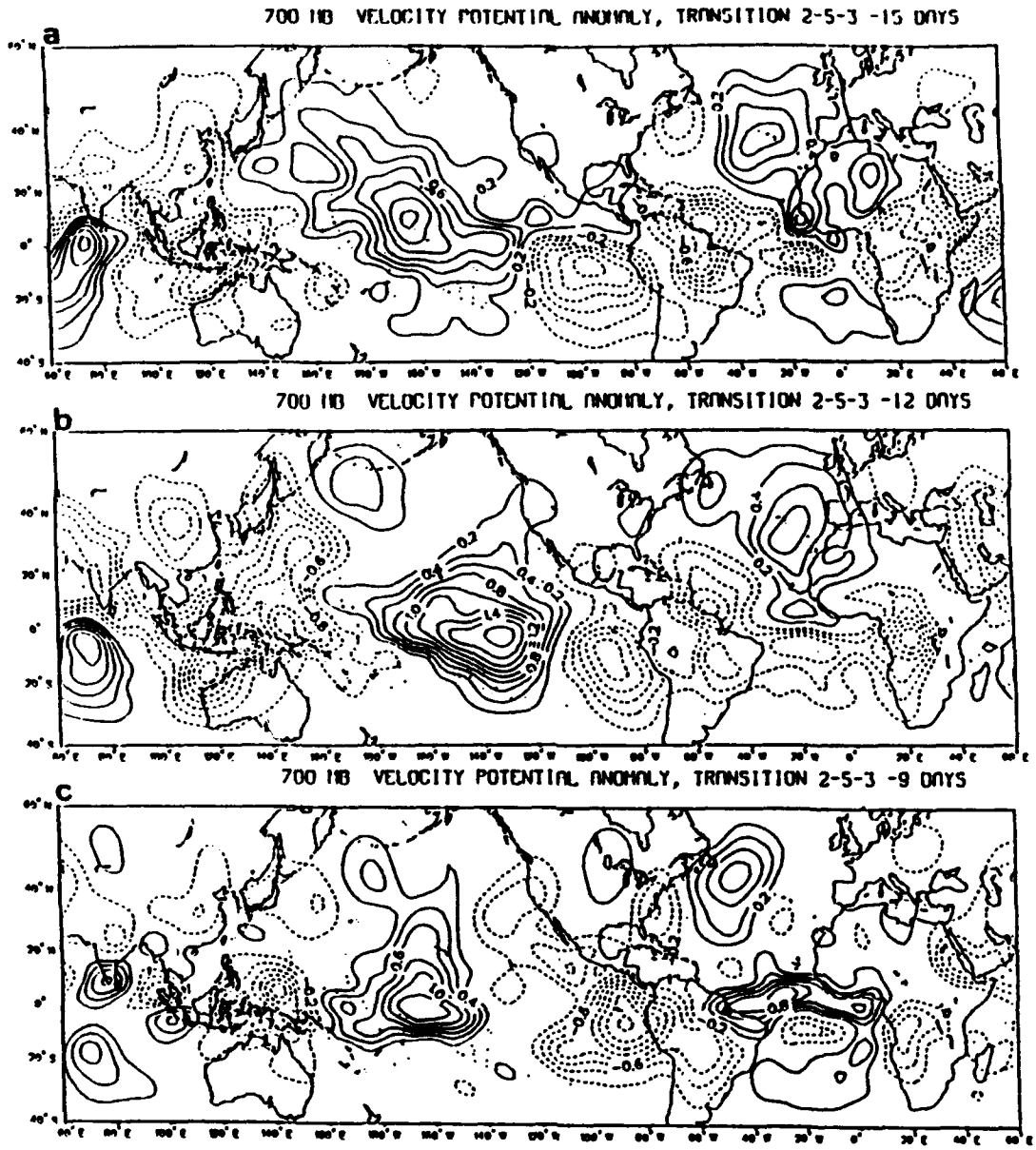


**Fig. 89** As in Fig. 88, except for 700 mb.

mb convergence anomaly located slightly eastward at 130°W, the dominant feature is an anomalous Walker circulation with large-scale ascent over the maritime continent and western equatorial Pacific with descent over the central and eastern Pacific.

At -9 days (Figs. 88c, 89c), this large Walker circulation splits into two circulations with ascent over the maritime continent, descent at the dateline, ascent at 150°W, and descent at 110°W. The large-scale divergent circulation anomalies continue to become oriented into smaller-scale features throughout the remainder of the 6-5-3 transition path (not shown).

### *d. Tropical Cyclone Characteristics*

The transition from the set of clusters associated with active tropical cyclone periods to clusters associated with inactive periods is evident in the evolution of the large-scale circulations discussed above. At the end of the 6-5-3 transition path, the region of the monsoon trough is dominated by anticyclonic circulation anomalies that are indicative of reduced tropical cyclogenesis. A significant difference between the 1-6-5-4 transition and this 6-5-3 transition regards the role of tropical cyclones during the transition. A combination of passive and active tropical cyclone roles was described in the 1-6-5-4 transition. However, the 6-5-3 transition is dominated by other features such as the TUTT and alignment with a midlatitude Rossby-like wave train.

### *e. Summary*

This transition path has some similarities to the 1-6-5-4 path described above. The variations of the equatorial zonal winds and the apparent eastward propagation of convection anomalies along the equator suggests that the large-scale circulations also

dominate this transition path. Between -5 and -10 days, large-scale cyclonic anomalies again begin to consolidate into northwestward-moving features that are associated with tropical cyclones and have trailing anticyclonic anomalies to the southeast. In this case, the anticyclonic anomaly moved northwestward as if coupled to the cyclonic anomaly.

A second interesting aspect of this 6-5-3 transition path concerns the relationship with the subtropical cyclonic circulation that is associated with the TUTT. A linkage between this anomaly and the active monsoon trough is established early in the composite period. However, large anticyclonic anomalies to the north in the midlatitudes seem to prevent any northward movement. The large cyclonic anomaly that covers the entire Philippine Sea at -9 days is similar to the "monsoon gyre" described by Lander (1993). Lander associates the gyre with a southward-moving upper-level cyclonic circulation that helps initiate the convection necessary to support the gyre. In Lander's description, the gyre circulation is capable of spawning several small tropical cyclones, or the monsoon gyre may evolve into a large tropical cyclone. This seems to be occurring between days -9 (Fig. 85c) to day 0 (Fig. 85e) in the composite anomaly patterns, and can only be confirmed by examining individual cases.

Other comparisons between the two active to inactive transition paths concern the connection with midlatitude circulation anomalies that only involve the circulation anomalies associated with the TUTT in the 6-5-3 path, but involve the entire monsoon trough circulation in the 1-6-5-4 path. In both cases, the connection with a midlatitude circulation is related to the phase of a Rossby wave-train pattern that may be forced by the anomalous convection associated with the active monsoon trough. In the 6-5-3 transition, the wave

appears to retrograde due to the intensification of a large anticyclonic anomaly that is east of Japan. The phase of this pattern results in a large anticyclonic circulation over the subtropical western Pacific. Therefore, the phasing between the tropical and Rossby-wave train circulations may be a factor in transition path differences that originated from similar tropical circulation evolutions.

### 3. Transition 3-5-2-1

The primary transition path leading from inactive to active clusters proceeds 4-3-5-2-1. This path is observed 12 times during the 1979-87 period. The average length of time required to complete the path is 10.1 days with a standard deviation of 6.4 days.

#### *a. 700 mb Anomalies and OLR Anomalies*

At -15 days, the 700 mb wind anomaly pattern is representative of cluster 4 with anticyclonic anomalies over the monsoon trough region, and cyclonic anomalies over the subtropical western Pacific (Fig. 90a). Positive OLR anomalies (below-average convection) are consistent with the inactive monsoon trough condition, whereas negative OLR anomalies (enhanced convection) are associated with the weak cyclonic anomaly (weak subtropical ridge). Another large area of negative OLR anomalies straddles the equator between 60°-100°E. At -10 days, the negative OLR anomalies over the equatorial Indian Ocean have moved eastward and northward. The cyclonic anomaly over the subtropical western Pacific has propagated northwestward and the primary region of anticyclonic anomalies has shifted westward and northward to cover the entire Philippine Sea (Fig. 90b). At -5 days, anticyclonic anomalies continue to dominate the monsoon trough region and the subtropical ridge remains strong (Fig. 90c). Although the region of enhanced convection over

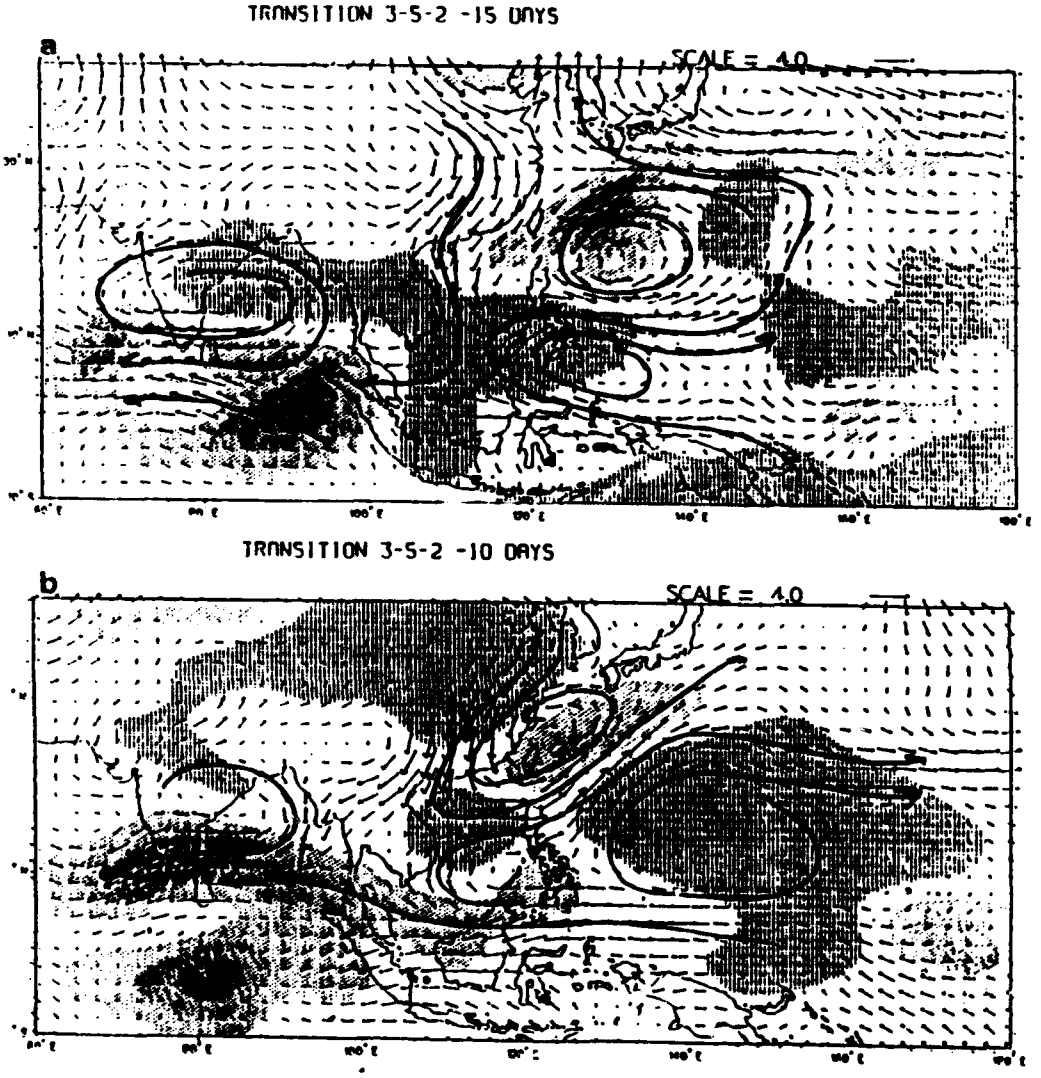


**Fig. 90** Composite for 700 mb wind anomalies and OLR anomalies for the 3-5-2 transition path at **(a)** -15 days, **(b)** -10 days, **(c)** -5 days and **(d)** 0 days prior to the entrance into cluster 2. Vector units are m $s^{-1}$. Dense shading marks enhanced convection regions with OLR anomalies less than -5 W $m^{-2}$. Light shading marks below average convection regions with OLR anomalies greater than 5 W $m^{-2}$.

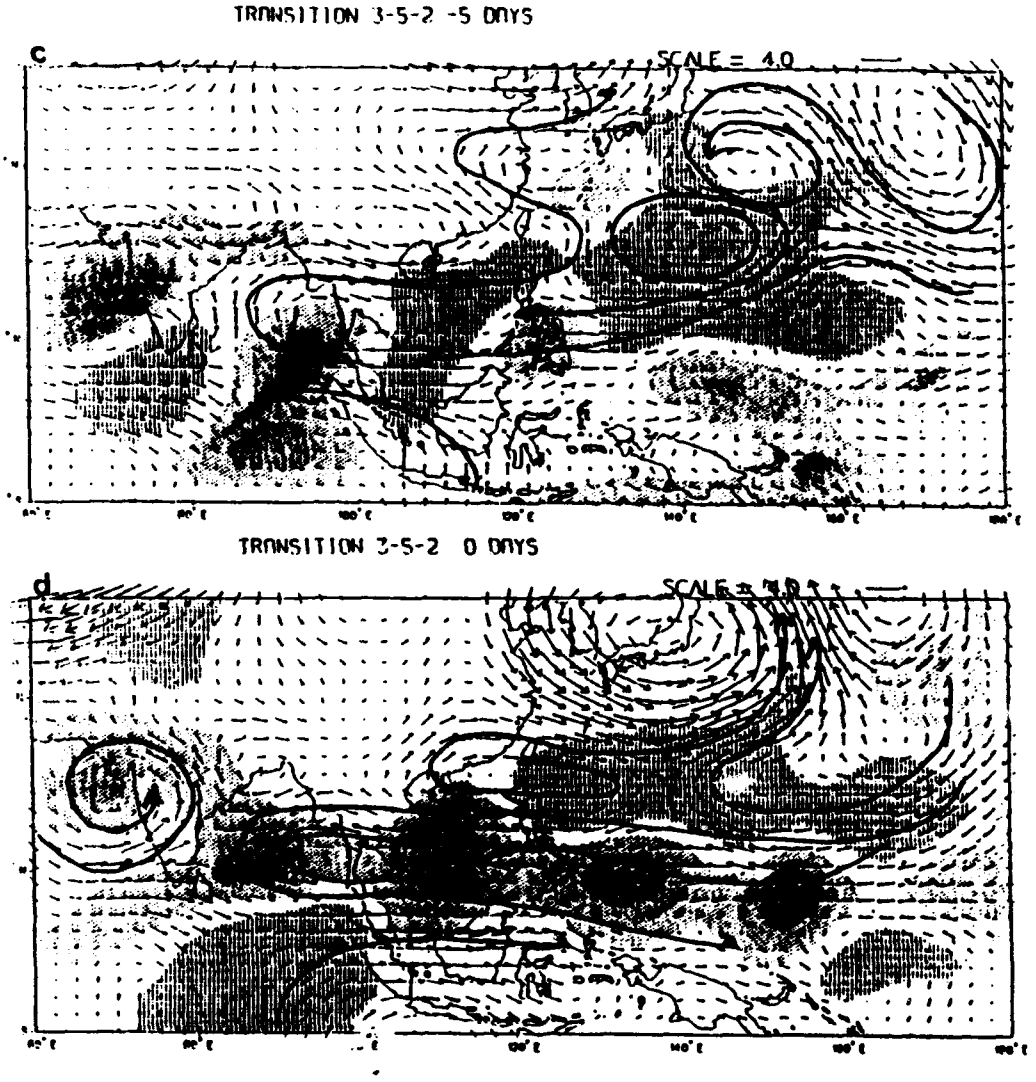


**Fig. 90** (continued).

the equatorial Indian Ocean has not moved, a new region of enhanced convection exists near 5°N, 150°E. This convective region moved westward between -10 days and -5 days, and is now associated with a weak cyclonic anomaly. At day 0 (Fig. 90d), the transition to a cluster 1 pattern is complete with an active monsoon trough marked by a northwest to southeast band of enhanced convection and cyclonic anomalies. Although the subtropical ridge over the western Pacific continues to remain slightly stronger than normal, a strong cyclonic anomaly is also present over Japan.

The evolution of this pattern is very similar to the evolution of the western Pacific component of the global-scale 30-60 day oscillation (Madden and Julian 1972; Knutson and Weickmann 1987). Unlike the transitions from active to inactive clusters, the 3-5-2 transition path does not contain any noticeably smaller scale features. Rather, a smooth transition from an inactive monsoon trough to an active trough appears to begin over the Indian subcontinent with the presence of cyclonic anomalies at -5 days. The monsoon trough continues to extend eastward until at day 0 it meets a region of enhanced convection and cyclonic anomalies that is moving westward from the central Pacific. The stretching of the negative OLR anomaly across Indonesia that leads to a merger of the eastern and western branches of the monsoon trough is similar to observations by Weickmann and Khalsa (1990), who studied the propagation of filtered OLR anomalies associated with the 30-60 day oscillation.

### *b. Streamfunction Anomalies*

At -15 days, the 200 mb (Fig. 91a) and 700 mb (Fig 92a) streamfunction anomalies have a series of waves along the northern midlatitudes. The vertical

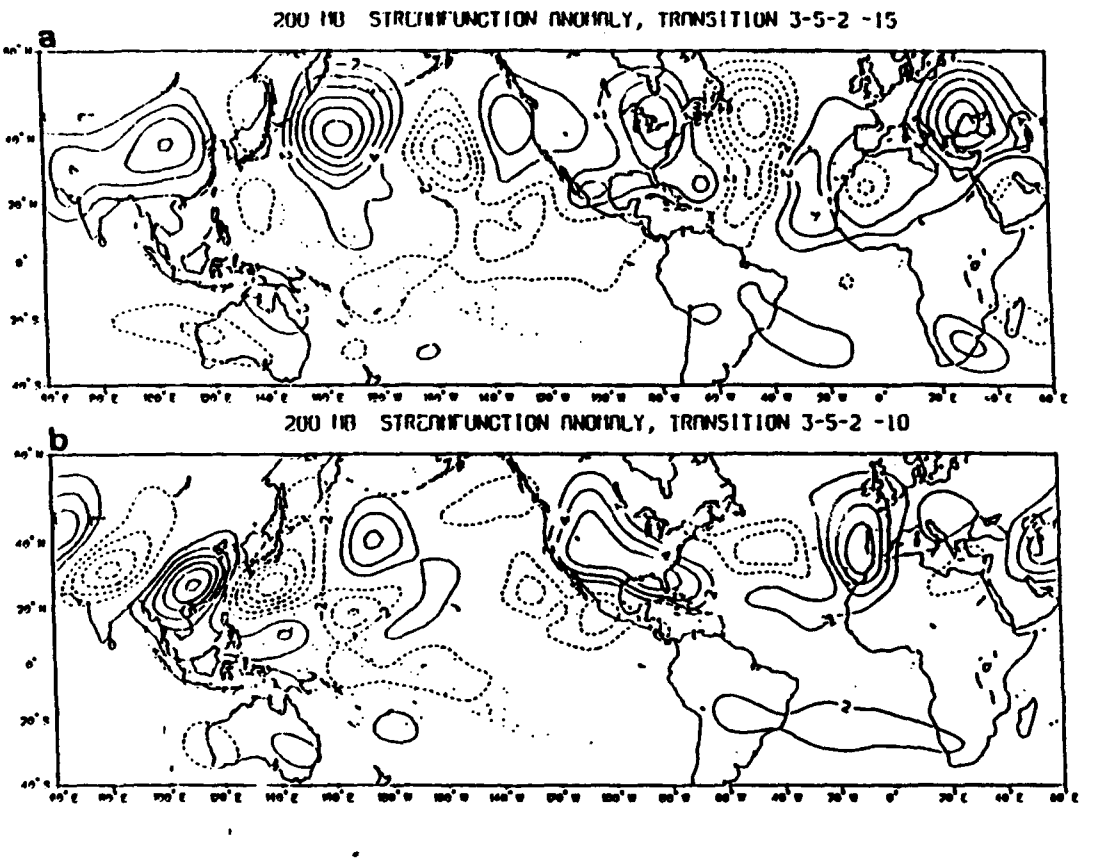


**Fig. 91** Composite for 200 mb wind streamfunction anomalies for the 3-5-2 transition path at **(a)** -15 days and **(b)** -10 days prior to the entrance into cluster 2. The contour interval is 2.0 x $10^6$ $m^2$ $s^{-1}$. Negative contours are dashed.

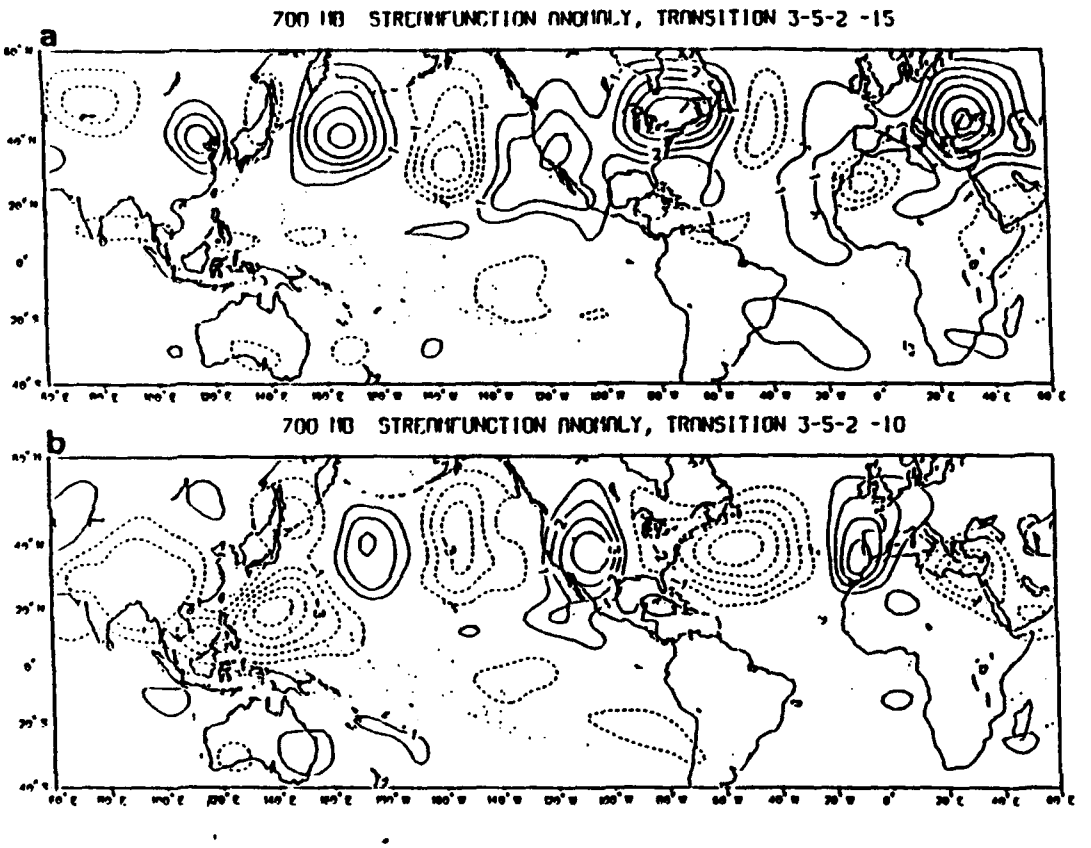


Fig. 92 As in Fig. 91, except for 700 mb.

structure of these anomaly patterns suggest that the waves are equivalent barotropic. The orientation of the anomaly circulations suggests that the features are not related to the deep tropics except perhaps for the anticyclonic circulation over the eastern North Pacific (Fig. 91a).

An interesting change occurs by day -10, when a 200 mb wave pattern (Fig. 91b) is evident from Eurasia towards the southwest and into the western Pacific. The phase of the wave places an anticyclonic anomaly over the subtropical western Pacific, which acts to strengthen the subtropical ridge. This wave feature is similar to a large-scale wave that was observed by Hsu et al. (1990) to be associated with the enhancement of equatorial convection during a particular Northern Hemisphere winter 30-60 day oscillation event. A strong anticyclonic anomaly at 700 mb covers the entire western Pacific and monsoon region (Fig. 92b). Over the remaining period (not shown), the 700 mb and 200 mb streamfunction anomalies do not take on any unique character. Thus, it is not clear what the role of the 200 mb wave train from Eurasia has to do with the 3-5-2-1 transition described above in terms of the 700 mb wind anomalies or OLR anomalies.

### *c. Velocity Potential Anomalies*

The 200 mb (700 mb) velocity potential anomalies at -15 days (Figs. 93a, 94a) indicate convergence (divergence), which is consistent with the inactive monsoon trough and anticyclonic anomalies. Although the evolution of the OLR anomalies appears to be similar to descriptions of propagating features associated with the 30-60 day oscillation, the 200 mb velocity potential anomalies do not indicate a global wavenumber 1 circulation pattern, which is indicative of the oscillation (Knutson and Weickmann 1987). Nevertheless,

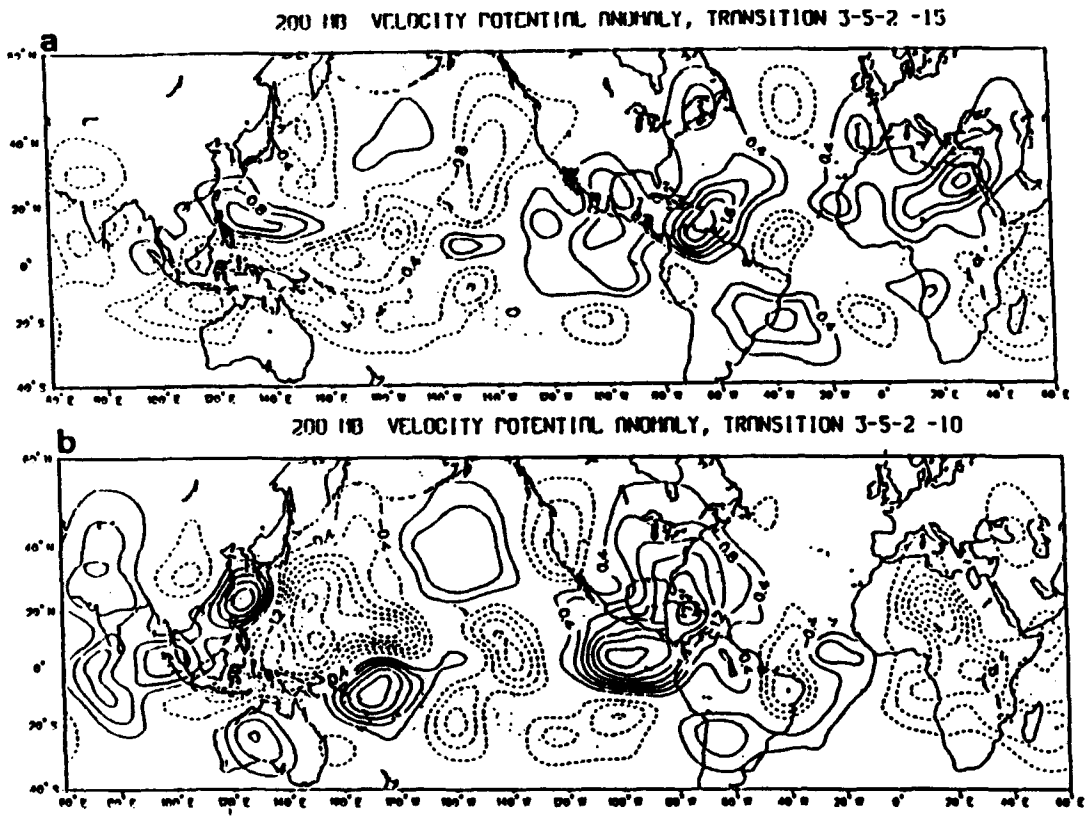


**Fig. 93** Composite for 200 mb wind velocity potential anomalies for the 3-5-2 transition path at (a) -15 days, (b) -10 days, (c) -5 days and (d) 0 days prior to the entrance into cluster 2. The contour interval is 0.2 x $10^6$ $m^2$ $s^{-1}$. Negative contours are dashed.

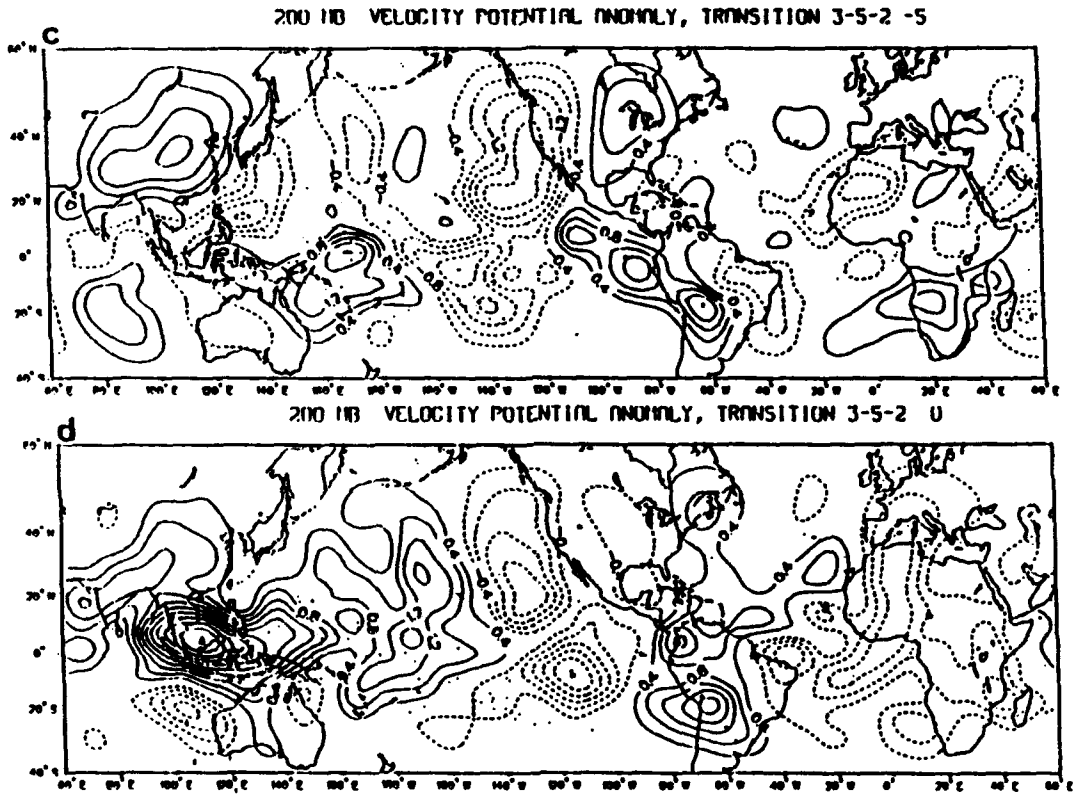


**Fig. 93** (continued).

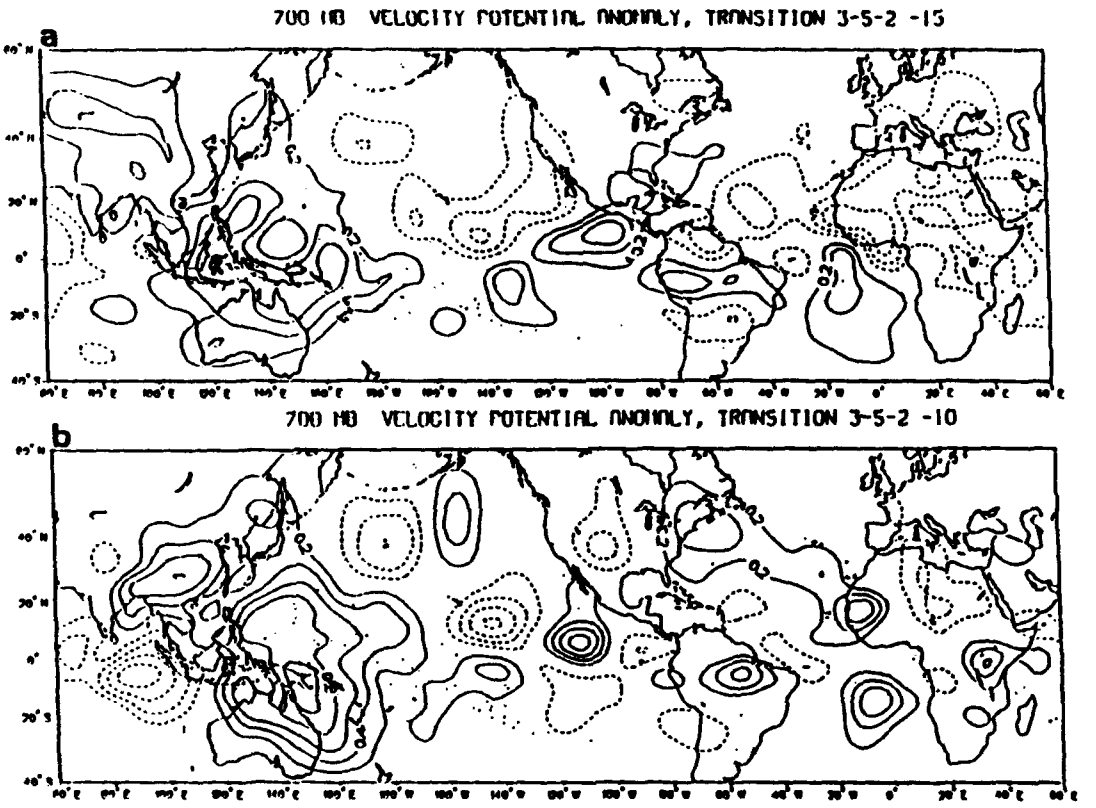


**Fig. 94** As in Fig. 93, except for 700 mb.

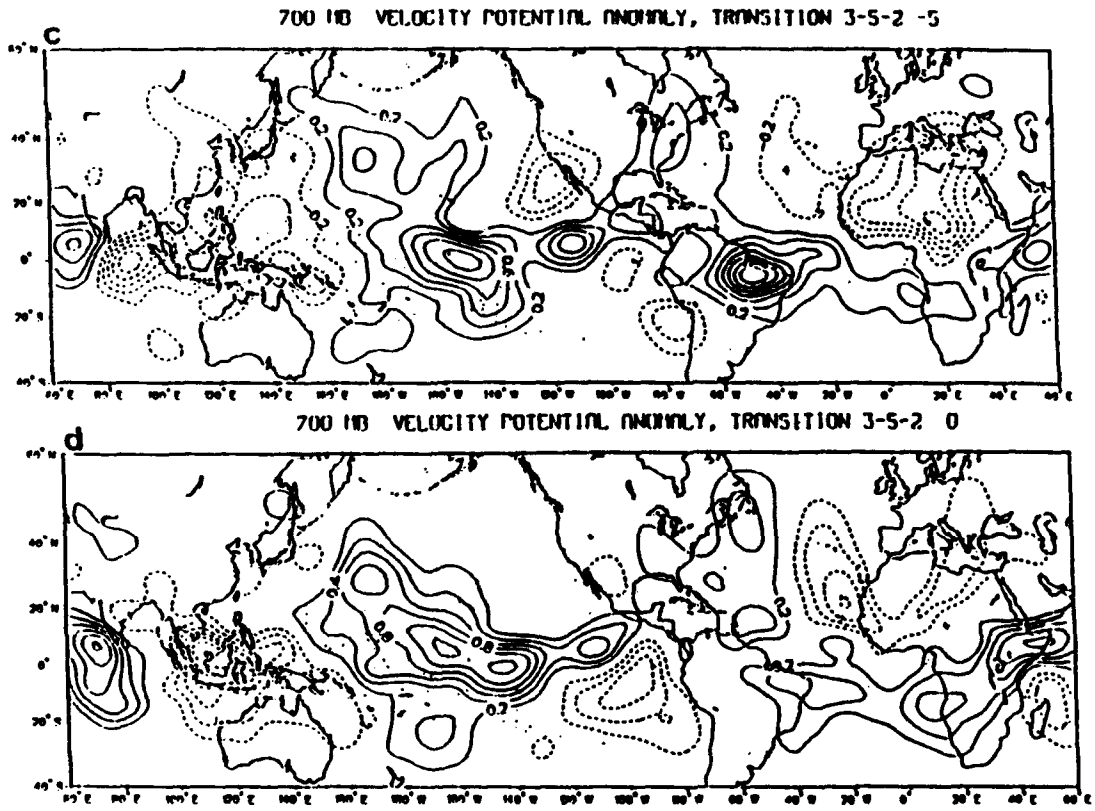


**Fig. 94** (continued).

the 200 mb convergence anomalies at -15 days change to divergent anomalies above the monsoon trough at day 0 (Figs. 93a-d). At 700 mb, an eastward-moving convergence anomaly that extends to 70°E appears along the western boundary at day -15. This feature, which straddles the equator, propagates to about 120°E at day 0. The 700 mb divergence anomaly located over the maritime continent at day -15 also moves eastward and is centered near 160°E at day 0. Therefore, the 700 mb velocity potential anomalies indicate more evidence of a large-scale eastward-moving circulation than the 200 mb circulation. This is consistent with studies of the 30-60 day oscillation during the Northern Hemisphere summer and its relation to the monsoon circulation (Knutson and Weickmann 1987; Lau and Peng 1990). The close connection between the large-scale convection associated with the monsoon and the divergent circulations may tend to alter the primary upper-level signal, which has primarily been examined during winter seasons.

### *d. Tropical Cyclone Characteristics*

The 4-3-5-2-1 transition results in a change from an inactive tropical cyclone pattern to an active tropical cyclone pattern. Although the major changes occur over the monsoon trough region, the subtropical ridge becomes slightly stronger than normal. The combination of these factors in cluster 1 indicates a preference for the straight-moving track type.

## E. DISCUSSION

The above section describes two transition paths that proceed from active clusters to inactive clusters and one path that proceeds from the inactive clusters to the active clusters. Physical descriptions of each path are based upon the evolution of three-dimensional

structures of the anomalous large-scale circulations. Each of the three primary transition paths could be characterized by a set of unique attributes. These evolutions of atmospheric variability along the transition paths involve scales of motion including tropical cyclones, synoptic-scale waves, monsoon circulations, and global-scale rotational and irrotational circulations. In the case of the two transition paths from the active clusters to the inactive clusters, the interactions between these various scales of motion are critical for determining which path will be followed.

The fact that major transitions of large-scale circulation features involve many scales and processes is not surprising given the complex nature of atmospheric motions. However, the ability of the cluster analysis to represent this complexity within a rather simple framework of recurrent circulation patterns with a relatively small set of preferred transition paths between them is remarkable. Although several studies have examined midlatitude circulation variability using the concept of transitions between recurrent states (Mo and Ghil 1988; Molteni et al. 1990), none have resulted in transition matrices with such a large number of empty cells as found with regard to the large-scale tropical circulation variability. Much of the success of the cluster algorithm is due to the rigorous definition of the large-scale circulation variability in terms of the VEOF analysis of the anomalous wind components.

Finally, the evolution of the large-scale circulation anomalies provides more detailed information regarding the relationships between each cluster pattern and tropical cyclone occurrences and track types. The physical associations between each cluster pattern, which represents an instantaneous depiction of recurrent circulation patterns, and the typical tropical cyclone characteristics remain intact during transitions between the clusters. Therefore, the

association between changing cluster patterns and tropical cyclone characteristics increases the utility of the cluster analysis as a potential prediction scheme for tropical cyclone activity/inactivity and track type.

# VI. SUMMARY AND CONCLUSIONS

The major hypothesis examined in this study is that the observed low-frequency variability in tropical cyclone characteristics over the tropical western North Pacific is directly attributed to the variability of the large-scale circulation. The investigation builds upon a preliminary study by Harr and Elsberry (1991) that is summarized in Chapter II. The primary results of that study are that a weak climatological control upon tropical cyclone track types can be identified based upon the time and location of tropical cyclone genesis. Although preliminary climatological analysis demonstrates a control on tropical cyclone characteristics, the relationship is not significant enough to explain the observed variability of tropical cyclone characteristics. However, the physical distribution of the climatological control identifies two separate classes of recurving tropical cyclones. One class, which is labeled recurve-south, contains tropical cyclones that follow recurving tracks after forming over regions where no climatological preference exists between a straight or a recurving track. The second class, which is labeled recurve-north, contains recurving tropical cyclones that form over regions where there is a definite climatological preference for recurving tracks. This distinction between recurving tropical cyclones is carried throughout the analysis.

A second result of the preliminary analysis is the identification of distinct anomalous large-scale 700 mb zonal wind patterns for each track type and inactive periods that were identifiable during the initial stages of the life of the tropical cyclone. The 700 mb anomaly patterns are defined using a compositing technique that is based upon the existence of a tropical cyclone following a specific track type, or the existence of an inactive period. These

patterns can be summarized by the latitudinal variation of the 700 mb zonal wind anomalies over the western Pacific. These results from Harr and Elsberry (1991) form the basis for the remainder of the investigation of the hypothesis defined above.

To extend this research, a logical approach has been followed in which each analysis step builds upon the results of the previous steps. Because the major conclusions of this study are based on inferences concerning the variability of the basic structure of the atmosphere over the tropical western Pacific, it is important to emphasize the steps taken to insure integrity of the results with reference to possible sampling errors. Several statistical methodologies have been employed throughout the progression of this research, and the results of each analysis have been subjected to conventional examinations of the statistical variability. A hierarchy of EOF analyses has been used to define the basic structure of the variance of the atmospheric fields. The standard errors associated with the eigenvalues (North et al. 1982) have been examined to insure that the EOF analyses are not contaminated by sampling problems. The cluster analysis has been executed upon many partitions of the total data set to examine the robustness of the recurrent circulation patterns. Composite analyses have been examined (see Appendix A) following the procedure of Livezey and Chen (1983). That is, appropriate examinations are made to insure that the conclusions regarding physical characteristics of the variability of the large-scale circulation over the tropical western Pacific are not based upon misrepresentations caused by sampling errors. Finally, the physical consistency demonstrated over different atmospheric variables and between vertical levels provide further evidence that results are not contaminated by sampling errors.

A basic goal of this research is to define recurrent large-scale circulation patterns that are characteristic of the basic structure of the total atmospheric variability over the tropical western Pacific. Relationships between these circulation patterns and tropical cyclone characteristics are then sought, rather than starting from the tropical cyclone characteristics first and defining their associated circulation patterns. That is, the variability of the tropical circulation is represented in terms of the recurrent patterns that describe a significant fraction of the tropical atmospheric variations irregardless of whether a tropical cyclone is present or not. After demonstrating that the transitions between recurrent patterns describe well the evolution of the atmosphere, their relation to tropical cyclone occurrence and track types is studied. The major conclusions are summarized in the following sections.

## A. PROPERTIES OF THE LARGE-SCALE CIRCULATION VARIABILITY AS DEFINED BY THE TROPICAL CYCLONE-BASED CIRCULATION PATTERNS

The properties of large-scale 700 mb circulation anomalies using the tropical cyclone-based patterns may be used to classify periods when a particular anomaly pattern is persistent or when no particular pattern persists. These classifications led to a schematic depiction (Figs. 10, 11) of the large-scale circulation variability as a set of four primary patterns that are based upon tropical cyclone occurrence and track types, plus two transient states that are classified according to the sense of the equatorial zonal wind anomalies. The variability of the large-scale circulation may then be described by passages around this schematic state description. Although transitions are possible between all pairs of states, identification of the significant transitions provides a first-order depiction of the large-scale circulation variability that is quite symmetric about the direction of large-scale 700 mb zonal wind anomalies. Whereas

this an appealing result, its practical utility is limited because direct transitions between the four primary states do not occur very often. Rather, transitions from a tropical cyclone-based circulation pattern are to a transient pattern in which the circulation may persist for some time before eventually transitioning to another tropical cyclone-based pattern.

It may be concluded that this depiction of the large-scale circulation variability is due to two factors. The first factor is that only the zonal wind is used to define the circulation patterns. The second factor is that the circulation patterns were only based upon the occurrence of tropical cyclones, so they do not specifically define the basic structure of the atmospheric variability.

## B. BASIC STRUCTURE OF THE VARIABILITY OF THE LARGE-SCALE CIRCULATION OVER THE TROPICAL WESTERN PACIFIC

A scalar EOF analysis is first applied to the anomalous 700 mb zonal wind data to identify the basic structure of the circulation variability that is defined by the internal variance structure of the data set rather than by the occurrences of tropical cyclones. The important result is that these leading EOF structures are indeed directly related to the large-scale circulation patterns that were first identified with tropical cyclone characteristics. However, these scalar EOF structures are still only based upon a partial depiction of the circulation variability (i.e., zonal wind component).

A vector EOF analysis is then applied to the total anomalous 700 mb wind vector Because of the increased number of degrees of freedom associated with a vector EOF analysis, rigorous examinations of the VEOF results are required to identify the most parsimonious representation of the large-scale circulation variability. The leading VEOF

patterns, which are oriented along preferred phase directions, are also significantly related to the tropical cyclone-based circulation patterns. Indeed, these VEOF structures represent much larger scale variability that can be associated with the primary circulation features over the tropical western Pacific and Indian Oceans (e.g., monsoon trough, subtropical ridge, reverse-oriented monsoon trough, 30-60 day zonal wind oscillations, etc.)

Because of the importance of large-scale convection over the tropical regions, a scalar EOF analysis is also applied to the anomalous OLR data to identify a relationship between tropical convection, large-scale circulation variability, and tropical cyclone-based circulation patterns. The leading OLR EOFs provide a physically consistent depiction of the variability in tropical convection associated with large-scale circulation features and tropical cyclone activity. These OLR anomalies, which are satellite-based measurements, are independent of the GBA wind analyses. Therefore, consistency between the OLR anomalies and large-scale convergence/divergence anomalies provides additional confidence in the ability of the Global Band Analysis to accurately depict the tropical circulation features.

A consistent conclusion from the scalar and vector EOF analyses of the wind, and the OLR EOF analysis, is that the scales of motion identified are much larger than the horizontal scales based only on tropical cyclone characteristics. Nevertheless, these large-scale circulations have similar relationships with the basic tropical cyclone characteristics. Because an EOF analysis is a statistical procedure originally utilized in meteorology as a data-reduction method, no guarantee exists that physically meaningful patterns of variability will be identified. Therefore, the rigorous establishment of physical relationships between the

structures defined by the EOF analyses was a necessary intermediate step for ultimately defining recurrent circulation patterns of the tropical atmosphere.

## C. RECURRENT LARGE-SCALE CIRCULATION PATTERNS

The exhaustive analysis of the basic structure of the large-scale circulation variabilities provides the framework for identification of recurrent large-scale circulation patterns. Because of the many degrees of freedom associated with atmospheric motions, it is imperative that the basic structure of the circulation variability be defined in the most complete manner possible. This basic structure is provided by the VEOF analysis.

A fuzzy cluster analysis has been applied to the two leading VEOF representations of the anomalous 700 mb large-scale circulations. The cluster analysis identifies six primary clusters. Anomaly maps that could not be identified with one of these clusters are placed into a seventh cluster that represents the large diffuse region of the phase space defined by the clusters. It is shown that the six clusters describe the variability associated with the monsoon trough and subtropical ridge over the western Pacific. A large fraction of the cases fall into cluster 5, which is identified as a representation of only small variations about the climate mean. Although the clusters are based upon 700 mb circulation anomalies, the physical attributes of each cluster have been identified using other meteorological variables and at different vertical levels. That is, the cluster patterns are associated with coherent variability over scales of motion ranging from tropical cyclones, synoptic-scale waves, and global-scale rotational and divergent circulations. Furthermore, preferred transition paths between the cluster centers are identifiable and statistically significant compared to random transitions among the clusters. Physical descriptions of the preferred transition paths among the clusters

identifies a rich structure that spans many spatial scales and includes both dynamic and diabatic mechanisms.

Two primary results are obtained from the cluster analysis. The first result is that the generally complex attributes of tropical atmospheric variability may be satisfactorily represented by this cluster analysis. The success of this application is undoubtedly due to the ability of the VEOF analysis to identify the basic variability structures within a two-dimensional framework. It might have been anticipated that the application of the combined EOF and cluster analyses would provide limited results that were only representative of the basic circulation features over the tropical western Pacific. However, the combination of the two analyses provides a very complete description of large-scale circulation variability that links many physical attributes of atmospheric motion systems.

The second major result is that a physically and statistically significant relationship is documented between tropical cyclone characteristics and the cluster patterns. Individual cluster patterns are related to synoptic regimes that are favorable or unfavorable to the genesis location and to the track types. That is, the cluster centers, which represent instantaneous depictions of the circulation variability, define recurrent patterns that may be associated with tropical cyclone characteristics. In addition, a small set of preferred transition paths between the clusters has been identified. This is a significant result since the values of the membership coefficients associated with each cluster at each time can used to infer the sequences of the atmospheric circulations around the phase space defined by the cluster system. This is expected to provide a sound basis for extended range predictions of expected tropical cyclone characteristics based upon the expected evolution of the atmospheric state.

The only disappointing result from the cluster analysis is that the standard deviations associated with passage times through clusters or along the preferred transition paths are large. This is probably due to the interactions and feedbacks among the various scales of motion within the cluster patterns. Because these interactions and feedbacks are nonlinear, they are expected to result in greater variance associated with movements around the cluster phase space. Even with the variable time components, only a limited number of preferred transition paths from each cluster are found. Also, the rate of change with respect to the membership coefficients may provide a basis to estimate how rapidly the atmospheric system is passing through a cluster.

A final implication of the results of this study regards the predictability of tropical cyclone characteristics. If the large-scale circulation anomalies represent small deviations about the climate mean state (i.e., cluster 5), then there is no indication of a preferred tropical cyclone track type. Therefore, forecasts of tropical cyclone motion may be less accurate in these instances. Conversely, a clear identification of the anomalous circulation with a cluster that has a strongly preferred track type would suggest that more confidence can be attached to the track forecast.

## D. CONCLUSION

The above results and discussion lead to the conclusion that the observed low frequency variability in tropical cyclone characteristics is directly attributable to the existence of recurrent large-scale circulation patterns. Preferred transition paths between these circulation patterns lead to periods of similar large-scale circulation characteristics that are directly related to tropical cyclone genesis and motion. Furthermore, these transition paths are

related to physically consistent relationships among many components of the atmospheric system.

The utility of this conclusion, which has direct bearing upon recommended future research, may be illustrated by examining the variability of the large-scale circulation during the summer of 1990, which was the period of a field experiment (TCM-90) of an Office of Naval Research tropical cyclone motion research initiative. The anomalous 700 mb circulation data, which were obtained from the Naval Operational Global Atmospheric Prediction System (NOGAPS), are projected onto the leading VEOFs and then assigned to the cluster patterns. The cluster analysis correctly identified a 1-6-5-4 transition path during late July, which was associated with the reverse orientation of the monsoon trough and movement of the trough to the subtropics (Fig. 95). Tropical cyclones that occurred during August and September 1990 (TCM-90 period) are listed in Table 12 along with the observed track type and cluster assignment based upon the time that each cyclone reached tropical storm intensity (35 kt). Comments regarding transitions that began to occur during the lifetime of the tropical cyclone are included. Transitions are defined by changes in the cluster membership coefficients. The relationships between the tropical cyclones that occurred during the TCM-90 period and the cluster assignments for that time period are similar to the nine-year sample used to define the cluster patterns (Table 12).

Several interesting features are associated with Table 12. Based upon a cluster 1 anomaly pattern, Typhoon Zola would have been forecast to follow a straight track. However, a transition from cluster 1 to cluster 6 occurred during the lifetime of Zola. Typhoon Becky and Tropical Storm Cecil, which were short-lived circulations over the South

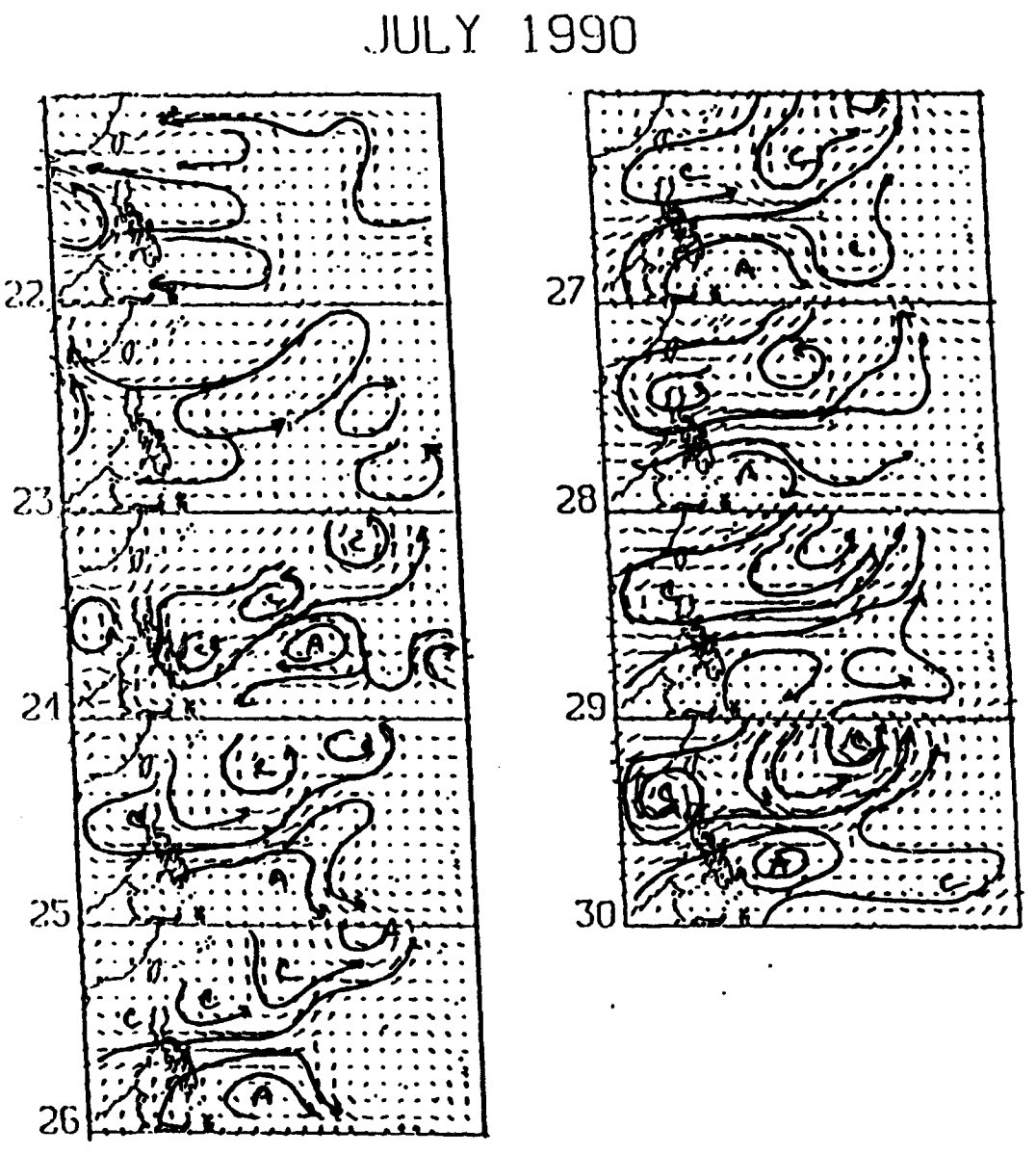


**Fig. 95** Anomalous 700 mb wind vectors at 00 UTC 22 July 1990 through 00 UTC 30 July 1990.

China Sea and eastern Asia near Taiwan, were associated with cluster 5 that does not have a strong circulation anomaly. Supertyphoon Flo was associated with a weak 6-5-3 transition that resulted in a period of reduced convective activity over the tropical western Pacific.

**TABLE 12** CLUSTER ASSIGNMENTS ASSOCIATED WITH TROPICAL CYCLONES DURING TCM-90.

| TROPICAL CYCLONE | TRACK TYPE | CLUSTER NUMBER | COMMENTS |
|---|---|---|---|
| Winona | Recurve-north | 4 | |
| Yancy | Straight | 1 | |
| Zola | Recurve-south | 1 | Beginning transition to 6 |
| Abe | Recurve-south | 6 | |
| Becky | Straight | 5 | |
| Cecil | Other | 5 | |
| Dot | Straight | 1 | |
| Ed | Straight | 1 | Beginning transition to 6 then 5 |
| Flo | Recurve-south | 5 | Transitioning to 3 |

## E. FUTURE RESEARCH

Future research should concentrate on two basic questions raised by this study. The first question concerns the implication that the large-scale circulation can evolve very differently depending upon which transition path is followed. Comparisons between the 1-6-5-4 and 6-5-3 transition paths in Chapter V suggest that very different paths may be followed depending upon the orientations of large-scale circulations over the midlatitudes.

The second question relates to an application of the results obtained in this study to the prediction of tropical cyclone characteristics in a manner similar to that illustrated during the TCM-90 time period. Cluster analysis combined with a discriminant analysis has been used as the basis for an operational forecast scheme over the midlatitudes (Maryon and Storey 1990). The results of the fuzzy cluster analysis used in this research provide additional information that could be utilized to estimate the stability of atmospheric patterns and expected durations within a cluster or movement along a transition path. A forecast scheme of this type would have great utility to operational planning of military and civilian activities that are impacted by tropical cyclones.

## APPENDIX A

## STATISTICAL SIGNIFICANCE OF COMPOSITE RESULTS

The statistical significance of the composite results is examined following the two-level procedure described by Livezey and Chen (1983), and will be described in this Appendix in relation to one of the tropical cyclone-based composite patterns. Initially a t-test is applied at every grid point of each composite to determine if the anomaly value is significantly different from zero (climatology). Following Livezey and Chen (1983), the outcomes of N 95% significance tests may be described by a binomial distribution with N trials and the probability of a success (test passed) P equal to 0.05. Local significance, at the 95% level, will be evaluated by comparing the number of significant points within the area between 5°S-30°N and 90°-150°E to the critical value from the binomial distribution with N equal to 384 (number of grid points in the region) and P equal to 0.05. From the binomial distribution with these parameters, 27 of 384 points (7%) must be significant.

It is assumed that the members of each composite are temporally independent. Recall that composites are created from combinations of anomaly maps based on different occurrences of a particular criterion. These sets are typically separated by more than 10 days, which is longer than the typical decorrelation time for atmospheric fields (Leith 1973).

The assumption of spatial independence among the grid points is examined in a second-level test, or global significance test. This global test is only relevant after establishing local significance, which assumes spatial independence. Global significance is examined by comparing the number of significant points to a distribution obtained from the

number of significant points defined in 200 random composites. The random composites are constructed using the same number of maps as the physical composite, except that the cases are chosen using a random number generator.

As an example, the locally significant points for the straight-moving tropical cyclone-based composite are presented in Fig. A1. Clearly, more than 27 points over the region of interest are locally significant. Nearly all of the significant points are within the region of anomalous easterlies associated with the subtropical ridge. The distribution of significant points between 5°S-30°N and 90°-150°E for the 200 mb composites that simulate the track-type composite is shown on Fig. A2. Only 2% of the random composites contained more significant points in the region of interest, which leads to the conclusion that the straight-moving pattern is significant at a 95% confidence level.

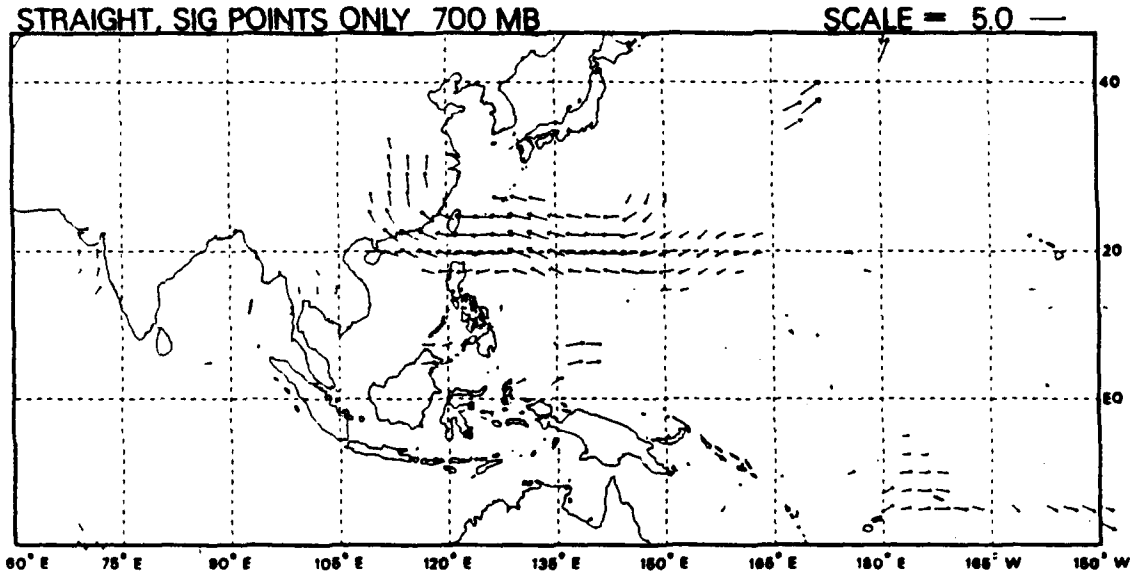


**Fig. A1** Locally significant 700 mb anomalous wind vectors (m $s^{-1}$) from the straight-moving composite (Fig. 3).

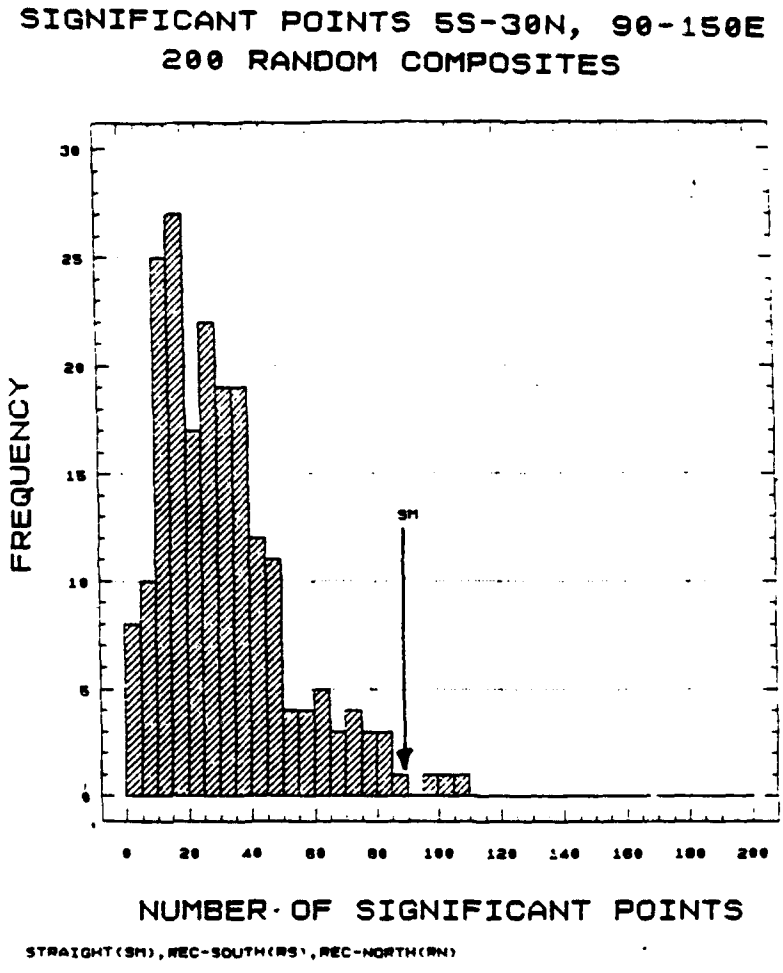


**Fig. A2** Distribution of locally significant points in the 200 random composites that simulate the straight-moving track type composites.

## APPENDIX B

## EMPIRICAL ORTHOGONAL FUNCTION ANALYSIS

Empirical orthogonal function analysis (EOF) is a powerful method that is used to summarize data by objectively examining the structure of variability within the data set. It is based upon the more general principal component analysis (Hotelling 1933), and has been extensively applied in meteorological research since its introduction by Lorenz (1957) (Richman 1987 and references therein). An EOF analysis may be used to describe physical attributes of a data set provided adequate examination of the functions indicate a relationship between the structure of the EOF and the characteristic spatial structures of the data set.

Many different definitions of the technique have been developed. The approach outlined here follows Kutzbach (1967). There are N observations of a vector $s_n$, which represents a spatial distribution of a variable such as the anomalous 700 mb zonal wind component or OLR anomaly over N grid points. The M sets of observations are collected in the observation matrix S such that the nth column contains $s_n$, and the element $s_{mn}$ contains the mth observation at point n. The objective of EOF analysis is to define a vector **e** that represents the structure of the observations in an optimal manner. The relationship between the observations $s_n$ and **e** is defined by their inner product. This product is divided by the total number of observations N to insure that the projection of **e** onto the data set is not biased by the length of the data set. It is also divided by the amplitude of **e** to remove any bias related to the length of **e**. The relationship between the observations and **e** is defined as

$$\frac{1}{N}\frac{(\boldsymbol{eS})^2}{\boldsymbol{ee}^T}, \tag{B1}$$

which is equivalent to $\mathbf{e}^T\mathbf{Re}$ with the condition $\mathbf{e}^T\mathbf{e} = 1$, and

$$\boldsymbol{R} = \frac{1}{N}\boldsymbol{SS}^T \tag{B2}$$

is the covariance matrix of the observation matrix S.

The maximization of (B1) proceeds by assuming that the maximum value of the squared projection of **e** onto the observations S is

$$\boldsymbol{e}^T\boldsymbol{Re} = \lambda. \tag{B3}$$

Multiplying the left side by **e** and using $\mathbf{e}^T\mathbf{e} = 1$ provides

$$\boldsymbol{Re} = \boldsymbol{e}\lambda. \tag{B4}$$

This is equivalent to

$$(\boldsymbol{R} - \lambda\boldsymbol{I}) = 0, \tag{B5}$$

which can only be true if

$$|\boldsymbol{R} - \lambda\boldsymbol{I}| = 0. \tag{B6}$$

Therefore, $\lambda$ is an eigenvalue of the real symmetric matrix **R**, which has a set of M positive eigenvalues. Generally, (B4) is expressed in matrix form as

$$\boldsymbol{RE} = \boldsymbol{EL}, \tag{B7}$$

where L is an M by M diagonal matrix where the ith diagonal element contains the ith eigenvalue. The matrix **E** is an M by M orthogonal matrix that contains the $\mathbf{e}_i$ eigenvectors.

Using (B2) and (B7) and the matrix property that the transpose of an orthogonal matrix is equal to the inverse results in

$$E^T S S^T E = LN. \tag{B8}$$

A M by N matrix may be defined as $C = E^T S$, which leads to

$$S = EC. \tag{B9}$$

An individual observation vector is then defined from

$$s_n = \sum_{i=1}^{M} c_{in} e_i. \tag{B10}$$

The element $c_{in}$ is defined as the principal component or the eigencoefficient associated with the ith eigenvector for the nth observation. Using (B9) in (B8) provides

$$CC^T = LN, \tag{B(11)}$$

which indicates that not only are the eigenvectors ($e_i$) orthogonal, but so are the principal components.

The percent of total variance explained by the ith eigenfunction is the ith eigenvalue divided by the sum of all eigenvalues times 100%.

## LIST OF REFERENCES


Anderberg, M. R., 1973: *Cluster Analysis for Applications.* Academic Press, New York, New York, 359 pp.

Barnston, A. G., and R. L. Livezey, 1987: Classification, seasonality and persistence of low-frequency atmospheric circulation patterns. *Mon. Wea. Rev.*,**115**, 1083-1126.

Bock, H.H.,1987: On the interface between cluster analysis, principal component analysis and multidimensional scaling. In *Multivariate Statistical Modeling and Data Analysis.* B. Bosdogan and G. Gupta, Eds., Reidel Publishing, Dordrecht Holland, 190 pp.

Chan, J. C.-L., 1985a: Identification of the steering flow for tropical cyclone motion from objectively analyzed wind fields. *Mon. Wea. Rev.*,**113**, 106-116.

Chan, J. C.-L, 1985b: Tropical cyclone activity in the northwest Pacific in relation to El Nino/Southern Oscillation phenomenon. *Mon. Wea. Rev.*,**113**, 599-606.

Charney, J. G., and J. G. DeVore, 1979: Multiple flow equilibria in the atmosphere and blocking. *J. Atmos. Sci.*, **36**, 1205-1216.

Dole, R. M., and N. M. Gordon, 1983: Persistent anomalies of the extratropical northern hemisphere wintertime circulation: Structure. *Mon. Wea. Rev.*,**114**, 1567-1586.

Elsberry, R. L., 1987: Tropical cyclone motion. *A Global View of Tropical Cyclones.* R. L. Elsberry, Ed., Office of Naval Research, 189 pp. [ Available from Dept. of Meteorology, Naval Postgraduate School, Monterey, CA 93943].

Freund, J. E., 1971: *Mathematical Statistics*, Prentice-Hall Inc., Englewood Cliffs, New Jersey, 463 pp.

Gambo, K., and K. Kudo, 1983: Teleconnection in the zonally asymmetric height field during the northern hemisphere summer. *J. Meteor. Soc. Japan*, **61**, 829-838.

George, J. E., and W. M. Gray, 1976: Tropical cyclone motion and surrounding parameter relationships. *J. Appl. Meteor.*, **15**, 1252-1264.

Gray, W. M., 1979: Tropical cyclone origin, movement, and intensity characteristics based on data compositing techniques. NAVENVPREDRSCHFAC Contractor Report CR 79-06. Naval Research Laboratory- Monterey, Monterey, CA 93943, 126 pp.

Gray, W. M., 1985: Tropical cyclone global climatology. WMO Tech. Document WMO/TD-No. 72, Vol I, WMO Geneva, Switzerland, 3-19.

Ghil, M., 1987: Predictability of planetary flow regimes: Dynamics and statistics. In *Toward Understanding Climate Change: The J. O. Fletcher Lectures on Problems and Prospects of Climate Analysis and Forecasting*. Uwe Radok, Ed., Westview Press, Boulder, Colorado, 151 pp.

Grayson, T. H., 1971: Global band sea level pressure and surface wind analysis. FNWC Tech Note 71-3, 28 pp. [Available from United States Navy Fleet Numerical Oceanography Center, Monterey, VA 93943].

Gruber, A., and A. F. Krueger, 1984: The status of the NOAA outgoing longwave radiation data set. *Bull. Amer Meteor. Soc.*, **65**, 958-962.

Gutzler, D. S., 1991: Interannual fluctuations of intraseasonal variance of near-equatorial zonal winds. *J. Geophys. Res.*, **96**, 3173-3185.

Hanson, A. R., and A. Sutera, 1986: On the probability density distribution of planetary-scale atmospheric wave amplitude. *J. Atmos. Sci.*, **43**, 3250-3265.

Hardy, D. M., 1977: Empirical eigenvector analysis of vector observations. *Geophys. Res. Lett.*,**4**, 319-320.

Hardy, D. M., and J. J. Walton, 1978: Principal components analysis of vector wind measurements. *J. Appl. Meteor.*, **17**, 1153-1162.

Harr, P. A., and R. L. Elsberry, 1991: Tropical cyclone track characteristics as a function of large-scale circulation anomalies. *Mon. Wea. Rev.*,**119**, 1448-1468.

Horel, J. D., 1985a: Persistence of the 500 mb height field during the northern hemisphere winter. *Mon. Wea. Rev.*,**113**, 2030-2042.

Horel, J. D., 1985b: Persistence of wintertime 500 mb height anomalies over the central Pacific. *Mon. Wea. Rev.*,**113**, 2043-2048.

Hoskins, B. J., and D. J. Karoly, 1981: The steady linear response of a spherical atmosphere to thermal and orographic forcing. *J. Atmos. Sci.*, **38**, 1179-1196.

Hotelling, H., 1933: Analysis of a complex of statistical variables into principal components. *J. Educ. Psychol.*, **24**, 417-441.

Hsu, H.-H., B. J. Hoskins and F.-F. Jin, 1990: The 1985/86 intraseasonal oscillation and the role of the extratropics. *J. Atmos. Sci.*,**47**, 823-839.

Jolliffee, I. T., 1987: Rotation of principal components; Some comments. *J. Climatol.*,7, 509-512.

Kalkstein, L. S., G. Tan and J.A Skindlov, 1987: An evaluation of three clustering procedures for use in synoptic climatological classifications. *J. Climate and Appl. Meteor.*, **26**, 717-730.

Kaufman, L., and P. J. Rousseeuw, 1990: *Finding Groups in Data: An Introduction to Cluster Analysis.*, John Wiley and Sons, Inc., New York, New York, 342 pp.

Kiladis, G. N., and K. M. Weickmann, 1992: Circulation anomalies associated with tropical convection during northern winter. *Mon. Wea. Rev.*,**120**, 1900-1923.

Klink, K., and C. Willmott, 1989: Principal components of the surface wind field in the United States: A comparison of analyses based upon wind velocity, direction and speed. *J. Climatol.*, **9**, 293-308.

Knutson, T. R., and K. M. Weickmann, 1987: 30-60 day atmospheric oscillations: Composite life cyclones of convection and circulation anomalies. *Mon. Wea. Rev.*,**115**, 1407-1436.

Krishnamurti, T. N., P. K. Jayakumar, J. Sheng, N. Surgi and A. Kumar, 1985: Divergent circulations on the 30-50 day time scale. *J. Atmos. Sci.*, **42**, 364-375.

Kurihara, K., and T. Tsuyuki, 1987: Development of the barotropic high around Japan and its association with Rossby wave-like propagations over the north Pacific: Analysis of August 1984. *J. Meteor. Soc. Japan*, **65**, 237-246.

Kutzbach, J. E., 1967: Empirical eigenvectors of sea-level pressure, surface temperature, and precipitation complexes over North America. *J. Appl. Meteor.*, **6**, 791-806.

Lander, M. A., 1993: The northward-displaced, self-sustaining, solitary (NSS) monsoon gyre. *Wea. and Forecasting*, (submitted).

Lau, K.-H., and N.-C. Lau, 1990: Observed structure and propagation characteristics of tropical summertime synoptic scale disturbances. *Mon. Wea. Rev.*, **118**, 1888-1913.

Lau, K.-H., and N.-C. Lau, 1992: The energetics and propagation dynamics of tropical summertime synoptic-scale disturbances. *Mon. Wea. Rev.*, **120**, 2523-2539.

Lau, K.-M., and P. H. Chan, 1985: Aspects of the 40-50 day oscillation during the northern summer as inferred from outgoing longwave radiation. *Mon. Wea. Rev.*,**114**, 1889-1909.

Lau, K.-M., and T. J. Phillips, 1986: Coherent fluctuations of extratropical geopotential height and tropical convection in intraseasonal time scales. *J. Atmos. Sci.*, **43**, 1164-1181.

Lau, K.-M., and L. Peng, 1990: Origin of low frequency (intraseasonal) oscillations in the tropical atmosphere. Part III: Monsoon dynamics. *J. Atmos. Sci.*, **40**, 1443-1462.

Lau, K.-M., L. Peng, C. H. Sui and T. Nakazawa, 1989: Dynamics of super cloud clusters, westerly wind bursts, 30-60 day oscillations and ENSO: A unified view. *J. Meteor. Soc. Japan*, **67**, 205-219.

Legler, D. M., 1983: Empirical orthogonal function analysis of wind vectors over the tropical Pacific Region. *Bull. Amer. Meteor. Soc.*, **64**, 234-241.

Legras, B., and M. Ghil, 1985: Persistent anomalies, blocking and variations in atmospheric predictability. *J. Atmos. Sci.*, **42**, 433-471.

Leith, C. E., 1973: The standard error of time-average estimates of climatic means. *J. Appl. Meteor.*, **12**, 1066-1069.

Liebmann, B., and H. H. Hendon, 1990: Synoptic-scale disturbances near the equator. *J. Atmos. Sci.*, **47**, 1463-1479.

Livezey, R. E., and W. Y. Chen, 1983: Statistical field significance and its determination by Monte Carlo techniques. *Mon. Wea. Rev.*, **111**, 46-59.

Lorenc, A. C., 1984: The evolution of planetary scale 200 mb divergent flow during the FGGE year. *Quart. J. Roy. Meteor. Soc.*, **110**, 427-441.

Lorenz, E. N., 1957: Empirical orthogonal functions and statistical weather prediction. Science Report 1, Statistical Forecasting Project, Department of Meteorology, Massachusetts Institute of Technology. [NTIS AD 110268] 49 pp.

Lorenz, E. N., 1963: Deterministic nonperiodic flow. *J. Atmos. Sci.*, **20**, 130-141.

Love, G., 1982: The role of the general circulation in western Pacific tropical cyclogenesis. Atmospheric Science Paper No. 340, Colorado State University, Ft. Collins, CO 80523, 215 pp.

Madden, R. A., 1986: Seasonal variation of the 40-50 day oscillation in the tropics. *J. Atmos. Sci.*, **43**, 3138-3158.

Madden, R. A., and P. R. Julian, 1972: Description of a global-scale circulation cell in the tropics with a 40-50 day period. *J. Atmos. Sci.*, **29**, 1109-1123.

Madden, R. A., and D. S. Gutzler, 1989: Seasonal variation is the spatial structure of intraseasonal tropical wind fluctuations. *J. Atmos. Sci.*, **46**, 641-660.

Magana, V., and M. Yanai, 1991: Tropical-midlatitude interaction on the time scale of 30-60 days during the northern summer of 1979. *J. Climate.*, **4**, 180-201.

Maryon R. H., and A. M. Storey, 1985: A multivariate statistical model for forecasting anomalies of half-monthly mean surface pressure. *J. Climatology.* **5**, 561-578.

McBride, J. L., and R. Zehr, 1981: Observational analysis of tropical cyclone formation. Part I Comparison of nondeveloping versus developing systems. *J. Atmos. Sci.*, **38**, 1132-1151.

Miller, R. J., T. L. Tsui and A. J. Schrader, 1988: Climatology of North Pacific tropical cyclone tracks. NAVENVPREDRSCHFAC Tech Rep. TR 88-10. Naval Research Laboratory-Monterey, Monterey, CA 93943, 511 pp.

Mo, K. C., 1986: Quasi-stationary states in the southern hemisphere. *Mon. Wea. Rev.*.**114**, 808-823.

Mo, K. C., and M. Ghil, 1987: Statistics and dynamics of persistent anomalies. *J. Atmos. Sci.*, **44**, 877-901.

Mo, K., and M. Ghil, 1988: Cluster analysis of multiple planetary flow regimes. *J. Geophys. Res.*, **93D**, 10927-10952.

Molteni, F., 1988: Empirical orthogonal function analysis of the zonal and eddy components of 500 mb height fields in the northern extratropics. ECMWF Technical Report No. 61, 36 pp.

Molteni, F., S. Tibaldi and T. N. Palmer, 1990: Regimes in the wintertime circulation over northern extratropics. I: Observational evidence. *Quart. J. Roy. Meteor. Soc.*, **116**, 31-67.

Moritz, R. E., and A. Sutera, 1981: The predictability problem: Effects of stochastic perturbations in multi-equilibrium systems. *Advances in Geophysics*, Vol. 23, Academic Press, New York, New York, 345-383.

Nitta, T., 1987: Convective activities in the tropical western Pacific and their impact on the northern hemisphere summer circulation. *J. Meteor. Soc. Japan*, **41**, 373-390.

Nitta, Ts., 1990: Unusual summer weather over Japan in 1988 and its relationship to the tropics. *J. Meteor. Soc. Japan*, **68**, 575-587.

North, G. R., T. L. Bell, R. F. Cahalan and F. J. Moeng, 1982: Sampling errors in the estimation of empirical orthogonal functions. *Mon. Wea. Rev.*.**110**, 699-706.

Pazan, S. E., T. P. Barnett, A. M. Tubbs and D. Halpern, 1982: Comparison of observed and model wind velocities. *J. Appl. Meteor.*, **21**, 314-320.

Richman, M. B., 1986: Rotation of principal components. *J. Climatol.*, **6**, 293-335.

Richman, M. B., 1987: Rotation of principal components: A reply. *J. Climatol.*, 7, 511-520.

Rui, H., and B. Wang, 1990: Development characteristics and dynamic structure of tropical intraseasonal convection anomalies. *J. Atmos. Sci.*, **47**, 357-379.

Sandgathe, S. A., 1987: Opportunities for tropical cyclone motion research in the northwest Pacific region. Tech. Rep. NPS-63-87-006, Naval Postgraduate School, Monterey, CA 93943, 36 pp.

Sardeshmukh, P. D., and B. J. Hoskins, 1988: The generation of global rotational flow by steady idealized tropical divergence. *J. Atmos. Sci.*, **45**, 1228-1251.

Schott, T. B., J. C.-L. Chan and R. L. Elsberry, 1987: Further applications of empirical orthogonal functions of wind fields for tropical cyclone motion studies. *Mon. Wea. Rev.*, **115**, 1225-1237.

Scott, A. J., and M. J. Symons, 1971: Clustering methods based on likelihood ratio criteria. *Biometrika*, **27**, 387-397.

Shukla, J., and K. R. Saha, 1974: Computation of nondivergent streamfunction and irrotational velocity potential from the observed winds. *Mon. Wea. Rev.*, **102**, 419-425.

Simmons, A. J., J. M. Wallace and G. W. Branstator, 1983: Barotropic wave propagation and instability, and atmospheric teleconnection patterns. *J. Atmos. Sci.*, **40**, 1363-1391.

Sui, C. H., and K.-M. Lau, 1992: Multiscale phenomena in the tropical atmosphere over the western Pacific. *Mon. Wea. Rev.*, **120**, 407-430.

Sutera, A., 1987: Probability density distribution of large scale atmospheric flow. *Adv. Geophys.*, **29**, 319-338.

Vautard, R., 1990: Multiple weather regimes over the North Atlantic: Analysis of precursors and successors. *Mon. Wea. Rev.*, **118**, 2056-2081.

Wallace, J. M., and D. S. Gutzler, 1981: Teleconnections in the geopotential height field during the northern hemisphere winter. *Mon. Wea. Rev.*, **109**, 784-812.

Weickmann, K. M., and S. J. S. Khalsa, 1990: The shift of convection from the Indian Ocean to the western Pacific Ocean during a 30-60 day oscillation. *Mon. Wea. Rev.*, **118**, 964-978.

Wylie, D. P., B. B. Hinton, M. R. Howland and R. J. Lord, 1985: Autocorrelation of wind observations. *Mon. Wea. Rev.*, **113**, 849-857.

## INITIAL DISTRIBUTION LIST

| | | No. Copies |
|---|---|---|
| 1. | Defense Technical Information Center<br>Cameron Station<br>Alexandria VA 22304-6145 | 2 |
| 2. | Library, Code 052<br>Naval Postgraduate School<br>Monterey CA 93943-5002 | 2 |
| 3. | Chairman (Code MR/Hy)<br>Department of Meteorology<br>Naval Postgraduate School<br>Monterey, CA 93943-5000 | 1 |
| 4. | Prof. Russell L. Elsberry (Code MR/Es)<br>Department of Meteorology<br>Naval Postgraduate School<br>Monterey, CA 93943-5000 | 4 |
| 5. | Office of Naval Research (Code 1122MM)<br>800 N. Quincy Street<br>Arlington, VA 22217-5000 | 1 |
| 6. | Commanding Officer<br>Fleet Numerical Oceanography Center<br>Monterey, CA 93943 | 1 |
| 7. | Commanding Officer<br>US NAVOCEANCOMCEN<br>COMNAVMAR Box 12<br>FPO San Francisco, CA 96630-2926 | 1 |
| 8. | Superintendent<br>Naval Research Laboratory, Monterey<br>Monterey, CA 93943-5000 | 1 |

9. Patrick A. Harr (Code MR/Hp) 2
Department of Meteorology
Naval Postgraduate School
Monterey, CA 93943-5000